Aromatic hydroxylations over titanium-substituted crystalline silicates

Dipl.-Ing. Uwe Wilkenhöner

Submitted in fulfillment of the requirements for the degree of

Doctor of Philosophy

Department of Chemical Engineering
University of Cape Town
Cape Town, South Africa.

September 2001

Declaration

I hereby declare that this submission is my own work and that, to the best of my knowledge and belief, it contains no material previously published or written by another person nor material which has been accepted for the award of any other degree of diploma of the university or other institute of higher learning, except where due acknowledgement has been made in the text.

Acknowledgements

First of all I thank my supervisors Prof. Eric van Steen and Dr. David Gammon; this would not have been finished without their support, input and guidance.

Thanks also to Prof. Cyril O'Connor and Prof. Hans Schulz, who established the link between the University of Cape Town and the Technical University of Karlsruhe, which brought me to this unique place and to a beautiful country.

I thank the Department of Chemical Engineering and the NRF for the funding they gave to this work.

A special thanks to the guys of the Fine Chemicals group of the Catalysis unit: Bryan Brack, Gillian Moon and Phalali Motsoetsoe. Many thanks also to the other members of the Catalysis Research Unit for their friendship and assistance, particularly to Natasha Ristic and Heiko Manstein for taking care of the group spirit by organising many social events.

I express my appreciation to the laboratory assistance of Helen, Maria and Shireen who always tried their very best to help me. The technical support received from Peter Dobias and Joachim Macke was equally appreciated as was the help from Granville de la Cruz (thanks also for the crayfish diving advice), Bill Randall and Craig Balfour with computer hardware and software.

Special thanks to the LINUX god Warwick Duncan and to Michael Halhead (thanks also for some stunning dives), who were always there for me and showed impressive patience when the next software disaster was looming. I would also like to thank my dear friend Peter, who listened to my woes and gave some good advice when the going was tough.

A very special thank-you goes to Sylvie, who probably suffered as much as myself in rough times, for her support and love. My gratitude also goes to my family, particularly to my mother, whose support was important despite the distance.

Thanks are also due to the group of Prof. P. A. Jacobs in Leuven and the group of Prof. G. Baron in Brussels; the fruitful collaboration with both groups in Belgium greatly contributed to this work. I particularly like to mention Gunther Langhendries and Frederik van Laar for their valuable advice and friendship (not only concerning science but also for the introduction to Belgium beer etc...).

Last but not least I salute my surfing buddies and friends Assaf, Lance and Dudley - not for the rapid completion of this thesis but for helping me to keep perspective.

Synopsis

This work focuses on aromatic hydroxylations over titanium-substituted zeolites of different pore sizes (TS-1, Al-free Ti-beta and Ti-HMS) using aqueous H_2O_2 as the oxidant. The aim was to gain a deeper understanding of the key factors controlling activity and selectivity, which implied an investigation of the reaction kinetics and the adsorption and diffusion properties of reactants and products in the various catalysts using different solvents. The role of shape selectivity inside the micropores of the solids and the reaction at their external surface was also examined.

In the course of this work, titanium-containing molecular sieves with different pore and crystal sizes have been synthesised. Physico-chemical characterisation methods confirmed the high quality of all samples. Comparing the product distributions obtained with catalysts of different pore sizes allows for investigation of shape selectivity in the zeolite pores, whereas variation of the crystal size represents a method of evaluating the influence of (i) the external surface and (ii) diffusional limitations on the rate of reaction. The influence of the external surface was further investigated by successfully applying the cycle-wise chemical vapour deposition (CVD) of tetraethoxysilane (TEOS) technique to completely deactivate the external surface of nano-size ($d_{crystal}$ = 0.1 μm) TS-1 crystals. It was shown that the application of this technique leads to deactivation of the external surface without imposing additional mass transfer resistances on diffusing molecules through narrowing or blocking of the pore mouth. A kinetic model was developed to represent the reaction data for the hydroxylation of phenol, anisole and toluene and good model fits were achieved. The application of this model to reaction data obtained from non-modified and surface-deactivated small TS-1 crystals allowed for decoupling of the activity of the internal and external surface of the zeolite. A chromatographic HPLC technique was used to characterise the adsorption properties and the liquid-phase ZLC method was chosen to measure the transport properties in the zeolites with different solvents.

The adsorption of reactants and products in both TS-1 and Al-free Ti-beta is the key factor for their excellent catalytic properties in aromatic hydroxylations. The hydrophobicity of both catalysts renders the intraporous H_2O_2 concentration low and inhibits readsorption and subsequent overoxidation of reaction products. Furthermore, framework hydrophobicity ensures their stability towards leaching of titanium, which was observed in the much more hydrophilic mesoporous titanosilicate Ti-HMS. A stronger adsorption of the aromatic reactant is also responsible for the activity of TS-1

and Al-free Ti-beta in different solvents, which decreased in the order water >> methanol > acetone.

The intraporous diffusion of aromatics in TS-1 and Al-free Ti-beta was found to be solvent-dependent and decreased with increasing adsorption of the aromatic compound, suggesting that the diffusion of the aromatic is influenced by its interactions with the zeolite walls. The measured intracrystalline diffusion coefficient of phenol in TS-1 was about an order of magnitude higher than reported in the literature. The discrepancy might be explained by the fact that literature values were determined under reaction conditions, whereas the diffusivities measured with the ZLC method are binary counterdiffusivities. The activation energy determined for the diffusion of phenol in TS-1 was 20.4 kJ/mol, which is in agreement with literature values for similar systems. The intracrystalline diffusivity of phenol was about a factor of 8 larger in Al-free Ti-beta compared to TS-1.

Reaction rates of aromatic hydroxylations over TS-1 and Al-free Ti-beta become strongly diffusion limited for larger crystals. Small crystals ($d_{crystal} < 0.3$ μm) of TS-1 have to be used to avoid major mass transfer limitations. Despite faster diffusion in Al-free Ti-beta, intraporous mass transfer resistance also influences the phenol hydroxylation in the smaller crystals synthesised ($d_{crystal} \approx 0.9$ μm). On the basis of the observed kinetic constants and the adsorption and diffusion measurements, the intrinsic activity of TS-1 was found to be slightly higher than the one of Al-free Ti-beta.

The selectivities and the different activities obtained with phenol, anisole and toluene are consistent with an electrophilic substitution reaction initiated by a titanium hydroperoxo species formed upon reaction of framework titanium with H_2O_2. The reactivity decreased in the order phenol > anisole > toluene. Ortho- and para-hydroxylation was observed in the phenol and anisole hydroxylation, whereas all three isomers were obtained in the toluene hydroxylation. A reaction mechanism involving the electrophilic attack of the terminal OH of the Ti-OOH group is proposed.

The selectivities obtained in aromatic hydroxylations over TS-1 and Al-free Ti-beta were strongly solvent dependent. In the case of the phenol hydroxylation over TS-1, the p/o-product isomer distribution was reversed when changing from a protic to an aprotic solvent. Higher para-selectivities were generally obtained in protic solvents for all reactions. Various configurations of the titanium active site are discussed and coordination of protic solvent molecules to the titanium atom is proposed. The size of the active site is significantly increased with coordinated solvent molecules, which imposes a geometric constraint in the micropores of TS-1 and enhances para-hydroxylation. Protic solvents can therefore play an active role in the reaction path and a reaction mechanism consistent with the selectivities observed is suggested.

A comparison of TS-1 and Al-free Ti-beta in the phenol hydroxylation confirms the presence of shape selectivity in TS-1 since much higher para-selectivities were obtained with the latter. Protic solvents enhance shape selectivity through coordination to the titanium site. In the anisole and toluene hydroxylation however, more para-hydroxylation was observed with Al-free Ti-beta. This can be explained by the ability of aromatic molecules to adopt a different configuration in Al-free

Ti-beta. Apolar substituents at the aromatic ring can point away from the polar active site towards the zeolite wall, a configuration that favours para-hydroxylation and is not possible in TS-1.

A comparison of parent and external surface-deactivated TS-1 revealed that the role of the external surface is important. All hydroxylation reactions proceeded at an order of magnitude faster rate at the external surface, which originates from higher H_2O_2 concentrations at the active sites. External surface sites are exposed to the peroxide concentrations in the bulk solution, which are much higher than in the pores, hence showing much higher activity. Undesired side reactions such as hydrogen peroxide decomposition and tar formation also mainly take place at the external surface. The external surface also exhibited different selectivities compared to the internal surface. In all cases, higher para-selectivities were obtained for the internal reaction, confirming a shape selective reaction inside the micropores of TS-1.

Al-free Ti-beta is a suitable catalyst for aromatic hydroxylations and can also be applied to the hydroxylation of naphthalenes due to its larger pores. 1-Naphthol and 2-methyl-naphthalene were taken as model compounds to demonstrate the activity of Al-free Ti-beta for this type of reaction.

Table of Contents

List of Figures

List of Tables

Nomenclature

Symbols

A_i	peak area of compound i, eq. D.5
C, C_i	concentration of compound i in the bulk solution [$\frac{mol}{l}$ or weight %]
d	diameter of spherical particles [m]
D_c	intracrystalline micropore diffusivity [$\frac{m^2}{s}$]
D_∞	intracrystalline self-diffusivity [$\frac{m^2}{s}$]
D_m	diffusivity in the bulk liquid phase [$\frac{m^2}{s}$]
D_{eff}	effective diffusivity under reaction conditions, eq. 5.3 and 5.4 [$\frac{m^2}{s}$]
E_A	heat of adsorption, eq. 2.4 or activation energy for diffusion, eq. 4.13 [$\frac{kJ}{mol}$]
F	flow rate [$\frac{ml}{min}$]
$\triangle_R$G	Gibbs free energy of reaction [$\frac{kJ}{mol}$]
$\triangle_R$H	heat of reaction [$\frac{kJ}{mol}$]
$\vec{j_c}$	micropore flux [$\frac{1}{m^2 \cdot mol \cdot s}$]
$\vec{j_s}$	surface flux [$\frac{1}{m^2 \cdot mol \cdot s}$]
k_f	mass transfer coefficient in the bulk liquid phase [$\frac{m}{s}$]
k_i,k_{obs}	observed second order rate constant for formation/consumption of compound i per surface area of catalyst [$\frac{l}{mol \cdot s \cdot m^2_{cat}}$]
k_{intr}	intrinsic second order rate constant for formation/consumption of compound i per surface area of catalyst [$\frac{l}{mol \cdot s \cdot m^2_{cat}}$]

k_{react}	intrinsic second order rate constant in catalyst pores, per unit volume of catalyst $[\frac{m^3}{mol \cdot s}]$
K_0	pre-exponential factor in eq. 2.4
K_{eq}	equilibrium constant
K	Henry's adsorption constant, eq. 2.2
l	thickness of slab-shaped particles [m]
L	coefficient extracted from ZLC desorption curves, eq. 2.10
L_{cat}	length of catalyst bed [m]
m	mass [g]
n_i	number of moles of compound i [mol]
q	concentration in micro-particles $[\frac{mol}{l}]$
$\overline{q}$	average concentration in micropores $[\frac{mol}{l}]$
r	radial coordinate of crystals [m]
R	ideal gas constant $[\frac{J}{mol \cdot K}]$
R_c	radius of crystals [m]
R_m	measured diffuse UV-VIS reflection, eq. C.1
R_∞	diffuse UV-VIS reflection for standard, eq. C.1
R^2	correlation coefficient
Δ_RS	entropy of reaction $[\frac{J}{mol \cdot K}]$
S, S_{int}, S_{ext}	BET surface area of catalyst $[\frac{m^2}{g}]$
S_i	selectivity on the basis of species i [%]
SF_i	sensitivity factor of compound i $[\frac{1}{mol}]$
t_R	reaction time [s]
T	temperature [K] or [°C]
u_f	superficial fluid velocity $[\frac{m}{s}]$

V_s,V_{cat} volume of catalyst [ml]

V_f,V_{cat} volume of fluid phase in catalyst bed [ml]

V_R volume of reactor [ml]

X_i conversion of species i [%]

Greek

α partition coefficient

β_n roots of eq. 2.11

γ activity coefficient

δ_f thickness of stagnant fluid layer around catalyst particles [m]

ε_{ext} porosity of catalyst bed

ε_r dielectric constant

ϕ Thiele modulus, eq. 5.4 and 5.3

λ wavelength [nm]

μ_1 first moment, eq. 2.1

η effectiveness factor, eq. 5.2

ρ_f density of reaction mixture [$\frac{g}{ml}$]

σ^2 second moment, eq. 2.3

Abbreviations

AAS atomic adsorption spectroscopy

BET Brunauer, Emmett and Teller isotherm

CVD chemical vapour deposition

DRS diffuse reflectance spectroscopy

DTA differential thermal analysis

EDX electron diffraction

EQ	environmental coefficient
ESR	electron spin resonance
EXAFS	X-ray absorption fine structure
FID	flame ionization detector
FT-IR	Fourier-transform infrared
GC	gas chromatography
HPLC	high-performance liquid chromatography
LC	liquid chromatography
TBHP	tert-butyl-hydroperoxide
SEM	scanning electron microscopy
TEM	transmission electron microscopy
TCD	thermal conductivity detector
TGA	thermogravimetric analysis
UV-VIS	ultraviolet-visible
WHSV	weight hourly space velocity
XANES	X-ray absorption near edge structure
XPS	X-ray photoelectron spectroscopy
ZLC	zero length column

Indices

ext,e	external
int,i	internal
P	phenol
A	anisole
T	toluene

t	tars
0	initial
obs	observed
o	ortho
m	meta
p	para
PBQ	para-benzoquinone
MB	monosubstituted benzene (phenol, anisole, toluene)
Naph	substituted naphthalene (1-naphthol, 2-methyl-naphthalene)
dec	decomposition

Chapter 1

Introduction

1.1 Oxidations in the synthesis of fine chemicals

Heterogeneous catalytic reactions for selective oxidation of hydrocarbons occupy a prominent place in both the science of catalysis and catalysis-based modern chemical industry. They represent major routes for functionalisation of hydrocarbon molecules. More than 20% of industrial organic chemicals are obtained by catalytic oxidation or ammoxidation of hydrocarbons [Shanani et al. (1996)]. Today catalytic oxidation is one of the largest industrial scale operations for the production of intermediates, pharmaceuticals and fine chemicals and the basis of the production of almost all monomers used in the manufacture of synthetic fibres, plastics, paints, adhesives etc. (see Table 1.1). While

Table 1.1: Industrial chemicals produced by hydrocarbon oxidation in 1996 [Shanani et al. (1996)]

Chemical	U.S. capacity (million ton/year)
Acetaldehyde	0.23
Acrylonitrile	1.38
1,4-Butanediol	0.31
Caprolactam	0.65
Ethylene oxide	3.52
Maleic anhydride	0.24
Phenol	1.89
Phthalic anhydride	0.47
Propylene oxide	1.75
Terephthalic acid/dimethyl terephthalate	3.53
Vinyl acetate	1.32
Vinyl chloride	5.86

Table 1.1 highlights the importance of catalytic oxidation processes in the chemical industry in general, one of the most interesting areas is fine chemicals production, where oxidations play an equally

important role. Due to the generally higher profit margins in the synthesis of fine chemicals, intermediates or pharmaceuticals, many chemical companies have increased their activities and research efforts in this area.

1.2 General catalytic process options

The focus of this work is heterogeneously catalyzed liquid-phase oxidations as highlighted in Figure 1.1, which shows the general process options for catalytic hydrocarbon oxidation reactions. The pro-

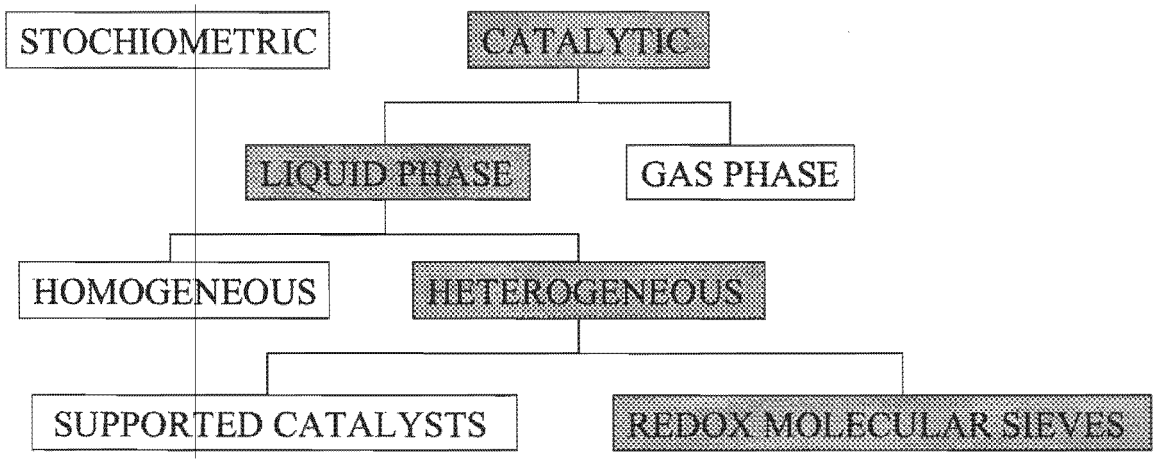

Figure 1.1: Catalytic process options for fine chemicals production [Sheldon and Dakka (1994)]

cess of choice, if possible, will always be a gas-phase oxidation using oxygen or air as the oxidant. Oxygen and air are inexpensive and the process can be run continuously, allowing large-scale production. However, since dioxygen has a triplet ground state, reactions with most organic molecules are spin-forbidden and exhibit high activation energies, consequently requiring relatively high reaction temperatures [Sheldon (1990)].

The term "fine chemicals" is not always precisely defined, but it usually refers to compounds that have:

- a relatively high molecular weight and thus
- a relatively high boiling point
- multiple functionalities (especially intermediates for pharmaceuticals etc.)
- limited thermal stability

Due to the above properties it is clear that the application of gas-phase processes using air/O_2 requiring high temperatures is generally not favoured for the synthesis of fine chemicals. Furthermore,

since fine chemicals are often produced in batch processes and have high value, a high selectivity is more important than a high activity in the process. The use of dioxygen (or air) as the oxidant in gas-phase oxidations always implies that side reactions such as total oxidation to water and carbon dioxide (the thermodynamically favoured products) lower the selectivity of the process. Dioxygen generally shows little chemo- or regioselectivity in its reactions with organic substrates and the primary oxidation products are more easily oxidised than the hydrocarbon substrate.

In liquid-phase oxidations, a range of (more selective) oxidants can be used. The reaction conditions are generally relatively mild. Traditionally, selective liquid-phase oxidations for high-value products is done using stochiometric quantities of the oxidants (e.g. CrO_3, $KMnO_4$ or $K_2Cr_2O_7$) that are simply added to the reaction mixture. Since these processes involve the production of large amounts of byproducts with associated undesirable economic and environmental effects, the development of new, catalytic processes is preferred.

To achieve the required highly selective catalytic transfer of oxygen from the oxidant to the substrate, a transition metal and an oxidant other than O_2 is needed. To date, homogeneous catalysis has dominated liquid-phase catalytic oxidations. The catalysts used are soluble transition metal complexes, with which high turnover numbers can be achieved. However, the disadvantage of a homogeneous process is obvious, since catalyst recovery is often not feasible or not economically viable. The catalyst ultimately remains associated with the product or is lost in waste or by-products, which is not only a cost factor but also of environmental concern, since transition metal complexes are expensive and often toxic. Heterogeneous catalysis offers the advantage of regenerability of the catalyst, which also saves costs on purification and separation of the desired products.

1.3 Environmental impact of fine chemicals production

Fine chemicals are produced on a scale orders of magnitude lower than bulk and intermediate chemicals (see Table 1.2). Due to the often complicated and multi-step synthesis procedures, a batch process is generally used. As Table 1.2 shows, fine chemicals production involves the generation of large amounts of by-products per kg product. Although the total amount of by-products produced is smaller in fine chemicals than in bulk due to smaller annual tonnage, the nature of the by-product has to be taken into account. By-products from fine chemicals production are often toxic and environmentally harmful, which has been described by a high 'environmental quotient' (EQ) by Sheldon and Dakka (1994).

The profit margin in fine chemicals production is high and thus, until recently, little attention has been paid to minimisation of environmentally harmful by-products. However, due to increasingly strict regulations on the chemical industry in Europe and the United States, there is a demand for cleaner processes which is finally impacting on the fine chemicals industry. The trend towards more

environmentally friendly processes is also reflected in research. In the literature, many articles on more environmentally friendly chemistry have been published during the past few years. The recent appearance of the journal "Green Chemistry", which is devoted to more environmentally friendly processes/synthesis, reflects the importance of this area of research.

Table 1.2: Scale and by-product generation of industrial chemicals production [Sheldon (1997)]

Industry segment	U. S. annual tonnage (1996)	kg by-product / kg product	EQ
bulk chemicals	10^4-10^6	< 1	low
fine chemicals	10^2-10^4	5 - 50	high
pharmaceuticals	10 - 10^3	25 - >100	very high

1.4 Scope of this thesis

In the preceding paragraphs, the importance of cleaner, heterogeneously catalyzed hydrocarbon oxidations for fine chemical production has been highlighted.

In the past decade, numerous publications have appeared in the area of heterogeneous catalytic hydrocarbon oxidation with both O_2 and peroxides as the oxidant. The immobilisation of transition metals, traditionally used as soluble complexes in homogeneous catalysis, increases the catalyst stability and enables the recovery and regeneration of the catalyst. Thus, this approach becomes more and more interesting for industrial applications and has attracted great attention from research groups all over the world.

The discovery of TS-1, the titanium-substituted analogue of ZSM-5, by Enichem researchers in Italy opened up a whole new area of research. Due to its remarkable catalytic properties, TS-1 was soon followed by the invention of a number of new redox molecular sieves with potential applications for many useful oxidation reactions.

However, despite the discovery of more and more promising new materials, various aspects of the catalyzed oxidation reactions are not fully understood. Even for the phenol hydroxylation over TS-1, a reaction carried out in an industrial production plant since 1986 [Clerici (1991), Clerici (1993)] (and to date the only industrial application of redox zeolites), many details such as the reaction mechanism, are not reported in literature.

In this work, aromatic hydroxylations over titanium-substituted molecular sieves were thoroughly studied to gain a deeper understanding of the mechanism(s) governing activity and selectivity.

Attention was paid to engineering aspects such as selective adsorption and transport phenomena. Intracrystalline diffusivities and kinetic and adsorption constants were determined to evaluate catalyst effectiveness factors for selected reactions. The presence of shape selectivity effects in the

zeolite channels and the influence of the external surface of the zeolite was systematically investigated. For this purpose, the catalytic properties of titanium silicates with different pore sizes (TS-1, Al-free Ti-beta and Ti-HMS) were compared. The pronounced solvent effects observed in aromatic hydroxylations over titanium-substituted zeolites were examined and a reaction mechanism consistent with the measured data was proposed.

For a recently discovered material, aluminium-free zeolite titanium beta, the catalytic properties for the hydroxylation of mono-substituted aromatics, not yet reported in literature, were explored. As a potential industrial application for this novel material, the hydroxylation of naphthalenes with Al-free Ti-beta was investigated.

Chapter 2

Literature review

2.1 Heterogeneous catalysis for liquid-phase fine chemicals synthesis

To selectively transfer the oxygen to the substrate, the presence of a transition metal is required. The transition metal containing catalyst first reacts with the oxidant to form the active species which then oxidises the substrate; re-oxidation of the catalyst occurs and the catalytic cycle is closed. A schematic drawing of the catalytic cycle is shown in Figure 2.1. For the process to be heteroge-

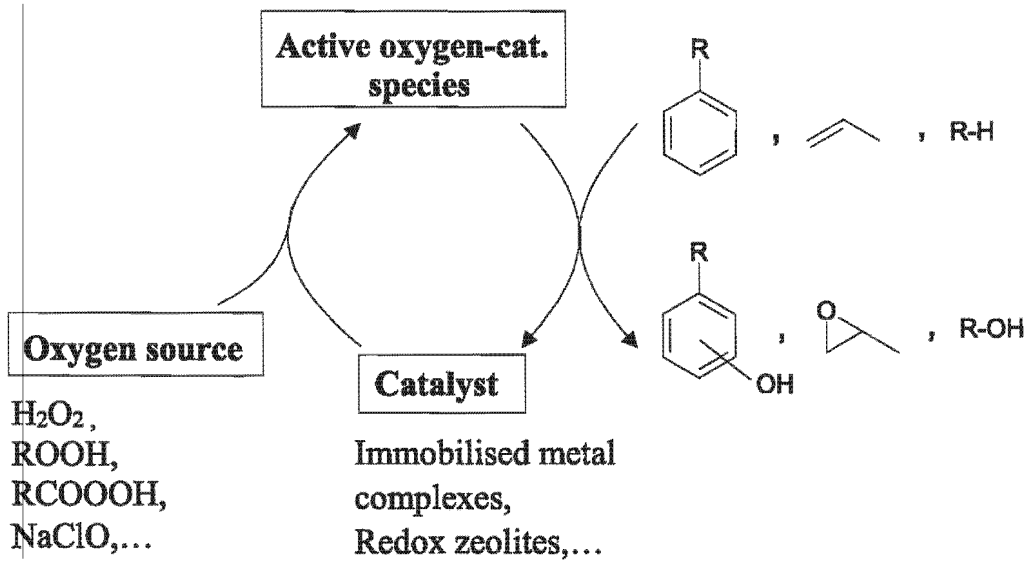

Figure 2.1: Catalytic cycle for partial oxidation reactions [Moro-oka (1998)]

neously catalyzed, the transition metal has to be immobilised. Principally, this immobilisation can be achieved in several ways:

- Occlusion of transition metal complexes in a polymer, such as polydimethylsiloxane (PDMS) via a sol-gel process; immobilisation is achieved via physical entrapment in the host network [Langhendries (1999), Neys et al. (1997)];
- Association of the transition metal with dendrimers which are large enough to be separated from the reaction mixture [Kimura et al. (1999)];
- Dissolution of transition metal complexes in a (non-volatile) solvent immiscible with the reagents [Wan and Davis (1994)];
- Ion-exchange of soluble transition-metal complexes on resins [Sheldon (1990)];
- 'Ship-in-a-bottle' catalysts, where transition metal complexes are synthesised from transition metal ions and ligands inside zeolite cavities [Parton et al. (1991), Schulz-Ekloff and Ernst (1999)];
- Supported transition metal oxides [Clerici (1993), Aiken III and Finke (1999)];
- Immobilisation of transition metals (or transition metal complexes) on zeolitic supports (generally referred to as redox molecular sieves).

A major recurrent problem with all varieties of immobilisations is leaching of the transition metal. Ion-exchange based methods in particular are not very suitable since the transition metal is easily leached into solution unless the reaction medium is completely non-polar. The same applies for transition metal oxides on supports; the transition metal rapidly dissolves in the reaction medium especially in the presence of polar solvents. A similar problem is encountered if the transition metal (as ion or complex) is dissolved in a second solvent which is immiscible with the reactants since there will always be a certain degree of exchange between the two phases.

Organic or hybrid polymers seem to be a quite stable environment for the occlusion of transition metal complexes. However, if polar solvents are present, the polymer matrix can swell and the transition metal is leached more easily. Another disadvantage can be mass transfer resistances within the polymer [Langhendries (1999)].

In the past years, significant progress has been made in the synthesis of dendrimers, and macromolecular dendrimers with associated transition metals of a micrometer scale have been synthesised. Although these dendrimers are potentially large enough to be filtered from the reaction medium, they are very expensive and oxidative degeneration of the dendrimer structure is a problem.

'Ship-in-a-bottle' catalysts have also received significant attention in recent years. Transition metal complexes such as ironphthalocyanines, synthesised in zeolite cavities such as zeolite Y supercages, offer a truly heterogeneous oxidation catalyst. The metal complex is too bulky to diffuse through the zeolite channels and is thus physically entrapped in the zeolite matrix. Although heterogeneity of these catalysts has been proven, the major problem is degradation of the complex ligands and thus instability of the transition metal complex [Sheldon et al. (1998b)].

A general problem with all immobilisation methods using complexes of transition metals is the regeneration of the deactivated catalyst. Deactivation during oxidation reactions occurs through formation of undesired high-molecular weight side products (polymers or tars) at or near the active sites. Due to the limited thermal stability of the complexes, simply heating the catalyst in air and combustion of the tars is not possible, and hence regeneration to restore the initial activity can be difficult.

A way to ensure both easy thermal regeneration of the catalyst and convincing stability towards leaching of the transition metal is to chemically bind the transition metal to an inorganic matrix. The inorganic matrix can be an amorphous oxide or have a regular structure like zeolites. The latter type of catalysts is generally referred to as redox molecular sieves.

2.1.1 The choice of the catalyst - redox molecular sieves

Zeolites not only offer the advantage of great thermal stability and thus facile regenerability, they also have a well-defined pore system that is able to discriminate between organic molecules with a precision of less than 1 Å, which is why they are also called molecular sieves. Due to the uniform size distribution of their micropores in which most of the reactive centres are located, zeolites can offer more selective reaction pathways. Shape selectivity effects can be divided into three categories:

- reactant shape selectivity: the zeolite excludes reactants that are too bulky from entering its pore structure
- product shape selectivity: the reaction equilibrium inside the zeolite pores is shifted towards the product(s) with the smallest kinetic diameter, which can then diffuse out of the channels
- transition-state shape selectivity: transition-states requiring more space than available in the channels are prevented

In oxidation chemistry, reactions are generally irreversible and product shape selectivity effects are therefore not observed. In fine chemicals synthesis, relatively pure feedstocks are usually applied, so that reactant shape selectivity is also not a major factor. Transition-state shape selectivity thus offers the greatest potential for zeolite-based oxidation catalysts; undesired consecutive reactions can be

prevented and the reaction can be driven towards the path with the least space-demanding transition state.

Generally, zeolites are defined as crystalline microporous solids, whose framework consists mainly of interconnecting MO_4 tetrahedra. $(SiO_2)_n$ is the main building unit of silica-based zeolitic materials, but a proportion of the silicon(IV) can be replaced by other metal ions. The best known examples are the aluminosilicates, where the Si/Al ratio can in principle range from 1 to infinity. Related to such materials are the microporous and mesoporous aluminophosphates (AlPO's) which consist of alternating AlO_4- and PO_4-tetrahedra. For both classes of zeolitic materials, isomorphous substitution of transition ('redox') metals into the framework is possible; in this case, the term 'redox molecular sieve' was suggested [Sheldon et al. (1998b)].

Figure 2.2 shows the building units, chemical composition and framework characteristics of redox molecular sieves. Apart from the chemical composition, the framework topology of (redox)

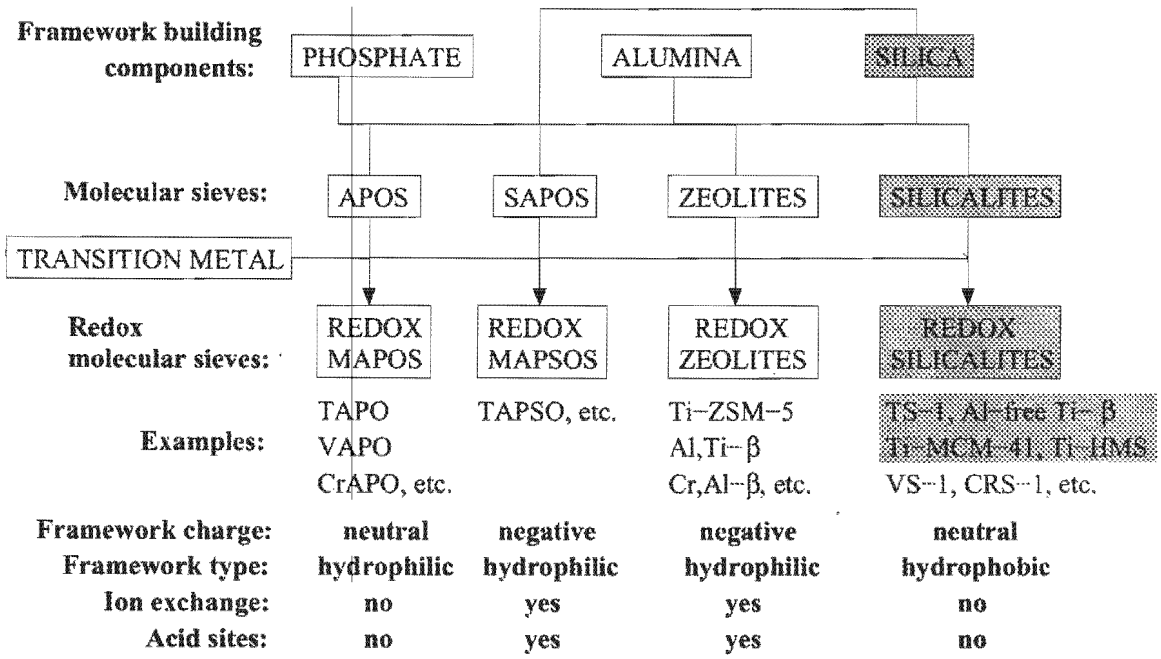

Figure 2.2: Composition of redox molecular sieves [Sheldon et al. (1998b)]

zeolites is an important characteristic. Zeolite topologies are categorised on the basis of their pore diameters into small pore (< 0.4 nm), medium pore (0.4-0.6 nm), large pore (0.6-0.8 nm), extralarge pore (0.8-1.4 nm) and mesoporous (1.5-10 nm). The pore system can be one-, two- and three-dimensional, which can significantly influence the accessibility of the active sites as multidimensional pore systems offer alternative diffusion paths. Generally, zeolitic materials have a hydrophilic framework. Their framework charge (generated by the MO_4 tetrahedra with non-tetravalent metal ions) is compensated by the presence of countercations. The only exceptions are silicalites, highly

siliceous materials where either only a small fraction of the silicon(IV) is substituted or the isomorphously substituted ion is also tetravalent. A comprehensive review on titanium-substituted zeolites was given by Notari (1996).

The attention in this work will be focused on redox silicalites as highlighted in Figure 2.2, since these materials possess the most interesting properties such as a hydrophobic framework. The advantage of a hydrophobic framework is the preferential adsorption of non-polar organic compounds and the exclusion of polar compounds such as water or polar solvents, which renders these materials particularly stable towards leaching. The synthesis of transition-metal incorporated silicates (and other redox zeolites) can be done in various ways which are described below.

2.1.1.1 Post-synthesis modifications

A number of post-synthesis modifications, where the transition metal is introduced into the lattice after zeolite synthesis, have been reported. Post-synthesis modification methods have the advantage that the redox molecular sieve can be prepared from commercially available materials. This can be achieved in different ways:

'Ship-in-a-bottle' catalysts These catalysts have transition metal complexes entrapped in zeolite cavities. A number of complexes with various ligands (phthalocyanines, polypyridines, aromatic Schiff bases, etc.) have been synthesised in zeolites (which must have supercages like zeolite X or Y) and although some exhibit remarkably high catalytic activity, their stability is sometimes a matter of debate. The problem of deactivation and regeneration usually limits the catalyst lifetime.

Ion exchange As Figure 2.2 shows, a number of zeolites have ion-exchange properties. The counterbalancing cations can be exchanged with transition metal ions, thereby achieving redox functionalisation of molecular sieves. Ion exchange in aqueous solutions as well as solid-state ion exchange have been reported. However, the transition metal obviously remains highly mobile and the leaching stability in polar solvents will be low.

Grafting and tethering The principle of these two methods is to create a chemical bond between the zeolite lattice and the transition metal.

In the case of grafting, reactive transition metal compounds (such as $MeCl_x$ or $Me(OR)_x$) are chemically bonded to defect (SiOH) sites in the zeolite framework. The process can be carried out in the gas phase using chemical vapour deposition (CVD) or in the liquid-phase [Rigutto et al. (1994), Reddy and Sayari (1995), Di Renzo et al. (2000)]. The required defect sites are always present in zeolites, but can also be generated, e.g by dealumination of aluminosilicates or steaming (generation

of 'silanol-nests'). After reaction with the transition metal compound, the zeolite is usually calcined and thus functionalised with a redox metal oxide chemically bonded to its lattice.

Tethering follows the same principle, except that the silanol groups are first reacted with a 'spacer' (a reactive bifunctional organic compound), to which the transition metal is subsequently bound. The main application of this method is the immobilisation of transition metal complexes on zeolitic materials via a chemical bond (e.g. the covalent attachment of Mn-triazacyclononanes to mesoporous silicates [Sheldon et al. (1998b)]).

The advantage of grafting and tethering methods is that a great variety of transition metals or transition metal complexes can be attached via a covalent bond to zeolite frameworks; the choice of transition metals suitable for incorporation via direct hydrothermal synthesis is more limited. However, grafting and tethering is rather based on anchoring of the transition metal species to framework defect sites; a disadvantage of these methods could be the deposition of TiO_2 or an imperfect incorporation of Ti. The isomorphous substitution via hydrothermal synthesis ideally offers a perfect incorporation of the transition metal as MeO_4 tetrahedra and should provide a more stable environment.

2.1.1.2 Framework substitution via hydrothermal synthesis

Molecular sieves are generally crystallised from aqueous gels containing a source of the framework building elements (Al, Si, P, see Figure 2.2), a mineraliser (OH^-, F^-) that regulates dissolution and condensation during the crystallisation, and a structure-directing template (organic amines or ammonium salts). These gels are then crystallised in autoclaves at temperatures between 80 and 200°C under autogeneous pressure for times varying from several hours to weeks. The synthesised material is subsequently calcined at ca. 500°C to destructively remove the template. Redox molecular sieves are similarly prepared by addition of redox metal salts or alkoxides during the crystallisation process, producing framework substituted redox metal sites.

However, for true framework substitution the transition metal should be able to adopt a tetrahedral coordination by oxygen atoms and it should fit in the lattice. The latter condition is only fulfilled if the ratio of the radii of the metal cation and the oxygen anion is between 0.225 and 0.414. Thus, the ion radius and coordination limits the number of transition metals that can be isomorphously substituted into zeolite frameworks during hydrothermal synthesis. Principally, these conditions are met by group IIa - VIIa transition metals and many of these metals (e.g. titanium, vanadium, chromium, germanium, tin and zirconium) have been incorporated into zeolite frameworks, mainly in the MFI structure. An important prerequisite for isomorphous framework substitution is the complete isolation of the transition metal sites. Neighbouring transition metal centres lead to di- or oligomerisation and a separate $(MO_2)_n$-phase is formed. Such μ-oxo-oligomers are catalytically inactive or, in the

worst case, may catalyze the decomposition of the oxidant.

In the past years, spectroscopic methods have been refined to identify these phase impurities in redox zeolites and in some cases it has been proven that the transition metal was not isomorphously substituted in the zeolite framework. To date convincing proof of true incorporation with sufficient characterisation data has only been given for titanium and vanadium substituted zeolites.

2.1.2 The choice of the oxidant

For the production of fine chemicals or pharmaceuticals, the use of O_2/air is often not possible as pointed out earlier. Thus, an alternative, more selective oxygen source has to be used. Table 2.1 shows potential oxidants for transition metal catalyzed, liquid-phase hydrocarbon oxidations. The

Table 2.1: Oxygen donors for fine chemicals oxidation reactions [Sheldon and Dakka (1994)]

Oxygen donor	Active oxygen (wt-%)	By-product
H_2O_2	47	H_2O
N_2O	36.4	N_2
O_3	33.3	O_2
t-BuOOH	17.8	t-BuOH
CH_3CO_3H	21	CH_3CO_2H
$NaClO_2$	35.6	NaCl
NaClO	21.6	NaCl
NaBrO	13.4	NaBr
$KHSO_5$	10.5	$KHSO_4$
$NaIO_4$	10	$NaIO_3$
HNO_3	25.4	HNO_2
PhIO	7.3	PhI

comparison of various oxidants shown in Table 2.1 clearly demonstrates why hydrogen peroxide (in aqueous solution) is the preferred oxidant. The major advantages of H_2O_2 are:

- the highest active oxygen content with respect to the weight of the oxidant
- the only by-product is water, thus making it very environmentally friendly
- aqueous H_2O_2 solutions are stable, easy and safe to handle
- it is readily available and the world market price is expected to decline

In particular, environmental considerations have focused the attention on aqueous H_2O_2 solutions as the oxidant of choice in liquid-phase oxidations. This underlines a world-wide trend towards 'greener' chemistry. However, the current method for industrial production of hydrogen peroxide

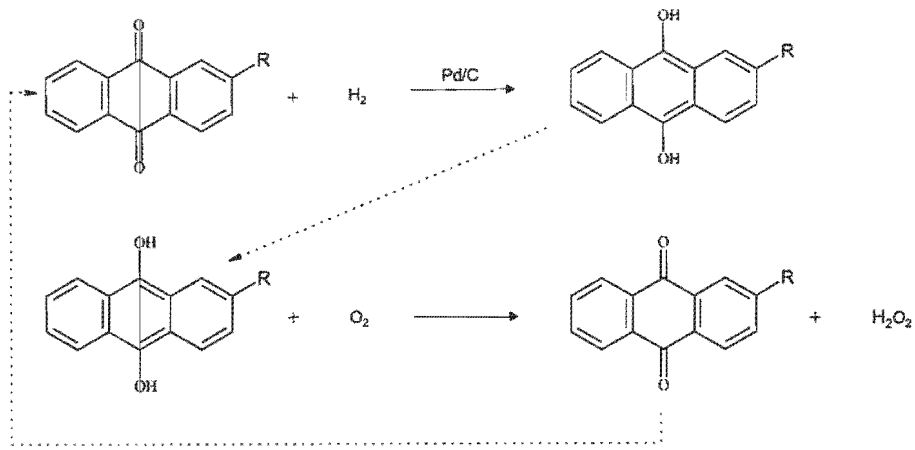

Figure 2.3: H_2O_2 production via anthraquinone route [Hess (1995)]

must be taken into consideration. The major route towards H_2O_2 production is via the anthraquinone process [Hess (1995)], shown in Figure 2.3. Substituted anthraquinones are first hydrogenated to their respective dihydroanthraquinones. Subsequently, in a separate reactor, re-oxidation with oxygen to the anthraquinones takes place, generating H_2O_2. Although the anthraquinone is continuously recycled, a part of it is lost in the process through oxidative degradation. These degradation products have to be removed in purification steps, rendering it a relatively energy-intensive and overall not-so-green process.

Recently, however, new processes have been developed to form H_2O_2 directly from O_2 and H_2 using noble metal catalysts. This is a promising route to environmentally friendly H_2O_2 production, although the engineering of this process is still a major challenge due to the large explosion limits of H_2/O_2 mixtures. A recent example was presented by Hancu and Beckmann (2001), where the direct generation of hydrogen peroxide from H_2/O_2 (outside the explosion limits) with CO_2 as the solvent is described. Additionally, the cost of transport has to be taken into account. Hydrogen peroxide is generally available as a 30% - 50% solution in water, so that major amounts of water have to be transported with the oxidant. To make oxidation processes using H_2O_2 economically viable, an on-site production in a separate plant is often necessary.

It must also be noted that the by-products from organic oxidants, such as tert-butylhydroperoxide (TBHP) and amine oxides, are recycled via reaction with hydrogen peroxide. Thus, the by-product of the overall process is also water, but one extra chemical step (with potential losses) is required to regenerate the organic oxidant.

This work is focused on the use of aqueous solutions of hydrogen peroxide as the oxidant; to clarify details about the reaction mechanism, TBHP is occasionally used for comparison. The nature of the active catalyst-oxygen species has to be taken into consideration when the reaction mechanism

of a catalyzed liquid-phase oxidation reaction is studied. The transition metal site can principally form three types of active species which then initiate different reaction pathways. The active species and reaction pathways are shown in Figure 2.4 (where M represents the transition metal and S the substrate). The generation of radicals as shown in scheme 1 of Figure 2.4 is generally undesired

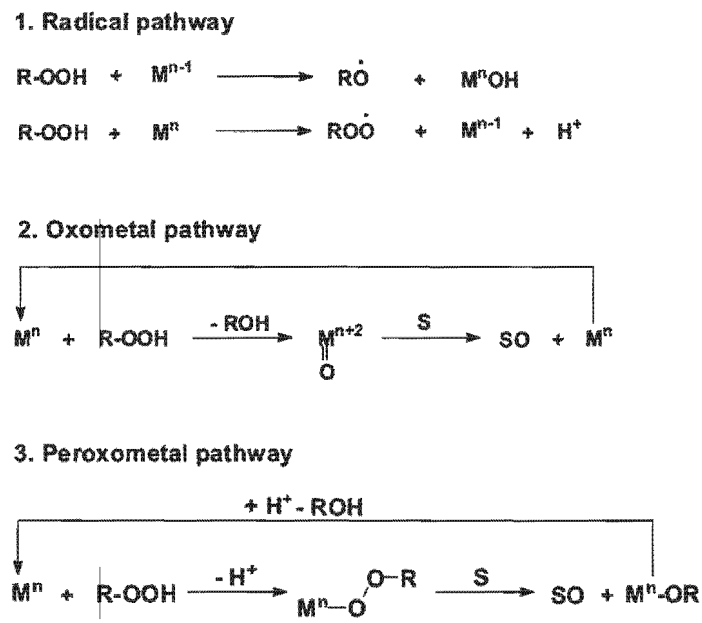

Figure 2.4: Mechanism of catalytic oxygen transfer by transition metals in the liquid phase [Sheldon (1997)]

since free-radical chemistry does not usually show the necessary selective oxygen transfer and side reactions become important. Thus, the active oxidant in the catalytic oxygen transfer process should be an oxometal or a peroxometal species. Early transition metals (Ti, Zr, Mo, W) react via peroxometal intermediates and late and first row transition metals (Cr, Mn, Fe) form oxometal species. Some metals, e.g. vanadium, react via both pathways depending on the reaction conditions. One major difference between the two pathways is that in the peroxometal pathway there is no change in oxidation state of the transition metal during reaction; the transition metal acts purely as a Lewis acid (for titanium see [Bittar and Kaliaguine (1992)]) and increases the oxidising power of the peroxo group. In contrast, the metal undergoes reduction and subsequent re-oxidation by the oxidant in the oxometal pathway.

2.1.3 The problem of leaching - is it really heterogeneous catalysis?

Leaching of the immobilised transition metal from the catalyst is one of the biggest problems of heterogeneous oxidation catalysis in the liquid phase. With the discovery of many new redox-

functionalised materials in the past years, characterisation methods have improved and the nature and environment of the redox sites in zeolitic materials is better understood. However, the ultimate test for their potential is a catalytic experiment with an adequate proof for leaching stability. Although stability is one of the most important conditions for industrial utility, this aspect has often been neglected in literature reports.

If leaching of the metal occurs, it may or may not be an active homogeneous catalyst in the solution. Filtration of the reaction mixture at reaction temperature was suggested by Sheldon *et al.* [Sheldon (1997), Sheldon et al. (1998a), Sheldon et al. (1998b)]: if the reaction continues in the filtrate, leaching has taken place and the transition metal is active as a homogeneous catalyst. An example of this type of leaching was found in reactions with chromium-substituted molecular sieves (CrAPO-5 and CrS-1) by Sheldon et al. (1998b), where leached chromium catalyzed the reactions homogeneously.

A second test for leaching involves testing the filtered, regenerated catalyst in further reaction cycles. If leaching has occurred and the transition metal is not an active homogeneous catalyst, the activity of the catalyst in consecutive reaction cycles should decline. Both tests accompanied by a physico-chemical characterisation of fresh and recycled catalyst are necessary to prove leaching stability. However, slow but practically insignificant leaching that is difficult to detect with most batch methods cannot be excluded and longevity tests will have also have to be performed.

2.2 Titanium-containing molecular sieves

The only cases where extensive testing and characterisation have proved that a redox zeolite is stable towards leaching is TS-1 and certain other titanium-substituted molecular sieves. Since titanium(IV) is a poor homogeneous catalyst and recycling experiments showed that the initial catalyst activity could be restored even after many reaction cycles, it can be assumed that liquid-phase oxidation reactions catalyzed by titanium-substituted zeolites are truly heterogeneous in nature.

On the basis of the numerous reports about the leaching stability of the titanium redox zeolites used in this work, no extensive leaching tests have been conducted. However, significant leaching was reported in the case of mesoporous titanium-substituted silicates when 30% H_2O_2 was used as the oxidant [Chen et al. (1997)]. Thus, results obtained from catalytic runs with mesoporous titanosilicates using aqueous hydrogen peroxide have to be interpreted with care.

2.2.1 Titanium silicalite-1 (TS-1)

Based on the well-known activity of titanium-based catalysts for the oxidation of organic compounds, the first process using a heterogeneous titanium catalyst was patented in 1971 for Shell Oil

[Wulff (1971)]. The developed catalyst was a TiO_2-SiO_2 mixed oxide and the catalyst is still in industrial use for the epoxidation of propylene with organic hydroperoxides. Amorphous titania-silica mixed oxides generally show good activities and selectivities for the epoxidation of alkenes as long as organic hydroperoxides are used. In the presence of water, however, rapid deactivation takes place and thus hydrogen peroxide cannot be used with this class of catalysts. Furthermore, these catalysts did not show good results for other selective organic oxidation reactions.

In 1983, researchers at Enichem [Taramasso and Perego (1983)] in Italy succeeded in synthesising TS-1, a catalyst with the MFI structure containing only silica and titanium. The remarkable catalytic potential of this new material soon became apparent and numerous publications dealt with the exploration of the catalytic properties of TS-1. However, initially, the good results obtained by the ENI group could not be reproduced by other research groups. It was later confirmed that the synthesis procedure is crucial; phase-impurities (mainly TiO_2 as anatase) due to poor titanium incorporation can be generated if certain conditions are not fulfilled.

Synthesis of TS-1 TS-1 and other titanium-substituted zeolites seem to be particularly sensitive to the presence of $(TiO_2)_n$-oligomers as they clearly show inferior catalytic properties if the latter are present. TiO_2 impurities are formed through hydrolysis and oligomerisation of the titanium source during its addition to the synthesis gel and in many publications, several reliable synthesis procedures have now been identified [Martens et al. (1993), Notari (1991), Thangaraj et al. (1992), Tuel (1998), Tuel and Ben Taarit (1994a)].

In a number of publications is was found that better incorporation can be achieved at low titanium contents; an upper limit for isomorphous titanium substitution of around 2.3 titanium atoms per unit cell has repeatedly been reported.

Another key factor is the purity of the reagents. TS-1 can be obtained from a variety of silica- and titanium-sources with good results [Tuel and Ben Taarit (1994a)], but the structure-directing template, tetrapropyl ammonium hydroxide (TPAOH), has to be of a very high purity. Exclusion of alkali ions ($Na^+$and K^+) is crucial as their presence in the template results in TS-1 samples with poor catalytic properties, even though spectroscopic characterisation methods indicate a highly pure material. It has been shown that alkali cations poison the titanium sites since the catalytic performance of TS-1 decreases as a function of the content of alkali metal cations in the synthesis gel [van der Pol and van Hooff (1992), Thangaraj et al. (1992)].

The crystallite dimensions also influence the catalytic performance. Crystallites larger than 0.2 - 0.3 μm show lower reaction rates and selectivities due to mass transfer limitations [van der Pol et al. (1992)]; this aspect is further investigated in this work.

Last but not least, the agglomeration of the crystallites is a very important point for industrial use as agglomerates of at least 20 - 30 μm are required for industrial use. After initial problems

in obtaining agglomerates of sufficient mechanical stability, a solution has been found with the formation of thin silica layers coating the crystallites [Clerici (1991)]. A template-silicalite solution was used to disperse the TS-1 crystallites and subsequent spray-drying and calcination resulted in mechanically stable agglomerates.

Structure of TS-1 TS-1 has a two-dimensional pore structure consisting of 0.56×0.53 nm straight ([010] direction) and 0.55×0.51 nm sinusoidal channels ([100] direction). Figure 2.5 shows the structure and pore opening of TS-1 in the [010] direction of the straight channels.

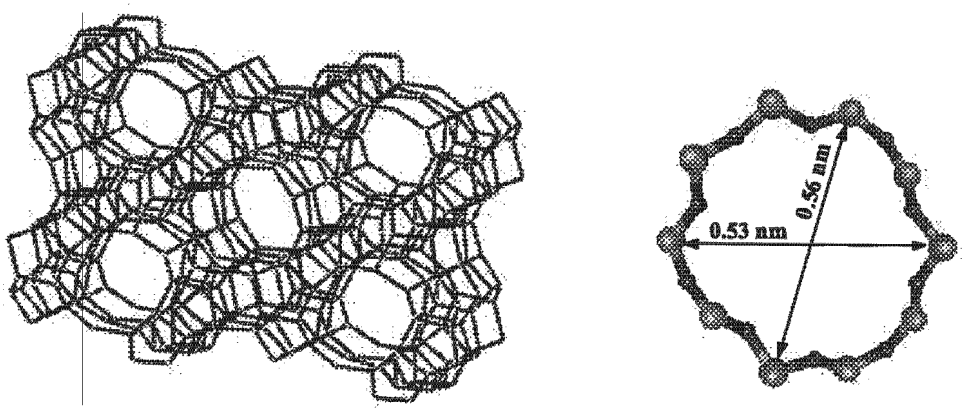

Figure 2.5: Pore structure and -opening of TS-1 in [010] direction

Characterisation of TS-1 After it was established that the quality of a TS-1 batch can vary significantly due to the many pitfalls in the synthesis procedures, much research effort went into the characterisation of TS-1. To date, dozens of publications have dealt with the evaluation of various physico-chemical and spectroscopic methods to characterise TS-1. All the techniques described in this paragraph also apply for other titanium-containing molecular sieves.

The structure and the degree of crystallinity of molecular sieves can conveniently be determined by X-ray diffraction. However, phase-impurities in the form of TiO_2-clusters are usually of nano-scale size and thus X-ray amorphous. X-ray diffraction has been used as an alternative method to determine the (incorporated) titanium content of the zeolite by determining the unit cell volume, although the accuracy is limited [Millini et al. (1992)]. A linear increase of the unit cell volume with titanium content was found (due to the larger diameter of incorporated Ti^{4+}). Determination

of the microporous (and mesoporous) volume using BET measurements give further information about the crystallinity and morphology of the catalyst. SEM and/or TEM pictures of the catalyst are widely used to gain information about the crystal size distribution and agglomeration of the catalyst crystallites and results can be compared to those of various other techniques to determine the crystal size. EDX or XPS analysis is used to confirm the homogeneous dispersion of Ti throughout the sample; for TS-1, a very homogeneous titanium dispersion has consistently been reported in the literature [Duprey et al. (1997)].

However, the above mentioned methods yield no information about the state of the titanium in the silicalite framework, which proved to be an important point for the catalytic properties of these materials. It was discovered that titanium-containing zeolites exhibit a characteristic band at 960 cm^{-1} in IR spectroscopy, which was first assigned to Ti=O or Ti-O vibrations. After the same band was later found in all-silica zeolites, it was reassigned to a stretching vibration of polarised $Si\text{-}O^{-}$ groups, caused either by defects or by the presence of neighbouring Ti^{4+} [Camblor et al. (1993)]. Winkhofer et al. (1994) found the same 960 cm^{-1} IR band in the characterisation of titanasilanesquioxanes, compounds that only contained Ti-O-Si bonds and assigned the band to a Ti-O-Si stretching. It is still debatable whether the presence of the band is a real proof for titanium incorporation; its absence however confirms that titanium has not been incorporated into the framework. Raman spectroscopy proved to be a more sensitive tool to detect extraframework titanium and a characteristic band at 144 cm^{-1} was assigned to the presence of anatase [Deo et al. (1993)]. However, the most powerful tool for characterising titanium incorporation is diffuse reflectance UV-VIS spectroscopy. This technique proved to be very sensitive to the presence of even minor amounts of anatase. Major amounts of TiO_2 in the form of anatase show strong absorption at wavelengths above 370 nm, minor amounts of Ti oxides may yield absorption shoulders down to 250-270 nm; the absence of absorption these regions thus confirms the phase-purity of the sample. Furthermore, the coordination of the incorporated titanium can be determined and a number of studies confirmed that tetrahedrally coordinated titanium is present in various titanium-containing molecular sieves. An absorption band at $\approx$ 210 nm indicates the presence tetracoordinated titanium, whereas an absorption at around 240 nm is responsible for penta- or hexacoordinated titanium. When major amounts of non-tetrahedrally coordinated titanium species were present in freshly calcined, dehydrated materials, inferior catalytic performances were observed. It was also discovered that the titanium changes coordination upon adsorption of certain polar compounds such as water and alcohols and upon reaction with hydrogen peroxide. The change to higher coordination was explained by a hydrolysis of one or two Ti-O-Si bonds, which is, in the case of TS-1, reversible since the original tetrahedral coordination can be restored through calcination. X-ray absorption spectroscopy (XANES-EXAFS) has been used more recently to identify the geometry and coordination of Ti in titanium silicalites [Bordiga et al. (1994b)], and an increase of titanium coordination to five or six upon adsorption of ammonia and water has also been reported

[Bolis et al. (1999)].

The exact nature of the titanium active site is still a matter of debate and will be discussed later as this is an important factor in the development of a reaction mechanism.

Catalytic properties of TS-1 As demonstrated above, care must be taken during synthesis, and the synthesised sample has to be characterised extensively especially for titanium incorporation. However, the ultimate proof for the quality of a synthesised catalyst is a catalytic experiment. The hydroxylation of phenol, extensively studied in this work, seems to be particularly sensitive to impurities in TS-1 and was suggested as a reliable test reaction for the quality of TS-1 samples by Kraushaar-Czarnetzki and van Hooff (1989). The catalytic properties of TS-1 and the other titanium-substituted molecular sieves are discussed in detail in section 2.3.

2.2.2 Zeolite titanium beta

Although TS-1 was certainly a milestone in heterogeneous oxidation catalysis, its medium-size pores restrict its use to relatively small molecules such as linear or simple branched hydrocarbon chains, or aromatics with small substituents. Larger molecules either cannot enter or their mass transfer through the pore system becomes too slow. Therefore, a larger-pore titanium containing zeolite is of great interest to open the area of heterogeneous oxidation catalysis with aqueous H_2O_2 to more bulky organic molecules. Another advantage is the possibility of using tert-butyl hydroperoxide as an alternative oxidant; the medium-pore TS-1 is completely inactive with the latter.

Structure of Ti-beta An obvious candidate for a large-pore titanium-substituted molecular sieve is zeolite beta, having a three-dimensional framework and pore openings of 0.76×0.64 nm ([100] direction) and 0.55×0.55 nm ([010] direction). Figure 2.6 shows the structure and pore opening of zeolite beta in the [100] direction (straight channels).

Synthesis of aluminium-free zeolite Titanium beta To ensure complete titanium incorporation, similar prerequisites apply for the synthesis of zeolite titanium beta as for TS-1. However, despite repeated attempts in many research groups, Ti-beta could only be crystallised in the presence of aluminium [Corma et al. (1996b), Blasco et al. (1993)]. The simultaneous presence of titanium and aluminium not only lowers the amount of titanium that can be incorporated in the zeolite framework, but also creates a bifunctional catalyst. The Brønsted acidity generated by framework aluminium sites can cause undesirable side reactions such as the ring-opening of epoxides to glycols after their formation at titanium sites [Trong On et al. (1996), Kapoor et al. (1997)]. Additionally, it renders the framework more hydrophilic which results in preferential adsorption of polar solvents or water and

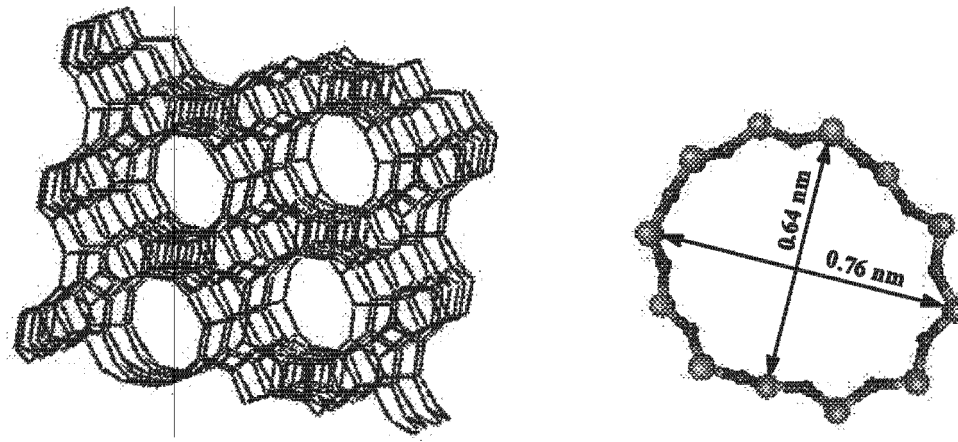

Figure 2.6: Schematic diagram of the BEA structure and pore opening in [100] direction

increases peroxide decomposition. Recently, the synthesis of aluminium-free Ti-beta was finally achieved [Blasco et al. (1998), van der Waal et al. (1998a), Dartt and Davis (1996)], and it was confirmed that a highly hydrophobic, stable material could be obtained [Blasco et al. (1998)].

Catalytic properties of aluminium-free Ti-beta The excellent catalytic properties for this novel material have been demonstrated for the epoxidation of olefins; bulky olefins could be epoxidised with both tert-butyl hydroperoxide and aqueous H_2O_2 as the oxidant [Blasco et al. (1998), van der Waal et al. (1998b), van der Waal and van Bekkum (1997)]. In the case of epoxidation reactions, acid-catalyzed ring-opening of epoxides was minimised and higher epoxide yields were achieved. However, no literature reports on the catalytic activity of Al-free Ti-beta in aromatic hydroxylation reactions are available. The application of Al-free Ti-beta for aromatic hydroxylations was evaluated in this work and the selectivities obtained were compared to TS-1. Both materials were synthesised in the course of this work and have similar chemical compositions and multi-dimensional frameworks, but with different pore dimensions. Thus, the product distributions in aromatic hydroxylations using these materials can be used to identify shape-selective effects generated by the zeolite. The role of the solvent was also investigated in this context.

2.2.3 Mesoporous titanium-containing molecular sieves

The successful synthesis of Ti-beta opened up heterogeneous oxidations with titanium-containing zeolites to more bulky molecules such as terpenes [van der Waal et al. (1998b)]. However, a material with ultralarge pores was soon sought to oxidise molecules that are too large even for Ti-beta. The

so-called M41S family is a mesoporous class of catalysts with has a hexagonally ordered structure and pore openings ranging from 2 to 10 nm. Figure 2.7 shows the mesopores of a M41S-type catalyst.

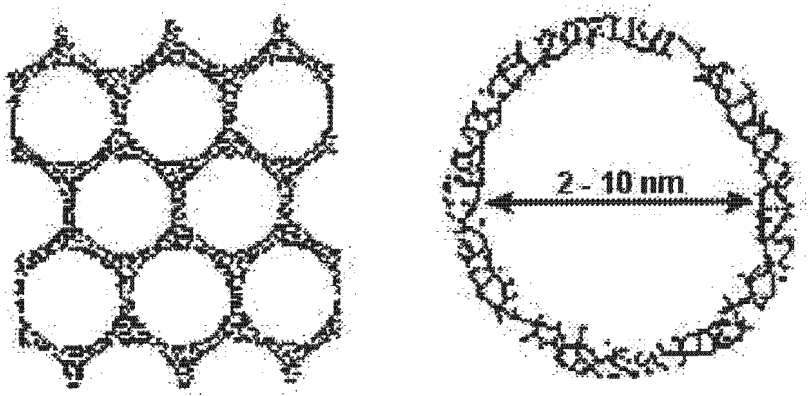

Figure 2.7: Mesopores of Ti-HMS and Ti-MCM-41

Synthesis of mesoporous titanium-containing molecular sieves The synthesis of Ti-M41S catalysts has been reported using various templates. Materials with very high surface areas of up to 1200 m^2/g were obtained and good titanium incorporation has been proven. However, due to the presence of large amounts of defect sites, the framework of Ti-M41S catalysts is very hydrophilic and leaching of titanium as well as framework instability under reaction conditions has been reported by Rhee and Lee (1996) and Chen et al. (1997). The two major representatives of this catalyst class are Ti-HMS and Ti-MCM-41, the latter having a slightly more ordered structure. Ti-HMS can be synthesised at room temperature with C_{12} - C_{18} amines as templates, whereas long-chain quarternary ammonium salts and higher temperatures are used for Ti-MCM-41.

Catalytic properties of Ti-HMS (and Ti-MCM-41) Mesoporous titanosilicates have been compared to TS-1 and Ti-beta for a number of reactions. A lower activity and peroxide selectivity is generally observed for the mesoporous materials, particularly when aqueous hydrogen peroxide is the oxidant. This is generally ascribed to the hydrophilicity of these catalysts, which approaches that of amorphous silica-titania oxides and leads to deactivation through adsorption of polar compounds and decomposition of the oxidant. The latter aspect of mesoporous titanosilicates has been investigated by Trong On et al. (1996) and Trong On et al. (1997), who described hydrogen peroxide decomposition by surface silanols with Ti-MCM-41. Depending on reaction conditions, leaching of titanium [Chen et al. (1997)] and even collapse of the framework [Chen et al. (1997), Rhee and Lee

(1996)] has been reported when aqueous solutions of H_2O_2 were used as the oxidant. Most literature reports focus on the use of organic hydroperoxides such as THBP with mesoporous titanium silicates to oxidise very bulky substrates that cannot be oxidised with TS-1 or Ti-beta.

Due to their ultralarge pores, no shape selective effects are observed with mesoporous materials and they can thus be taken as a 'reference' for non shape-selective reactions over titanium-containing molecular sieves.

2.2.4 Other titanium-containing molecular sieves

The first titanium-substituted redox zeolite to follow TS-1 was TS-2, a medium-pore zeolite with MEL topology, a pore size of the same order as TS-1 and very similar catalytic properties. In several research reports over the past years, the incorporation of titanium in a number of other zeolitic materials has been claimed. The synthesis of TS-48, the titanium analog of the mesoporous ZSM-48 and a range of amorphous titanium silicates was reported. Other examples of titanium-substituted zeolites are ETS-10 and titanium ZSM-12, which were obtained via hydrothermal synthesis. Post-synthesis modifications mainly with $TiCl_4$ were used to obtain titanium-containing versions of zeolites that could not successfully be synthesised via hydrothermal synthesis; examples are mordenite, zeolite X and Y.

Titanium has also been incorporated into the framework of many materials based on phosphorus, aluminium (APOs, see Figure 2.2) and silica (SAPOs). Few reports on the catalytic properties of this class of catalysts are available [Hsu and Cheng (1999)]. The general problem is the very hydrophilic framework TAPOs and TAPSOs which limits their application to non-polar environments.

Some of the materials mentioned above showed good results for epoxidation reactions, but with the exception of TS-2, satisfactory activities and selectivities for aromatic hydroxylation reactions were not achieved and often no proof for leaching stability of the catalyst was given.

2.3 Liquid-phase oxidations catalyzed by titanium-containing molecular sieves

The exceptional range of reactions catalyzed by TS-1 with 30% hydrogen peroxide is illustrated in Figure 2.8 with the reactions studied in this work highlighted. The majority of the reactions shown are also catalyzed by Ti-beta and Ti-HMS although lower activities and selectivities were reported as compared to TS-1.

The epoxidation of olefins is of great industrial interest and excellent selectivities at high conversions have been reported by many groups [Clerici and Ingallina (1993), Langhendries et al. (1999)].

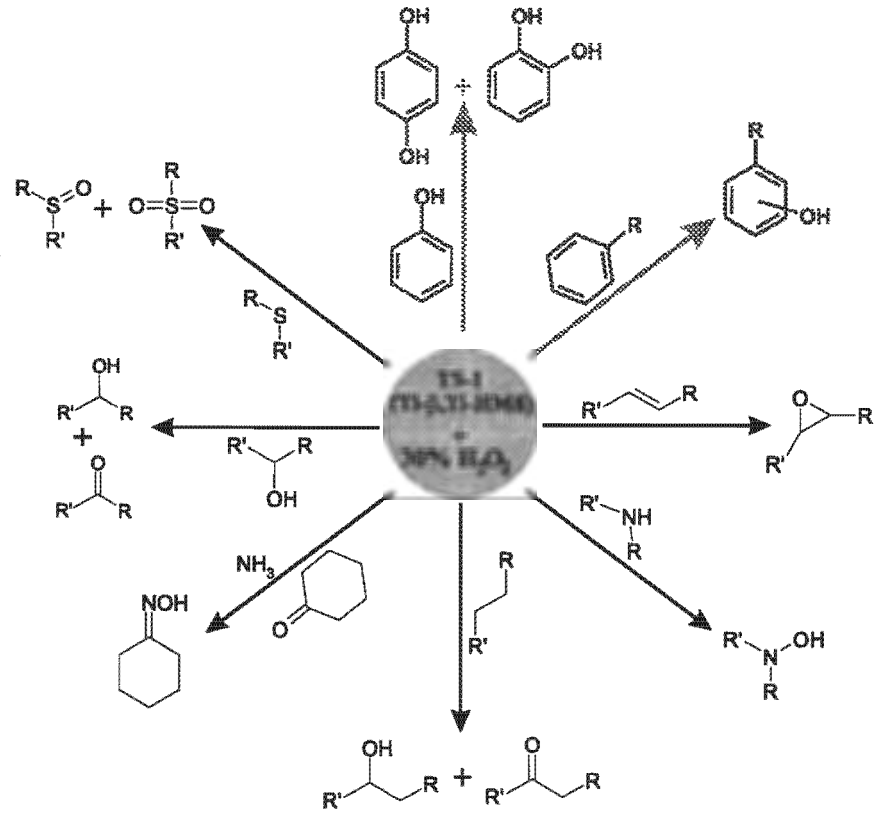

Figure 2.8: Catalytic properties of TS-1 (redrawn and extended from Sheldon et al. (1998b))

However, catalyst deactivation has been described by Langhendries et al. (1999) and presumably occurs through strong readsorption of the epoxides with subsequent formation of high molecular weight compounds in the pores. A solution to the deactivation problem has been found (by the addition of ammonia in the ppm range) and pilot plants are currently being optimised for the epoxidation of propylene using TS-1 and 30% H_2O_2 on an industrial scale.

The ammoximation of cyclic ketones is another industrially important reaction since the resulting oximes are easily rearranged to the corresponding cyclic lactams, the monomers for the production of Nylon. Selectivities in excess of 95% at complete peroxide conversion have been reported [Thangaraj et al. (1991b)] and pilot plants for the ammoximation of cyclohexanone with TS-1 were built. However, leaching of titanium in the presence of ammonia was observed [Petrini et al. (1991)].

Alcohols can be oxidised to their respective aldehydes and ketones [Maspero and Romano (1994), van der Pol and van Hooff (1[illegible]3)] and even saturated hydrocarbons can be oxidised in the liquid-phase under relatively mild [illegible]ditions [Huybrechts et al. (1990), Khouw et al. (1994)]. The oxidation of thioethers to sulfoxides and sulfones [Moreau et al. (1997)] and the hydroxylation of secondary amines [Reddy and Jacobs (1996)] has also been described.

The hydroxylation of phenol was, however, the first industrial application of TS-1; a plant producing around 10000 t/a of hydroquinone and catechol using 30% H_2O_2 was operated for a decade in Ravenna, Italy. The hydroxylation of phenol and other aromatics was thoroughly investigated in this work and a brief overview of the existing literature reports is given below.

2.3.1 Hydroxylation of phenol

Since the process was patented [Taramasso and Perego (1983)], the phenol hydroxylation has received much attention in the literature and many reaction parameters have been investigated to optimise the catalytic activity and selectivity.

In the early work on the reaction, phenol hydroxylation was identified as a suitable test reaction for the quality of the TS-1 catalyst batch [Kraushaar-Czarnetzki and van Hooff (1989)]. The selectivity towards the dihydroxybenzenes and the peroxide efficiency are very sensitive towards incomplete titanium incorporation and/or the presence of TiO_2 impurities. This aspect was used again later when the European Association of Catalysis launched a collaborative research project for the standardisation of TS-1. The synthesis, characterisation and catalytic properties of a standard EUROTS-1 catalyst was described by four independent research groups throughout Europe [Martens et al. (1993)]. Major differences in the catalytic reaction results from the different groups were recorded. The phenol hydroxylation was found to be dependent not only on the quality of the catalyst but also on a number of other parameters such as reaction temperature and -time, amount of catalyst, amount and nature of solvent, phenol/H_2O_2 ratio and method of H_2O_2 addition.

Although many of these parameters have been studied in various publications, a comparison of the results obtained is often difficult due to the different reaction conditions chosen by the authors, and some of the conclusions found in the literature are contradictory.

Thangaraj et al. (1991a) reported the formation of para-benzoquinone, the consecutive oxidation product of hydroquinone, only for reaction temperatures below 43 °C. The analysis method, however, was GC analysis and the formation of para-benzoquinone during GC analysis was reported at low H_2O_2 conversions; this effect is described in more detail in section 3.4.3. In more recent publications, most authors do not report the formation of para-benzoquinone.

One of the most interesting and most studied aspects of the phenol hydroxylation catalyzed by TS-1/H_2O_2 is the product distribution. Principally, hydroquinone is the more desired product and thus reaction conditions with maximum peroxide efficiency and hydroquinone yield are generally sought.

An increase in titanium content of TS-1 results in the expected increase in activity, but no effect on the product distribution was observed [Thangaraj et al. (1991a)]; the selectivity of the reaction is thus rather insensitive towards the titanium content of the catalyst.

A strong influence of reaction time and catalyst concentration on the product distribution has been found [Thangaraj et al. (1991a)]; more of the para-isomer was formed with increasing reaction time and increasing catalyst concentration. Both these effects are very likely to originate from different phenol conversions. The selectivity strongly depends on phenol conversion and several authors have reported a shift towards more hydroquinone with increasing conversion. Selectivities can thus only be compared at the same conversion levels and the conclusions in some reports do not take this into account.

The product distribution as well as the change in selectivity with conversion also strongly depend on the solvent used. In protic solvents, hydroquinone is the preferred product, whereas catechol is preferentially formed in aprotic solvents. Thangaraj et al. (1994) tested various protic and aprotic solvents for the phenol hydroxylation with TS-1/H_2O_2 and found an increase in phenol conversion with the polarity of the solvent. An explanation for this trend would be adsorption effects: the hydrophobic environment in the TS-1 pores leads to preferential adsorption of non-polar compounds and with increasing polarity, less solvent and more phenol could be present in the pores. However, no adsorption study of phenol and other aromatics in different solvents can be found in the literature and is presented in this work for both TS-1 and Al-free Ti-beta.

Satisfactory peroxide efficiencies and high reaction rates have only been obtained for water, methanol and acetone as the solvents. This can be accounted for by TS-1 catalyzed solvent oxidation; water and acetone are inert, whereas the relatively rapid oxidation of alcohols to their respective aldehydes or ketones has been reported [van der Pol and van Hooff (1993)]. The exception is methanol, which is converted to formaldehyde, formic acid, dimethyether and CO/CO_2 at a very low reaction rate [Maspero and Romano (1994)]. For bulky solvent molecules such as longer-chain ketones or tert-butanol, the reaction rates decrease probably as a result of preferential adsorption of these solvents, causing a significant reduction of the space available for reaction in the pores. Shape selectivity through space restrictions in the TS-1 micropores is generally invoked to explain for the higher para-selectivity compared to homogeneous processes; a comparison of some processes for the hydroxylation of phenol using H_2O_2 is given in Table 2.2. Although a shape selectivity effect is

Table 2.2: Industrial processes for the hydroxylation of phenol with H_2O_2 [Notari (1988)]

Process	Reagents/method	X_{phenol} %	S_{phenol} %	$S_{H_2O_2}$ %	p/o ratio
Rhone-Poulenc (homogeneous)	Fe^{2+}/ Co^{2+} Radical catalysis (Fenton-type)	5	90	70	0.7-0.8
Brichima (homogeneous)	$HClO_4$, H_3PO_4 Acid catalysis	10	80	50	0.4-0.5
Enichem (heterogeneous)	TS-1 continuous fixed-bed	30	92	82	0.8-2.0

undoubtedly present in TS-1, no systematic study of this aspect is found in the literature. Titanium-

containing molecular sieves with medium, large and ultralarge pores (TS-1 → Al-free Ti-beta → Ti-HMS) were compared in this work and conclusions in terms of shape selectivity were based on the product distributions obtained. As the shape selectivity observed in TS-1 can be enhanced by the solvent, the influence of the latter in the different pore environments was also investigated in this study.

Not only the concentration of the reactants and products, but also their transport properties in the pore system are of great importance. This key parameter was identified by van der Pol et al. (1992), who investigated the influence of the crystal size on the catalytic activity of TS-1 in the phenol hydroxylation with H_2O_2. These authors found that the reaction was strongly mass transfer limited if the crystal size is larger than 0.3-0.4 μm, which they attributed to very low intracrystalline diffusivity values for phenol in TS-1. Their observation was based on a kinetic study and the calculation of the Thiele modulus for TS-1 samples of different crystal sizes, but the diffusivity values had to be estimated. In contrast, the present study documents the measurement of intracrystalline diffusivities of phenol and other aromatics in TS-1 and Al-free Ti-beta using two different methods. Values for the counterdiffusion of aromatics in these catalysts (using different solvents) are not yet reported in the literature.

The use of very small crystals to avoid mass-transfer limitations in aromatic hydroxylation reactions implies that another parameter becomes important: the external surface of the catalyst particles. The desired shape selective effects are not present on the external surface as the reaction on external surface sites is not limited by geometric constraints generated by the microporous structure. Additionally, external reactive centres are exposed to the concentrations in the bulk solution, which can be different from the concentrations present in the pores as pointed out earlier. The role of the external surface in the phenol hydroxylation over TS-1 was subject of a study by Tuel et al. (1991). These authors used a non-calcined catalyst for a phenol hydroxylation experiment in methanol and acetone as solvents. A very high selectivity towards catechol was observed and their conclusion was that catechol is almost exclusively formed on the external surface. A more pronounced shift towards more hydroquinone with increasing conversion was observed in methanol than in acetone as the solvent. This was explained by a poisoning of the external surface with tars in the course of the reaction. As the external sites are preferentially producing catechol and are poisoned during reaction, more hydroquinone is observed with increasing phenol conversion. In acetone as the solvent, the external surface poisoning is partly prevented or delayed due to the dissolving power of acetone for tars. Although this seems a valid explanation for the role of the external surface sites, there are still contradictions in the literature. In the same study, Tuel et al. (1991) reported a high activity of the external surface whereas van der Pol et al. (1992) found a very low activity. Additionally, if a non-calcined catalyst is taken for a catalytic experiment, the role of the template, still in the pores and possibly also on the external surface, is unclear. A different approach is presented in this work:

instead of preventing reaction in the pores by blocking the latter, deactivation of the external surface by SiO_2 deposition using a CVD technique was applied to discriminate between external and internal activity of TS-1.

An interesting detail is the dependence of peroxide efficiency and product distribution on the method of peroxide addition as reported by Thangaraj et al. (1991a). Drop-wise addition of the H_2O_2 solution resulted in higher peroxide efficiencies and hydroquinone selectivities than addition of the whole amount in one portion. Thus, low concentration levels of hydrogen peroxide favour hydroquinone formation and decrease peroxide decomposition. A patent describing a continuous phenol hydroxylation process with multi-stage H_2O_2 addition into the catalyst bed is based on this concept [Ratnasamy and Sivasanker (1996)].

The influence of many parameters such as the reaction conditions, quality and crystal size of the TS-1 sample etc. renders a comparison of literature data difficult; in some cases, important information is not given in the reports. Table 2.3 shows a selection of literature results for the phenol hydroxylation over TS-1 with aqueous H_2O_2. Higher para-selectivities are generally reported in protic solvents, although the reported values differ substantially. This overview of the literature clearly demonstrates that phenol hydroxylation over TS-1/H_2O_2 is by no means a simple reaction. Although this reaction has been the subject of numerous publications and has been running on an industrial scale for many years, a detailed reaction mechanism explaining the activities and selectivities observed is not yet reported and many aspects such as the influence of the external surface are not yet fully understood.

2.3.2 Other aromatic hydroxylations

Other substituted benzenes and benzene itself can also be hydroxylated over TS-1 with aqueous H_2O_2. Larger aromatics such as substituted naphthalenes seem too bulky to enter the TS-1 pores under mild reaction conditions. If the benzene ring has more than one substituent or the substituent is too bulky, low reaction rates were observed [Bhaumik and Kumar (1995), Vayssilov et al. (1997), Wu et al. (1998)], presumably due to mass transfer limitations. In the hydroxylation of alkylbenzenes, Wu et al. (1998) observed that the reaction rates decreased in the order toluene >> ethylbenzene > cumene. These authors also presented the only study of transport properties of alkylated benzenes in TS-1. Vayssilov et al. (1997) investigated the hydroxylation of toluene, ethylbenzene, and 1- and 2-propyl-benzene over TS-1 with H_2O_2. For toluene, only ring hydroxylation was observed whereas for all other aromatics, side-chain oxidation was the major reaction.

Substituted benzenes with electron-withdrawing groups do not react [Höft et al. (1996)], indicating that deactivated aromatic rings cannot be hydroxylated with TS-1/H_2O_2 under mild reaction conditions.

Table 2.3: Literature data for TS-1/H_2O_2 catalyzed phenol hydroxylation

T [°C]	solvent	X_{ph} [%]	$X_{H_2O_2}$ [%]	S_{ph} [%]	$S_{H_2O_2}$ [%]	p/o	Experimental conditions	Ref.
70	water	17.2	-	-	85.0	1.44	t_R = 6 h, 20 g solvent,	Thangaraj
	methanol	16.9	-	-	79.0	2.69	1 g TS-1(Si/Ti=33),	et al.
	acetone	16.2	-	-	82.0	0.94[1]	phOH/H_2O_2 = 5,	(1994)
	t-butanol	10.0	-	-	48.6	2.91[1]	2.5 g H_2O_2[2]	
	2-butanone	8.4	-	-	43.0	0.67[1]		
	acetonitrile	9.0	-	-	48.0	0.93[1]		
80	methanol	31.8	83.0	-	-	2.7	t_R = 6 h, 28 ml solvent,	Kulawik
							0.5 g TS-1(Si/Ti=48),	et al.
							9.4 g phOH, 4.4 ml H_2O_2[2]	(1994)
80	acetone	24.0	-	-	-	0.2	0.4 g TS-1(Si/Ti=40),	Astorino
							10 g phOH, 4 ml H_2O_2	et al.
								(1995)
70	methanol	18.0	-	-	89.0	2.0	t_R = 6 h, 15 ml solvent,	Tuel
							0.5 g TS-1, 9.4 g phOH,	et al.
							2.4 ml H_2O_2	(1994)
80	acetone	21.4	-	-	-	1.1	1 g phOH, 8 g solvent,	Kumar
							0.2 g TS-1(Si/Ti=27)	et al.
								(1994)
70	ethanol	20.0	-	-	95.0	1.9	t_R = 1 h, 20 ml solvent,	Tuel
							0.5 g TS-1(Si/Ti=109),	et al.
							9.4 g phOH, 2 ml H_2O_2	(1996)
80	methanol	-	-	-	92.0	2.1	t_R = 2 h, 15 ml solvent,	Tuel
							0.5 g TS-1(Si/Ti=25),	et al.
							9.4 g phOH, 2.3 ml H_2O_2	(1994)
60	ethanol	-	100	89.0	93.0	2.0	t_R = 3 h, 16 ml solvent,	Tuel
							0.5 g TS-1(Si/Ti=50),	et al.
							9.4 g phOH, 2.3 ml H_2O_2	(1998)
57	acetone	24.6	-	-	75.0	0.75	t_R = 6 h,	Thangaraj
	2-butanone	14.4	-	-	43.0	0.62[1]	TS-1(Si/Ti=23)/phOH = 0.1,	et al.
	acetonitrile	15.3	-	-	48.0	0.62[1]	phOH/H_2O_2 = 3	(1991)
	methanol	25.2	-	-	81.0	1.86		
25	acetone	30.0	-	-	81.0	0.92[2]		
100	acetone/H_2O	27.0	100.0	91.0	82.0	1.0	t_R = 1h, 20.7 g phOH,	Martens
69	methanol	21.0	-	66.0	-	2.5[1]	0.72 g TS-1 (Si/Ti=35),	et al.
							6.8 g solvent, 5.46 g H_2O_2[2]	(1993)
60 -	methanol	20.0	100.0	91.0	70.0	1.85	phOH/H_2O_2 = 3.3 - 5	Perego
100	acetone	26.1	100.0	92.0	80.0	0.75	TS-1(Si/Ti=40)	et al.
								(1990)

[1]major amounts of para-benzoquinone reported; [2]H_2O_2 (30 - 35% solution in water) was injected dropwise over 10 - 60 min

The hydroxylation of benzene mainly yields phenol and para-benzoquinone [Thangaraj et al. (1990)], and phenol selectivities > 90% could be achieved depending on the solvent. Kumar and Bhaumik (1998), Bhaumik et al. (1998) and Kumar et al. (1999) presented a series of studies on aromatic hydroxylations with TS-1 under triphase conditions. Higher reaction rates and para-selectivities were reported for toluene and anisole. The same authors also described a solvent effect similar to the one observed in the phenol hydroxylation; protic solvents favour para hydroxylation whereas more ortho hydroxylated products were formed in aprotic solvents. The higher reaction rates in triphase conditions were ascribed to preferential adsorption of the aromatics in the presence of water. The higher para selectivities were explained with the same effect as the reaction takes place in the pores to a much larger extent and shape selectivity effects become more dominant. Kumar and Bhaumik (1998) and Bhaumik and Kumar (1995) also described the hydroxylation of benzyl chloride, benzyl alcohol and acetophenone [Bhaumik et al. (1996)] to a mixture of hydroxylated and side-chain oxidised products.

Table 2.4: Literature data for TS-1/H_2O_2 catalyzed anisole and toluene hydroxylation

substrate	solvent	X_A	$X_{H_2O_2}$	S_A	$S_{H_2O_2}$	%o	%m	%p	p/o	Ref.
anisole	acetone	11.9	98	90	73	64	-	36	1.78	Perego
toluene	acetone	7.1	98	90	65	15	15	70	4.67	et al. (1990)[1]
	water	7.5	98	85	65	26	29	45	1.73	
anisole	methanol	5.9	19.1	-	-	35	-	65	1.8	Kulawik et al. (1994)[2]
anisole	acetone	42.2	-	-	43.5	66.6	-	30.3	0.45	Kumar
	methanol	45.2	-	-	46.2	31.8	-	67.2	2.11	et al. (1998)[3]
	t-butanol	38.0	-	-	40.4	24.4	-	74.0	3.03	
	water	66.5	-	-	67.9	25.6	-	72.3	2.82	
toluene	acetone	5.5	-	-	5.6	69.7	-	28.4	0.41	
	water	14.8	-	-	15.2	41.4	-	55.9	1.35	
anisole	acetonitrile	42.2	100	-	-	66.6	-	30.3	0.46	Bhaumik
	water	66.5	100	-	-	25.6	-	72.3	2.82	et al. (1995)[4]
toluene	acetonitrile	5.5	100	-	-	69.7	-	28.4	0.41	Ratnasamy
	water	14.8	100	-	-	41.4	-	55.9	1.35	et al. (1995)[4]
toluene	water	-	100	-	-	25	30	45	1.8	Marchal et al. (1993)[5]
anisole	acetonitrile	7.5	-	-	37.5	55	-	45	0.82	Kumar
	methanol	9.0	-	-	45.0	60	-	40	0.67	et al. (1999)[6]
	water	17.5	-	-	87.5	25	-	75	3.0	

[1] T = 60 - 100°C, aromatic/H_2O_2 = 0.1; [2] t_R = 4 h, T = 80°C, 20 g solvent, 1 g TS-1(Si/Ti=48), 20 g phOH, 4 ml H_2O_2; [3] T = 60 - 80°C, 10 mmol aromatic, 10 mmol H_2O_2, 0.2 g TS-1(Si/Ti=30), t_R = 6 - 12 h; [4] T = 80°C, 10 mmol aromatic, 10 mmol H_2O_2, 0.2 g TS-1(Si/Ti=30), t_R = 6 - 16 h; [5] T = 80°C, 10 ml solvent, 0.5 g TS-1(Si/Ti=50), 0.1 mol aromatic, 0.02 mol H_2O_2; [6] T = 80°C, 54 g solvent, 0.1 mol aromatic, 2.1 g TS-1(Si/Ti=32), 0.02 mol H_2O_2;

In this work, only reactions where exclusive ring hydroxylation occurs were investigated, e.g. the anisole and toluene hydroxylation, using the same approach as for the phenol hydroxylation. Table 2.4 shows literature results for the hydroxylation of anisole and toluene. The results for the anisole and toluene hydroxylation reported in the literature, particularly the effect of the solvent on the product distribution, show considerable inconsistency.

The role of the external surface has not yet been investigated in the literature and no comparison to a larger pore titanium-containing zeolite, which could identify shape selectivity effects, has been reported. Solvent effects were also examined and a reaction mechanism consistent with the experimental results was developed.

For the catalytic properties of Al-free Ti-beta in aromatic hydroxylations, no data is currently available in the literature and the application of this novel catalyst for these reactions is evaluated.

A very interesting and potential industrial application of Al-free Ti-beta is the hydroxylation of naphthalenes to their corresponding naphthoquinones. The feasibility of this reaction was demonstrated by Anunziata et al. (1999), who studied the conversion of 2-methyl-naphthalene to 2-methyl-1,4-naphthoquinone over titanium- and iron-substituted large pore zeolites and mesoporous materials. This reaction and the hydroxylation of 1-naphthol with aqueous H_2O_2 was examined in this work as another application of Al-free Ti-beta.

2.4 Adsorption of hydrocarbons on microporous solids

One of the most interesting properties of zeolites is their ability to selectively adsorb molecules, which leads to an accumulation of preferentially adsorbed compounds in the pore system. In the case of titanium-substituted silicalites such as TS-1 and Al-free Ti-beta, their hydrophobic framework is expected to preferentially adsorb non-polar compounds.

Without knowing the concentrations in the pores, it is difficult to evaluate the (intrinsic) activity of a microporous catalyst as most of the active sites are located inside the pores. Since a kinetic study is presented in this work, the (competitive) liquid-phase adsorption of reactants, products and solvents in the zeolites used was investigated using both a batch and a chromatographic technique.

In a separate investigation, a gas-phase adsorption study was used to examine the effect of external surface deactivation on the pore mouth of TS-1. The adsorption of molecules with a kinetic diameter close to the pore openings of TS-1 was taken as a measure for potential pore entrance narrowing or -blocking generated by deposition of inert material on the external surface.

2.4.1 Gas-phase adsorption

The chromatographic method is a well-established technique to determine adsorption constants of hydrocarbons in microporous and mesoporous materials. The method consists of the injection of a hydrocarbon pulse into a column packed with the adsorbing material at elevated temperatures. The first and second moment of the response peak can then be used to calculate the adsorption constant and the diffusivity of the tracer compound in the zeolite pores, respectively. This work deals only with liquid-phase reactions, and thus the aim of the gas-phase adsorption study conducted was not to determine the adsorption properties of certain compounds in the vapour phase in TS-1, but to evaluate changes in adsorption behaviour on progressive silanisation of the external surface.

Using the pulse gas-phase chromatographic technique, it could be shown that the pores of silicalite-1 can be narrowed through silica deposition on the external surface to an extent that branched paraffins were excluded from entering the pores [Sealy and Möller (1998)], whereas linear alkanes were still strongly adsorbed. Thus, this technique is an appropriate tool to characterise pore mouth narrowing upon silanisation. From the response of the pulse-injection of 50 - 100 μl of saturated hydrocarbon vapour (1 - 4 μmol), the first moment μ_1 can be calculated by integration of the FID detector signal. From the first moment, the Henry's constant of the tracer compound on the solid can be determined:

$$\mu_1 \equiv \int_0^\infty \frac{C(t) \cdot t \cdot dt}{\int_0^\infty C(t) \cdot dt} = \frac{L_{cat}}{u_f}(\varepsilon_{ext} + (1 - \varepsilon_{ext})K) \tag{2.1}$$

The adsorption isotherm is assumed to be in the linear region, hence Henry's law is valid:

$$K = \frac{q}{C} \tag{2.2}$$

The second moment of the pulse response can be calculated by integration of the FID detector signal using the first moment:

$$\sigma^2 \equiv \frac{\int_0^\infty C(t) \cdot (t - \mu_1)^2 dt}{\int_0^\infty C(t) \cdot dt} \tag{2.3}$$

The temperature dependence of the adsorption constant K is given by the van't Hoff-type equation:

$$K = K_0 \cdot exp(-\frac{E_A}{R \cdot T}) \tag{2.4}$$

2.4.2 Liquid-phase adsorption

In the gas phase, the influence of the carrier gas on adsorption can generally be neglected. In the liquid phase, however, adsorption is always competitive since not only reactants and products but

also solvents are present in the system. The adsorption of reactants and products was therefore measured in TS-1 and Al-free Ti-beta using different solvents. Adsorption constants in the liquid phase were determined by means of a batch and a chromatographic technique. Langhendries et al. (1999) highlighted the importance of the adsorption properties of reactants and products in liquid-phase epoxidation reactions over TS-1 and Al-free Ti-beta using the same experimental technique that was used in this work. Surprisingly, a systematic study of the adsorption of aromatics in TS-1 and Al-free Ti-beta with different solvents is not available in the literature.

2.5 Intracrystalline diffusion of hydrocarbons in microporous solids

Kinetics of heterogeneous chemical reactions in microporous solids can be influenced either by the reaction itself or by the mass transport of the reactants or products. The phenol hydroxylation over TS-1 was identified as a strongly mass transfer limited reaction by van der Pol et al. (1992) for zeolite crystals larger than 0.3 μm. However, the intracrystalline diffusivities were estimated through the calculation of a relative Thiele modulus for different crystal sizes. No reliable data for the diffusion of aromatics in TS-1 and Al-free Ti-beta in the liquid phase are available in the literature. This work presents a study on the intracrystalline counter-diffusivities of various aromatics in TS-1 and Al-free Ti-beta in the different solvents used for reactions. Together with kinetic data from catalytic reaction experiments, the measured diffusivity values then allow an exact evaluation of the influence of the crystal size.

2.5.1 The liquid-phase ZLC method

The zero length column (ZLC) method of measuring micropore diffusivities in microporous solids was first introduced by Eic and Ruthven (1988) for gas-phase adsorption systems. Many more publications followed and useful and consistent data can be extracted from the model, which has been continuously improved since the establishment of the technique. One of the advantages of the technique is its simplicity. The ZLC technique depends on following the transient desorption curve when a very small sample of zeolite crystals (a bed of 'zero length'), presaturated at a known, low concentration, is desorbed by purging with an inert carrier at a relatively high flow rate, under conditions such that the desorption rate is controlled by diffusion within the zeolite crystals. The intracrystalline diffusivity and the Henry constant can be extracted from the long-time region (i.e. the 'tail') of the monitored transient desorption curve.

The application of this technique to liquid systems is, however, experimentally much more dif-

ficult. Ruthven and Stapleton (1993) presented the first extension of the ZLC method to liquid systems, and this was followed by an improved modelling of the system by Brandani and Ruthven (1995). These are to date the only publications that deal with liquid-phase systems using the ZLC technique. In a gaseous system, because of the low molecular density, neglect of the external (fluid-phase) hold-up is generally a very good approximation and it is possible to use a very simple model to interpret the experimental desorption curves. In liquid-phase adsorption systems the hold-up in the external fluid is of much greater importance and can be of the same order as that in the adsorbed phase. Another problem is that the sensitivity of the available detectors is not as high in the liquid phase as in the gas phase. Careful characterisation of the system with special attention to the blank response is thus necessary. The (original) ZLC model is derived from the following equations, assuming spherical catalyst particles, the validity of Henry's law and Fick's second law of diffusion, and a well-mixed (differential) adsorber:

Solid-phase (sorbate bed) mass balance using Fick's second law in spherical coordinates:

$$\frac{\partial q}{\partial t} = D\left(\frac{\partial^2 q}{\partial r^2} + \frac{2}{r}\frac{\partial q}{\partial r}\right) \tag{2.5}$$

Fluid-phase mass balance:

$$V_s\frac{\partial \overline{q}}{\partial t} + V_f\frac{\partial c}{\partial t} + F \cdot C = 0 \tag{2.6}$$

with the initial conditions

$$\begin{aligned} q(r,\, t=0) &= K \cdot C_0 \\ C(t=0) &= C_0 \end{aligned} \tag{2.7}$$

and the boundary conditions, assuming the validity of Henry's law (linear isotherm)

$$\begin{aligned} q(r = R_c,\, t) &= K \cdot C\,, \\ \left(\tfrac{\partial q}{\partial r}\right)_{r=0} &= 0 \end{aligned} \tag{2.8}$$

With a negligible interstitial fluid hold-up, these equations can be solved to yield the relation for ZLC desorption curves:

$$\frac{C}{C_0} = 2L\sum_{n=1}^{\infty}\frac{exp(-\beta_n^2(D/R_c^2)t)}{\beta_n^2 + L(L-1)} \tag{2.9}$$

where

$$L = \frac{characteristic\ diffusion\ time}{characteristic\ convection\&adsorption\ time} = \frac{FR_c^2}{3V_sKD} = \frac{\varepsilon_{ext}v_fR_c^2}{3(1-\varepsilon_{ext})L_{cat}KD} \tag{2.10}$$

and β_n is given by the roots of

$$\beta_n cot(\beta_n) + L - 1 = 0 \tag{2.11}$$

For sufficiently long times, only the first term of the sum in equation 2.9 has to be taken into account:

$$\frac{C}{C_0} = \frac{2L \cdot exp(-\beta_1^2 (D/R_c^2)t)}{\beta_1^2 + L(L-1)} \tag{2.12}$$

For large values of L, i.e.for sufficiently high purge flow rates and with $\beta_1 \approx \pi$ for long times, this can be written as

$$ln\left(\frac{C}{C_0}\right) \approx ln(\frac{2}{L}) - t \cdot \pi^2 \frac{D}{R_c^2} \tag{2.13}$$

Under these conditions, the desorption is controlled by intracrystalline diffusion to the crystal surface. The diffusional time constant D/R^2 and the parameter L can then be extracted from the slope and intercept of the ZLC desorption curve in a semi-logarithmic plot of C/C_0 versus t, respectively.

The other limit is obtained for very low purge flow rates. Intracrystalline diffusion is then fast enough to maintain an essentially uniform concentration through each crystal and the desorption rate is controlled by the convective removal of the sorbate. In this case, L→0, $\beta_1^2 \rightarrow 3L$ and the desorption curve becomes

$$ln\left(\frac{C}{C_0}\right) = \frac{-\varepsilon_{ext} v_f \cdot t}{(1-\varepsilon_{ext}) K L_{cat}} \tag{2.14}$$

Under these conditions, the desorption is equilibrium controlled and the transient desorption curve contains no information about diffusion. Hence, care must be taken to choose a sufficiently high purge flow rate to operate at large values of L and therefore monitor a diffusion-controlled ZLC desorption curve. A variation of the flow rate is necessary to verify this condition.

It has to be noted that the above equations are derived for spherical particles. Cavalcante Jr. et al. (1997) and Duncan and Möller (2001) presented a study about the main diffusion path length in ZLC desorption curves using non-spherical crystals and a crystal size distribution, respectively. For slab-shaped crystals, the crystal radius R_c in equation 2.13 has to be replaced with the half-thickness (l/2) of the slab-shaped crystals. For other particle shapes, the main diffusion path length can be represented by the ratio of pore volume to surface area. Further details for the derivation of the ZLC model and the interpretation of ZLC desorption curves are described elsewhere [Duncan and Möller (2001), Eic and Ruthven (1988), Cavalcante Jr. et al. (1997), Kärger and Ruthven (1992), Ruthven

et al. (1991), Ruthven and Stapleton (1993)].

2.5.2 The liquid-phase pulse method

The liquid-phase pulse method relies on the same principles as the ZLC method described above and the same assumptions are made. Instead of following the transient desorption curve after a step input, the response of a pulse of saturated hydrocarbon solution is monitored. Mathematically, the pulse method can be described as the time derivative of the ZLC method. The pulse model relies on the same assumptions and is derived in a similar way as the ZLC model; a detailed derivation is described elsewhere [Schwan (2001)]. In principle, the same problems are encountered as for the ZLC method, and in particular the axial dispersion can be a problem. However, application of the pulse method is more limited: the zeolite has to strongly adsorb the tracer compound and the diffusion has to be slow. If these conditions are not fulfilled, the amount of hydrocarbon adsorbed by the zeolite bed is low. Consequently, the hydrocarbon concentration during desorption is also low and the sensitivity of the detector is not sufficient to accurately measure the response curve.

2.6 Inertisation of the external surface sites of microporous solids

Diffusion limited reactions are common especially with microporous solids in the liquid phase; this aspect was further investigated in this work. The application of nano-sized catalyst crystallites offers a solution to overcome mass transfer limitations in heterogeneously catalyzed reactions. However, small catalyst particles have a significant portion of the active sites located at the external surface where no shape selectivity effects take place. Figure 2.9 shows the calculated ratio of external surface area to total surface area for TS-1 as a function of crystal size, assuming spherical particles with a perfectly smooth surface (S_{total} for TS-1 taken from the t-plots of BET measurements). Due to surface roughness, the real values are expected to be higher.

Generally, when a zeolite is employed as a catalyst, shape selective effects generated by the microporous framework are desired. The inertisation of the external surface has therefore been extensively studied in the literature for a number of microporous solids using various methods. More recently, the deactivation of the external surface with SiO_2 using chemical vapour deposition of silanes received increasing attention. The advantage of this approach is that inertisation is permanent in contrast to external surface deactivation through coking. In case of further (internal) deactivation, the zeolite can be thermally regenerated with the silica layer still intact since it is chemically bonded to the surface.

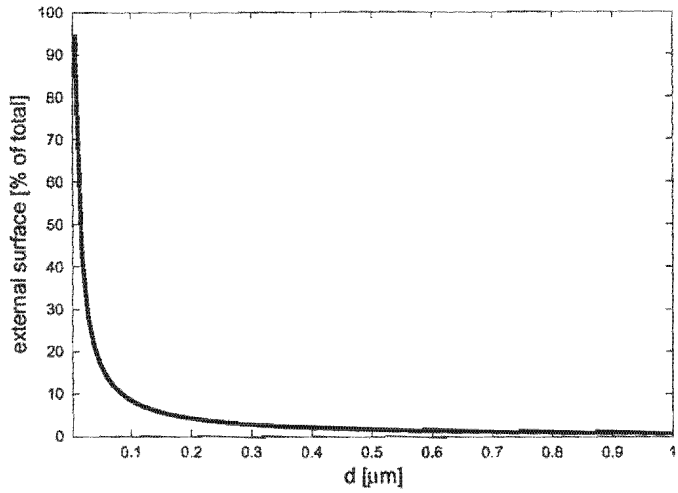

Figure 2.9: External surface area relative to total surface area for spherical TS-1 particles

2.6.1 Chemical vapour deposition (CVD) of tetraethoxysilane (TEOS)

The chemical vapour deposition (CVD) of silanes on zeolitic aluminosilicates, especially ZSM-5, is a well-established technique for inertising the acid sites on the external surface [Wang et al. (1988)]. For external surface site inertisation, a silane with a kinetic diameter larger than the pore openings of the zeolite is chosen, e.g. tetraethoxysilane (TEOS). Silica deposition proceeds via chemical reaction of TEOS molecules with active sites at the external surface, which can be either Brønsted acid sites [Chu et al. (1989), Weber (1998)], silanol groups [Bartram and Moffat (1996), Sealy and Möller (1998)] or other surface sites, as described in detail by Impens et al. (1999). The inertisation may lead to improvement in selectivity towards the product with the smallest kinetic diameter, as was observed in the toluene disproportionation to benzene and xylenes over H-ZSM-5. A cycle-wise CVD deposition of TEOS on H-ZSM-5 was described by Röger et al. (1998) and Ceijka et al. (1996). With increasing number of cycles the para-xylene content in the fraction of xylenes increased up to 99%, which was explained in terms of pore mouth narrowing [Röger et al. (1998)].

In this work, CVD of TEOS was used to inertise the external surface of TS-1. At low temperatures (RT - 200°C), TEOS molecules react with external surface groups; the remaining organic groups are subsequently combusted in a high-temperature calcination step. Figure 2.10 shows a schematic drawing of the possible interactions of a TEOS molecule with TS-1.

The external surface deactivation through silica deposition can principally be achieved in three different ways:

- exclusive reaction of TEOS with external active centres at a low coverage, such that the pore entrances are not significantly affected
- slow, selective SiO_2 deposition with a controlled narrowing of the pore mouth

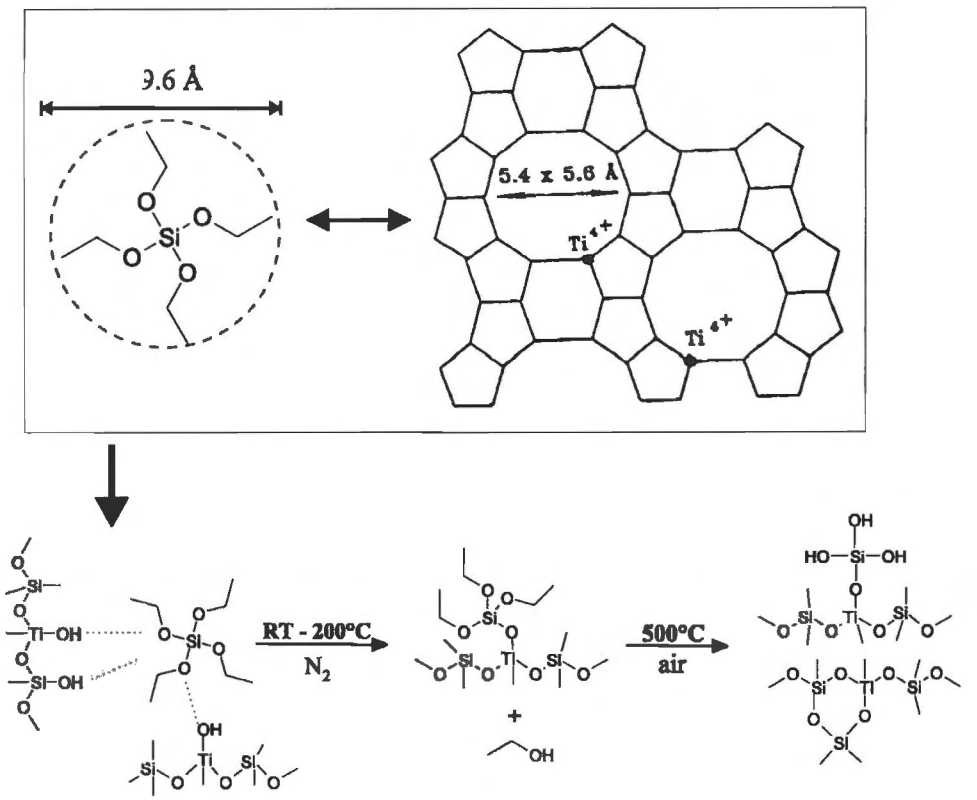

Figure 2.10: Possible reaction of TEOS with TS-1 external surface groups

- non-selective deposition with a rapid build-up of an amorphous silica layer, resulting in pore blockage

The key parameter to a selective deactivation of the external surface is the CVD temperature. At low temperatures, small amounts of silica are deposited and a selective reaction of the silane with reactive centres at the external surface takes place. The pore entrances are ideally completely unaffected under such conditions. If the procedure is repeated often enough or the temperature is increased carefully, a controlled narrowing or partial blockage of the zeolite pores can be achieved. In this case, desired shape-selective effects of the zeolite can be enhanced without a significant increase in mass transfer resistance. At high temperatures, large amounts of silica are deposited and the silane starts to oligomerise at contact with the external surface; in this case, progressive blocking of the pore mouth takes place on a large scale. If the TEOS deposition is done at a low temperature, selective reaction with surface defect sites can be expected. After reaction, the remaining alkoxy groups of chemisorbed TEOS molecules are removed through a calcination step at a high temperature in air. At low temperatures and low TEOS partial pressures, the deposited amount is also low and the procedure has to be repeated a number of times. In this work, the aim was a selective deactivation of the external surface of TS-1 without affecting the pore opening of the zeolite since additional mass

transfer resistances are not desired. The cycle-wise deposition technique allows for monitoring of the inertisation process. After a number of TEOS deposition cycles, TS-1 was tested for its catalytic properties in an aromatic hydroxylation reaction and for pore mouth narrowing by adsorption of compounds with a kinetic diameter close to that of the pore openings. Whereas many reports on external surface silica deposition on the isostructural ZSM-5 are available, this technique has not yet been applied to TS-1. The influence of a selective external surface silanisation on the catalytic properties of TS-1 is presented in this work.

Chapter 3

Experimental methods

3.1 Catalyst synthesis and preparatory treatment

The importance of the synthesis procedure and the purity of reagents used were described earlier. In this work, only well-established synthesis procedures were used and all catalyst samples obtained were extensively characterised. Since it is known that even trace amounts of alkali ions in the template have to be avoided (see section 2.2.1), template solutions from various suppliers were tested for their alkali content prior to use. It was found that the majority of commercially available template solutions contained high amounts of alkali ions (up to 10000 ppm). The alkali content in all templates used for synthesis in this work was less than 50 ppm as confirmed by AAS.

3.1.1 Titanium silicalite-1 (TS-1)

Large crystals of TS-1

Large crystals of TS-1 (Si/Ti = 34) were synthesised according to the procedure of Milestone and Sahasrabudhe (1999). A typical synthesis mixture consisted of 1 g SiO_2 (Aerosil 200), 0.5 g TPABr, 1.6 ml of tetrapropylammonium hydroxide (TPAOH, 40 % solution in H_2O), 0.6 g NH_4F, 0.11 g $(NH_4)_2TiF_6$ and 20 ml of deionised water. The salts and the TPAOH were dissolved in the water and Aerosil added and mixed until a homogeneous gel was obtained. The molar composition of the initial mixture was as follows:

0.034 TiO_2 : 1 SiO_2 : 66.93 H_2O : 0.47 TPAOH : 0.11 TPABr : 0.98 NH_4F

The synthesis mixture was autoclaved in teflon-lined stainless steel autoclaves and heated statically at autogeneous pressure at 170°C for 48 h. After crystallisation, the solid was recovered, washed with deionised water, dried and calcined in static air at 550°C for 8 h to remove the template.

Small crystals of TS-1

Small crystallites of TS-1 were synthesised (Si/Ti = 34) according to the method described by Thangaraj et al. (1992). In a typical synthesis, 24.4 g of tetraethyl orthosilicate (TEOS) was hydrolysed with 29.3 g of TPAOH (20 % solution in H_2O). A solution of 1.23 g tetrabutyl orthotitanate (TBOT) in 5.55 g of dry isopropyl alcohol was then added drop-wise. Subsequently, 9.8 g of TPAOH solution and 22.76 g of deionised water were added. Before autoclaving, the reaction mixture was heated to 80°C to remove the alcohol. The molar composition of the initial mixture was as follows:

0.035 TiO_2 : 1 SiO_2 : 25 H_2O : 0.32 TPAOH : 0.77 i-PrOH

This gel was then heated statically in Teflon-lined stainless steel autoclaves at autogeneous pressure at 170°C for 48 h. The resulting solid was recovered, washed with deionised water, dried and calcined in static air at 550°C for 8 h to remove the template.

3.1.2 Aluminium-free zeolite titanium beta

Large crystals of Al-free Ti-beta

Aluminium-free zeolite titanium beta was synthesised according to a procedure adopted by Blasco et al. (1998). In a typical synthesis, 80 g of tetraethyl orthosilicate (TEOS), 91.26 g of tetraethylammonium hydroxide (TEAOH, 34.8% in H_2O), 15.45 g of hydrogen peroxide solution (30% in water) and 1.42 g deionised water were mixed in a polypropylene beaker under magnetic stirring. This solution was kept stirring for 2 h at 25°C for complete hydrolysis of the TEOS. To this solution, 3.50 g of tetraethyl orthotitanate ($Ti(OEth)_4$) were added dropwise under stirring. The titanium source was added directly from the bottle to avoid pre-hydrolysis and thus TiO_2 formation. The titanium source dissolved to yield a yellow, clear solution. The solution was kept stirring at 25°C until the ethanol formed during hydrolysis of TEOS and $Ti(OEth)_4$ was evaporated. This process takes several hours, but can be accelerated by heating the solution to 50-60°C and using a gentle purge flow of nitrogen. The resulting solution was loaded into Parr general purpose bombs with 24 ml teflon liners. 10.78 g of hydrofluoric acid (40% in water) was added to the solution dropwise and slowly and a yellow, solid gel was obtained. During the evaporation of the ethanol, water was also evaporated and before autoclaving, the water loss was compensated by adding deionised water to obtain a gel with the following molar composition:

1 TiO_2 : 25 SiO_2 : 14 TEAOH : 189 H_2O : 14 HF

This gel was heated at 140°C for 20 days under rotation (60 rpm). The resulting solid was filtered on 0.45 μm Millipore filters and washed intensively with deionised water. The product was then dried and calcined in static air at 550°C for 8 h to remove the template.

Small crystals of Al-free Ti-beta

The synthesis procedure of smaller crystals of Al-free Ti-beta was identical to the one for larger crystals except that dealuminated (nanoscale) zeolite beta seeds were added to the final synthesis gel just before autoclaving. For seeding, 0.05 g dealuminated nanoscale zeolite beta seeds were added per gram of gel. The gel was heated at 140°C for 72 h under rotation (60 rpm).

Synthesis and dealumination of nanoscale zeolite (Al-) beta seeds In a typical synthesis, 40 g of tetraethyl orthosilicate (TEOS), 45.24 g of TEAOH (40% solution in H_2O), 1.85 g of $AlCl_3 \cdot 6H_2O$ and 4.33 g deionised water were mixed in a polypropylene beaker under magnetic stirring. This solution was kept stirring for several hours at 25°C until the ethanol formed during hydrolysis was evaporated. The resulting gel was loaded into Parr general purpose bombs with 24 ml teflon liners. The molar ratios given below refer to the molar composition of the final gel before autoclaving:

SiO_2 : 0.04 Al : 0.56 TEAOH : 6.5 H_2O

This gel was heated at 140°C for 72 h at autogeneous pressure. After crystallisation, the mixture was centrifuged at 18000 rpm for 30 min to separate the gel-type solid from the mother solution. The zeolite was then repeatedly washed (and centrifuged) with deionised water until pH around 9 and dried at 100°C.

The resulting solid was dealuminated by treating the as-made, dried zeolite with HNO_3 (55 wt%) using 60 g of acid per gram of beta-seeds. This solution was kept under magnetic stirring and reflux at 85°C for 12 h. The dealuminated seeds were subsequently extensively washed with deionised water and dried at 100°C.

3.1.3 Mesoporous titanosilicates (Ti-HMS)

A mesoporous hexagonally ordered titanium-containing silicate (Ti-HMS) was synthesised according to a procedure adopted by Tanev et al. (1994). For a typical synthesis, two solutions were prepared. Solution A was prepared through addition of 1.27 g of tetraorthobutyltitanate (TBOT) and 31.2 g of TEOS to 9 g of dry isopropyl alcohol and 45 g dry ethanol under magnetic stirring. Solution B was prepared through addition of 7.5 g dodecylamine to 95 g deionised water and 3 ml 1N hydrochloric acid. Solution A was slowly added to solution B under mechanical stirring. The molar composition of the initial mixture was as follows:

0.025 TiO_2 : 1 SiO_2 : 36.2 H_2O : 0.27 Dodecylamine : 0.02 HCl : 6.53 EtOH : 1 i-PrOH

Precipitation of Ti-HMS started after several minutes. The solution was left stirring overnight at room temperature. The Ti-HMS was then recovered by filtration on a 0.45 μm Millipore filter, extensively washed with deionised water (500 ml water per gram of solid) and ethanol and dried at 100°C. The solid was then calcined in static air at 550°C for 8 h.

3.2 Catalyst characterisation

3.2.1 Catalyst structure and morphology

X-ray diffraction (XRD)

Powder X-ray diffraction spectra of TS-1, Al-free Ti-beta and Ti-HMS were obtained from a Philips X'PERT diffractometer generating Cu-Kα radiation (λ = 1.542 Å) operating at 40 kV and 25 mA. Scanning was done between 4 and 12° 2Θ and between 4 and 55° 2Θ for Ti-HMS with a step size of 0.02° 2Θ and 2.0 s counting time. The samples were kept at ambient conditions prior to analysis. Relative crystallinities were obtained by integrating the peak areas of three largest peaks in the range 26-29° 2Θ for TS-1 and the peak in the range 21-24° 2Θ for Al-free Ti-beta, where the peak areas were normalised with respect to a 100% crystalline reference sample as discussed below.

Scanning electron microscopy (SEM)

Crystallite morphologies and -sizes were assessed from Electron micrographs obtained using a Leica LEO S440 Scanning Electron Microscope. The samples were mounted on aluminium stubs with a carbon/glue mixture and subsequently coated with Au/Pd film. Care was taken to select representative micrographs of the sample. The instrument was operated at an accelerating voltage of 40 keV, a tilt angle of 0° and aperture size 30 μm, and a working distance of 7 mm was used.

Nitrogen adsorption (N_2-BET)

The micropore volumes and surface areas of the samples were determined using a Micromeritics ASAP 2000. 0.5 g of sample were first dried at 500°C under vacuum. Nitrogen was then adsorbed at liquid nitrogen temperature until ambient pressure was reached.

All nitrogen adsorption data were repeated on a Coulter OMNISORP 360 under similar conditions. The data from both measurements were in good agreement. For evalutation, the desorption branch was used and the BJH method applied to calculate the pore diameters. Surface areas were determined by the t-plot method.

Thermogravimetric analysis (TGA/DTA)

The thermogravimetric spectra of the calcination of the freshly-prepared zeolite samples and the combustion of deposited coke on samples after reaction were recorded using a Stanton Redcroft STA-780 Series Thermal Analyser with a sample mass of 25 mg.

For the tar content analysis after reaction, the sample was recovered by filtration on a 0.45 μm Millipore filter, extensively washed with deionised water and ethanol and dried at room temperature.

In the Thermal Analyser, the sample was first heated in nitrogen (60 ml(NTP)/min) at 5°C/min to 150°C to desorb water. Subsequently, the carrier gas was changed to air (60 ml(NTP)/min) and the sample was heated at 5°C/min to 550°C and kept at this temperature for 4 h.

3.2.2 Catalyst composition and titanium incorporation

Diffuse reflectance ultraviolet spectroscopy (DRS)

Diffuse reflectance UV-VIS spectra were recorded from 600 to 200 nm on a UV-VIS-NIR Varian Cary 5 spectrophotometer with a certified standard of Labsphere (SRS-99-010) as reference.

Atomic absorption spectroscopy (AAS)

The silicon, titanium and alkali contents of the samples were determined by atomic absorption spectroscopy on a Varian Spectra AA-100 spectrometer, attached to a DSD 30 data station. Samples (100 mg) were prepared by placing them in a 24 ml Teflon Parr acid digestion bomb, where they were wetted with a few drops of deionised H_2O, followed by 5 ml of cold 40% HF. The Parr bomb was then heated in an oven to 70°C for 4 h. The content of the Teflon bombs was subsequently diluted with deionised water to 100 ml in a polypropylene volumetric flask. Standards were prepared using amounts of SiO_2 and TiO_2 equivalent to the amounts that were present in the zeolite sample.

3.3 Silanisation of the external surface of TS-1

3.3.1 Experimental apparatus

A flow system was used for the CVD of TEOS on TS-1, which has the advantage of removal of (potentially inhibiting) reaction products from the catalyst bed after reaction of TEOS with external surface sites. An additional advantage of a flow design is that excess (physisorbed) TEOS can efficiently be flushed from the reactor after the deposition cycle.

Figure 3.1 shows a schematic drawing of the experimental setup used for the silanisation of TS-1. All heated zones and the temperature ramping were PID controlled and the gas flow was regulated by mass flow controllers. All gases were dried before entering the system. The TEOS saturator was cooled to 15°C to avoid condensation of TEOS in the lines leading to the reactor. The up-flow operation ensured that the pressure drop over the reactor, filled with TS-1 powder, was within acceptable limits. To avoid potential contamination of the TS-1 catalyst with metal, the reactor was made of quartz glass and silanised glass wool was used to keep the catalyst bed in position.

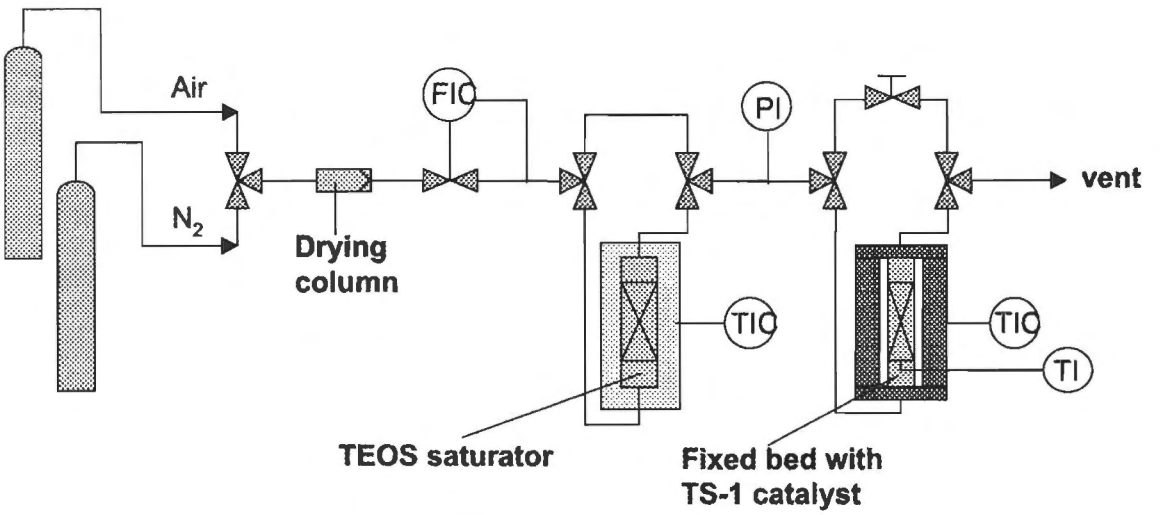

Figure 3.1: Experimental rig for external surface silanisation of TS-1

3.3.2 Experimental conditions and procedure

The external surface of small TS-1 crystals, synthesised according to the method described by Thangaraj et al. (1992), was silanised using a low temperature deposition of tetraethoxysilane (TEOS) [Röger et al. (1998)]. Nitrogen carrier gas (100 ml(NTP)/min) was led through a TEOS containing saturator at 15 °C. The TEOS-loaded carrier then passed through the TS-1 catalyst bed ($d_{crystal}$ = 0.1 μm) for 1 h at 100°C, the space velocity being 2.43 mg/(g·min). Subsequently, TS-1 was flushed with pure N_2 (100 ml(NTP)/min) for 15 min, heated in air (100 ml(NTP)/min) at 5 °C/min to 500°C, and kept at this temperature for 4 h. This procedure was repeated up to twenty times. Figure 3.2 shows the temperature-time profile of a CVD cycle.

3.4 Aromatic hydroxylation reactions

3.4.1 Experimental apparatus

The catalytic reactions were carried out in a 24 ml glass batch reactor equipped with a teflon sample port (mininert reactor) or a 100 ml reflux glass batch reactor with magnetic stirring (1000 rpm), immersed in a large silicon oil bath. The oil bath was placed on a magnetic stirrer/heater unit equipped with a thermocouple and a PID controller (temperature control within ± 0.5°C). The use of teflon sample ports with silicone septa as well as sample syringes with teflon valves ensured that samples were only in contact with glass and teflon and that evaporation was avoided.

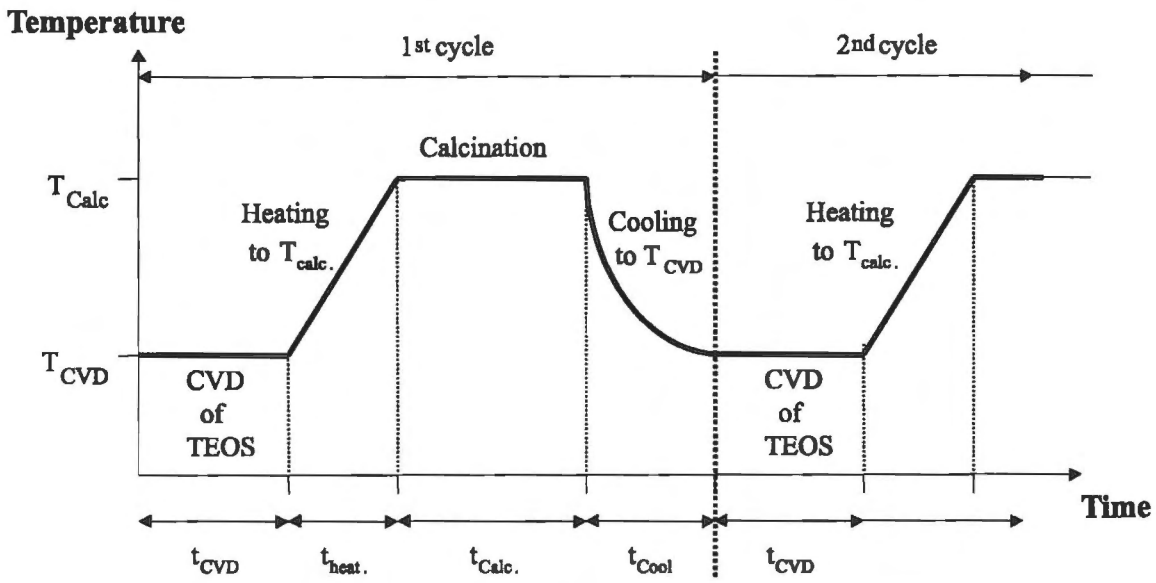

Figure 3.2: Temperature-time profile for CVD of TEOS on TS-1

3.4.2 Experimental conditions and procedure

All aromatic hydroxylation reactions were carried out at 60°C. Catalytic tests for the completion of the silanisation procedure were carried out in a 100 ml batch reactor fitted with reflux condenser. 1.2 g of phenol was dissolved in 30 g water, 0.12 g of small TS-1 crystals added, and the suspension allowed to attain adsorption equilibrium (stirring for 12 h at reaction temperature). All other hydroxylation reactions were carried out in a 24 ml mininert reactor (see above). After dissolution of 1.2 g of the aromatic substrate (phenol, anisole, toluene, 1-naphthol or 2-methyl-naphthalene) in 5 ml of the solvent (water, methanol or acetone), the catalyst (TS-1, Al-free Ti-beta or Ti-HMS) was added and adsorption equilibrium was attained at 60°C by allowing the suspension to stir for 12 hours before reaction.

For the hydroxylation of phenol, 0.12 g of catalyst was used, whereas for anisole and toluene hydroxylation, 0.18 g and 0.30 g catalyst were used, respectively. To start the reaction 4.6 mmol of H_2O_2, i.e. 0.6 g of a 30 wt % aqueous solution, was added in a single portion. In the hydroxylation of 1-naphthol and 2-methyl-naphthalene, 0.24 g of catalyst and 1.0 and 1.4 ml of H_2O_2 solution were used, respectively. 0.2 ml samples of the reaction mixture were withdrawn and analysed using HPLC. After reaction, the catalyst was recovered by filtration on a 0.45 μm Millipore filter, extensively washed with deionised water and dried at room temperature.

3.4.3 Analysis

It has been reported that HPLC analysis is generally a better choice for the analysis of reaction mixtures of aromatic hydroxylations with H_2O_2. A comparison between gas chromatography (GC) and high-performance liquid chromatography (HPLC) analysis of the reaction products in the phenol hydroxylation has been published by van der Pol et al. (1993), in which it was clearly shown that HPLC analysis is the preferred technique for analysing the reaction mixtures when hydrogen peroxide has not been completely converted. Para-benzoquinone was detected by GC analysis in high concentrations, whereas only small amounts were found using HPLC analysis, suggesting that residual H_2O_2 in the reaction mixture reacts in the high-temperature injector port of gas chromatographs and leads to the overoxidation of hydroquinone to para-benzoquinone. A very similar observation has been reported by Tuel and Ben Taarit (1994b), who also concluded that unreacted hydrogen peroxide leads to para-benzoquinone formation in the GC injector.

These findings were confirmed in this work; GC analysis results were dependent on the injector port temperature when phenol hydroxylation reaction mixtures still containing H_2O_2 were injected. The analysis method used in this work is thus HPLC analysis. Gas chromatography was occasionally used to compare the chromatograms obtained from HPLC to ensure that all products formed were detected by the diode array detector used for HPLC. The use of internal standards for TS-1/H_2O_2 catalyzed reactions is not recommended in the literature. Martens et al. (1993) concluded that internal standards such as pentafluorobenzoic acid might block active sites or reduce the accessibility of the micropores in the phenol hydroxylation over TS-1. No internal standard was therefore used in this work and the analytical equipment was regularly calibrated with standard solutions.

The analysis system used was a Beckman HPLC equipped with a C_{18} reverse-phase column (Luna) using acetonitrile/water mixtures and methanol/water mixtures as mobile phase and a Beckman 168 diode array detector operating at 280 nm. Analysis conditions for the various product mixtures are described in more detail in appendix E. The H_2O_2 content was monitored by means of a standard iodometric titration [Vogel (1959)].

Special attention had to be paid to the analysis of the toluene hydroxylation reaction mixtures. A mixture of cresols was obtained, which cannot be separated on standard columns by both HPLC or GC analysis. Unless specialised equipment is used (e.g. fatty acid capillary columns for GC), identical retention times for para- and meta-cresol were observed. A close look at results given in the literature reveals that this problem has occurred in many cases; high para-selectivities were often reported with no mention of formation of meta-cresol, suggesting that the para- and meta-isomers have not been separated [Bhaumik and Kumar (1995), Kumar and Bhaumik (1998)].

The addition of a complexing agent (in a procedure adopted and modified from Zukowski et al. (1985)), β-cyclodextrin, to the mobile phase resulted in a perfect separation of all cresol isomers

in HPLC analysis using a standard reverse-phase C_{18} column. The β-cyclodextrin molecule has a cavity with similar dimensions to the cresol isomers and strong interactions of the cresol isomers with β-cyclodextrin leads to a very good separation.

3.5 Adsorption studies of aromatic hydrocarbons on titanium-containing zeolites

3.5.1 Experimental apparatus

3.5.1.1 Liquid-phase chromatographic method

The adsorption of aromatics in TS-1 and Al-free Ti-beta was determined from water, methanol and acetone as solvents using a pulse chromatographic technique with standard HPLC equipment. The experimental set-up was the one used by Langhendries et al. (1999) and is shown in Figure 3.3.

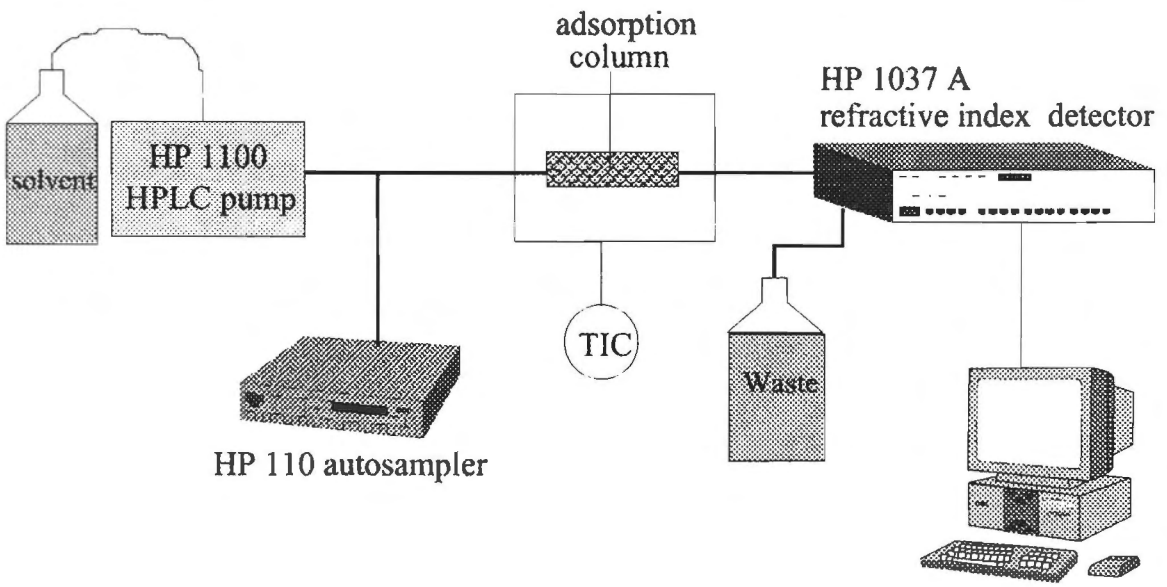

Figure 3.3: Experimental setup used for liquid-phase chromatographic adsorption measurements

To achieve a clear pulse-response without tailing, a good column packing without voids is essential. Columns for liquid-phase adsorption studies were carefully packed using HPLC pumps at high flow rates and pressures. Good column packing was confirmed by injection of 1,3,5-triisopropylbenzene, a tracer compound that cannot enter the zeolite pores. A sharp and symmetrical response peak was obtained. Figure 3.4 shows a stainless-steel adsorption column for liquid-phase adsorption experiments. Zeolite columns of 4 cm length and 0.4 cm I.D., previously dehydrated under vacuum at 300°C, were used for adsorption experiments.

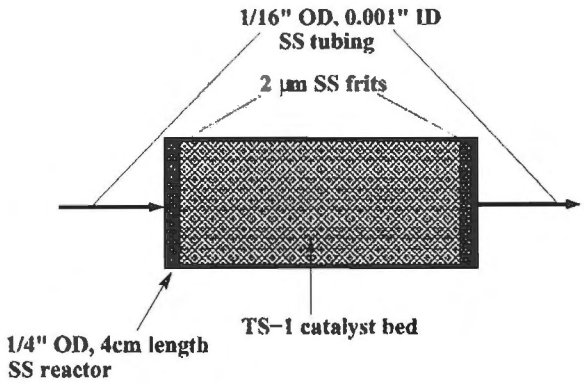

Figure 3.4: Column for liquid-phase adsorption experiments

3.5.1.2 Gas-phase chromatographic method

Pore mouth narrowing due to silanisation was investigated by a gas-phase chromatographic technique using an experimental set-up similar to that of Denayer and Baron (1998), taking cyclohexane, 2-methyl-pentane, 3-methyl-pentane, 2,3-dimethylbutane, n-hexane, and toluene as tracer components.

A scheme of the experimental setup is shown in Figure 3.5. Attention was paid to the packing

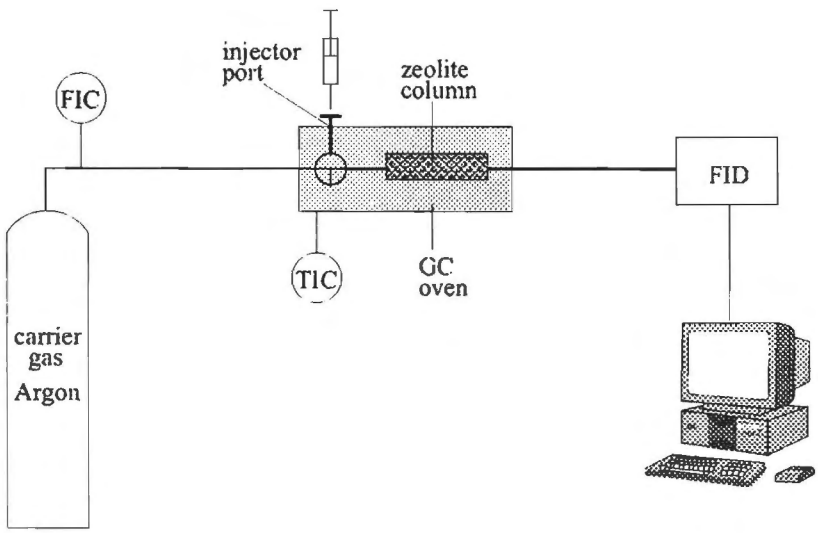

Figure 3.5: Experimental setup for gas-phase chromatographic adsorption measurements

of the adsorption columns: to ensure good reproducibility, pulse gas-phase adsorption experiments were repeated with repacked columns. Figure 3.6 shows a packed TS-1 column for pulse gas-phase adsorption experiments. A TS-1 bed of 1 cm length (0.05 g) was packed between chromatographic sand beds of 4 cm length in a 10 cm quartz glass tube of 0.4 cm I.D.

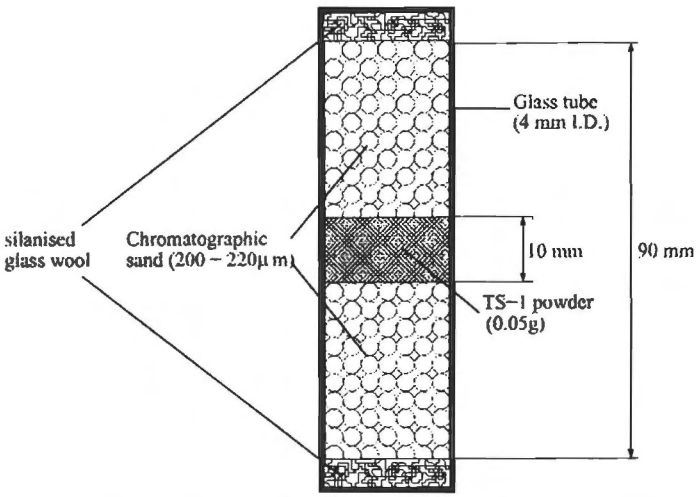

Figure 3.6: Adsorption column for gas-phase adsorption studies on parent and silanised TS-1

3.5.1.3 Liquid-phase batch method

A batch setup identical to the one used for aromatic hydroxylation reactions was used to determine the partition coefficient, α, as the ratio of adsorbed aromatic in the molecular sieve and solvent phase. Sample analysis was done using a HP 5890 GC equipped with FID and TCD detectors.

3.5.2 Experimental conditions and procedure

In the liquid-phase batch adsorption method, 0.1 g of zeolite catalyst was suspended in a solution of 1.2 g phenol and 5 ml solvent at 25°C. A liquid sample (0.2 ml) was taken after adsorption equilibrium was established (24 h).

For gas phase pulse adsorption studies, a hydrocarbon pulse (typically 1-4 μmol of hydrocarbon vapour in argon) was injected in a carrier gas (argon, 30 ml(NTP)/min), which was led over a 1 cm column (4 mm internal diameter) containing 0.05 g of parent or inertised zeolite powder. The column was mounted in a GC equipped with FID detector. The response on the pulse was monitored at temperatures ranging from 175-275 °C and the shift in the first and second moments of the peaks were taken as a measure for changes in the sorption behaviour of TS-1 on inertisation.

For liquid-phase pulse adsorption studies, 2-5 μl of saturated aromatic solution was injected in the pure solvent carrier (water, methanol and acetone) with flow rates between 0.01 and 0.5 ml/min, which was led over the zeolite column (TS-1 and Al-free Ti-beta). The column was mounted in a temperature-controlled compartment and the pulse response monitored at temperatures ranging from 30 - 60°C. Henry's adsorption constants were calculated from the response peaks first moments.

3.6 Liquid-phase measurement of intracrystalline diffusivities of aromatic hydrocarbons in titanium-containing zeolites

3.6.1 Experimental apparatus

Figure 3.7 shows a sketch of the experimental apparatus used for the ZLC diffusion measurements. Special care was taken to minimise dead volumes. All lines were of 0.007" I.D. stainless steel tubing

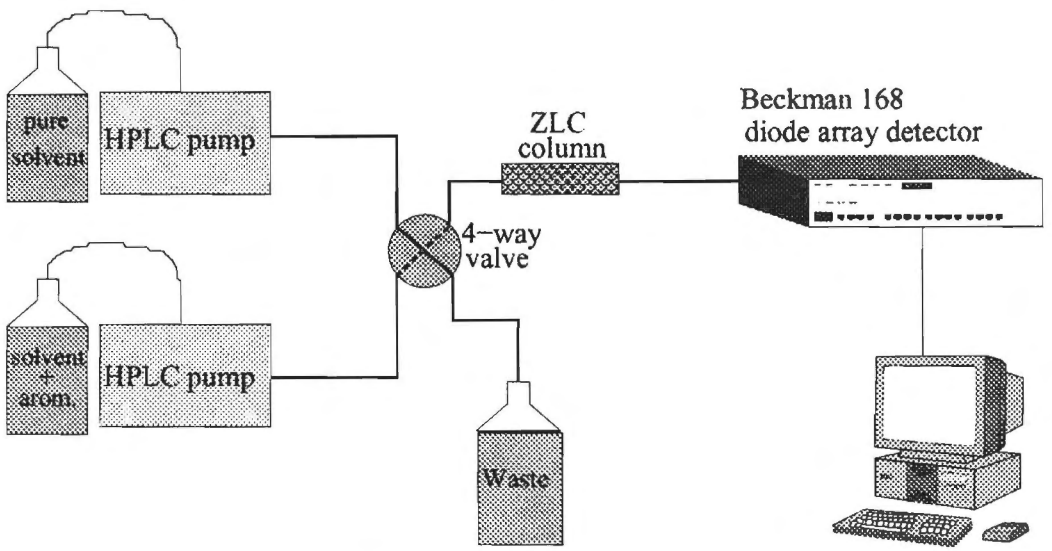

Figure 3.7: Liquid-phase ZLC rig

and as short as the experimental setup allowed. The dead volume of the diode array detector used is negligible. The adsorption column was immersed in a large PID controlled oil bath to ensure isothermal conditions. A schematic drawing of a column used for ZLC and pulse diffusion studies is given in Figure 3.8.

3.6.2 Experimental conditions and procedure

The transient desorption curves of phenol, catechol, hydroquinone, toluene and anisole were measured with water and methanol as the solvent at temperatures ranging from 0 - 80°C. Catalyst amounts of 70 mg (TS-1 and Al-free Ti-beta) were used in ZLC columns. Flow rates were varied between 0.5 and 3 ml/min to ensure that the monitored response curves were not governed by interstitial fluid hold-up or axial dispersion. Additional blank experiments with no catalyst in the reactor confirmed this assumption and the dead time of the system was measured at different flow rates. The independence of the transient desorption curve of concentration was confirmed by variation of the initial concentration of the aromatic compound from 0.1-1 wt.%. Identical desorption

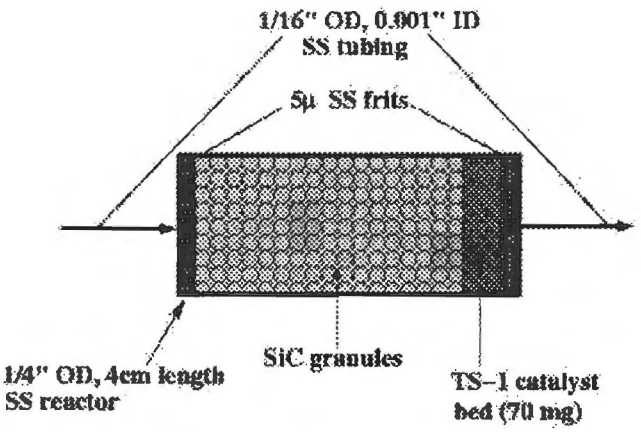

Figure 3.8: ZLC column

curves in the long-time region were taken as a proof that the isotherm was indeed in the linear region.

Chapter 4

Results

4.1 Physical and chemical catalyst characterisation

Additional characterisation data for the catalyst batches used in this work are shown in appendix C.

4.1.1 Synthesised titanium-containing molecular sieves

All synthesised TS-1 and Al-free Ti-beta samples showed their typical structural X-ray diffraction patterns (see Figure C.1-C.3) and were 100 % crystalline, Table 4.1 summarises the results from powder X-ray diffraction measurements. The XRD patterns of all samples are given in Appendix C. The large TS-1 crystals showed very sharp and intense reflections, whereas the XRD pattern of the

Table 4.1: Relative crystallinities of catalysts used

Catalyst	relative crystallinity [%][1]		
	as-synthesised	calcined	recycled
TS-1 small[2]	100	100	100
TS-1 large[3]	100	100	100
Al-free Ti-beta[4]	100	95	95

[1]± 5%, based on peak areas of most intensive reflections; intensity of large TS-1 crystals and large Al-free Ti-beta crystals were taken as a reference for 100% crystallinity; [2]$d_{crystal}$ = 0.1 μm; [3]$d_{crystal}$ = 3×10×45 μm; [4]$d_{crystal}$ = 0.9 - 5 μm

dealuminated zeolite beta seeds was not well resolved and shows line broadening due to the nano-size of the crystals. The Ti-HMS sample showed the typical reflections for MCM-type materials at low angles of 2Θ; these reflections were however relatively weak suggesting that amorphous material was also present in this sample. For Al-free Ti-beta, a partial loss of crystallinity after reaction or exposure to water has been reported by Carati et al. (1999). However, a different synthesis method was used in that study, resulting in a much more hydrophilic Al-free Ti-beta sample. The higher

hydrophilicity might facilitate framework disintegration by interaction with polar compounds such as water. The Al-free Ti-beta samples used in this work were synthesised using the fluoride method. They have been reported to be very hydrophobic [Blasco et al. (1998)]. No loss of crystallinity was detected when the catalysts were used for several (3-5) reaction cycles (aromatic hydroxylation reactions under standard conditions and subsequent calcinations), confirming the stability of the zeolite framework under reaction conditions. The only loss of crystallinity observed was a $\approx$ 5% decrease in crystallinity upon calcination for the Al-free Ti-beta.

The phase purity of all catalyst samples used for reaction work was proven by UV-VIS diffuse reflectance spectroscopy. The spectra of small and large TS-1 crystals, Al-free Ti-beta and Ti-HMS are shown in Figure 4.1. For comparison, the spectrum of anatase is added. The two TS-1 samples

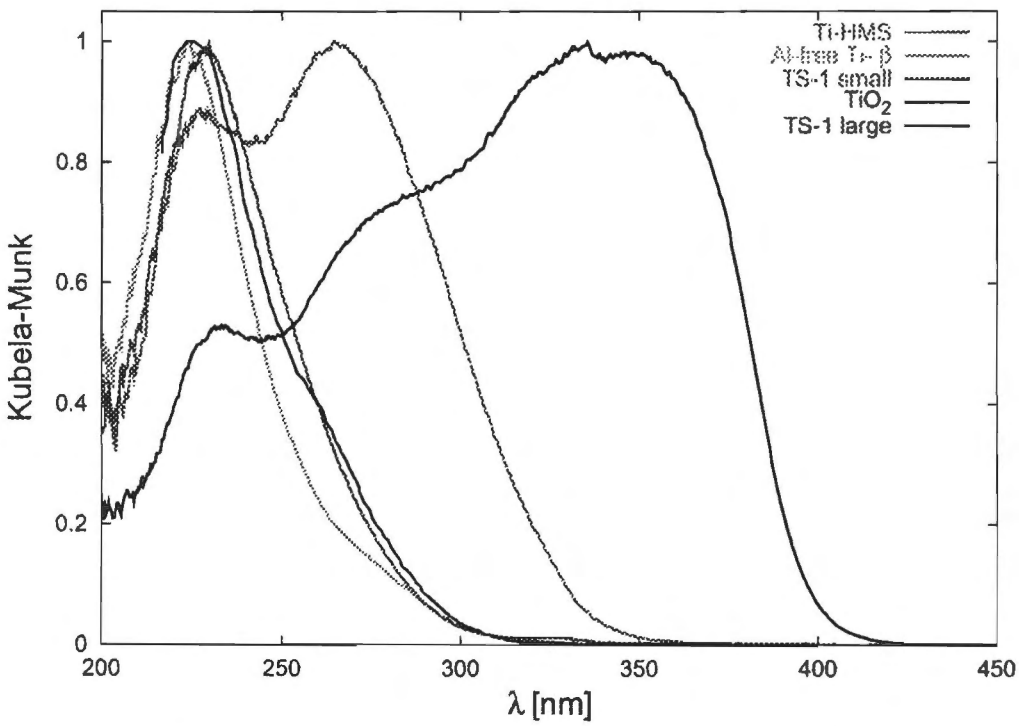

Figure 4.1: Normalised diffuse reflectance UV-VIS spectra

used in this work and Al-free Ti-beta show a single absorption band at 215-220 nm, generally assigned to titanium in tetrahedral coordination. For Ti-HMS, a significant amount of hexacoordinated titanium was present. The sample was, however, not dehydrated. Water is easily coordinated to the titanium sites in mesoporous titanosilicates due to their hydrophilicity, resulting in higher coordination for a fraction of the titanium sites upon uptake of water. Comparing the spectrum of Ti-HMS to a typical DR UV-VIS spectrum of anatase, it can be assumed that the Ti-HMS sample was also free of (bulk) TiO_2, but the presence of some inherently hexacoordinate Ti species cannot be excluded.

The results of the BET measurements are in good agreement with literature data [Blasco et al. (1998), Ferrini and Kouwenhoven (1990), Tanev et al. (1994), Zhang et al. (1995)]. Table 4.2 shows the micropore volumes and BET surface areas of the catalyst samples used for reactions. For Al-free Ti-beta and both TS-1 samples, BET measurements indicated no significant presence of mesopores. For Ti-HMS, an average pore size of 2.8 nm was determined by BET plots. For the small TS-1

Table 4.2: BET micropore volumes and surface areas of catalyst samples

Catalyst	micropore volume $[\frac{cm^3}{g}]$	total BET area $[\frac{m^2}{g}]$	external surface area $[\frac{m^2}{g}]$
TS-1 small[1]	0.176	442	82
TS-1 small (sil.)[2]	0.169	460	86
TS-1 large[3]	0.188	422	5
Al-free Ti-beta[4]	0.241	574	8
Ti-HMS	0.931	1097	-

[1]TS-1 of $d_{crystal}$ = 0.1 μm; [2]small TS-1 crystals after CVD of TEOS for 20 cycles; [3]TS-1 of $d_{crystal}$ = 3×10×45 μm; [4]Al-free Ti-beta of $d_{crystal}$ = 2 - 5 μm

crystals only ca. 82% of the total surface area is located in the pores of the crystal whereas the larger TS-1 and the Al-free Ti-beta crystals have 98.5% of their Ti sites inside the pores. This indicates that the external surface could have a much higher influence on the catalytic properties for the small crystals, one of the major aspects investigated in this work.

Scanning electron micrographs of the small TS-1 crystals show a 'cauliflower' morphology with an average diameter of 0.1 μm and a very narrow size distribution. The large crystallites of TS-1 were slab-shaped with dimensions of about 45×10×3 μm with little intergrowth. Only minor amounts of nano-sized crystallites were present in the sample. The large and small crystallites (obtained from non-seeded and seeded synthesis) of Al-free Ti-beta were well faceted truncated bipyramids of 2 - 5 μm and 0.9 μm, respectively. SEM pictures of the dealuminated zeolite titanium beta seeds show very small crystals of about 30 - 50 nm, whereas only amorphous structures are visible on SEM pictures of Ti-HMS. Figures 4.2 - 4.5 show Scanning Electron Micrographs of the catalyst batches synthesised.

The chemical composition of all catalysts was determined by AAS of the dissolved catalysts and EDX analysis of the solids. Both measurements were in agreement within the error of analysis. All samples showed a similar titanium content; a Si/Ti-ratio of 33, 42 and 50 was found for the TS-1 samples, the Al-free Ti-beta samples and the Ti-HMS sample, respectively.

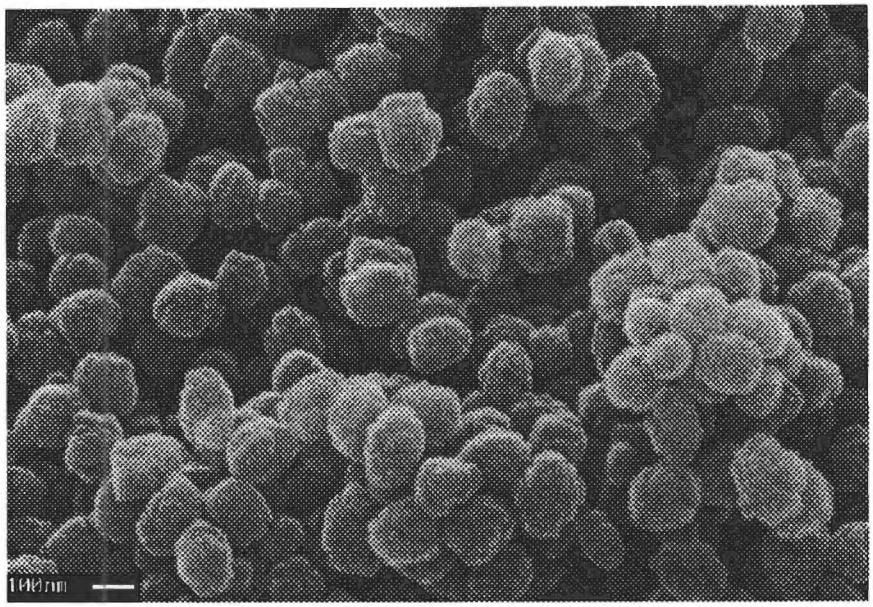

Figure 4.2: SEM picture of small TS-1 crystals

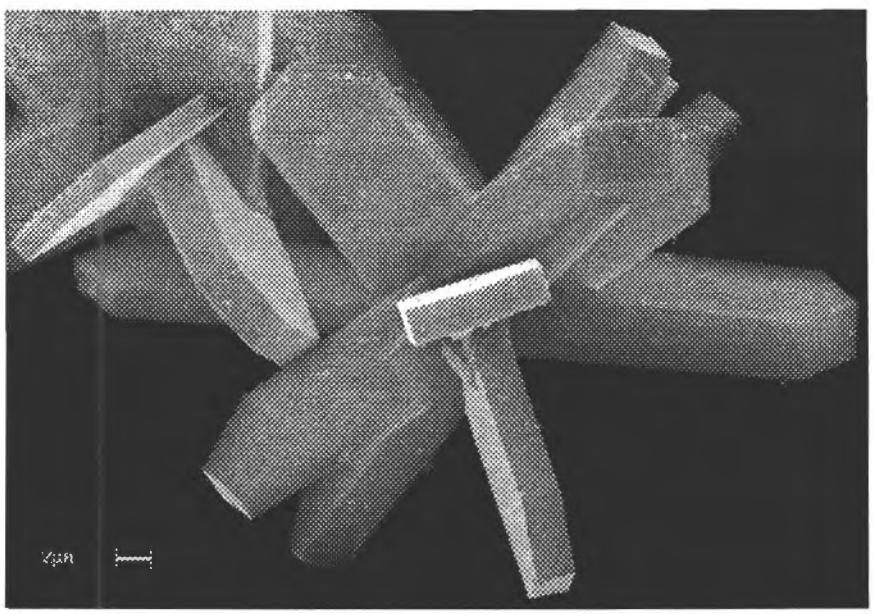

Figure 4.3: SEM picture of large TS-1 crystals

4.1.2 Characterisation of external surface Inertisation by cycle-wise CVD of TEOS

4.1.2.1 Physico-chemical characterisation of modified TS-1

The physico-chemical characterisation of the small TS-1 crystals silanised for 20 cycles (using the CVD of TEOS deposition technique) was compared to the parent, non-modified sample.

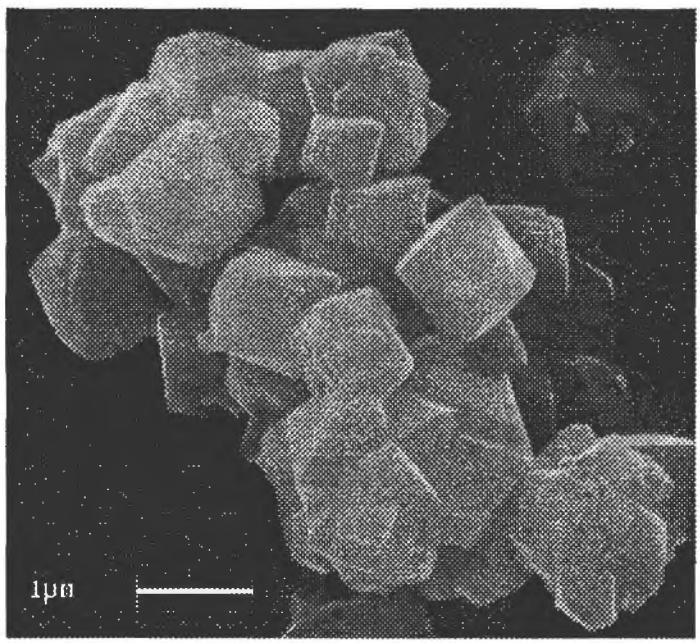

Figure 4.4: SEM picture of small crystals of Al-free Ti-beta

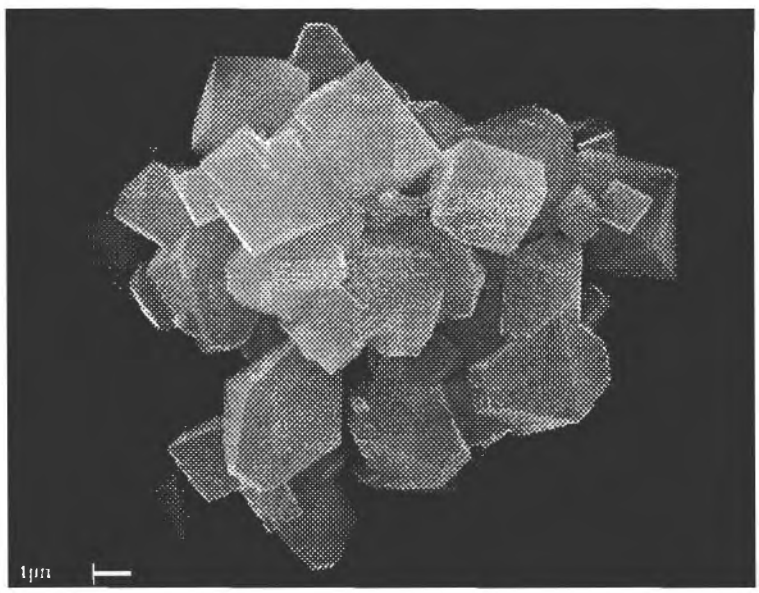

Figure 4.5: SEM picture of large crystals of Al-free Ti-beta

XRD diffraction patterns and diffuse reflectance UV-VIS spectra for parent and silanised TS-1 were identical. IR spectra also essentially remained unchanged.

SEM pictures of parent and silanised TS-1 samples also showed no change, indicating that the agglomeration degree of the small crystallites remained unchanged.

BET measurements also showed no significant change, pointing to the absence of major pore

blocking upon silanisation. Pore mouth blocking or -narrowing upon silanisation is further studied and discussed in section 5.3.3.1.

EDX of parent and silanised TS-1 showed an increase of the average Si/Ti-ratio from 33 to 60, confirming the increase of the Si/Ti-ratio of the external rim of the crystals and thus the deposition of silica on the external surface.

4.1.2.2 Thermogravimetric study of CVD of TEOS on TS-1

The TEOS uptake by TS-1 and the amount deposited after one deposition cycle was determined using a thermogravimetric setup. Figure 4.6 shows the change in sample mass with time during a typical TEOS deposition cycle. Adsorption and desorption steps in the TG/DTA setup were carried

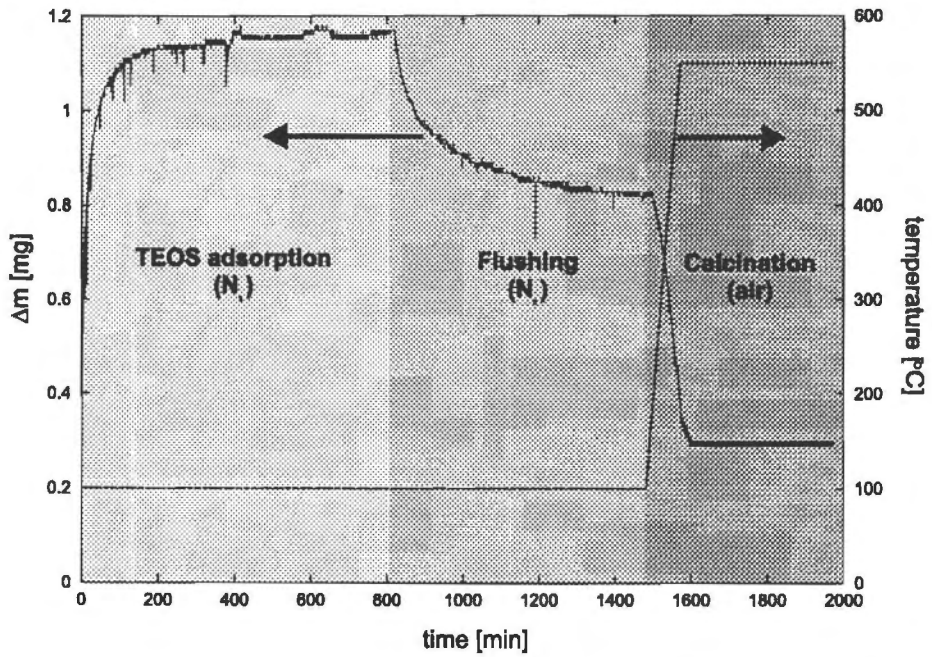

Figure 4.6: Thermogravimetric profile of a CVD of TEOS cycle on small TS-1 crystals
T = 100 - 500 °C, F = 30 ml/min, m_{cat} = 52 mg, WHSV = 2.43 $mg_{TEOS}/(g_{cat} \cdot min)$

out for longer times than in the experimental CVD of TEOS setup since in the TG/DTA setup the carrier gas passes over the sample as opposed to through the catalyst bed. Temperatures and TEOS partial pressure were identical to the ones used for silanisation.

TEOS was first adsorbed onto the TS-1 sample (52 mg) until adsorption equilibrium was attained. The system was then flushed with pure N_2 carrier to purge the TG/DTA setup and to desorb physisorbed TEOS from the sample. After the completion of the desorption step, the TEOS-loaded sample was calcined in air.

Assuming a diameter of 0.96 nm for the TEOS molecule, the coverage of the external surface

during a CVD cycle can be estimated from the thermogravimetric data. After the desorption step, the TEOS amount chemisorbed corresponds to a theoretical coverage of ≈ 40 % of the external surface. After calcination, the mass gain was ≈ 0.4 %, proving the deposition of SiO_2 on the TS-1 external surface. The thermogravimetric study presented in Figure 4.6 shows that the deposited amount does not correspond to a full monolayer, explaining the necessity for a repetition of the CVD cycle. The amounts deposited in subsequent CVD cycles are however unknown; the thermogravimetric study therefore only represents an estimation for the TEOS adsorption and, after calcination, SiO_2 deposition at the external surface.

4.1.2.3 Gas-phase adsorption properties of progressively silanised TS-1

As described earlier (see section 2.6.1), CVD of silanes on zeolites can lead to a (partial) blocking or narrowing of the micropores, depending on the CVD conditions. The gas-phase chromatographic setup used in this work is a suitable technique to characterise pore mouth narrowing due to silanisation [Sealy and Möller (1998)]. The injection of tracer compounds with a kinetic diameter similar to the pore openings yields information about the accessibility of the pores and about additional diffusional resistances that could be caused by the silanisation procedure. After injection of a small pulse of the tracer compound, the first and second moment of the response can be used to calculate the Henry's constant and the peak asymmetry, respectively. Significant changes in the Henry's constant would indicate that the adsorption properties were altered, the extreme case being that the tracer is no longer able to enter the pores of the zeolite, whereas an increasingly asymmetrical peak response would indicate the presence of increased diffusional resistances.

The peak response was determined with 2-methyl-pentane, 3-methyl-pentane, 2,3-dimethylbutane, cyclohexane and toluene as tracer components at temperatures from 175 °C to 275 °C. Using equation 2.1 and 2.4, the first moment of the response and the activation energy for adsorption can be determined, respectively. Figure 4.7a shows typical peak responses for the compounds injected into the TS-1 adsorption columns and Figure 4.7b shows the van't Hoff plots calculated from the peak first moments at different temperatures. A perfectly linear van't Hoff plot as shown in Figure 4.7b was obtained for all compounds with all catalyst samples, confirming the suitability of the the experimental setup.

In Figure 4.8a and 4.8b the adsorption constants and the peak variances are plotted as a function of the number of silanisation cycles.

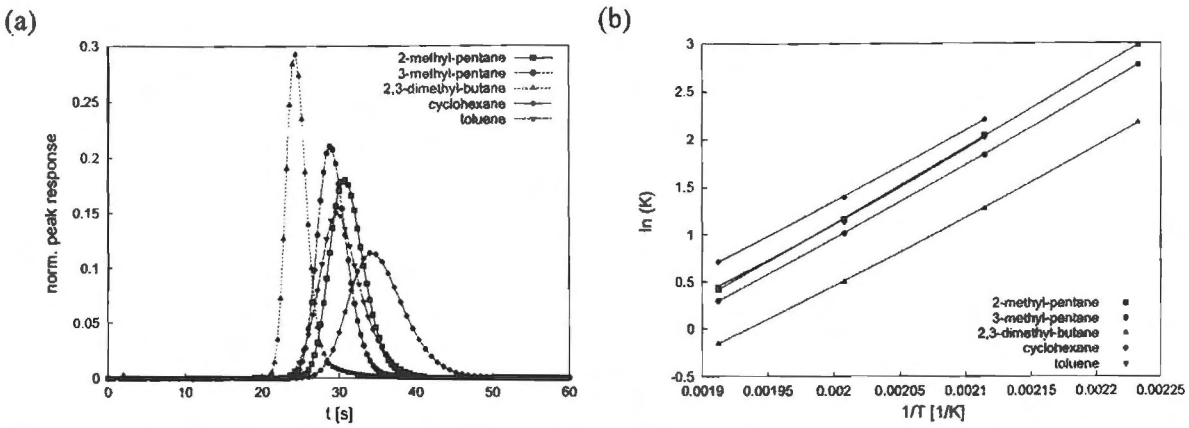

Figure 4.7: (a) typical pulse response (T = 225 °C) and (b) van't Hoff plots from pulse response first moments of tracer compounds injected into parent TS-1 ($d_{crystal}$ = 0.1 μm)

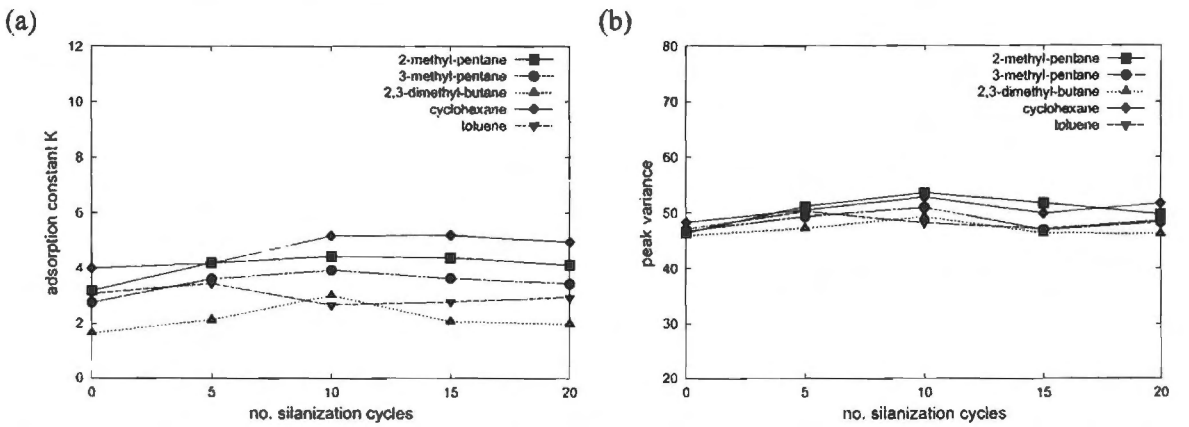

Figure 4.8: (a) adsorption constants and (b) peak variance of injected tracer compounds (T = 225 °C) as a function of the number of silanisation cycles of TS-1 ($d_{crystal}$ = 0.1 μm)

4.2 Hydroxylation of substituted benzenes using titanium-substituted molecular sieves and H_2O_2

4.2.1 External mass transfer resistance

If the mass transport to and from the outer surface of the catalyst particle to the bulk solution is rate limiting, it is generally referred to as external mass transfer resistance. It is caused by a slow diffusion of reactants in the bulk liquid phase to the outer surface of the catalyst and can be important if a relatively fast reaction occurs at the catalyst surface. Although usually much smaller than the internal mass transfer resistance in porous particles, a brief evaluation of the external resistance to mass transfer for the reactions investigated in this work is given below.

One of the general approaches to describe external diffusional resistance is the so-called film

model, where a stagnant boundary layer around the catalyst particle is assumed to exist. With a linear concentration gradient in this film, the diffusional flux to the catalyst surface is given by

$$\vec{j_s} = k_f(C - C_s) \ , \quad with \ k_f = \frac{D_m}{\delta_f} \tag{4.1}$$

where δ_f is the film thickness, D_m the diffusivity in the liquid phase, C the reactant concentration in the bulk solution, C_s the reactant concentration at the catalyst surface and k_f the mass transfer coefficient. Whereas the film thickness δ_f is generally unknown, the mass transfer coefficient k_f can be described by the Sherwood number, which equals 2.0 for a laminar flow around a spherical particle:

$$Sh = \frac{k_f d}{D_m} \approx 2 \tag{4.2}$$

Under flow conditions such as a well-stirred reaction vessel, the Sherwood number is expected to be much larger, hence the equation above represents the 'worst case' in terms of external mass transfer. Equating the steady state flux of the reactant through the external film to the rate of reaction within the particle ($\vec{js} = \vec{jc}$) yields

$$4\pi R_c^2 k_f(C - C_s) = \frac{4}{3}\pi R_c^3 \eta k_{react} C_s C_{H_2O_2} \tag{4.3}$$

which can be rearranged to

$$\frac{C_s}{C} = \frac{k_f}{k_f + \frac{R_c}{3}\eta k_{react} C_{H_2O_2}} \tag{4.4}$$

External mass transfer resistance can therefore not be neglected if the ratio of the surface reactant concentration to the bulk solution reactant concentration (C_s/C) is significantly lower than unity. With R_c = 0.05 μm (small TS-1 crystals) - 1.5 μm (large TS-1 or Al-free Ti-beta crystals) and $D_m \approx 10^{-9}\frac{m^2}{s}$, the lowest value of k_f is $\approx 0.0013 \ \frac{m}{s}$. With typical values for observed reaction rates and hydrogen peroxide concentrations in this work, the lowest value of C_s/C practically equals unity, confirming the absence of external mass transfer resistances in the reactions investigated.

4.2.2 Kinetic model

A kinetic study was conducted using the concentration-time data obtained from the hydroxylation reactions, applying a simplified reaction scheme as displayed in Figure 4.9. Severe deactivation of TS-1 has been reported in epoxidation reactions in the literature [Langhendries et al. (1999)]. Rate constants for this reaction were determined from initial reaction rates. For aromatic hydroxylations, a slight deactivation through formation of high-molecular compounds (tars) was observed, though

by far not as severe as for epoxidation reactions. This was taken into account by weighting of initial concentration-time data.

The data obtained for the hydroxylation of phenol, anisole and toluene were fitted in concentration-time profiles with following kinetic expressions:

$$\frac{dC_{MB}}{dt} = -k_1 C_{MB} C_{H_2O_2} \tag{4.5}$$

$$\frac{dC_{H_2O_2}}{dt} = -k_1 C_{MB} C_{H_2O_2} - k_2 C_{H_2O_2}^2 - k_6 C_{H_2O_2} C_O - k_7 C_{H_2O_2} C_M - k_8 C_{H_2O_2} C_P \tag{4.6}$$

$$\frac{dC_O}{dt} = -k_3 C_{MB} C_{H_2O_2} - k_6 C_{H_2O_2} C_O \tag{4.7}$$

$$\frac{dC_M}{dt} = -k_4 C_{MB} C_{H_2O_2} - k_8 C_{H_2O_2} C_M \tag{4.8}$$

$$\frac{dC_P}{dt} = -k_5 C_{MB} C_{H_2O_2} - k_7 C_{H_2O_2} C_P \tag{4.9}$$

$$k_T = k_1 - k_3 - k_4 - k_5 \tag{4.10}$$

Equation 4.5 represents the consumption of the aromatic reactant either to hydroxylated products or tars. The consumption of the second reactant, hydrogen peroxide, is described by equation 4.6; non-selective peroxide decomposition and overoxidation of hydroxylated products are taken into account by additional second-order terms. Formation of ortho-, meta- or para-hydroxylated products is fitted with the kinetic expressions 4.7, 4.8 and 4.9, respectively; overoxidation is taken into account using the same additional terms as in equation 4.6. The kinetic model used in this work is simplified and based on the reaction scheme in Figure 4.9, which shows the simplified reaction paths with the rate constants used for fitting the reaction data. In the phenol and anisole hydroxylation, no meta-hydroxylated products were observed, thus the constants k_5 and k_8 equal zero for these reactions.

A good fit was obtained for all experiments, showing that the overall second-order kinetic model describes the reaction well. The choice of the kinetic model and the reaction order is further elaborated in appendix F.1. However, a high error was found for the rate constants for subsequent overoxidation of the hydroxylated products (k_6-k_8). The rate constant representing tar formation was thus obtained by subtracting the product formation rate constants from the reactant consumption rate constant as shown in equation 4.10.

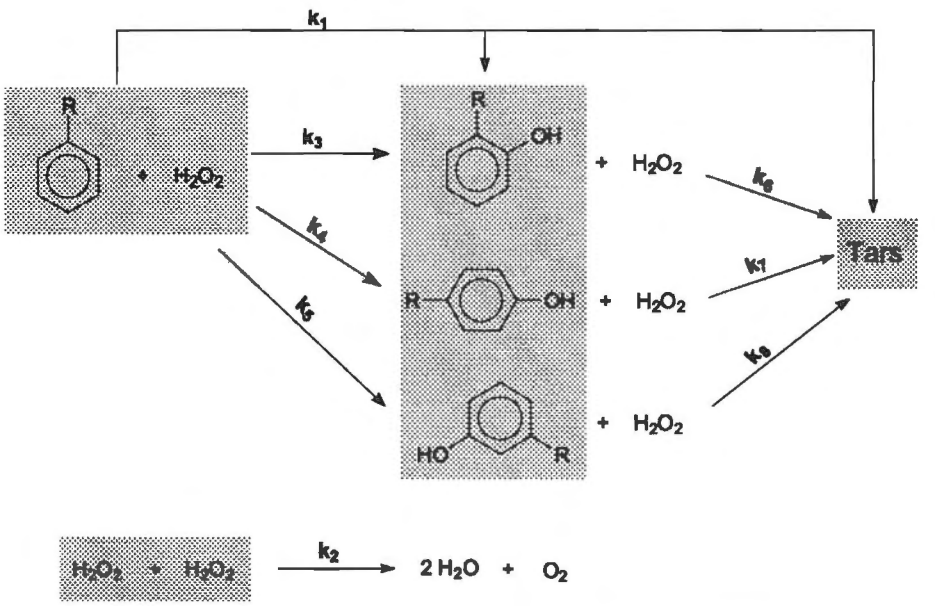

Figure 4.9: Reaction scheme of aromatic hydroxylations

4.2.3 Reaction kinetics for progressively silanised TS-1

The external surface of small TS-1 crystals was deactivated using the cycle-wise CVD of TEOS technique. The progressive surface deactivation through deposition of SiO_2 was monitored by removing the catalyst from the silanisation setup for a catalytic test reaction. The phenol hydroxylation in water was chosen as the test reaction to monitor the deactivation after a number of silanisation cycles. Figure 4.10 shows a plot of the kinetic constants obtained (applying the model described in paragraph 4.2.2) as a function of the number of CVD cycles. Only relatively small changes in the rate constants (within the error of the method) were observed between 15 and 20 cycles of TEOS deposition. It was thus assumed that the role of the external surface can be neglected after 20 cycles, *i.e.* the observed activity is then solely due to the activity of TS-1 in the pores.

On the basis of the rate constants obtained for parent and external surface inertised TS-1 (after 20 cycles of TEOS deposition), the contribution of the external surface to the overall catalytic activity can be determined. The contribution of the external surface activity and the contribution of the sites in the pore system of TS-1 can be evaluated as follows:

$$k_n S = k_{n,i} S_{int} + k_{n,e} S_{ext} \tag{4.11}$$

$$S = S_{int} + S_{ext} \tag{4.12}$$

For the small TS-1 crystals, the total surface area (S) and the external surface area (S_e) were

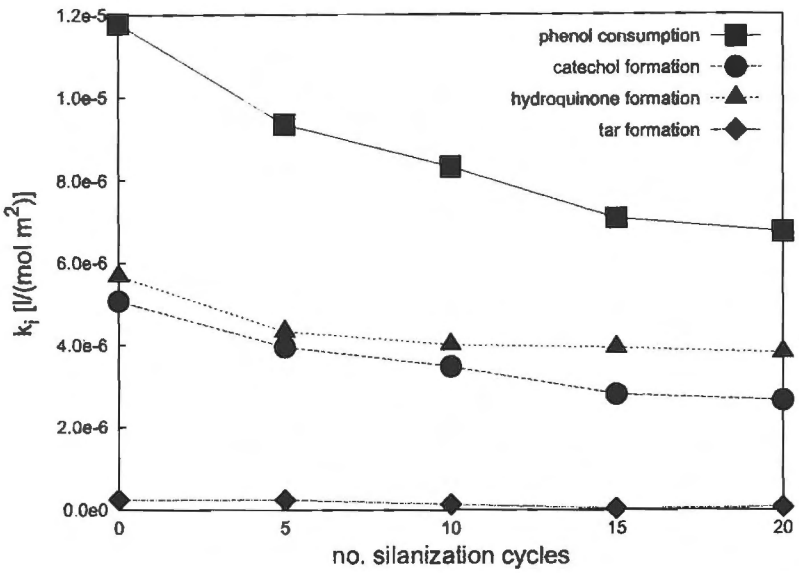

Figure 4.10: Overall rate constants as a function of the number of silanisation cycles for the phenol hydroxylation

T = 60 °C, 1.2 g phenol, 30 ml water, 0.12 g TS-1 ($d_{crystal}$ = 0.1 μm), 0.6 ml H_2O_2 (30 % soln. in H_2O)

determined to be 442 m^2/g and 82 m^2/g, respectively (from BET measurements, see Table 4.2). Rate constants determined from experiments with the parent TS-1 sample (k_n) represent total (internal + external) activity whereas rate constants from experiments with the silanised sample ($k_{n,i}$) were assigned exclusively to internal activity.

4.2.4 Decomposition of hydrogen peroxide

The non-selective reactions of H_2O_2 under typical reaction conditions, but in the absence of the aromatic reactant were quantified in the solvents used for reaction studies. Table 4.3 shows the non-selective conversion of H_2O_2 with TS-1 and Al-free Ti-beta in water, methanol and acetone and data for homogeneous (thermal) decomposition. The homogeneous decomposition of hydrogen peroxide under reaction conditions was negligible. However, with no other reactant in the system, the peroxide loss in the presence of small TS-1 crystals and Al-free Ti-beta was significant. Particularly in water, H_2O_2 was rapidly decomposed to O_2 and H_2O. The decomposition reaction was presumably also responsible for the loss of H_2O_2 in acetone, whereas titanium silicalites catalyze the oxidation of methanol to a mixture of formaldehyde, formic acid, dimethyl ether and CO/CO_2 as described by Deo et al. (1993), Maspero and Romano (1994) and other authors. Oxidation of the solvent is therefore an additional non-selective reaction of H_2O_2 in methanol, although Table 4.3 demonstrates that the reaction proceeds at a low rate as also reported by Maspero and Romano (1994). Table 4.3

Table 4.3: Non-selective conversion of H_2O_2 over TS-1 and Al-free Ti-beta in the absence of aromatic reactants

Solvent	water		methanol		acetone	
Catalyst	$X_{H_2O_2}$[%] after 4h	$X_{H_2O_2}$[%] after 8h	$X_{H_2O_2}$[%] after 4h	$X_{H_2O_2}$[%] after 8h	$X_{H_2O_2}$[%] after 4h	$X_{H_2O_2}$[%] after 8h
blank[1]	0.5	0.9	-	-	-	-
TS-1(small)[2]	40.0	62.5	25.9	46.0	15.2	28.9
TS-1(large)[3]	29.2	42.9	3.2	6.8	4.1	7.3
Al-free Ti-β[4]	54.4	96.1	28.6	46.8	14.0	21.5

T = 60°C, 0.12 g catalyst, 5 ml solvent, 0.6 ml H_2O_2 (30% in H_2O); [1]same conditions, but without catalyst; [2]$d_{crystal}$ = 0.1 μm;[3]$d_{crystal}$ = 3×10×45 μm; [4]$d_{crystal}$ = 0.9 μm

also shows that small TS-1 and Al-free Ti-beta crystals had similar activities for non-selective H_2O_2 reactions except for the reaction in water, where Al-free Ti-beta showed a very high activity for the decomposition of the peroxide. Large TS-1 crystals showed a lower rate of H_2O_2 decomposition than the smaller TS-1 crystals and Al-free Ti-beta. Only in water, large amounts of the peroxide were decomposed; in methanol and acetone, remarkably little peroxide was lost in the presence of large TS-1 crystals. For all catalysts, the reactivity decreased in the order water > methanol > acetone. Similar results have been reported by Trong On et al. (1997), Trong On et al. (1998) and Gallot and Kaliaguine (1997), who described the activity of silanol groups at the surface of titanium-containing zeolites for the decomposition of hydrogen peroxide.

4.2.5 Phenol hydroxylation

In Figure 4.11, the typical concentration-time profiles of reactants and products, as well as the fit of the kinetic model applied (equations 4.5-4.10) are given for the hydroxylation of phenol over TS-1. A good model fit was achieved not only in the initial region but for the entire concentration-time profile, indicating that catalyst deactivation did not significantly affect the kinetics of the phenol hydroxylation carried out as a batch reaction in this work. Reactions in other solvents showed similar good fits, justifying the overall second-order kinetic model used to determine kinetic reaction data. The only reaction products detected were hydroquinone, catechol and tars; only trace amounts of resorcinol (meta-hydroxy-phenol) or para-benzoquinone were observed. A typical chromatogram obtained from the HPLC analysis of a phenol hydroxylation reaction mixture is displayed in appendix E.1.

4.2.5.1 Influence of the H_2O_2 concentration

In section 2.3.1, the dependence of peroxide efficiency and product distribution on the method of peroxide addition was described. Thangaraj et al. (1991a) reported higher peroxide efficiencies and

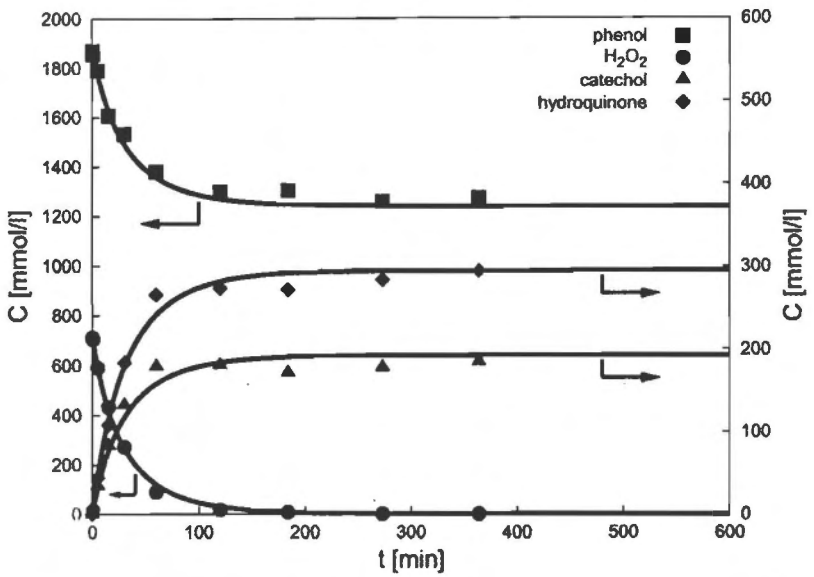

Figure 4.11: Concentration-time profile in the phenol hydroxylation over TS-1

T = 60 °C, 1.2 g phenol, 5 ml water, 0.12 g TS-1 ($d_{crystal}$ = 0.1 μm), 0.6 ml H_2O_2 (30 % soln. in H_2O)

hydroquinone selectivities using a drop-wise addition of the H_2O_2 solution as compared to an addition of the whole amount in one portion. However, the different methods of H_2O_2 addition were not compared under the same reaction conditions in their study. Table 4.4 shows the results for a phenol hydroxylation reaction over TS-1 in water using different methods of peroxide addition. In 'dilute'

Table 4.4: Influence of the method of H_2O_2 addition

	X_{phenol} [%]	$X_{H_2O_2}$[%]	S_{Phenol}[4][%]	H_2O_2 eff. [%]	$\frac{p}{o}$-ratio[4]
dropwise addition[1]	28.0	100	90	79	1.42
addition in one lot[2]	27.9	100	91.8	78	1.13
addition in one lot[3]	30.3	100	78	71	1.59

T = 60 °C, 30 ml H_2O, 1.2 g phenol, 0.12 g TS-1 ($d_{crystal}$ = 0.1 μm), 0.6 ml H_2O_2 (30% in H_2O), t_R = 6 h; [1]H_2O_2 was diluted with 2 ml H_2O and added over 35 min; [2]H_2O_2 was diluted with 2 ml H_2O and injected in one portion; [3]5 ml H_2O as solvent; [4]at X_{phenol} = 28 %

conditions (i.e. with 30 ml solvent), a drop-wise H_2O_2 addition resulted in a higher p/o-ratio, suggesting that low concentration levels of hydrogen peroxide favour hydroquinone formation. However, at higher concentrations of all reactants (i.e. with 5 ml solvent), more hydroquinone was formed and the selectivities were lower when the entire H_2O_2 amount was added in one portion. These phenomena are very likely to be related to the different rates of polymerisations of hydroquinone and catechol. The primary overoxidation products of the dihydroxybenzenes are the respective benzoquinones, which can subsequently undergo a large variety of coupling reactions as described by

Taylor and Battersby (1967) and Patai (1974), eventually leading to the formation of high-molecular compounds, e.g. tars. Whereas the para-benzoquinone formation was hardly observed in this work and was reported to be partly reversible in phenol hydroxylations catalyzed by aluminium-containing zeolites [Allain et al. (1994)], ortho-benzoquinone is not stable under reaction conditions and undergoes rapid overoxidation through rupture of the aromatic ring [Patai (1974), Taylor and Battersby (1967)]. Catechol is thus more likely to form tars than hydroquinone and care has to be taken with the interpretation of the reaction results. Due to the consecutive overoxidation reactions, product selectivities should be compared at identical reaction conditions and phenol conversions.

4.2.5.2 Influence of water

Solvent effects in the hydroxylation of phenol, anisole and toluene are documented in the literature and were thoroughly investigated in this work. Protic solvents such as alcohols and water generally enhance the selectivity towards para-hydroxylation. However, water is always present in the system as it is part of the hydrogen peroxide solution and a reaction product. A certain amount of the protic solvent water is therefore present even when aprotic solvents such as acetone are used. To investigate the influence of water when the reaction is carried out in aprotic solvents, a TS-1 catalyzed phenol hydroxylation with non-aqueous hydrogen peroxide solution was conducted with acetone as the solvent. The TS-1 sample was previously dehydrated at 500°C. The solvent acetone was also dehydrated using $MgSO_4$; furthermore, dehydrated $MgSO_4$ (0.5 g) was added to the reaction mixture to adsorb water formed during the reaction. Table 4.5 shows the results obtained for a phenol hydroxylation over TS-1 in acetone using aqueous and water-free hydrogen peroxide. In the absence of the protic solvent water, a higher ortho-selectivity was expected. However, a higher p/o-ratio, hence more hydroquinone was obtained when water-free H_2O_2 solution was used. Furthermore, a slightly higher phenol conversion and significantly lower selectivities were obtained with the non-aqueous hydrogen peroxide solution. These observations indicate that water and hydrogen peroxide might compete for adsorption at the titanium site. As described in the previous paragraph, overoxidation and polymerisation of reaction products to tars is more likely for catechol than for hydroquinone. The presence of more H_2O_2 at the active sites under water-free conditions might therefore be responsible for catechol being overoxidised more rapidly compared to hydroquinone, which would result in lower selectivities (based on peroxide and phenol) and a higher hydroquinone content in the final reaction mixture.

4.2.5.3 Influence of the oxidant

This work focuses on the use of hydrogen peroxide as the oxidant. A comparison of the reaction results obtained with H_2O_2 to a reaction with TBHP as the oxidant could however clarify details of

Table 4.5: Influence of water in the phenol hydroxylation over TS-1 in acetone

	X_{phenol} [%]	$X_{H_2O_2}$[%]	S_{Phenol}[1][%]	H_2O_2 eff. [%]	$\frac{p}{o}$-ratio[1]
aqueous H_2O_2	19.6	82.7	87	72	0.75
water-free H_2O_2	21.1	79.4	81	60	1.18

T = 60 °C, t_R = 6 h, 1.2 g phenol, 0.12 g TS-1 ($d_{crystal}$ = 0.1 μm), 5 ml dried acetone, 0.6 ml H_2O_2 (30% in water or acetone), [1]at X_{phenol} = 19 %

the reaction mechanism. It is known that TS-1 is inactive with TBHP as the oxidant [Corma et al. (1996a), Corma et al. (1996b)], presumably because the titanium peroxo species formed with TBHP is too bulky to allow a reaction in the medium-size pores. There is however sufficiently space in the pores of Al-free Ti-beta for the use of TBHP as the oxidant, as has been proven for epoxidation reactions, where Al-free Ti-beta was reported to be very active [Blasco et al. (1998), van der Waal et al. (1998b), van der Waal and van Bekkum (1997), van der Waal (1998)]. Table 4.6 shows the results of a phenol hydroxylation reaction in water with Al-free Ti-beta using aqueous H_2O_2 and TBHP as the oxidants. Al-free Ti-beta was completely inactive for the hydroxylation of phenol with

Table 4.6: Influence of the oxidant on the phenol hydroxylation over Al-free Ti-beta

Oxidant	X_p [%]	$X_{Oxidant}$[%]	S_P [%]	Oxidant eff. [%]	$\frac{p}{o}$-ratio
H_2O_2	18.8	88.7	70.0	48.3	0.42
TBHP	< 1	3.3	-	-	only tars

t_R = 6 h, T = 60 °C, 1.2 g phenol, 5 ml water, 0.12 g Al-free Ti-β ($d_{crystal}$ = 0.9 μm), 0.6 ml H_2O_2 (30 % soln. in H_2O) or TBHP (70 % soln. in water)

TBHP as the oxidant. Even after 24 h of reaction time, no hydroxylation products were detected in the phenol hydroxylation with TBHP; only decomposition of the oxidant and tar formation was observed.

4.2.5.4 Solvent effects

The pronounced effect of the solvent on activity and selectivity in the phenol hydroxylation over TS-1 with aqueous H_2O_2 has been reported in the literature; a brief overview was given in section 2.3.1. The complete inversion of selectivities in protic and aprotic solvents is a particularly interesting phenomenon that was further investigated. Water, methanol and acetone were chosen as solvents since these are the only solvents where high conversions and selectivities can be achieved, the former two representing protic and the latter being an aprotic solvent.

Figure 4.12 shows the phenol conversion in water, methanol and acetone as a function of reaction time. The solvent clearly influences the activity of TS-1 for the phenol hydroxylation. Some pseudo-first order rate constants can be found in the literature [Kulawik et al. (1995), van der Pol et al.

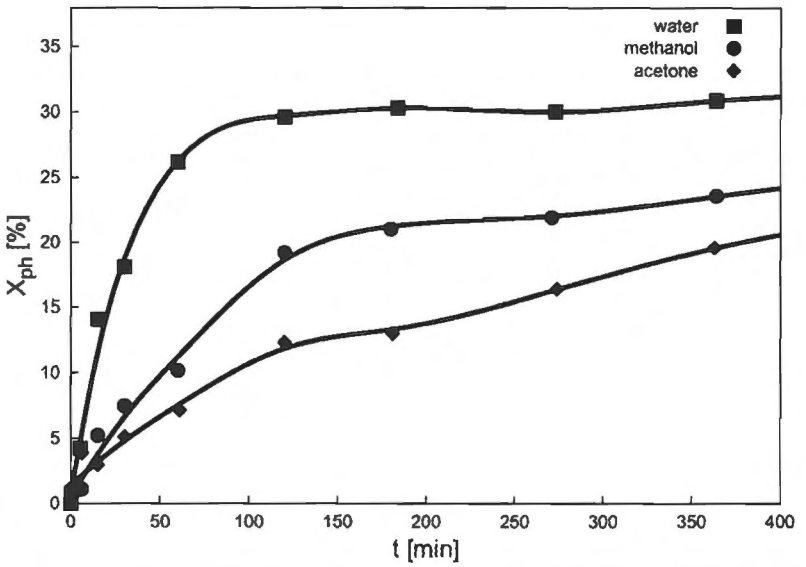

Figure 4.12: Phenol conversion vs. reaction time in different solvents

T = 60 °C, 1.2 g phenol, 5 ml solvent, 0.12 g TS-1 ($d_{crystal}$ = 0.1 μm), 0.6 ml H_2O_2 (30 % soln. in H_2O)

(1992)], but no systematic kinetic study comparing the activity of TS-1 for the phenol hydroxylation in different solvents is available. The rate constants for phenol consumption, peroxide decomposition and formation of products and tars in different solvents were determined using the kinetic model introduced in section 4.2.2 and are shown in Table 4.7. The highest catalytic activity, expressed as

Table 4.7: Influence of solvent on the observed rate constants for phenol hydroxylation over small TS-1 crystals

$k_i[\frac{l}{mol \cdot s \cdot m^2}]$	k_1 Phenol	k_2 $H_2O_{2\ dec}$	k_3 Catechol	k_4 Hydroquinone	k_t Tar	Tar[1] [mg/g_{cat}]
Water	5.32e-6	2.94e-6	1.61e-6	2.43e-6	1.46e-6	84.2
Methanol	1.38e-6	2.88e-6	3.23e-7	6.94e-7	3.59e-7	57.0
Acetone	7.93e-7	3.32e-8	3.32e-7	2.57e-7	2.04e-7	47.0

T = 60 °C, 1.2 g phenol, 5 ml solvent, 0.12 g TS-1 ($d_{crystal}$ = 0.1 μm), 0.6 ml H_2O_2 (30 % soln. in H_2O); [1]Tar deposition after 24 h reaction time

observed rate constant for phenol consumption (k_1), was obtained with water as a solvent, followed by methanol and acetone. Tar formation followed a similar trend to phenol conversion (water > methanol > acetone), which is shown by the rate constants for tar formation (k_t) and by the deposition of tars on the catalyst as determined by TG/DTA. The tar deposition on the catalyst surface decreased when the tar components or precursors are more soluble in the solvent. The para-selectivity was higher in protic solvents, confirming literature reports; hydroquinone was the preferred product in methanol and water, whereas catechol formation was favoured in acetone.

In several literature reports, a shift in product selectivity towards more para-hydroxylated product with increasing phenol conversion is mentioned [Thangaraj et al. (1991a), Thangaraj et al. (1994), Tuel et al. (1991)]. Figure 4.13 shows the ratio of hydroquinone to catechol formed in the phenol hydroxylation with water, methanol and acetone as a solvent as a function of reaction time. Figure

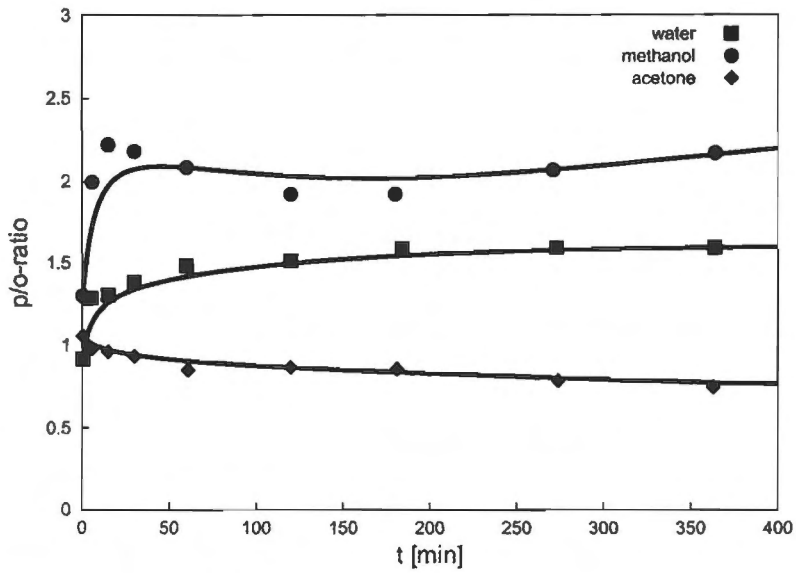

Figure 4.13: Ratio of the amount of hydroquinone formed relative to the amount of catechol formed as a function of reaction time

T = 60 °C, 1.2 g phenol, 5 ml solvent, 0.12 g TS-1 ($d_{crystal}$ = 0.1 μm), 0.6 ml H_2O_2 (30 % soln. in H_2O)

4.13 clearly shows that the product selectivity changes with reaction time and thus phenol conversion. With water and methanol as solvents, the para-content in the reaction products increased with reaction time, whereas the opposite trend was observed in acetone. Selectivities should therefore only be compared at similar phenol conversion levels, which is neglected in many literature reports.

4.2.5.5 Influence of pore geometry and external surface

To further investigate the solvent and shape selectivity effects in the phenol hydroxylation over TS-1, the experimental results were compared to larger-pore zeolites such as Al-free Ti-beta and Ti-HMS. If shape selectivity plays a major role in the TS-1 catalyzed phenol hydroxylation with aqueous H_2O_2, the selectivities should be different in larger-pore systems. The same applies for the solvent effects observed for TS-1; if these solvent effects are caused by steric effects inside the micro-channels, they should be less pronounced for larger pores.

Shape selectivity effects can also be identified by comparing the product distribution obtained from the reaction inside the pores to the reaction at external surface of the zeolite, as no shape

selective effects are expected for a reaction at the external surface. External surface deactivation by cycle-wise CVD of TEOS was described in section 2.6.1 as a tool to obtain information about the catalytic reaction inside the pores. Another approach is to block the access to the pore system, forcing the reaction to occur at the external surface. Tuel et al. (1991) used a non-calcined TS-1 for a phenol hydroxylation reaction with the aim of obtaining the product distribution generated exclusively by the external surface. In this study, a high activity and a very high selectivity towards catechol (> 95 % for the first 60 min of the reaction) of the external surface was reported. These findings could not be confirmed in this work; a low activity was observed when a non-calcined TS-1 was taken for a phenol hydroxylation experiment and only a slight excess of catechol was obtained when compared to a calcined catalyst at the same phenol conversion. A comparison of the phenol hydroxylation results for a non-calcined TS-1 and a TS-1 calcined at 550 °C is shown in Table 4.8.

Table 4.8: Comparison of calcined and as-synthesised TS-1 for the phenol hydroxylation

Catalyst	X_p [%]	$X_{H_2O_2}$[%]	H_2O_2 eff. [%]	$\frac{p}{o}$-ratio[1]
non-calcined TS-1 (run 1)	2.1	9.2	48	0.91
non-calcined TS-1 (run 2)	3.0	14.5	40	0.66
calcined TS-1	28.1	100	78	0.72

t_R = 6 h, T = 60 °C, 1.2 g phenol, 5 ml water, 0.12 g TS-1 ($d_{crystal}$ = 0.1 μm), 0.6 ml H_2O_2 (30 % soln. in H_2O); [1] determined at X_P of 1.6 %

The results for the phenol hydroxylation with a non-calcined TS-1 were not reproducible. The results were found to be dependent on the treatment of the sample after the synthesis, especially on the washing of the solid obtained after crystallisation. In the two runs using a non-calcined catalyst shown in Table 4.8, the TS-1 sample used for run 2 was washed more extensively with deionised water than the sample for run 1 and the results were clearly different. The remaining template could be attached to the external surface of the non-calcined TS-1, altering the properties of the former. Furthermore, the (strongly basic) template molecules could influence the pH of the solution; another unknown factor is the interaction of template and hydrogen peroxide.

The 'classical' way of obtaining information about shape selectivity in microporous solids is to change the ratio of internal and external surface by changing the crystal size. Larger crystals have a smaller external surface and thus a smaller fraction of the active sites located at the external surface.

The tar formation in the phenol hydroxylation can be used as an alternative method for external surface inertisation. Thus, a TS-1 sample was used for a phenol hydroxylation in water (where the tar formation is most pronounced, see Table 4.7), washed extensively with deionised water and, without regeneration, used for another reaction cycle with water as a solvent. Table 4.9 shows the influence of the external surface and the crystal size of TS-1 on activity and product selectivity in the phenol hydroxylation. A decrease in crystal size of TS-1 leads to an enhancement in phenol and

Table 4.9: Influence of crystal size and external surface activity on the phenol hydroxylation over TS-1

$d_{crystal}$ [μm]	X_p [%]	$X_{H_2O_2}$[%]	S_P[1][%]	H_2O_2 eff. [%]	$\frac{p}{o}$-ratio[1]	tar [mg/g][2]
3×10×45	5.8	18	72.1	48	1.31	-
0.1	30.3	100	78.4	71	1.31	84.2
0.1 (sil.)	27.8	100	94.5	78	1.54	53.0
0.1 (coked)[3]	23.8	100	65.4	61	1.39	91.5

t_R = 6 h, T = 60 °C, 1.2 g phenol, 5 ml water, 0.12 g TS-1, 0.6 ml H_2O_2 (30 % soln. in H_2O); [1] determined at X_P of 5.8 %; [2]amount of tar deposited after 24 h of reaction; [3]TS-1 previously coked by 1 reaction cycle without calcination

H_2O_2 conversion. This increase in the conversion cannot be attributed to the increase in the external surface, since in comparable conditions the conversion with the silanised sample of TS-1 was still significantly larger than with the large crystals of TS-1. This suggests that the phenol hydroxylation over large crystals is strongly diffusion limited. van der Pol et al. (1992) obtained a similar conclusion by comparing the activity of different crystal sizes of TS-1 in the phenol hydroxylation. Thus, with large crystals of TS-1, the phenol hydroxylation only occurs within a small layer of the catalyst close to the external surface. When the product selectivities of large and small crystals are compared at the same phenol conversion, the results did not show a clear trend, as shown in Figure 4.14. At very low phenol conversions (X_{ph} < 5%), the large crystals showed a similar p/o-product ratio whereas the p/o-ratio was higher for phenol conversions > 5%. Since the peroxide efficiency was much lower for the larger TS-1 crystals, phenol conversions higher than 10 % could not be obtained with the latter under the standard reaction conditions used in this work. However, the final p/o-ratio (obtained at 10 % phenol conversion) with the large crystals was 1.81 and thus significantly higher than with the small crystals.

Silanisation of TS-1 leads to a decrease in the amount of coke formed, pointing to a decreased activity of the external surface, and an enhanced formation of the para-hydroxylated isomer. Similar observations are noted for a coked TS-1 sample; no significant additional amount of tar was formed (7.3 mg tar/g catalyst additionally deposited on the catalyst). However, a decrease in phenol conversion as well as hydrogen peroxide efficiency was observed and the increase in the product p/o-ratio was not as pronounced as for the silanised sample.

Having a similar diffusional path length, the comparison of the large TS-1 crystals and the Al-free Ti-beta sample yields direct information on the effect of the pore structure on the phenol hydroxylation. Table 4.10 shows a comparison of TS-1 and Al-free Ti-beta for the phenol hydroxylation. The phenol conversion over large crystals of TS-1 was much lower than over Al-free Ti-beta. This confirms again that mass transfer controls the reaction rate in large TS-1 crystals. Intracrystalline diffusion is expected to be faster using Al-free Ti-beta. With the larger pores of Al-free Ti-beta,

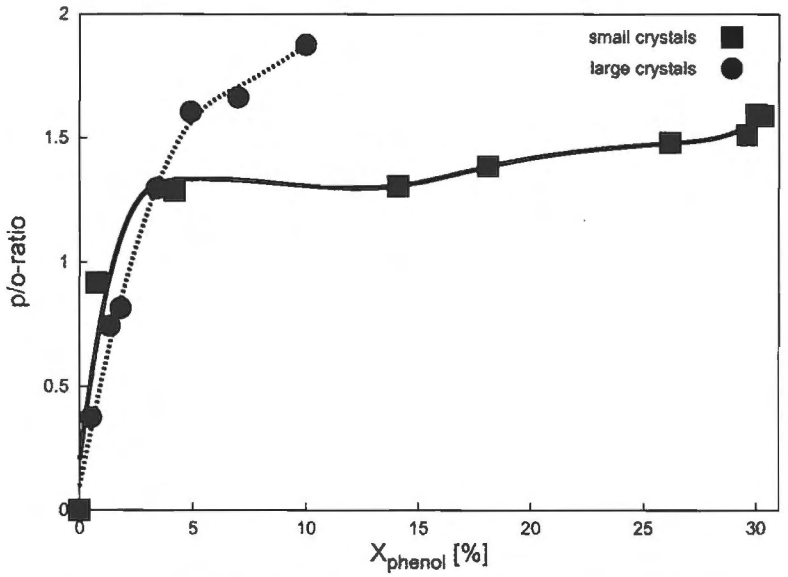

Figure 4.14: Product p/o-ratio vs. phenol conversion for small and large TS-1 crystals

T = 60 °C, 1.2 g phenol, 5 ml water, 0.12 g TS-1, 0.6 ml H_2O_2 (30 % soln. in H_2O)

Table 4.10: Influence of the zeolite crystal structure on the phenol hydroxylation

Catalyst	X_p [%]	$X_{H_2O_2}$[%]	S_P[3][%]	H_2O_2 eff. [%]	$\frac{p}{o}$-ratio[3]	tar [mg/g][4]
TS-1[1]	5.8	18.1	72.1	48.1	1.31	-
Al-free Ti-β[2]	18.8	88.7	70.0	45.3	0.45	118.0

t_R = 6 h, T = 60 °C, 1.2 g phenol, 5 ml water, 0.12 g catalyst, 0.6 ml H_2O_2 (30 % soln. in H_2O); [1]TS-1 crystals of 3×10×45 μm; [2]Al-free Ti-beta of 2 - 5 μm; [3] determined at X_P of 5.8 %; [4]amount of tar deposited after 24 h of reaction

catechol was the preferred product whereas hydroquinone was preferentially formed in TS-1. This shows that the zeolite pore size controls the product formation.

Although a faster intracrystalline diffusion is expected for the large Al-free Ti-beta crystals, the reaction rate could also be governed by mass transfer limitations. To investigate this aspect, Al-free Ti-beta of two different crystal sizes were synthesised and compared for a phenol hydroxylation reaction in water. Figure 4.15 shows the phenol conversion as a function of time obtained with small ($d_{crystal}$ = 0.9 μm) and large ($d_{crystal}$ = 2-6 μm) crystals of Al-free Ti-beta. The smaller Al-free Ti-beta crystals were clearly more catalytically active as phenol conversions were higher. This strongly suggests that the phenol hydroxylation over Al-free Ti-beta was also diffusion limited. However, as it is an irreversible reaction, the selectivity of the phenol hydroxylation can be compared to TS-1, provided that the comparison is done at the same phenol conversion.

The effect of the pore structure on the product selectivity was further investigated using methanol, the solvent with the highest para-selectivity, as the solvent. Figure 4.16 shows the product p/o-ratios

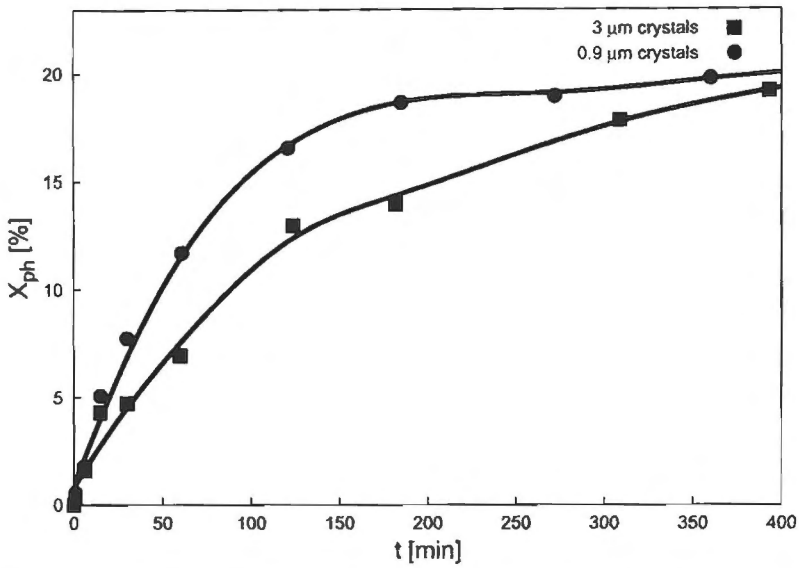

Figure 4.15: Effect of crystal size in phenol hydroxylation over Al-free Ti-beta

T = 60 °C, 1.2 g phenol, 5 ml water, 0.12 g Al-free Ti-beta, 0.6 ml H_2O_2 (30 % soln. in H_2O)

obtained as a function of phenol conversion for TS-1, silanised TS-1, Al-free Ti-beta and Ti-HMS. The para-selectivity was higher for TS-1 than for Al-free Ti-beta, indicating that the solvent ef-

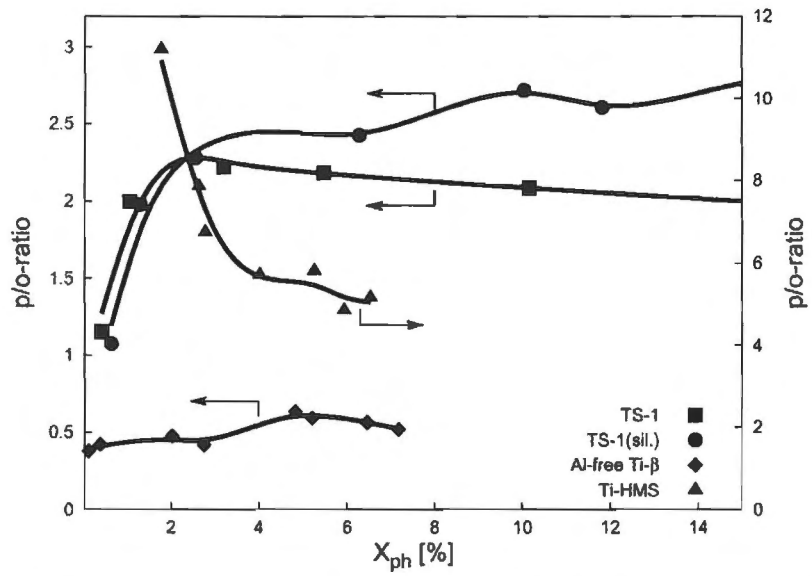

Figure 4.16: Product p/o-ratio as a function of phenol conversion for titanium-containing molecular sieves of different pore size and external surface activity

T = 60 °C, 1.2 g phenol, 5 ml methanol, 0.12 g catalyst (TS-1: $d_{crystal}$ = 0.1 μm, Ti-β: $d_{crystal}$ = 0.9 μm), 0.6 ml H_2O_2 (30 % soln. in H_2O)

fects observed for TS-1 could be generated by steric constraints in the micropores. Figure 4.16

also shows that the p/o-ratio increases with silanisation of the external surface of TS-1, confirming again the presence of a para-directing effect inside the pores. The very high p/o-ratio obtained for Ti-HMS is intriguing. However, rapid tar formation through product overoxidation was observed in the phenol hydroxylation over Ti-HMS. Major amounts of para-benzoquinone, the product of subsequent oxidation of hydroquinone, were detected. Ortho-benzoquinone, the corresponding oxidation product of catechol, is not expected to be stable under reaction conditions [Taylor and Battersby (1967)]. Once formed, it rapidly polymerises to form tars and is thus not detected in the reaction mixture, explaining the high p/o-ratio in the products. A very poor product selectivity (3.2 %, based on phenol) and peroxide efficiency (15.5 %) demonstrates that the phenol hydroxylation was not the dominating reaction; the main reaction was H_2O_2 decomposition and product overoxidation to tars. Exclusive formation of para-hydroxylated products in the phenol hydroxylation with aqueous H_2O_2 over Ti-MCM-41 was also reported by Kulawik et al. (1995). The reported phenol conversion and peroxide efficiency were very low and the results in that publication are likely to originate from the same effects that were observed for Ti-HMS in this work. Defects in the walls of the mesoporous structure and the resulting presence of large amounts of silanol groups are held responsible for the pronounced hydrophilicity of mesoporous crystalline titanosilicates [Chen et al. (1997), Rhee and Lee (1996)]. As a result of the hydrophilic properties of the framework, high H_2O_2 concentrations are likely to be present at the titanium sites. This could facilitate the observed overoxidation and peroxide decomposition reactions. Due to the fact that the above mentioned side-reactions dominate under the reaction conditions, the results obtained from Ti-HMS catalyzed hydroxylations of monosubstituted benzenes cannot be compared to TS-1 or Al-free Ti-beta.

Table 4.6 summarises the results obtained for the phenol hydroxylation over titanium-substituted zeolites. In the blank reaction (e.g. without catalyst), only a slow hydrogen peroxide decomposition reaction and phenol conversion to tars was observed. The solvent effects observed for TS-1 were much less pronounced for Al-free Ti-beta. Although, as observed for TS-1, protic solvents (methanol and water) lead to a higher para-selectivity, the ortho-isomer catechol was always the preferred product in the Al-free Ti-beta catalyzed phenol hydroxylation. In all solvents tested, the p/o-ratio was higher for TS-1. This strongly confirms the presence of shape selective effects in the TS-1 micropores.

Silanisation of the external surface of small TS-1 crystals lead to an increase in para-selectivity for all solvents, supporting the hypothesis that the reaction taking place at the external surface of TS-1 shows less shape selectivity. In Table 4.6, the experimental results for a parent and a silanised TS-1 are compared for a fixed reaction time or phenol conversion. Applying the kinetic model introduced in section 4.2.2 and extracting the rate constants from the experimental data, the contribution of internal and external surface to the total activity and selectivity can be decoupled and quantified by using equation 4.11 and 4.12. Table 4.12 shows the rate constants for internal and external

Table 4.11: Influence of solvent on the phenol hydroxylation after 6 h of reaction time

Catalyst	Solvent	X_P [%]	$X_{H_2O_2}$[%]	S_P [%]	H_2O_2 eff. [%]	$\frac{p}{o}$-ratio[5]	tar [mg/g][6]
blank[1]	Water	< 1	3.5	-	-	only tars	-
TS-1[2]	Water	30.3	100	78.4	72	1.29	84.2
	Methanol	22.8	100	71.1	58	2.14	57.0
	Acetone	19.6	82.8	76.4	68	0.84	47.0
TS-1 (sil.)[3]	Water	27.8	100	94.5	78	1.49	53.0
	Methanol	21.6	92.1	90.4	68	2.50	46.1
	Acetone	15.1	52.0	79.7	72	1.06	46.7
Al-free Ti-β[4]	Water	18.8	88.7	70.0	48.3	0.42	118.0
	Methanol	7.2	37.1	35.2	33.7	0.56	-
	Acetone	2.9	19.7	51.5	40.7	0.38	-
Ti-HMS	Methanol	6.8	89.6	3.2	15.5	5.2[7]	-

T = 60 °C, 1.2 g phenol, 5 ml solvent, 0.12 g catalyst, 0.6 ml H_2O_2 (30 % soln. in H_2O); [1]no catalyst added; [2]$d_{crystal}$ = 0.1 μm; [3]$d_{crystal}$ = 0.1 μm after 20 cycles of CVD of TEOS; [4]$d_{crystal}$ = 2 - 5 μm;[5]at X_P = 7 %; [6]amount of tar deposited on TS-1 after 24 h; [7](para-benzoquinone + hydroquinone)/catechol

surface of TS-1 in the phenol hydroxylation; values in brackets represent the contribution of total formation/consumption in percent. On the basis of the rate constants shown in Table 4.12, the

Table 4.12: Rate constants for internal and external activity in the phenol hydroxylation over small TS-1 crystals

rate const. $\frac{l}{mol \cdot m^2 \cdot s}$	Water		Methanol		Acetone	
	internal	external	internal	external	internal	external
k_1	2.02e-6 (31)	1.98e-5 (69)	9.23e-7 (54)	3.37e-6 (46)	3.45e-7 (36)	2.76e-6 (64)
k_2	1.70e-6 (47)	8.43e-6 (53)	1.30e-6 (37)	9.80e-6 (63)	1.14e-8 (28)	1.29e-7 (72)
k_3	7.07e-7 (36)	5.59e-6 (64)	2.10e-7 (53)	8.18e-7 (47)	1.29e-7 (32)	1.22e-6 (68)
k_4	1.23e-6 (41)	7.71e-6 (59)	6.24e-7 (73)	1.00e-6 (27)	1.46e-7 (46)	7.45e-7 (54)
k_6	2.36e-7 (18)	4.71e-6 (82)	1.41e-7 (51)	5.92e-7 (49)	1.51e-8 (16)	3.55e-7 (84)
k_7	4.15e-8 (13)	1.18e-6 (87)	1.04e-7 (58)	3.20e-7 (32)	4.04e-9 (52)	1.61e-8 (48)
k_t	8.23e-8 (4)	7.52e-6 (96)	8.86e-8 (20)	1.55e-6 (80)	6.98e-8 (28)	7.90e-7 (72)

Values in brackets: contribution to total rate of formation/consumption in %; T = 60 °C, 1.2 g phenol, 5 ml solvent, 0.12 g TS-1 ($d_{crystal}$ = 0.1 μm), 0.6 ml H_2O_2 (30 % soln. in H_2O)

product selectivity on the external surface and inside the pores can be evaluated. Table 4.13 shows internal and external product p/o-ratios in different solvents for the phenol hydroxylation over TS-1, expressed as the ratio of the rate constants for hydroquinone and catechol formation. The selectivities for the para isomer were always higher inside the pores. This effect can be further enhanced by protic solvents (see Table 4.12). The influence of the solvent was less pronounced at the external surface. However, even at the external surface, catechol formation was only preferred with acetone as the solvent.

Table 4.13: Internal and external p/o-ratios in different solvents for the phenol hydroxylation over TS-1

	Water	Methanol	Acetone
$\frac{k_p}{k_o}$ internal	1.74	2.97	1.13
$\frac{k_p}{k_o}$ external	1.38	1.23	0.61

T = 60 °C, 1.2 g phenol, 5 ml solvent, 0.12 g TS-1 ($d_{crystal}$ = 0.1 μm), 0.6 ml H_2O_2 (30 % soln. in H_2O)

4.2.6 Anisole hydroxylation

To investigate the influence of the substituent at the aromatic ring of the reactant, the results obtained in the TS-1 catalyzed phenol hydroxylation were compared to the hydroxylation of the methyl ether of phenol, e.g. anisole. As for the phenol hydroxylation, the influence of the external surface, the pore structure of the catalyst and the solvent were studied.

In Figure 4.17, the typical concentration-time profiles of reactants and products, as well as the fit of the kinetic model applied (equations 4.5-4.10) are given for the hydroxylation of anisole over TS-1 with methanol as the solvent. As for the phenol hydroxylation, good model fits were obtained

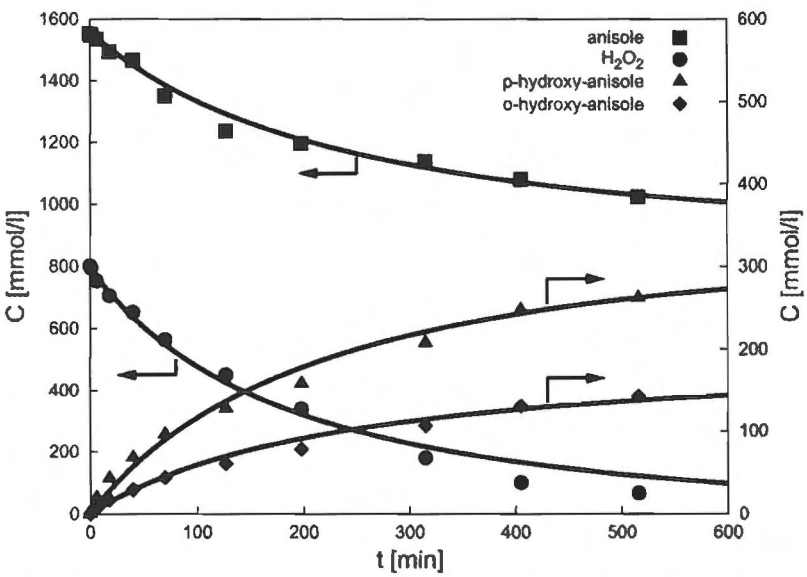

Figure 4.17: Concentration-time profile in the anisole hydroxylation over TS-1

T = 60 °C, 1.2 g anisole, 5 ml methanol, 0.18 g TS-1 ($d_{crystal}$ = 0.1 μm), 0.6 ml H_2O_2 (30 % soln. in H_2O)

to represent the experimental data. No meta-hydroxylated anisole nor any other products were found (see appendix E.2 for a typical HPLC chromatogram of an anisole hydroxylation reaction mixture).

4.2.6.1 Solvent effects

Given the strong influence of the solvent on the product selectivity in the phenol hydroxylation, the existence of similar solvent effects in the anisole hydroxylation was investigated. This could give further information about the reaction mechanism of aromatic hydroxylations over titanium-substituted zeolites.

The influence of the solvent on product selectivity and catalytic activity is not as well documented in the literature as for the phenol hydroxylation. However, a higher para-selectivity for protic solvents was found by Kumar and Bhaumik (1998) and Bhaumik and Kumar (1995) in the anisole hydroxylation over TS-1. In both publications, the anisole hydroxylation was also studied in triphase conditions, i.e. in the presence of a separate aqueous phase. However, triphase conditions introduce a number of additional parameters such as mass transfer limitations in the bulk liquid phase, homogeneous dispersion of the catalyst, unknown adsorption properties and concentrations in each phase etc., that would also have to be investigated. For water-immiscible reactants such as anisole, the catalytic hydroxylation reaction was studied with methanol and acetone as solvents, the former representing a protic and the latter representing a non-protic solvent.

Figure 4.18 and 4.19 show the influence of the solvent on the activity (expressed as anisole conversion) and product selectivity (expressed as p/o-ratio) in the anisole hydroxylation over TS-1 and Al-free Ti-beta.

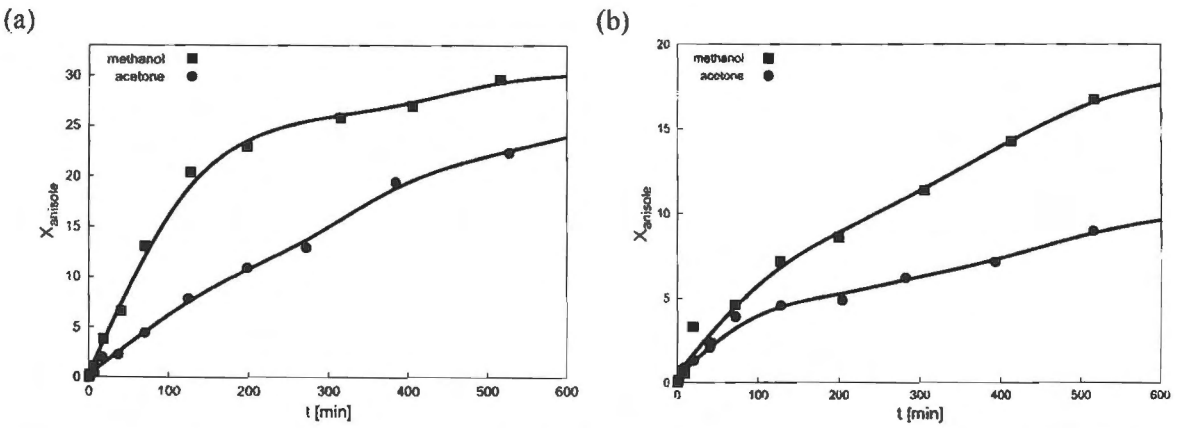

Figure 4.18: Influence of solvent on the activity of (a) TS-1 and (b) Al-free Ti-beta in the anisole hydroxylation

T = 60 °C, 1.2 g anisole, 5 ml solvent, 0.18 g catalyst (TS-1: $d_{crystal}$ = 0.1 μm, Ti-β: $d_{crystal}$ = 0.9 μm), 0.6 ml H_2O_2 (30 % soln. in H_2O)

Similar to the phenol hydroxylation, the activity in the anisole hydroxylation was higher with methanol than with acetone as the solvent for both TS-1 and Al-free Ti-beta. The effect of the solvent in the anisole hydroxylation also follows a similar trend as in the phenol hydroxylation. Using methanol as a solvent, more of the para-hydroxylated isomer was formed for both catalysts.

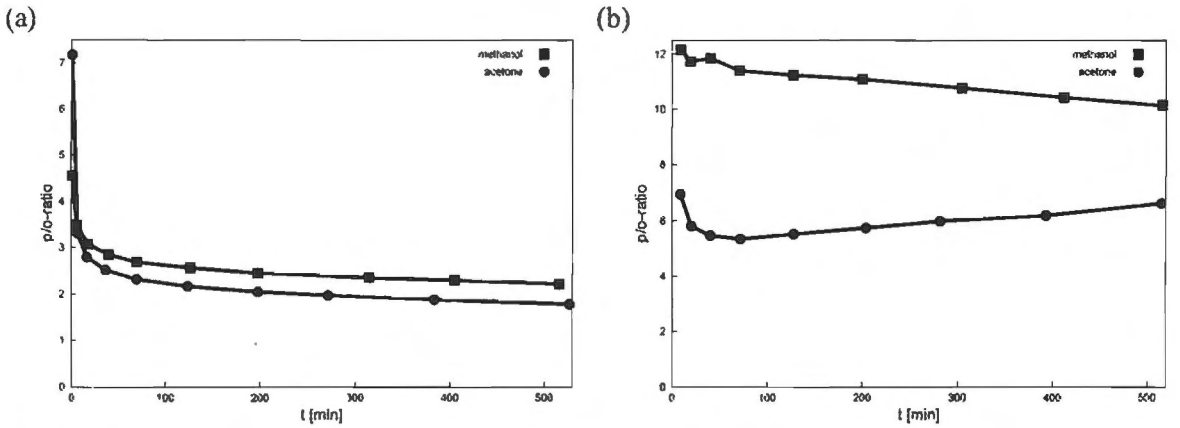

Figure 4.19: Influence of solvent on the product p/o-ratio in (a) TS-1 and (b) Al-free Ti-beta catalyzed anisole hydroxylation

T = 60 °C, 1.2 g anisole, 5 ml solvent, 0.18 g catalyst (TS-1: $d_{crystal}$ = 0.1 μm, Ti-β: $d_{crystal}$ = 0.9 μm), 0.6 ml H_2O_2 (30 % soln. in H_2O)

However, the effect of the solvent on the product distribution was much more pronounced for Al-free Ti-beta than for TS-1; the opposite was found in the phenol hydroxylation.

The rate constants for anisole consumption, peroxide decomposition and formation of products and tars in different solvents were determined for TS-1 using the kinetic model introduced in section 4.2.2 and are shown in Table 4.14. Although the smaller Al-free Ti-beta crystals ($d_{crystal}$ = 0.9 μm) were used, the reaction was likely to be mass transfer limited as was observed for the phenol hydroxylation; this aspect and the kinetic data for hydroxylation reactions over Al-free Ti-beta are discussed in section 5.2.

Table 4.14: Influence of solvent on the observed rate constants for anisole hydroxylation over small TS-1 crystals

$k_i[\frac{l}{mol \cdot s \cdot m^2}]$	k_1 Anisole	k_2 $H_2O_{2\ dec}$	k_3 2-OH-anisole	k_4 4-OH-anisole	k_t Tar
Methanol	5.67e-7	5.24e-7	1.23e-7	2.84e-7	1.60e-7
Acetone	2.05e-7	4.20e-7	5.89e-8	1.09e-7	3.70e-8

T = 60 °C, 1.2 g anisole, 5 ml solvent, 0.18 g TS-1 ($d_{crystal}$ = 0.1 μm), 0.6 ml H_2O_2 (30 % soln. in H_2O)

4.2.6.2 Influence of pore geometry and external surface

The effect of the pore structure and the external surface on the product selectivity was further investigated using methanol, the solvent with which the highest para-selectivity was obtained. Figure 4.20 shows the product p/o-ratios obtained as a function of anisole conversion for TS-1, silanised TS-1 and Al-free Ti-beta. More para-hydroxy-anisole was formed in the initial stages of the reaction for

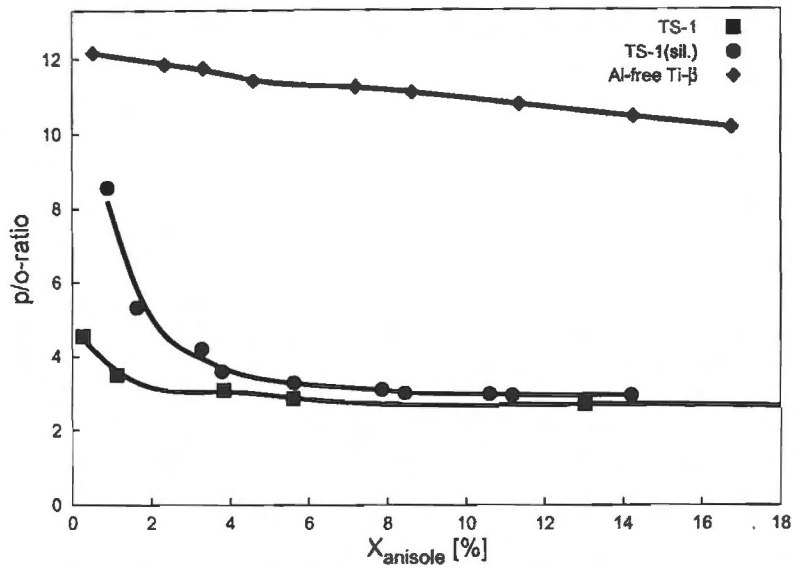

Figure 4.20: Product p/o-ratio as a function of anisole conversion for titanium-containing molecular sieves of different pore size and external surface activity

T = 60 °C, 1.2 g anisole, 5 ml methanol, 0.18 g catalyst (TS-1: $d_{crystal}$ = 0.1 μm, Ti-β: $d_{crystal}$ = 0.9 μm), 0.6 ml H_2O_2 (30 % soln. in H_2O)

both TS-1 and Al-free Ti-beta. In Table 4.15, the experimental results of the anisole hydroxylation over TS-1, silanised TS-1 and Al-free Ti-beta are summarised. Extremely high para-selectivities

Table 4.15: Influence of solvent and catalyst on the anisole hydroxylation after 8 h of reaction time

Catalyst	Solvent	X_A [%]	$X_{H_2O_2}$[%]	S_A [%]	H_2O_2 eff. [%]	$\frac{p}{o}$-ratio[4]
TS-1[1]	Methanol	28.2	94.5	69.7	48	2.75
	Acetone	21.5	71.4	81.9	62	2.08
TS-1 (sil.)[2]	Methanol	11.1	43.2	73.9	48	2.99
	Acetone	10.5	39.8	92.5	61	2.39
Al-free Ti-β[3]	Methanol	15.7	71.7	83.7	47	10.87
	Acetone	9.0	34.6	49.3	27	6.61

T = 60 °C, 1.2 g anisole, 5 ml solvent, 0.18 g catalyst, 0.6 ml H_2O_2 (30 % soln. in H_2O); [1]$d_{crystal}$ = 0.1 μm; [2]$d_{crystal}$ = 0.1 μm after 20 cycles of CVD of TEOS; [3]$d_{crystal}$ = 0.9 μm; [4]at X_A = 9 %

were obtained with Al-free Ti-beta. However, especially with acetone as the solvent, the peroxide efficiencies in the Al-free Ti-beta catalyzed anisole hydroxylation were low. Applying equation 4.11 to the kinetic data for the anisole hydroxylation of parent and silanised TS-1, the contribution of the external surface can be evaluated in the same way as for the phenol hydroxylation. Table 4.16 shows the rate constants for internal and external surface of TS-1 in the anisole hydroxylation; values in brackets represent the contribution of total formation/consumption in percent. On the basis of the rate constants shown in Table 4.16, the product selectivity on the external surface and inside

Table 4.16: Rate constants for internal and external activity in the anisole hydroxylation over small TS-1 crystals

rate constant $[\frac{l}{mol \cdot m^2 \cdot g}]$	Methanol		Acetone	
	internal	external	internal	external
k_1	9.01e-8 (16)	2.66e-6 (84)	1.08e-7 (44)	6.30e-7 (56)
k_2	2.25e-7 (44)	1.84e-6 (56)	2.19e-7 (43)	1.30e-6 (57)
k_3	1.82e-8 (15)	5.84e-7 (85)	2.98e-8 (42)	1.86e-7 (58)
k_4	4.85e-8 (18)	1.32e-6 (82)	7.05e-8 (54)	2.80e-7 (46)
k_6	1.39e-7 (93)	2.15e-7 (7)	6.80e-8 (60)	2.08e-7 (40)
k_7	3.04e-9 (64)	1.28e-8 (46)	1.26e-9 (4)	1.18e-7 (96)
k_t	2.34e-8 (15)	7.62e-7 (85)	8.03e-9 (18)	1.64e-7 (82)

Values in brackets: contribution to total rate of formation/consumption in %; T = 60 °C, 1.2 g anisole, 5 ml solvent, 0.18 g TS-1 ($d_{crystal}$ = 0.1 μm), 0.6 ml H_2O_2 (30 % soln. in H_2O)

the pores can be calculated. Table 4.17 shows internal and external product p/o-ratios in different solvents for the anisole hydroxylation over TS-1. The influence of the solvent and the external sur-

Table 4.17: Internal and external p/o-ratios in different solvents for the anisole hydroxylation over TS-1

	Methanol	Acetone
$\frac{k_p}{k_o}$ internal	2.67	2.37
$\frac{k_p}{k_o}$ external	2.26	1.51

T = 60 °C, 1.2 g anisole, 5 ml solvent, 0.18 g TS-1 ($d_{crystal}$ = 0.1 μm), 0.6 ml H_2O_2 (30 % soln. in H_2O)

face was not as pronounced for the anisole hydroxylation as for the phenol hydroxylation. Whereas ortho- and para-selectivities were reversed in protic and aprotic solvents in the phenol hydroxylation, the para-hydroxylated isomer was always preferentially formed in the anisole hydroxylation. Only with acetone as the solvent, the p/o-product ratios (based on the rate constants obtained for parent and silanised TS-1) for the internal and external surface differ substantially.

4.2.7 Toluene hydroxylation

Toluene was chosen as the third model compound for the hydroxylation of monosubstituted benzenes over titanium-substituted silicalites. Having a methyl group as the substituent, the toluene molecule is much less polar than phenol or anisole, but has similar dimensions. A comparison of the toluene hydroxylation to the anisole and phenol hydroxylation results could therefore give more information about the influence of the substituent and about the reaction mechanism(s) governing the selectivity for this type of reaction.

In Figure 4.21, the typical concentration-time profiles of reactants and products, as well as the fit of the kinetic model applied (see equations 4.5 - 4.10 in section 4.2.2) are given for the hydroxylation of toluene over TS-1. In the toluene hydroxylation, all three cresol isomers were detected (see

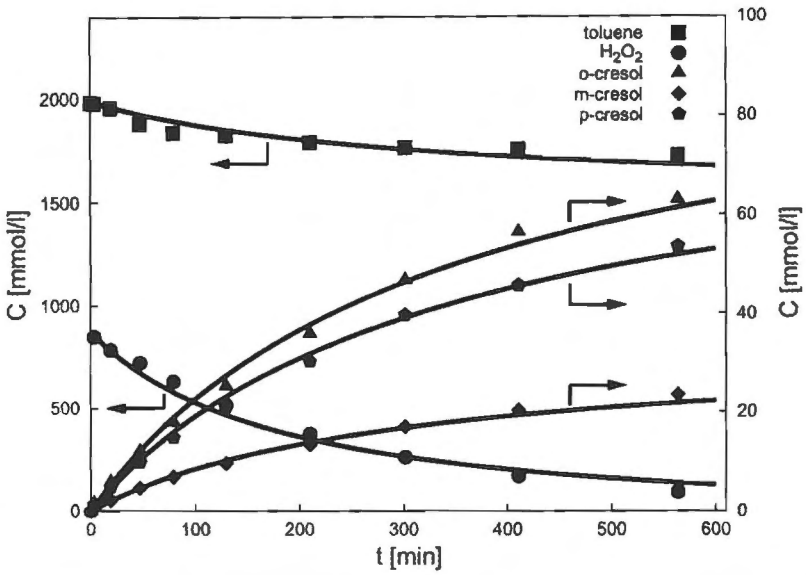

Figure 4.21: Concentration-time profile in the toluene hydroxylation over TS-1

T = 60 °C, 1.2 g toluene, 5 ml methanol, 0.3 g TS-1 ($d_{crystal}$ = 0.1 μm), 0.6 ml H_2O_2 (30 % soln. in H_2O)

appendix E.4 for a typical HPLC chromatogram of a toluene hydroxylation reaction mixture), thus the meta-hydroxylation path must be considered in the kinetic model. As Figure 4.21 shows, the same kinetic model used for the phenol and anisole hydroxylation (see section 4.2.2) could be applied with additional rate constants for the formation and subsequent over-oxidation of meta-cresol. A good fit for all concentration-time profiles was obtained in all systems investigated.

4.2.7.1 Solvent effects

For the toluene hydroxylation, even less data than for the anisole hydroxylation exist in the literature. Additionally, the existence of meta-cresol as a reaction product is not consistently reported by all authors, which renders a comparison of product selectivities difficult. Vayssilov et al. (1997) reported the absence of side-chain oxidation to benzyl alcohol or benzaldehyde, but ring-hydroxylation of toluene was only reported at the ortho and para position. Kumar and Bhaumik (1998) and Bhaumik and Kumar (1995) found trends similar to the phenol and anisole hydroxylation in the TS-1 catalyzed hydroxylation of toluene; in protic solvents, more para-cresol was formed. However, in both publications, the formation of meta-cresol was not mentioned. Marchal et al. (1993) and Wu et al. (1998) both reported meta-cresol as a reaction product, the former one being the only publication

where data for product selectivities including all three isomers are given.

As for the phenol and anisole hydroxylation, the influence of the solvent on the catalytic activity and product selectivity was investigated under the same aspects. The reaction was studied with methanol and acetone as solvents, the former representing a protic and the latter representing a non-protic solvent.

Figure 4.22, 4.23 and 4.24 show the influence of the solvent on the activity (expressed as toluene conversion) and product selectivity (expressed as p/o-ratio and meta-content in cresols) in the toluene hydroxylation over TS-1 and Al-free Ti-beta.

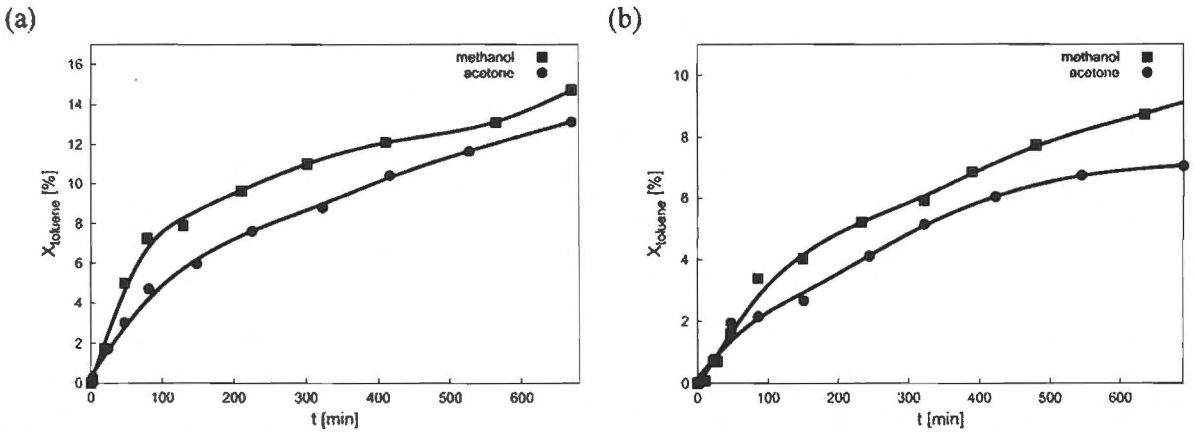

Figure 4.22: Influence of solvent on the activity of (a) TS-1 and (b) Al-free Ti-beta in the toluene hydroxylation

T = 60 °C, 1.2 g toluene, 5 ml solvent, 0.3 g catalyst (TS-1: $d_{crystal}$ = 0.1 μm, Ti-β: $d_{crystal}$ = 0.9 μm), 0.6 ml H_2O_2 (30 % soln. in H_2O)

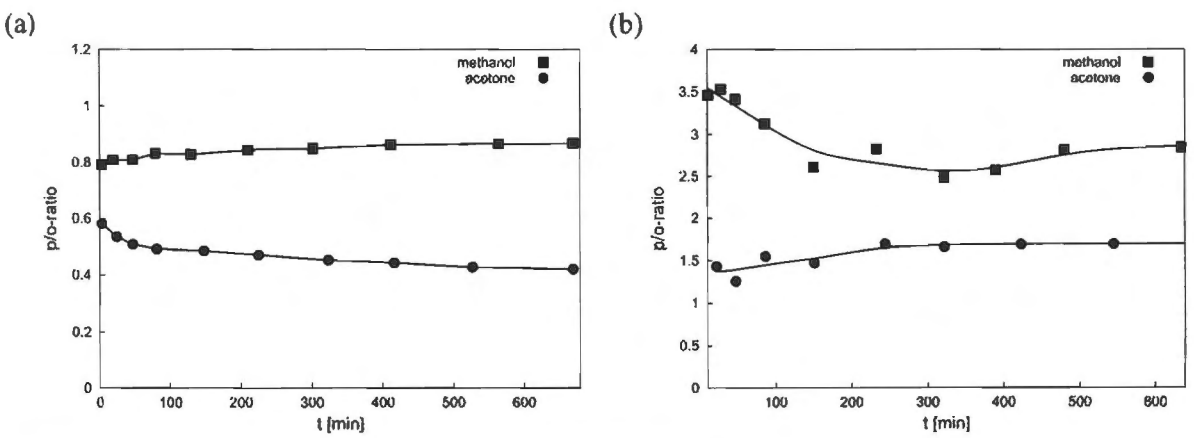

Figure 4.23: Influence of solvent on the product p/o-ratio in (a) TS-1 and (b) Al-free Ti-beta catalyzed toluene hydroxylation

T = 60 °C, 1.2 g toluene, 5 ml solvent, 0.3 g catalyst (TS-1: $d_{crystal}$ = 0.1 μm, Ti-β: $d_{crystal}$ = 0.9 μm), 0.6 ml H_2O_2 (30 % soln. in H_2O)

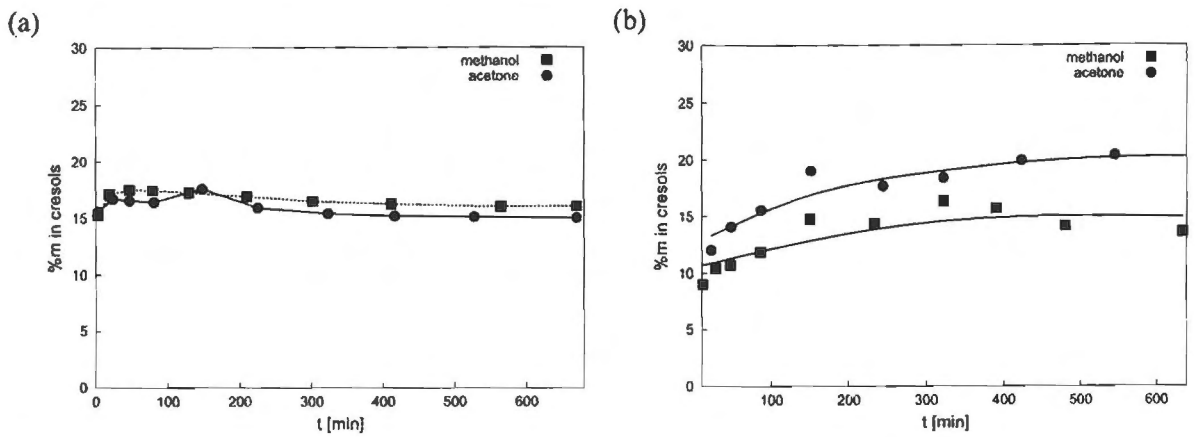

Figure 4.24: Influence of solvent on the meta-cresol content in the cresol fraction in (a) TS-1 and (b) Al-free Ti-beta catalyzed toluene hydroxylation

T = 60 °C, 1.2 g toluene, 5 ml methanol, 0.3 g catalyst (TS-1: $d_{crystal}$ = 0.1 μm, Ti-β: $d_{crystal}$ = 0.9 μm), 0.6 ml H_2O_2 (30 % soln. in H_2O)

As for the phenol and anisole hydroxylation, the activity in the toluene hydroxylation was higher with methanol than with acetone as the solvent for both TS-1 and Al-free Ti-beta. The effect of the solvent in the anisole hydroxylation also follows a similar trend as already seen in the phenol and anisole hydroxylation; in methanol, more of the para-hydroxylated isomer was formed for both catalysts. The effect of the solvent on the product distribution was more pronounced for Al-free Ti-beta than for TS-1. The formation of meta-cresol was not significantly affected by the solvent for TS-1; a significantly enhanced formation of meta-cresol was only observed for Al-free Ti-beta with acetone as the solvent.

The rate constants for toluene consumption, peroxide decomposition and formation of products and tars in different solvents were determined for TS-1 using the kinetic model introduced in section 4.2.2 and are shown in Table 4.18. Due to the possible presence of mass transfer limitations in Al-free Ti-beta crystals, a direct comparison to the activity of TS-1 is difficult; the product selectivities however can be compared to TS-1. The rate constants in Table 4.18 show that TS-1 was less active

Table 4.18: Influence of solvent on the observed rate constants for toluene hydroxylation over small TS-1 crystals

$k_i[\frac{l}{mol \cdot s \cdot m^2}]$	k_1 Toluene	k_2 $H_2O_{2\ dec}$	k_3 o-cresol	k_4 p-cresol	k_5 m-cresol	k_t Tar
Methanol	1.02e-7	5.69e-7	2.28e-8	1.95e-8	8.71e-9	5.14e-8
Acetone	6.73e-8	2.18e-7	2.25e-8	1.02e-8	5.95e-9	2.87e-8

T = 60 °C, 1.2 g toluene, 5 ml solvent, 0.3 g TS-1 ($d_{crystal}$ = 0.1 μm), 0.6 ml H_2O_2 (30 % soln. in H_2O)

for the hydroxylation of toluene than for anisole and phenol. Furthermore, it is confirmed that the

activity of TS-1 in the toluene hydroxylation is higher when methanol is used as the solvent.

4.2.7.2 Influence of pore geometry and external surface

The role of the external surface in terms of activity and product selectivity was examined for the hydroxylation of toluene using the same approach that was used for the phenol and anisole hydroxylation. Silanisation of the external surface of small TS-1 crystals was applied to gain information about the catalytic properties inside the pores and at the external surface of TS-1. The influence of the pore structure and thus the presence of shape selectivity effects for this reaction was investigated using Al-free Ti-beta for the toluene hydroxylation and comparing the selectivities obtained to TS-1.

The effect of the pore structure and the external surface on the product selectivity was characterised using methanol, the more selective solvent in terms of para-selectivity, as the solvent. Figure 4.20 shows the product p/o-ratios and content of the meta-isomer in cresols obtained as a function of toluene conversion for TS-1, silanised TS-1 and Al-free Ti-beta. The experimental results of the

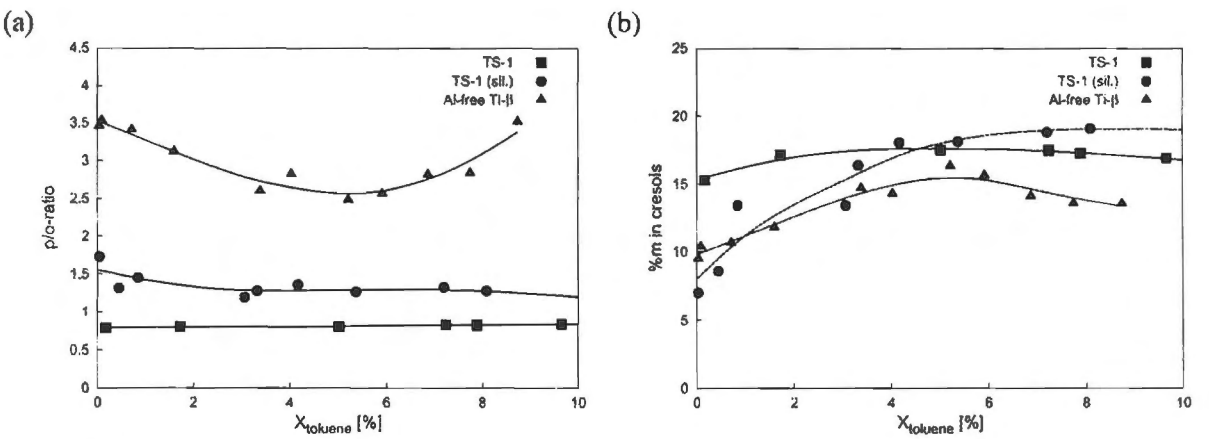

Figure 4.25: (a) product p/o-ratio and (b) %meta-isomer in cresols as a function of toluene conversion for titanium-containing molecular sieves of different pore size and external surface activity

T = 60 °C, 1.2 g toluene, 5 ml methanol, 0.3 g catalyst (TS-1: $d_{crystal}$ = 0.1 μm, Ti-β: $d_{crystal}$ = 0.9 μm), 0.6 ml H_2O_2 (30 % soln. in H_2O)

toluene hydroxylation (after 10 h of reaction time) over TS-1, silanised TS-1 and Al-free Ti-beta with methanol and acetone as the solvents are summarised in Table 4.19. The selectivities based on toluene and the peroxide efficiency were generally lower than observed for the phenol and anisole hydroxylation. Especially for Al-free Ti-beta, the toluene selectivities and peroxide efficiencies were poor; the selectivity towards para-cresol was however higher. For silanised TS-1, a lower activity but higher peroxide efficiency, toluene selectivity and product para-selectivity was observed than for parent TS-1. The influence of the external surface can be quantified by evaluating the kinetic constants for parent and silanised TS-1 in the same way as for the phenol and anisole hydroxylation.

Table 4.19: Influence of solvent and catalyst on the toluene hydroxylation after 10 h of reaction time

Catalyst	Solvent	X_T [%]	$X_{H_2O_2}$[%]	S_T [%]	H_2O_2 eff. [%]	o : m : p[4] [%]
TS-1[1]	Methanol	13.5	91.2	47.6	24	45 : 17 : 38
	Acetone	12.7	46.8	61.0	23	57 : 16 : 27
TS-1 (sil.)[2]	Methanol	7.5	74.7	57.9	57	35 : 19 : 46
	Acetone	9.5	38.1	61.2	49	55 : 16: 29
Al-free Ti-β[3]	Methanol	8.1	55.3	29.3	17	22 : 13 : 65
	Acetone	7.1	25.8	14.1	8	29 : 20 : 51

T = 60 °C, 1.2 g toluene, 5 ml solvent, 0.3 g catalyst, 0.6 ml H_2O_2 (30 % soln. in H_2O); [1]$d_{crystal}$ = 0.1 μm; [2]$d_{crystal}$ = 0.1 μm after 20 cycles of CVD of TEOS; [3]$d_{crystal}$ = 0.9 μm; [4]at X_T = 7 %

Table 4.20 shows the rate constants for internal and external surface of TS-1 in the toluene hydroxylation; values in brackets represent the contribution of total formation/consumption in percent. On the basis of the rate constants shown in Table 4.20, the product selectivity on the external

Table 4.20: Rate constants for internal and external activity in the toluene hydroxylation over small TS-1 crystals

rate constant $[\frac{l}{mol \cdot m^2 \cdot s}]$	Methanol		Acetone	
	internal	external	internal	external
k_1	4.15e-8 (37)	3.70e-7 (63)	3.11e-8 (41)	2.26e-7 (59)
k_2	3.04e-7 (49)	1.73e-6 (51)	1.31e-7 (54)	6.00e-7 (46)
k_3	8.99e-9 (36)	8.37e-8 (64)	1.06e-8 (42)	7.49e-8 (58)
k_4	1.18e-8 (55)	5.33e-8 (45)	5.88e-9 (52)	2.91e-8 (48)
k_5	4.55e-9 (48)	2.70e-8 (52)	3.19e-9 (48)	1.80e-8 (52)
k_6	2.12e-8 (65)	6.68e-9 (35)	7.18e-9 (19)	1.49e-7 (81)
k_7	5.19e-9 (23)	9.19e-9 (77)	9.87e-9 (56)	4.12e-8 (44)
k_8	3.10e-9 (52)	6.10e-9 (48)	6.55e-9 (12)	2.27e-7 (88)
k_t	5.70e-9 (29)	2.52e-7 (71)	1.14e-8 (36)	1.04e-7 (64)

Values in brackets: contribution to total rate of formation/consumption in %; T = 60 °C, 1.2 g toluene, 5 ml solvent, 0.3 g TS-1 ($d_{crystal}$ = 0.1 μm), 0.6 ml H_2O_2 (30 % soln. in H_2O)

surface and inside the pores can be evaluated. Table 4.21 shows internal and external product p/o-ratios in different solvents for the toluene hydroxylation over TS-1. The ortho-position was clearly

Table 4.21: Internal and external p/o-ratios in different solvents for the toluene hydroxylation over TS-1

	Methanol	Acetone
$\frac{k_p}{k_o}$ internal	1.31	0.55
$\frac{k_p}{k_o}$ external	0.64	0.39

T = 60 °C, 1.2 g toluene, 5 ml solvent, 0.3 g TS-1 ($d_{crystal}$ = 0.1 μm), 0.6 ml H_2O_2 (30 % soln. in H_2O)

favoured in the toluene hydroxylation over TS-1. The para-hydroxylated product was only preferentially formed inside the pores when methanol was the solvent. The formation of the meta-isomer was largely unaffected by the solvent; similar meta-selectivities were also obtained for internal and external surface of TS-1.

4.3 Hydroxylation of naphthalenes with Al-free Ti-beta and Ti-HMS

Being a novel material, the catalytic properties of Al-free Ti-beta were also tested for the hydroxylation of compounds that are too large to enter the TS-1 pores, such as substituted naphthalenes. 1-naphthol and 2-methyl-naphthalene were taken as 'model compounds' for this reaction class, yielding 1,4-naphthoquinone and 2-methyl-1,4-naphthoquinone as the main reaction products, respectively. 1,4-naphthoquinone is widely used as an anti-oxidant and 2-methyl-1,4-naphthoquinone is also known as vitamin K_3 or menadione, a very efficient anti-bleeding agent [Anunziata et al. (1999)]. Both reactions are therefore of interest for a potential industrial application [Sheldon et al. (1998a)]. Table 4.22 shows the reaction results for the hydroxylation of 1-naphthol over Al-free Ti-beta, Ti-HMS and TS-1. As for the hydroxylation of monosubstituted benzenes, only a slow

Table 4.22: Hydroxylation of 1-naphthol over titanium-substituted zeolites

catalyst	X_{Naph} [%]	$X_{H_2O_2}$ [%]	S_{Naph} [%][4]	H_2O_2 eff. [%][4]
blank[1]	0.5	4.1	-	-
TS-1[2]	2.5	8.0	-	-
Al-free Ti-β[3]	18.9	32.8	59.7	81.4
Ti-HMS	44.9	61.3	12.8	24.1

t_R = 8 h, T = 60 °C, 1,2 g 1-naphthol, 0.24 g catalyst, 5 ml acetone, 1 ml H_2O_2 (30 % in H_2O); [1]without catalyst; [2]$d_{crystal} = 0.1$ μm; [3]$d_{crystal} = 0.9$ μm; [4]selectivity towards 1,4-naphthoquinone

conversion of 1-naphthol and of hydrogen peroxide to tars and H_2O/O_2 was observed in the blank reaction, respectively. Similar results were obtained with TS-1. Since 1-naphthol is not expected to be able to enter the TS-1 pores, the conversion was low and tars were presumably formed at the external surface. Ti-HMS showed higher activity than TS-1, but selectivities based on 1-naphthol and H_2O_2 were low. Over Al-free Ti-beta however, satisfactory selectivities were obtained. The reaction results for the hydroxylation of 2-methyl-naphthalene over titanium-containing zeolites are shown in Table 4.23. Similar to the 1-naphthol hydroxylation, a selective formation of the naphthoquinone was only observed in the reaction over Al-free Ti-beta. The conversion of 2-methyl-naphthalene was however low.

Table 4.23: Hydroxylation of 2-methyl-naphthalene over titanium-substituted zeolites

catalyst	X_{Naph} [%]	$X_{H_2O_2}$ [%]	S_{Naph} [%][4]	H_2O_2 eff. [%][4]
blank[1]	< 1	3.2	-	-
TS-1[2]	0.3	8.1	2.1	8.7
Al-free Ti-β[3]	2.4	10.1	58.8	88.2
Ti-HMS	2.0	73.2	2.0	6.0

t_R = 8 h, T = 60 °C, 1,2 g 2-methyl-naphthalene, 0.24 g catalyst, 5 ml acetone, 1.3 ml H_2O_2 (30 % in H_2O); [1]without catalyst; [2]$d_{crystal}$ = 0.1 μm; [3]$d_{crystal}$ = 0.9 μm; [4]selectivity towards 2-methyl-1,4-naphthoquinone

4.4 Diffusivities of aromatics in TS-1 and Al-free Ti-beta in various solvents

4.4.1 Suitability and limits of the experimental setup

The assumptions made in the original ZLC model and the difficulties of the extension of this method from the gas-phase to the measurement of liquid-phase diffusivities in microporous solids were pointed out in section 2.5.1. One of the major prerequisites of the ZLC technique is a small, differential zeolite bed. Very small amounts of zeolite, generally less than 10 mg, are therefore used in gas-phase experiments [Duncan and Möller (2000), Eic and Ruthven (1988)] to fulfil the 'zero length' criterion. The conditions for the validity of this criterion has been evaluated by Duncan and Möller (2000). It was shown that the zeolite bed, assumed to be of 'zero length', can always be considered as being differential as long as the characteristic parameter L (extracted from the intercept of the long-time region of the ZLC curves) is larger than $\approx$ 10.

In liquid-phase ZLC experiments, the amount of catalyst in the catalyst bed has to be much larger than in the gas-phase, mainly due to the limited detector sensitivity as shown by Ruthven and Stapleton (1993). In this work, reliable measurements for all compounds were possible for catalyst amounts of 70 mg of large TS-1 crystals ($d_{crystal}$ = 5×10×45 μm)in the ZLC columns. However, the parameter L was greater than 100 for all experiments. Thus, it can be assumed that the 'zero length' criterion is fulfilled.

Being a novel technique, the suitability of the experimental setup of the liquid-phase ZLC method and the validity of the assumptions made in the theoretical model is demonstrated in the following paragraphs.

4.4.1.1 Reproducibility

To ensure that the desorption curves monitored in the ZLC experiments were not influenced by the packing of filling material or the catalyst, the ZLC column was repacked with catalyst and filling

material and the runs were repeated under standard conditions. Figure 4.26 shows ZLC transient desorption curves of phenol in TS-1 with water as the solvent; for each run, the column was repacked. All three runs shown in Figure 4.26 can clearly be represented by the same ZLC desorption curve.

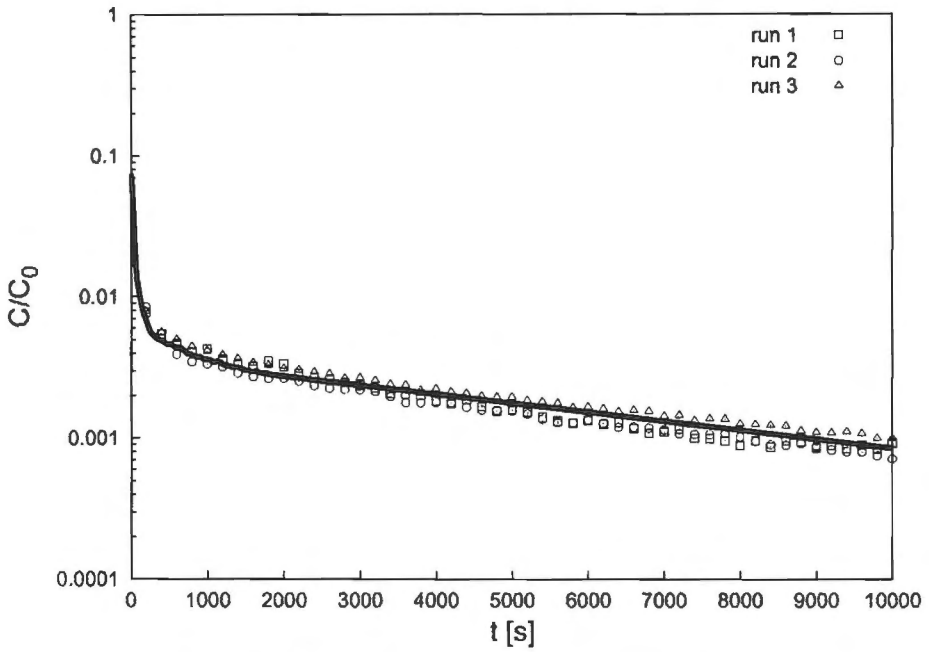

Figure 4.26: Reproducibility of ZLC experiments

T = 30 °C, F = 2 ml/min, 70 mg TS-1, $C_{0,phenol}$ = 0.2 wt.%, solvent: water

Particularly in the long-time region, where the diffusional time constant is extracted, all experimental desorption curves show a straight line with identical slopes. The reproducibility of the method is thus satisfactory.

4.4.1.2 Blank response

A very important factor in transient transport diffusion studies is the blank response of the system. The system and the ZLC column have to be designed in such a way that dead volumes and backmixing are minimised. Furthermore, the system has to be inert, e.g. especially the reactor filling material should not adsorb the diffusing compounds. A series of blank experiments was therefore conducted with various reactor filling materials; the setup was identical to the one used for the ZLC diffusion studies except that no catalyst was present in the column. Figure 4.27 shows a comparison of the desorption curves obtained from a run without column, with a ZLC column packed only with filling material, and a ZLC column packed with filling material and TS-1. Not all filling materials were suitable for the ZLC columns. Commercially obtained chromatographic sand for example showed significant adsorption of the aromatic compounds, even after calcination at 950 °C. SiC granules (d

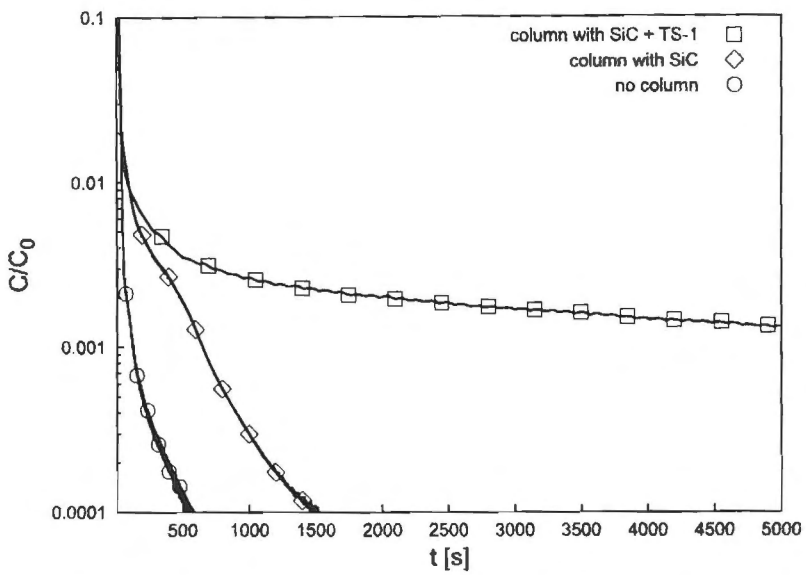

Figure 4.27: ZLC desorption curves for blank columns and for columns containing catalyst T = 30 °C, F = 2 ml/min, $C_{0,phenol}$ = 0.2 wt.%, solvent: water

= 350 μm) and silanised glass beads (d = 250 μm) were good filling materials due to their inertness as the response curve of a (blank) column filled with SiC granules displayed in Figure 4.27 shows. However, even for suitable packing materials, the response of a blank column shows some tailing and retention of the aromatic, probably caused by axial dispersion, backmixing and non-ideal flow patterns in the column. To a minor extent, the same effects were also observed when the column was bypassed, which is an indication for axial dispersion and backmixing in the lines, valves and/or in the detector cell. Ruthven and Stapleton (1993) modelled the blank response of the system using a combination of a plug- and a well mixed flow. The calculated values for the PFR-CSTR model of the blank reactor were then used to correct the ZLC desorption curves. However, in the latter study the short-time (initial) region of the desorption curves was fitted and as a consequence, the estimated diffusivities of the compounds investigated were orders of magnitudes higher than the ones investigated in this study.

The optimisation of the curve fit to the experimentally determined ZLC desorption curves was not the aim of this work, but reliable measurement of binary liquid-phase diffusion coefficients applying the ZLC technique. Although the comparison of a 'blank' column and a column packed with TS-1 shows that the initial region of the desorption curve is influenced by interstitial fluid hold-up, the blank response has no influence in the long-time region of the desorption curve, which is where the ZLC theoretical model is used to extract diffusivities and Henry's constants. As Figure 4.27 demonstrates, the tail of the desorption curve was governed only by diffusion of the aromatic compound from the zeolite crystals.

4.4.1.3 Independence of measured diffusivities on concentration and flow rate

Another assumption made in the modelling of transient ZLC desorption curves is that the isotherm is in the linear region, i. e. that Henry's law is obeyed in the region where diffusivity and adsorption constants are extracted. In most publications that use the ZLC method, the validity of this assumption was tested by repeating a ZLC experiment with different concentrations of the diffusing hydrocarbon. If the adsorption isotherm is indeed in the linear region, the slope of the transient desorption curve in long-time region (in a semi-logarithmic plot of C/C_0 vs. t) should be identical for all concentrations. Figure 4.28 shows two ZLC runs for hydroquinone diffusing in TS-1 at different initial concentrations with water as the solvent. Identical slopes in the long-time region of the des-

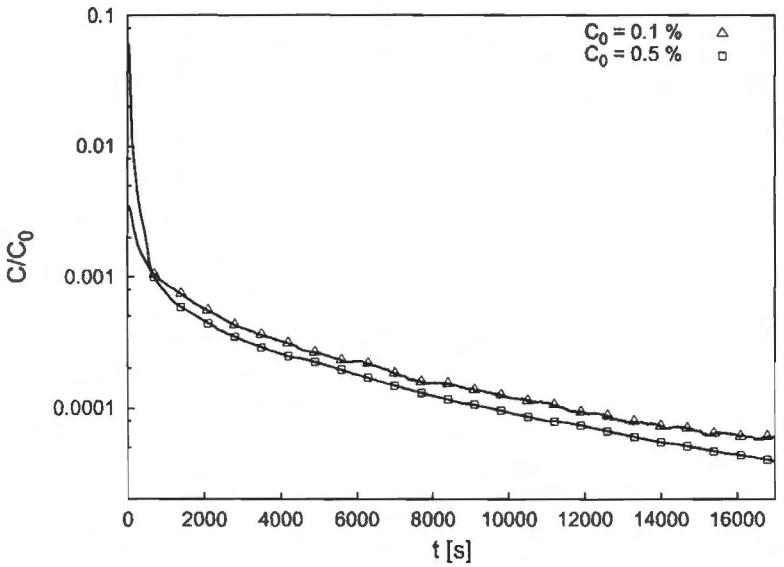

Figure 4.28: Independence of ZLC desorption curves of hydroquinone in TS-1 on concentration T = 30 °C, F = 2 ml/min, solvent: water

orption curves for hydroquinone at different initial concentrations demonstrate that the assumption of the isotherm being in the Henry's region is justified. However, Figure 4.28 also shows that the influence of background noise is less pronounced for higher concentration levels; concentrations of 0.2 - 0.5 % were therefore used for subsequent ZLC experiments.

In the previous paragraph, the importance of blank experiments and the independence of the monitored desorption curves of fluid hold-up in the long-time region was highlighted. To give further evidence that the long-time region of the ZLC curves is controlled only by intracrystalline diffusion, a ZLC diffusion experiment was repeated at different flow rates of the purging carrier solvent. Figure 4.29 shows the ZLC transient desorption curves of phenol diffusing in TS-1 at different flow rates. From Figure 4.29, it is evident that the tail of all transient desorption curves represents a straight line with the same slope for all flow rates. However, at higher flow rates the detector noise becomes more

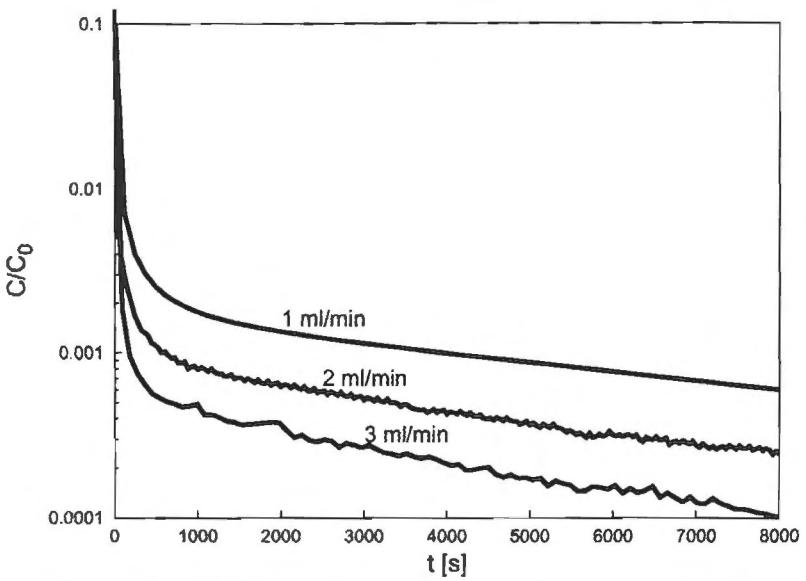

Figure 4.29: ZLC desorption curves for the diffusion of phenol in TS-1 at different purge flow rates T = 30 °C, $C_{0,phenol}$ = 0.2 wt.%, solvent: water

important since the concentration has to be measured at very low levels; flow rates of 1 - 2 ml/min were therefore used to obtain 'clean' curves of higher accuracy.

4.4.1.4 Model fit

The theoretical background of the ZLC model was described in section 2.5.1. The parameters D/R^2 and L were determined from the slope and intercept of the long-time region of the experimental desorption curves and used to calculate theoretical ZLC curves. Figure 4.30 shows experimental and calculated ZLC desorption curves for the diffusion of phenol in TS-1 with water as the solvent. A very good fit was obtained for the linear tail of the curve whereas a deviation in the short-time region is evident, probably originating from a non-linear detector response at high concentrations. A model fit of similar high quality was obtained for all compounds studied, proving the validity of the ZLC theory for the interpretation of the measured desorption curves.

4.4.2 Dependence of liquid-phase intracrystalline diffusion on the solvent

In the gas phase, the effect of counter-diffusing gas molecules can generally be neglected as their diffusivity is much larger and little interactions exist between the inert carrier gas and the hydrocarbon. In the liquid phase however, the counter-diffusing solvent could have an influence on the mobility of diffusing molecules, particularly if the kinetic diameter of these molecules are close to the pore dimensions of the microporous solid as it is the case for aromatics diffusing in TS-1 pores.

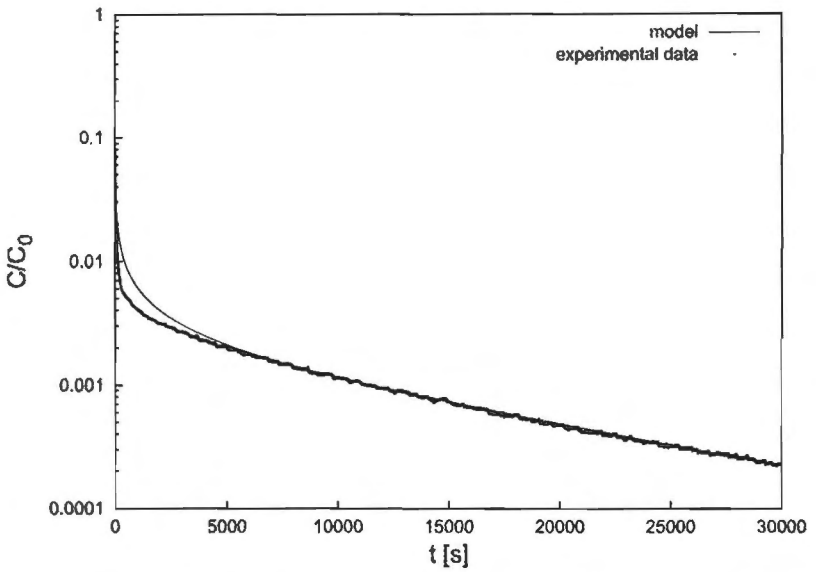

Figure 4.30: Experimental and calculated ZLC desorption curves for the diffusion of phenol in TS-1 T = 30 °C, F = 2 ml/min, $C_{0,phenol}$ = 0.2 wt.%, solvent: water

Few reports are available on the influence of the counter-diffusing solvent and no data at all are available for the diffusion of phenols in TS-1. The diffusivity of phenol, catechol and hydroquinone in TS-1 was therefore measured in water and methanol as the solvent under identical conditions; Table 4.24 shows the diffusivity values extracted from the ZLC desorption curves.

Table 4.24: Diffusivity and Henry's constant of phenol, hydroquinone and catechol in TS-1 with water and methanol as solvents

	Water		Methanol	
	D [$\frac{m^2}{s}$]	K[1]	D [$\frac{m^2}{s}$]	K[1]
Phenol	5.2e-17	77.7	4.4e-16	0.61
Catechol	8.2e-17	14.8	1.5e-16	0.64
Hydroquinone	1.0e-16	6.2	9.2e-17	1.02

T = 30 °C, $C_{0,aromatic}$ = 0.2 wt.%, F = 1 ml/min; [1]extracted from ZLC curve

4.4.3 Influence of the substituent at the aromatic ring on the diffusivity

The influence of the nature of the substituent attached to the aromatic ring on activity and selectivity in TS-1 was investigated in kinetic studies of the hydroxylation reaction. The influence of the substituent on the mass transport of monosubstituted benzenes was investigated applying the ZLC method. Table 4.25 shows the intracrystalline diffusivities of phenol, anisole and toluene in TS-1 with methanol as the solvent. Although the values in Table 4.25 are in the same order of magnitude, a significant difference in diffusivity in the order phenol > anisole > toluene was obtained.

Table 4.25: Diffusivities of phenol, anisole and toluene in TS-1

	D $[\frac{m^2}{s}]$
Phenol	4.4e-16
Toluene	1.2e-16
Anisole	2.2e-16

T = 30 °C, $C_{0,aromatic}$ = 0.2 wt.%, F = 1 ml/min, solvent: methanol

4.4.4 Temperature dependence of diffusion

As pointed out in section 3.6, there is generally a great deal of inconsistency concerning the values for intracrystalline diffusivities reported in the literature. Depending on the experimental method used and the model applied to extract the diffusivity, the values found in the literature vary by orders of magnitude. However, the activation energy of diffusion extracted from measurements at different temperatures are generally in good agreement. The activation energy for the liquid-phase diffusion of phenol in TS-1 was therefore measured with the ZLC method and compared to literature values.

The temperature dependence of the diffusivity is given by the following van't Hoff-type equation:

$$D_c(T) = D_\infty \cdot exp(-\frac{E_A}{RT}) \tag{4.13}$$

Table 4.26 shows the diffusivity of phenol in TS-1 obtained with the ZLC method at different temperatures. Figure 4.31 shows an van't Hoff plot of the measured diffusivity values at different

Table 4.26: Intracrystalline diffusivity of phenol in TS-1 at different temperatures

T [°C]	D_{phenol} $[\frac{m^2}{s}]$
0	2.4e-17
30	5.2e-17
60	7.7e-17
80	1.1e-16

F = 2 ml/min, $C_{0,phenol}$ = 0.2 wt.%, solvent: water

temperatures. The good linear fit obtained in Figure 4.31 shows the van't Hoff-type dependency of the diffusivity on the temperature. From the slope of the plot, an activation energy of 20.4 kJ/mol can be extracted for the diffusion of phenol in TS-1 with water as the counter-diffusing solvent.

4.4.5 Dependence of intracrystalline diffusivity on the pore structure

The liquid-phase ZLC method was successfully applied to measure the intracrystalline diffusivity of aromatics in TS-1 using different solvents. Although the diffusion in Al-free Ti-beta is expected to be faster due to the larger pores, the hydroxylation of phenol over the Al-free Ti-beta samples

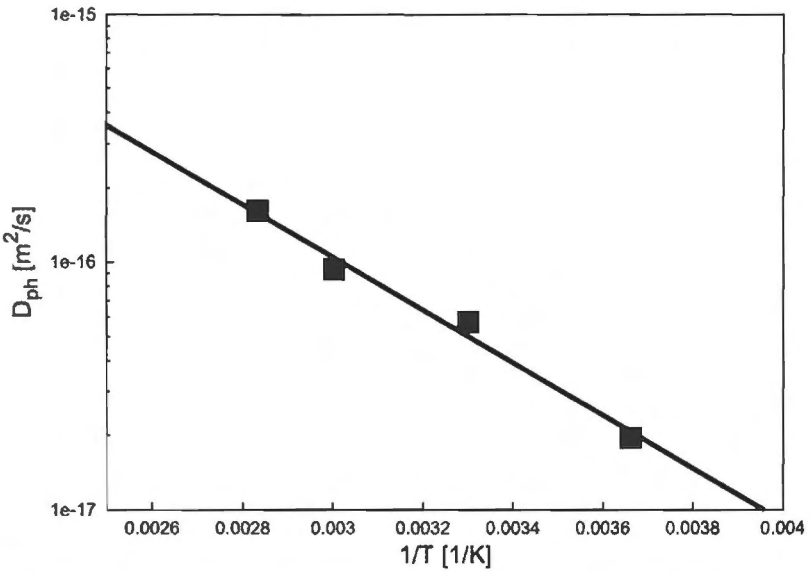

Figure 4.31: van't Hoff plot of the intracrystalline diffusivity of phenol in TS-1

F = 2 ml/min, $C_{0,phenol}$ = 0.2 wt.%, solvent: water

used in this work was also shown to be mass-transfer limited (see Figure 4.15). The measurement of intracrystalline diffusivities for aromatics in Al-free Ti-beta is thus of great interest, particularly for a comparison to the diffusivity values obtained for TS-1. Due to their small external surface area, the large Al-free Ti-beta crystals were suitable for diffusion studies and were used for a ZLC column packing, applying identical setups and procedures as for TS-1. Table 4.27 shows a comparison of the diffusivity values for phenol in TS-1 and Al-free Ti-beta, determined with the ZLC technique. The intracrystalline diffusion of phenol is about a factor of 8 faster in Al-free Ti-beta than in TS-1.

Table 4.27: Diffusivity of phenol in TS-1 and Al-free Ti-beta

catalyst	D_{phenol} [$\frac{m^2}{s}$]
TS-1	5.2e-17
Al-free Ti-beta	3.9e-16

T = 30 °C, F = 2 ml/min, $C_{0,phenol}$ = 0.3 wt.%, solvent: water

As expected, the larger pores of Al-free Ti-beta allow faster transport of the aromatic hydrocarbons through the microporous system. The intracrystalline diffusivity of phenol in Al-free Ti-beta with methanol as the solvent was determined to be $1.5 \cdot 10^{-15} m^2/s$ (T = 60 °C), hence much closer to the diffusivity of phenol measured for TS-1 with methanol ($4.4 \cdot 10^{-16} m^2/s$ at T = 30 °C).

4.4.6 Comparison of pulse and ZLC method

In the previous paragraphs, the suitability of the ZLC technique to measure liquid-phase intracrystalline diffusivities of aromatics in TS-1 and Al-free Ti-beta was shown. A pulse technique was applied in this work to measure Henry's constants with a different experimental setup (see section 3.5.1.1). However, a pulse method can be applied to measure intracrystalline diffusivities using the ZLC columns and the ZLC experimental setup if the adsorption of the compound is strong enough and the diffusivity sufficiently slow. These conditions were fulfilled for the adsorption and diffusion of phenol, catechol and hydroquinone in TS-1 with water as a solvent, thus the pulse method as described in section 2.5.2 (see also Schwan (2001)) was applied to measure the diffusivity and Henry's constants for these systems and to compare the results to the ZLC values. Instead of a step desorption response as for the ZLC method, the transient response curve of a pulse of the diffusion hydrocarbon is monitored and the diffusivity and Henry's constant can be extracted from the tail in a similar way as demonstrated for the ZLC method. Figure 4.32 shows a calculated and a measured pulse response curve. As for the ZLC method, the experimental response curve obtained by

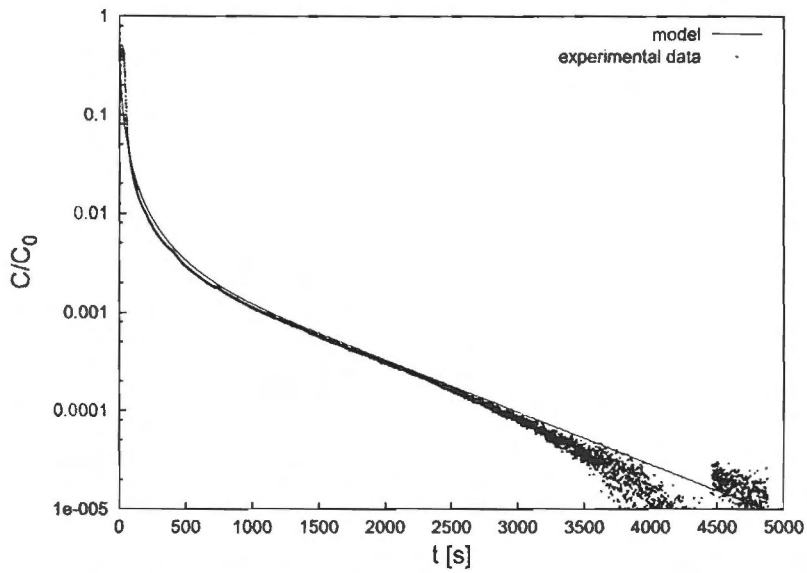

Figure 4.32: Experimental and calculated pulse response curves for phenol in TS-1

T = 30 °C, F = 1 ml/min, $C_{0,phenol}$ = 0.5 wt.%, solvent: water

the pulse method is represented very accurately by the theoretical model. The diffusivity of phenol, catechol and hydroquinone was determined using the pulse technique in water as the solvent. Table 4.28 shows a comparison of the intracrystalline diffusivity values determined using ZLC and pulse technique. The values obtained from the pulse method were in average about a factor of 2 - 4 higher than the values obtained from the ZLC method. This demonstrates again that absolute values for transport diffusivities are dependent on the experimental measurement technique. However,

Table 4.28: Diffusivity of phenol in TS-1: Comparison of ZLC and pulse technique

	ZLC technique[1]		Pulse technique[1]	
	D [m^2/s]	K	D [m^2/s]	K
Phenol	5.2e-17	77.7	2.3e-16	84.3
Catechol	8.2e-17	14.8	3.9e-16	9.2
Hydroquinone	1.0e-16	6.2	5.2e-16	6.1

[1] T = 30°C, F = 1 - 2 ml/min, $C_{0,aromatic}$ = 0.2 wt.%, solvent: water

considering that two completely different models and techniques are compared, the values were in good agreement. Furthermore, the pulse technique yielded consistently higher diffusivities for all compounds, confirming that the relative values are correct.

4.5 Adsorption of aromatics on TS-1 and Al-free Ti-beta in various solvents

4.5.1 Suitability and limits of the experimental setup

In the previous paragraph, a pulse technique was applied to measure intracrystalline diffusivities. The liquid-phase chromatographic technique used in this work to measure adsorption coefficients relies on a similar experimental technique; the response of a hydrocarbon pulse injected into a zeolite bed is monitored. However, despite this similarity the pulse and the chromatographic method are based on different principles. The former is based on monitoring a transient pulse response where mass transfer resistances create a concentration gradient in the microporous solid, whereas the latter method is based on the absence of diffusional resistances; the concentration in the pores is assumed to be uniform and in equilibrium with the concentration in the bulk solution. The equilibrium criterion represents the most important assumption made by applying the chromatographic technique to measure Henry's constants in the liquid phase. The principles and assumptions are essentially identical with the ones for the gas-phase pulse technique introduced in section 2.4.1 and the same equations are used to calculate the Henry's constants. The chromatographic technique has been applied in many publications and has been proven to be a suitable technique to determine adsorption coefficients [Awum et al. (1988), Boulicault et al. (1998), Langhendries et al. (1999), Lin and Ma (1989)]. The experimental setup used in this work was also used by Langhendries et al. (1999) and has been shown to be suitable for the measurement of Henry's constants in TS-1 and Al-free Ti-beta in the liquid phase. However, two major limitations have to be mentioned. Firstly, if the adsorption in the microporous solid is too strong, the peak first and second moments become too large and cannot be determined accurately. Secondly, the crystal size of the microporous solid has to be small

enough to ensure the absence of diffusional resistances.

4.5.2 Adsorption of substituted benzenes

4.5.2.1 Batch method

Since relatively high concentrations were used in the reaction studies, the adsorption isotherms were not expected to be in the linear region under reaction conditions. The batch adsorption method was therefore used to determine separation coefficients under reaction conditions and -concentrations and to compare the results to Henry's constants determined with the chromatographic technique. Table 4.29 shows the partition coefficients and the calculated activity coefficient for phenol in different solvents for TS-1 and a silicalite-1 sample as determined by the batch method. A very strong ad-

Table 4.29: Phenol partition (α) and activity (γ) coefficients in different solvents

Solvent	α(TS-1)[1]	α(S-1)[2]	γ[3]
water	33	19	9.05
methanol	$\approx$1	-	0.59
acetone	$\approx$1	-	0.31

T = 30 °C, 0.1 g catalyst, 5 ml solvent, 0.25 g phenol; [1]TS-1 of $d_{crystal}$ = 0.1 μm; [2]Silicalite-1 of $d_{crystal}$ = 0.2 μm; [3] calculated with UNIFAC at reaction conditions

sorption of phenol in TS-1 was found with water as the solvent whereas no preferential adsorption of phenol was observed in methanol and acetone. The strong adsorption of phenol in water was more pronounced for TS-1 than for S-1. Table 4.29 also shows that the partition coefficients measured correlate with the calculated activity coefficients for phenol.

4.5.2.2 Chromatographic method

The assumption of adsorption equilibrium in the chromatographic adsorption study was verified by changing the flow rate of the carrier solvent. A plot of the peak first moment μ_1 versus the ratio of bed length and superficial fluid velocity (L_{cat}/u_f) should show a linear relationship for all flow rates if equilibrium was attained (see equation 2.1 in section 2.4.1). The respective plots for TS-1 and Al-free Ti-beta are shown in Figure 4.33. A linear relationship was indeed found for flow rates between 0.05 and 0.3 ml/min, confirming the validity of the assumption that adsorption equilibrium was attained during the chromatographic measurements. Small deviations from linearity were observed at higher flow rates (> 0.3 ml/min); a flow rate of 0.1 ml/min was therefore used for the chromatographic liquid-phase adsorption study. The chromatographic method was used to determine the Henry's constants of various aromatics with water, methanol and acetone as the solvents in TS-1 and Al-free Ti-beta. Typical responses of pulse injections into a TS-1 adsorption column with

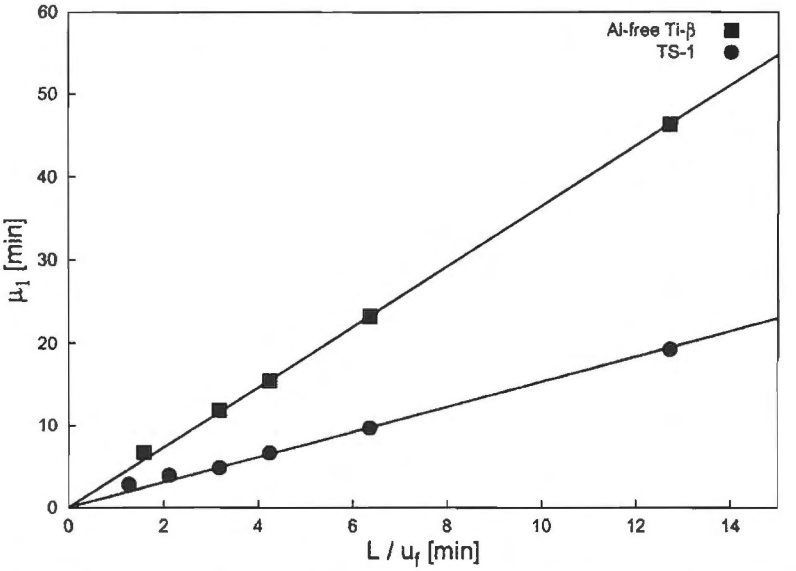

Figure 4.33: Equilibrium adsorption data for toluene adsorption in TS-1 and Al-free Ti-beta showing μ_1 plotted against L_{cat}/u_f (T = 30 °C); solvent: methanol

methanol as the carrier solvent are displayed in Figure 4.34. The peak first moments were deter-

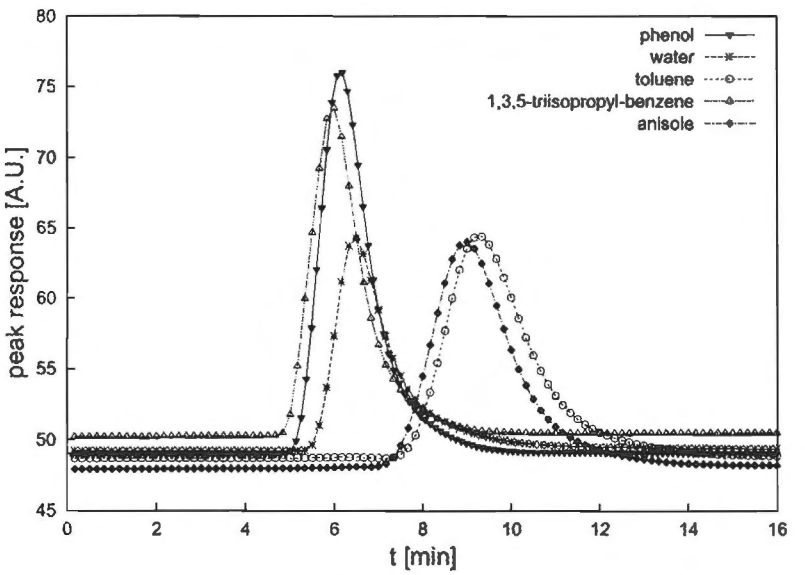

Figure 4.34: Typical chromatographic responses obtained for pulse injection of aromatics in a TS-1 column (T = 30 °C)

mined by integration (see equation 2.1) of the peak responses and the Henry's constants calculated for various substituted benzenes with water, methanol and acetone as the solvents. The dead time of the system was determined prior to the measurements and subtracted from the peak retention times obtained. The results are displayed in Table 4.30. Phenol, hydroquinone and catechol were the only

Table 4.30: Henry's constants for the adsorption of substituted benzenes in different solvents in TS-1 and Al-free Ti-beta

K_i for compound	TS-1[1]			Al-free Ti-beta[2]		
	Water[3]	Methanol	Acetone	Water[3]	Methanol	Acetone
Phenol	77.7	0.66	0.62	17.15	1.31	0.72
Hydroquinone	6.2	0.63	0.62	0.45	0.89	0.69
Catechol	14.8	0.67	0.66	1.11	8.50	1.34
p-benzoquinone	-	0.62	0.57	-	-	-
Anisole	-	1.32	0.62	-	4.21	0.81
p-hydroxy-anisole	-	0.66	0.61	-	1.91	-
Toluene	-	1.40	0.63	-	3.86	0.77
o-cresol	-	0.62	0.58	-	0.77	-
m-cresol	-	0.63	0.59	-	-	-
p-cresol	-	0.65	0.6	-	1.47	-
Acetanilide	-	0.80	0.66	-	1.61	0.77
p-hydroxy-acetanilide	-	0.64	0.67	-	1.15	-
Water	-	0.76	1.36	-	0.73	1.15
1,3,5-Triisopropylbenzene	-	0.60	0.56	-	0.62	0.58

T = 30 °C, F = 0.1 ml/min; [1]$d_{crystal}$ = 0.1 μm; [2]$d_{crystal}$ = 2 - 5 μm; [3]determined by ZLC pulse method

compounds studied with water as the solvent due to the limited solubility of the other aromatics in water. With water as a solvent, the peak first moment was too large to be accurately measured by the chromatographic method. The ZLC pulse method was therefore used as the experimental technique to determine the Henry's constants for the aromatic compounds in water. 1,3,5-Triisopropylbenzene was used as a reference compound for a non-adsorbing aromatic hydrocarbon since its kinetic diameter is larger than the pore openings of both TS-1 and Al-free Ti-beta. Thus, only compounds with a Henry's constant significantly greater than the one determined for 1,3,5-triisopropylbenzene are preferentially adsorbed in the micropores of the solid.

4.5.3 Adsorption of naphthalenes

The chromatographic setup was also used to determine the Henry's constants for the adsorption of various substituted naphthalenes in TS-1 and Al-free Ti-beta. Table 4.31 shows the results obtained. The small Henry's constant for the adsorption of 1-naphthol (similar to 1,3,5-triisopropylbenzene) in TS-1 indicates that substituted naphthalenes cannot enter the pores of TS-1 under reaction conditions. Only 2-methyl-naphthalene and, to a minor extent, 1-naphthol were preferentially adsorbed by Al-free Ti-beta when methanol was the solvent.

Table 4.31: Henry's constants for the adsorption of substituted naphthalenes in different solvents in TS-1 and Al-free Ti-beta

K_i for compound	TS-1[1]		Al-free Ti-beta[2]	
	Methanol	Acetone	Methanol	Acetone
1-Naphthol	0.62	0.6	0.78	0.63
1,4-naphthoquinone	-	-	0.63	0.6
2-methyl-naphthalene	-	-	5.33	0.64
2-methyl-1,4-naphthoquinone	-	-	0.70	0.64
1,3,5-Triisopropylbenzene	0.6	0.56	0.62	0.58

T = 30 °C, F = 0.1 ml/min; [1]$d_{crystal}$ = 0.1 μm; [2]$d_{crystal}$ = 2 - 5 μm

Chapter 5

Discussion

5.1 Selective liquid-phase adsorption of aromatics by titanium-containing molecular sieves

As both TS-1 and Al-free Ti-beta are known to be very hydrophobic materials, a very high adsorption coefficient for hydrocarbons was expected in water. This was shown by the strong adsorption of phenol, catechol and hydroquinone in water; the hydrophobic silicalite framework prefers the aromatic over the very polar water molecules. The polarity seems to be the key factor in determining the adsorption properties of the aromatic molecule. The more polarised the aromatic ring, the less strongly the molecule was adsorbed in TS-1 and Al-free Ti-beta with water and methanol as the solvent. This becomes more apparent by comparing the aromatic reactants with their hydroxylated reaction products. The hydroxylated isomers were consistently less strongly adsorbed since the addition of a hydroxyl group to the aromatic ring increases the polarity and hydrophilicity of the molecule. However, with acetone as the solvent, all adsorption constants were low, indicating that acetone was preferred over aromatic compounds in all cases.

A comparison of the adsorption constants for products and reactants also partially explains why the hydrophobic titanium silicalites are efficient catalysts for aromatic hydroxylations with aqueous hydrogen peroxide. The hydroxylated (primary) reaction products are principally more easily oxidised than the reactants, which is the reason for the generally lower selectivities observed in homogeneously catalyzed reactions. However, for the formation of tars or overoxidation products in TS-1 or Al-free Ti-beta, the hydroxylated aromatic molecules first have to re-adsorb onto the catalyst surface and subsequently react again with titanium hydroperoxo sites. Since the reactant is more hydrophobic and clearly preferred over the reaction products, competitive adsorption is in favour of the former. Readsorption and subsequent overoxidation of hydroxylated aromatics is thus suppressed. A second factor is the adsorption of hydrogen peroxide, which is presumably relatively

weak considering the polarity (and hydrophilicity) of the H_2O_2 molecule. Since immediate reaction of the peroxide with the titanium sites occurs, the adsorption properties of H_2O_2 could not be determined. No indications for possible intraporous H_2O_2 concentrations in TS-1 can be found in the literature. On the basis of the polarity of the molecule, water can be taken as a 'model' compound for H_2O_2. Table 5.1 shows dielectric constants (a measure for the polarity of the molecule) of solvents and reactants. Low K values for water (see Table 4.30) suggest that the intraporous concentration

Table 5.1: Dielectric constants for substrates and solvents

compound	dielectric constant ε_r [1]
water	80.4
acetone	20.7
methanol	33.0
hydrogen peroxide	70.7
phenol	28.1
anisole	4.3
toluene	2.4

[1] T = 298 K, taken from Thangaraj et al. (1994) and ASI Instruments (2001)

of hydrogen peroxide is also relatively low, which could be another key factor for the stability and excellent catalytic properties of titanium silicalites. Large crystals of TS-1 and Al-free Ti-beta (having small external surface areas) showed little activity for H_2O_2 decomposition with acetone and methanol as the solvent, supporting the assumption that the intraporous hydrogen peroxide concentration is low in these solvents. With water as the solvent, since H_2O_2 is less polar than H_2O, the H_2O_2 concentration in the pores is higher, resulting in a higher rate of decomposition. Under reaction conditions however, strong adsorption of the aromatic compound will lower intraporous H_2O_2 concentration levels. Excessive hydrolysis of Ti-O-Si bonds is prevented and peroxide decomposition suppressed through the control of the H_2O_2 concentration at the active sites, which results in very good peroxide efficiencies. The clearly inferior catalytic properties of hydrophilic materials such as mesoporous titanosilicates or amorphous SiO_2-TiO_2 with aqueous H_2O_2 support this argument.

5.2 Diffusion of aromatic compounds in TS-1 and Al-free Ti-beta from the liquid phase

The suitability of the ZLC method to determine liquid-phase intracrystalline diffusivities in TS-1 and Al-free Ti-beta has been shown in section 4.4.1.1 - 4.4.1.4. Good reproducibility and independence of the measured diffusivities of important parameters such as blank response of the system, concentration of diffusing compound and purge flow rate have been demonstrated. Furthermore, it has

been shown that the experimental data fit the theoretical model very well, confirming that reliable intracrystalline diffusivity values can be extracted from the measured ZLC desorption curves.

5.2.1 Intracrystalline diffusivities of substituted benzenes in TS-1

The intracrystalline diffusivities determined with the ZLC method in this work are about an order of magnitude larger than the values reported by Wu et al. (1998) and van der Pol et al. (1992). The former used a batch uptake rate method to determine the diffusivity of toluene in TS-1 and reported a value of $\approx 1 \cdot 10^{-18} \frac{m^2}{s}$ (T = 0°C), whereas the latter estimated the diffusivity of phenol in TS-1 to be $\approx 2 \cdot 10^{-18} \frac{m^2}{s}$ (T = 60°C) using kinetic data from samples with different crystal sizes. However, it has to be considered that in these studies, the diffusivity of the aromatic compound was measured under reaction conditions, i. e. in the presence of not only the solvent, but also H_2O and H_2O_2. Strong interactions between the aromatic substrate and the titanium hydroperoxo groups are expected and more severe space restrictions in the presence of 'open' titanium sites in the channels could also decrease the mobility of the aromatic molecules. The diffusion of aromatic molecules could therefore be lower under reaction conditions. It has to be emphasised that the diffusivities reported in this work are binary counterdiffusivities with only the solvent and the aromatic compound competing for adsorption and diffusion.

The influence of the counter-diffusing solvent on the intracrystalline diffusivity has rarely systematically been studied in the literature. In the few reports available, mostly sodium- and potassium-exchanged zeolites X and Y were studied and most authors report liquid-phase diffusivities similar to values obtained in the gas phase [Brandani and Ruthven (1995), Ching and Ruthven (1988), Lin and Ma (1989), Ruthven and Stapleton (1993)]. In some cases, the diffusivities measured for microporous solids in liquid systems were reported to be even larger than the corresponding gas-phase values [Boulicault et al. (1998)], which was explained by an expansion of the zeolite lattice at high loadings. In the above mentioned studies, it was generally concluded that the counter-diffusing solvent in liquid systems has little influence on the diffusivity in microporous solids. However, Awum et al. (1988) reported a significant reduction of the diffusivity of benzene in zeolite NaX when changing the solvent from hexane to cyclohexane.

From the ZLC diffusivities extracted from the transient desorption curves of phenol, hydroquinone and catechol in TS-1 it is clear that the solvent has a strong influence. The diffusivity of phenol in TS-1 increased by almost an order of magnitude when the solvent was changed from water to methanol. For catechol, the diffusivity increased only by a factor of 2 and the diffusivity of hydroquinone was hardly influenced by the solvent. The influence of the solvent is therefore strongly dependent on the interactions of solvent, zeolite and aromatic compound in the particular system. A comparison of the intracrystalline diffusivity values and the Henry's constant for a particular

compound-solvent combination suggests the existence of a correlation between the diffusion in the pores and the adsorption of the compound by the zeolite. The stronger the aromatic molecule was adsorbed, the slower the mass transport in the TS-1 channels. The same trend was observed when the diffusivities of phenol, anisole and toluene in TS-1 with methanol as the solvent were compared. The most strongly adsorbed compound toluene showed the slowest diffusion. In previous chapters it has been shown that geometric constraints exist for aromatics in the medium-size pores of TS-1. It is therefore consistent to assume that strong interactions of the aromatic molecule and the zeolite walls, expressed as a large Henry's constant, impose a restriction on the mobility of the molecule which translates into a slower diffusion. Since the adsorption of aromatics in TS-1 strongly depends on the solvent (as shown in Table 4.30), the latter also has an influence on the diffusivity.

Diffusivity values reported in the literature differ by several orders of magnitude, depending on the method and experimental setup used. The activation energies for diffusion are however generally in good agreement. The van't Hoff plot for the diffusion of phenol in TS-1 with water as the counter-diffusing solvent at different temperatures shows a good linear correlation (see Figure 4.31), and an activation energy of 20.4 kJ/mol was determined. No literature value exists for comparison, but the activation energy determined in this work is in the same range as values reported for aromatics in zeolite NaX and silicalite/ZSM-5. Awum et al. (1988) reported an activation energy of 14.7 kJ/mol for the diffusion of phenol in zeolite NaX with water as the solvent and 27.2 kJ/mol for the diffusion of benzene in NaX with hexane as counter-diffusing solvent; similar values were reported by Ruthven and Stapleton (1993). Table 5.2 shows literature values for measured liquid-phase counterdiffusivities of aromatics in silicalite/ZSM-5 (the isostructural analogues of TS-1) taken from Kärger and Ruthven (1992).

5.2.2 Intracrystalline diffusivities of substituted benzenes in Al-free Ti-beta

No comparison of liquid-phase intracrystalline mass transport in the medium-pore TS-1 and the large-pore Ti-beta is available in the literature. Although the large crystals of Al-free Ti-beta were generally suitable for diffusion measurements using the ZLC method, the diffusional path length could not be determined as accurately as for the TS-1 sample. The large TS-1 crystals showed a very narrow crystal size distribution and the diffusional path length can be assigned to the half-thickness of the slab-shaped crystals [Kärger and Ruthven (1992), Ruthven et al. (1991)]. The Al-free Ti-beta sample consisted of well faceted truncated bipyramids and showed a crystal size distribution between 1 and 5 μm. The shape was therefore approximated with the spherical model and the diffusional path length corrected ($l \approx 1.8$ μm) according to Duncan and Möller (2001).

A comparison of the diffusivity of phenol in TS-1 and Al-free Ti-beta (with water as the counter-diffusing solvent) under identical conditions showed that the mass transport of phenol in Al-free

Table 5.2: Diffusion of aromatics in silicalite/H-ZSM-5 from the liquid phase [Kärger and Ruthven (1992)]

sorbate/ solvent	sorbent	crystal size [μm]	Method	T [K]	D $[\frac{m^2}{s}]$	E_A $[\frac{KJ}{mol}]$
Benzene/ n-hexane	silicalite	27	ZLC	313 333	$2.5 \cdot 10^{-14}$ $4.0 \cdot 10^{-14}$	-
p-xylene/ n-hexane	silicalite	27	ZLC	313	$8.5 \cdot 10^{-15}$	-
ethylbenzene/ n-hexane	silicalite	27	ZLC	313	$3.1 \cdot 10^{-15}$	-
toluene/ cyclohexane	silicalite	1.2	LC	303 323	$8.0 \cdot 10^{-14}$ $1.2 \cdot 10^{-15}$	18
toluene/ iso-octane	H-ZSM-5	1.5	batch	306	$1.7 \cdot 10^{-17}$	-
p-xylene/ iso-octane	H-ZSM-5	1.5	batch	288 320	$1.3 \cdot 10^{-17}$ $3.6 \cdot 10^{-17}$	25.4
n-propylbenzene/ iso-octane	H-ZSM-5	1.5	batch	288 320	$2.1 \cdot 10^{-18}$ $8.5 \cdot 10^{-18}$	34

Ti-beta is about a factor of 8 faster than in TS-1. Thus, the phenol molecules are able to move significantly faster through the larger channels of Al-free Ti-beta, which confirms that the pores of Al-free Ti-beta impose less geometric constraints on monosubstituted benzenes than the ones of TS-1. With methanol as the solvent, the difference between TS-1 and Al-free Ti-beta for the diffusivity of phenol was much smaller.

5.3 Hydroxylation of substituted benzenes with TS-1, Al-free Ti-beta and Ti-HMS

5.3.1 Activity

5.3.1.1 Influence of the solvent

A pronounced effect of the solvent on the activity of the titanium-substituted zeolites was found for all hydroxylation reactions. In the phenol hydroxylation, the activity of both TS-1 and Al-free Ti-beta decreased in the order water >> methanol > acetone. In the hydroxylation of anisole and toluene, both catalysts were more active in methanol than in acetone. The exceptionally high activity for TS-1 and Al-free Ti-beta in the phenol hydroxylation with water as the solvent can be explained by the very strong adsorption of phenol in the zeolite pores. This results in higher reaction rates with water as the solvent. Adsorption effects can also explain the higher activity for both catalysts in the

anisole and toluene hydroxylation with methanol as compared to acetone. The Henry's constants for anisole and toluene were higher when methanol was the solvent. As for the water-phenol system, the higher concentration of the aromatic in the pores causes higher reaction rates with methanol as the solvent. However, the Henry's constants for phenol in TS-1 and Al-free Ti-beta as determined by the chromatographic and the batch method, shown in Table 4.30 and Table 4.29, respectively, were almost identical. Thus, adsorption phenomena cannot explain the higher activity of TS-1 and Al-free Ti-beta for the phenol hydroxylation in methanol.

To explain the lower activity in acetone, attention must be focused on the second reactant, i. e. hydrogen peroxide. The interactions of ketones and H_2O_2 are known in organic chemistry. This may lead to the formation of explosive peroxides [Davies (1961)]. A variety of peroxides and hydroperoxides can be also formed from the interaction of acetone with H_2O_2. Figure 5.1 shows various compounds formed by reactions of acetone with hydrogen peroxide. All reactions are equilibrium reactions and, except for the acid-catalyzed cyclisations (species **5**), they are possible in both basic and acidic environments [Davies (1961), Sauer and Edwards (1971)]. The reaction scheme shows commonly reported acetone-H_2O_2 reactions, but it does not cover all possible compounds formed and more pathways certainly do exist [Davies (1961)]. The formation of the primary adduct (species

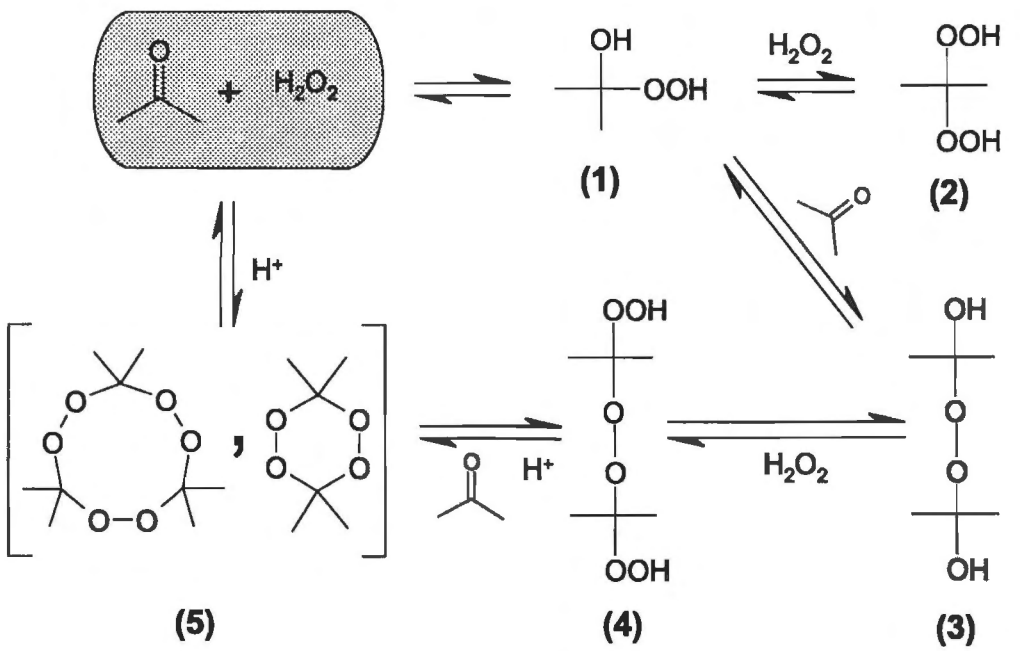

Figure 5.1: Reactions of acetone with hydrogen peroxide

1 in Figure 5.1) was intensively studied by Sauer and Edwards (1971). In their study, the equilibrium of the primary adduct reaction was determined at different temperatures and the thermodynamic parameters $\triangle_R H$ and $\triangle_R S$ are reported to be -29.29 kJ/mol and 117.15 J/(mol·K), respectively. The

equilibrium constant for the reaction

$$\boxed{\text{Acetone} + H_2O_2 \rightleftharpoons \text{2-hydroxy-2-hydroperoxy-propane (1)}}$$

is given by

$$K_e = \frac{c(Adduct\ 1)}{c(Acetone) \cdot c(H_2O_2)} = exp\left(-\frac{\triangle_R G}{R \cdot T}\right) \tag{5.1}$$

At 60 °C, the equilibrium constant K_e equals 0.0298. Hence, at equilibrium, 24% of the hydrogen peroxide has reacted to 2-hydroxy-2-hydroperoxypropane at the start of the reaction. Equilibrium should be easily attained, since Sauer and Edwards (1971) established that the rate of reaction for the formation of the adduct **1** is several orders of magnitude faster than the phenol hydroxylation. However, this calculation does not take the 'secondary' equilibria for the reaction of the primary adduct to species **2** and **3** into account. The equilibrium constants and thermodynamic parameters for these 'secondary' reactions are unknown. It is however reported that significant formation of species **2** and **3** can be expected in H_2O_2-rich solutions and acetone-rich solutions, respectively [Davies (1961), Sauer and Edwards (1971)]. Hence, the free hydrogen peroxide concentration should be even lower than estimated with the above calculation. Since these reactions are reversible, H_2O_2 can be 'restored' from the adducts as it is consumed in the hydroxylation reaction and the adduct reaction is shifted back to acetone and H_2O_2. Some loss of H_2O_2 due to decomposition of acetone-H_2O_2 adducts can however be expected.

5.3.1.2 Influence of the catalyst

The activity of TS-1, Al-free Ti-beta and Ti-HMS (or Ti-MCM-41) has often been compared in the literature for various reactions, the most studied ones being epoxidation reactions. A higher activity was consistently reported for TS-1 in the epoxidation of linear olefins, whereas Ti-beta was more active in the epoxidation of branched and cyclic olefins; mesoporous titanosilicates showed little activity with aqueous H_2O_2. From these results, it was generally concluded that TS-1 is intrinsically more active than Ti-beta [van der Waal and van Bekkum (1997), van der Waal et al. (1998b), van der Waal (1998), Corma et al. (1995)]; only when the substrate was restricted from entering the pores of TS-1 or diffusional resistances became important, Ti-beta showed higher activity.

The lower activity of mesoporous titanium molecular sieves can be explained by the pronounced hydrophilicity of these materials, which originates from a high concentration of Si-OH groups at their internal surface. Although a very high initial reactivity in the phenol hydroxylation over Ti-HMS was observed, rapid deactivation occurred through extensive tar formation. Overoxidation of hydroxylated reaction products to tars and peroxide decomposition were the dominant reactions, thus rendering a comparison to TS-1 and Al-free Ti-beta difficult. Rhee and Lee (1996) also used mesoporous titanosilicates (Ti-MCM-41) for phenol hydroxylation reactions and also reported rapid

catalyst deactivation and poor reproducibility of the results accompanied by framework disintegration and leaching of titanium. High concentrations of hydrogen peroxide in the Ti-HMS mesopores and readsorption of the (more polar) reaction products, caused by a high hydrophilicity of the framework, could explain this experimental result. Consequently, polar compounds such as water, protic solvents and hydrogen peroxide are much more strongly adsorbed than the hydrocarbon substrate, thus inhibiting the catalytic performance.

A similar explanation was given for the inferior activity of Al-containing Ti-beta; Brønsted acid sites generated by the presence of aluminium in the framework increase the hydrophilicity. However, after the successful synthesis of aluminium-free Ti-beta, epoxidation reaction results for TS-1 and Ti-beta showed the same trends. Van der Waal et al. [van der Waal et al. (1998b), van der Waal and van Bekkum (1997)], Dartt and Davis (1996) and Blasco et al. (1998) used different methods for the synthesis of Al-free Ti-beta and compared the activity to TS-1. In all cases, a higher activity in the epoxidation of linear alkenes (1-hexene, 1-octene) was found for TS-1; with cyclic alkenes [Dartt and Davis (1996)] and terpenes [van der Waal et al. (1998b)], Al-free Ti-beta was reported to be more active. Since both materials have very similar hydrophobicities [Blasco et al. (1998), Dartt and Davis (1996), van der Waal et al. (1998a)], it was concluded that the titanium sites in TS-1 are intrinsically more active than the ones in Al-free Ti-beta.

van der Waal (1998) however acknowledged that even for the epoxidation of 1-octene over Al-free Ti-beta, diffusional limitations might exist. Diffusional limitations for TS-1 are well documented [van der Pol et al. (1993)] and very small crystallites ($d_{crystal} < 0.3$ μm) are generally used for catalytic reactions whereas the Al-free Ti-beta samples in most literature reports consist of relatively large crystals ($d_{crystal} > 1$ μm or not reported) due to the synthesis method. Although intracrystalline diffusion is expected to be faster in Al-free Ti-beta, diffusional limitations might have played a role in some studies.

A second, very important factor is the adsorption of all compounds on the zeolite. Corma et al. (1996a) presented a kinetic study of the oxidation of alcohols over Al-containing Ti-beta and concluded that the kinetics cannot be adequately treated unless the adsorption equilibria on the catalyst, including the competing role of solvents, are considered. Langhendries et al. (1999) studied the adsorption of olefins on TS-1, Al-free Ti-beta and Ti-MCM-41 and came to a similar conclusion since major differences in the adsorption behaviour between these catalysts were observed.

5.3.1.3 Catalyst effectiveness factors for TS-1 and Al-free Ti-beta

The influence of internal diffusion on the reaction rate in a porous catalyst was first described by Thiele (1939) by the introduction of the effectiveness factor η. The effectiveness factor η describes the fraction with which the intrinsic reaction rate found for very small particles is reduced by the

presence of internal transport limitation for larger particles:

$$\eta = \frac{\text{observed reaction rate with diffusion}}{\text{intrinsic reaction rate}} \tag{5.2}$$

The effectiveness factor can be expressed by the Thiele modulus ϕ, which represents the ratio of reaction time over diffusion time. The definition of the Thiele modulus and the effectiveness factor for a second-order reaction in spherical and slab-shaped particles is given below [Levenspiel (1979), Smith (1981)].

For spherical particles:

$$\eta = \frac{1}{\phi}\left(\frac{1}{tanh(3\phi)} - \frac{1}{3\phi}\right); \quad with\ \phi = \frac{d}{6}\sqrt{\frac{k_{react}C_0}{D_{eff}}} \tag{5.3}$$

For slab-shaped particles:

$$\eta = \frac{tanh(\phi)}{\phi}; \quad with\ \phi = \frac{l}{2}\sqrt{\frac{k_{react}C_0}{D_{eff}}} \tag{5.4}$$

With $k_{react} = k_{intr}SV_R\rho_{cat}$ (k_{intr} is the intrinsic rate constant per surface area of catalyst, evaluated from the rate constant extracted with the kinetic model according to equation 4.5). In equation 5.3 and 5.4, d and l represent the crystal diameter and thickness, respectively, k_{reakt} represents the intrinsic reaction rate constant per unit volume of catalyst, C_0 the (initial) concentration of the second reactant (H_2O_2) and D_{eff} the effective diffusivity of the aromatic (phenol) under reaction conditions.

By measuring the reaction rate for significantly different particle sizes one can estimate the diffusivity and the intrinsic reaction rate, as was done for the phenol hydroxylation in TS-1 by van der Pol et al. (1993).

However, the diffusivity and the observed rate constant for the hydroxylation reactions have been measured in this work, hence the intrinsic rate constants, the Thiele moduli and the catalyst effectiveness factors can be calculated. Table 5.3 shows the calculated Thiele moduli and effectiveness factors for the phenol hydroxylation in small, spherical and the large, slab-shaped TS-1 crystals with water as the solvent. The calculated values for the Thiele modulus are based on equation 5.3 and 5.4, whereas the experimental value represents the ratio of observed to intrinsic rate constant according to equation 5.2. For the small crystals, the rate constant for phenol consumption from the silanised TS-1 sample was taken since it represents the reaction inside the pores where diffusional limitations can take place. For the nano-sized TS-1 crystals the effectiveness factor is close to 1, confirming the absence of diffusional limitations in the experiments with this sample. The reaction in the large, slab-shaped crystals was found to be severely diffusion limited, which is confirmed by the low effectiveness factor; only $\approx$ 7-8 % of the active sites in this sample are used. The reaction therefore

Table 5.3: Calculated Thiele moduli and catalyst effectiveness factors for the phenol hydroxylation over TS-1 in water

$d_{crystal}$ [μm]	$k_{observed}$ [$\frac{l}{mol \cdot s \cdot m^2_{cat}}$]	ϕ	$\eta_{calculated}$	$\eta_{experimental}$
0.1 (spherical)	2.1e-6	0.16	1	0.986
3.0 (slabs)	1.4e-7	12.53	0.079	0.069

T = 60 °C, 0.12 g TS-1, 1.2 g phenol, 0.6 ml H_2O_2(30% in H_2O), 5 ml water

only takes place in a small layer close to the external surface of these crystals. Figure 5.2 shows the catalyst effectiveness factor η for the phenol hydroxylation over TS-1 in water as a function of crystal size and Thiele modulus ϕ (calculated according to equation 5.4 and equation 5.3). The

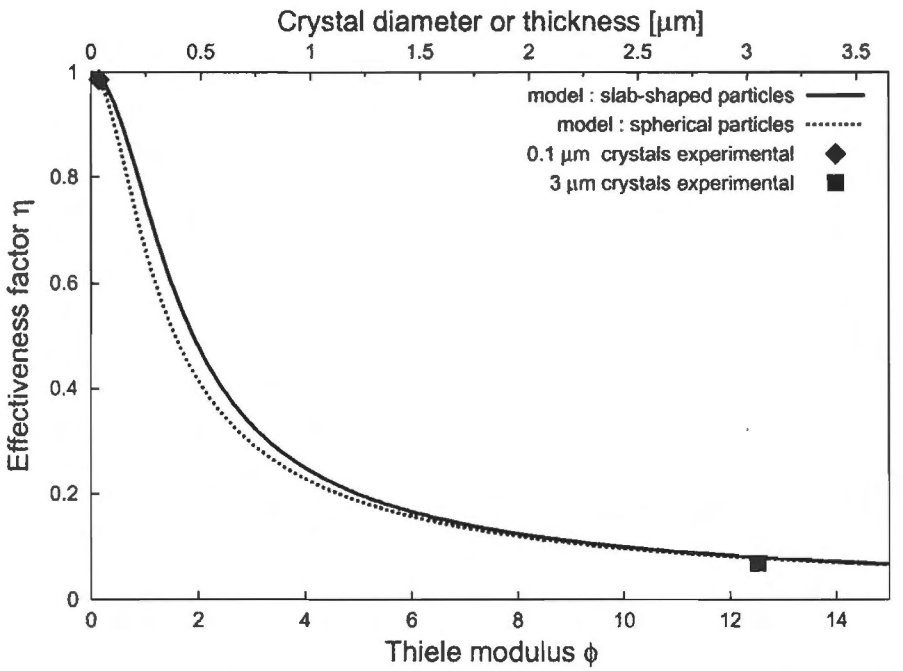

Figure 5.2: Catalyst effectiveness factors η as a function of crystal size and Thiele modulus ϕ for the phenol hydroxylation over TS-1

T = 60 °C, 1.2 g phenol, 0.12 g TS-1, 5 ml water, 0.6 ml H_2O_2 (30 % soln. in H_2O)

evaluation for diffusional limitations was also done for the two Al-free Ti-beta samples of different crystal size synthesised in this work. Table 5.4 shows the calculated Thiele moduli and effectiveness factors for the phenol hydroxylation in Al-free Ti-beta samples of different crystal size with water as the solvent. The calculated (intrinsic) rate constant for the phenol consumption in Al-free Ti-beta with water as the solvent was $1.8 \cdot 10^{-7} \frac{l}{mol \cdot s \cdot m^2_{cat}}$. Figure 5.3 shows the catalyst effectiveness factor η for the phenol hydroxylation over TS-1 in water as a function of crystal size and Thiele modulus ϕ (calculated according to equation 5.4 and equation 5.3). A comparison of the 'intrinsic' rate constants with water as the solvent calculated for Al-free Ti-beta ($1.8 \cdot 10^{-7} \frac{l}{mol \cdot s \cdot m^2_{cat}}$) and TS-

Table 5.4: Calculated Thiele moduli and catalyst effectiveness factors for the phenol hydroxylation over Al-free Ti-beta in water

$d_{crystal}$ [μm]	$k_{observed}$ [$\frac{l}{mol \cdot s \cdot m^2_{cat}}$]	ϕ	$\eta_{calculated}$	$\eta_{experimental}$
0.9	1.2e-6	0.72	0.78	0.77
3.0	6.3e-7	2.16	0.39	0.41

T = 60 °C, 1.2 g phenol, 0.12 g Al-free Ti-beta, 5 ml water, 0.6 ml H_2O_2 (30 % soln. in H_2O)

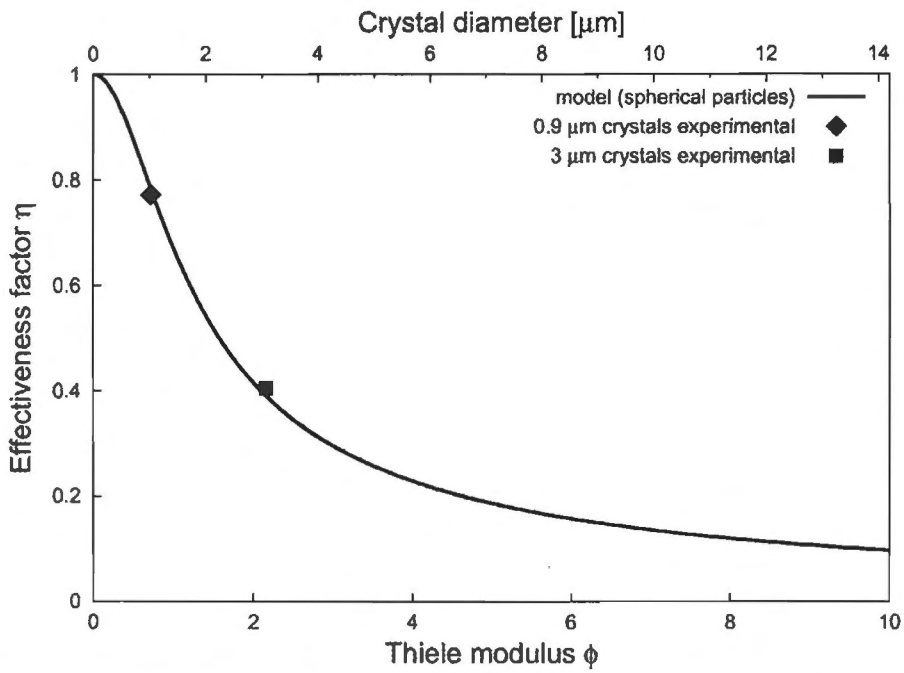

Figure 5.3: Catalyst effectiveness factors η as a function of crystal size and Thiele modulus ϕ for the phenol hydroxylation over Al-free Ti-beta

T = 60 °C, 1.2 g phenol, 0.12 g Al-free Ti-beta, 5 ml water, 0.6 ml H_2O_2 (30 % soln. in H_2O)

1 ($2.1 \cdot 10^{-7}$ $\frac{l}{mol \cdot s \cdot m^2_{cat}}$) could lead to the conclusion that TS-1 is intrinsically slightly more active. However, it has to be emphasised that the observed rate constants were based on the concentrations in the bulk liquid phase; Table 4.30 demonstrates that at least the concentration of the aromatic compound in the zeolite pores can be very different. Particularly for the reaction in water the intraporous concentration of phenol is much higher than in the bulk phase with TS-1 showing a higher K value than Al-free Ti-beta. Adsorption of both reactants must be accounted for by the multiplication of the adsorption coefficient K with the reaction rate of sorbed molecules k_{react}. However, a correction of the calculated rate constants is possible for the concentration of the aromatic since the adsorption constant was measured, but the adsorption equilibrium of H_2O_2 remains unknown. The hydrogen peroxide concentration in the pores of both catalysts are generally expected to be low due to the hydrophobicity of their frameworks. Whereas higher concentrations of phenol are present in the TS-1 pores compared to Al-free Ti-beta with water as the solvent, higher concentrations of H_2O_2 would

be expected in the larger pores of the latter. A comparison of the 'intrinsic' rate constants calculated for TS-1 and Al-free Ti-beta is therefore difficult.

However, the phenol hydroxylation in methanol could give an indication to the true intrinsic activities of both catalysts. Both catalysts showed similar (small) adsorption constants for both phenol and water with methanol as the solvent. Taking water as a 'model' compound for hydrogen peroxide, it can be assumed that similar concentration levels of H_2O_2 and phenol exist in both TS-1 and Al-free Ti-beta with methanol as the solvent. The phenol consumption 'intrinsic' rate constants for the phenol hydroxylation in methanol were therefore determined using the same approach as shown above for the reaction in water. The values for TS-1 and Al-free Ti-beta are $9.3 \cdot 10^{-7}$ and $2.2 \cdot 10^{-7} \frac{l}{mol \cdot s \cdot m^2_{cat}}$, respectively. This result suggests that the titanium sites in TS-1 are indeed intrinsically more active than the ones in Al-free Ti-beta for the hydroxylation of phenol.

Sastre and Corma (1999) performed quantum-chemical calculations simulating the environment of the titanium active site in TS-1 and Al-free Ti-beta. Force-field calculations for atom clusters representative for the structure of TS-1 and Al-free Ti-beta revealed that, although the Ti-O bond distance is identical for both materials, the bond angles are different. They concluded that this effect alters the Lewis-acidity of Al-free Ti-beta and could potentially lead to a different activity of the titanium site in this material compared to TS-1. The fact that Al-free Ti-beta is more active than TS-1 for the the ring-opening of epoxides [Blasco et al. (1998), Camblor et al. (1996)], a reaction catalyzed by Lewis (and Brønsted) acids, seems to support the conclusion that Al-free Ti-beta possesses a higher Lewis-acidity. However, these calculations were performed for a 'closed' titanium site, i. e. for a non-hydrated titanium centre in perfect tetrahedral coordination. These sites are very unlikely to be present after reaction of the zeolite with water and hydrogen peroxide. As Ti-O-Si bonds are hydrolysed upon reaction with water or H_2O_2, a new configuration of the titanium site is created and coordination as well as bond angles change. It is therefore questionable whether conclusions about the activity of the titanium site in TS-1 and Al-free Ti-beta can be based on quantum-chemical calculations if the 'real' configuration of the active site under reaction conditions is not taken in to account.

The general difficulties in comparing catalyst effectiveness factors and catalytic activity in general were pointed out in this paragraph: all adsorption equilibria, the intraporous diffusivity under reaction conditions and the kinetic constants have to be known to be able to make exact statements. The calculated higher intrinsic phenol consumption rate constant for TS-1 in the phenol hydroxylation in methanol as compared to Al-free Ti-beta is however an indication that TS-1 possesses intrinsically more active titanium centres.

5.3.1.4 Influence of the substrate

The reactivity of both TS-1 and Al-free Ti-beta for aromatic hydroxylation decreased in the order phenol > anisole > toluene. The rate constants obtained for consumption of the aromatic reactant in the hydroxylation reactions over TS-1 are comparable in acetone since no preferential adsorption was observed in this solvent. TS-1 was 3.9 and 11.8 times less active in the anisole and toluene hydroxylation compared to the phenol hydroxylation, respectively. If the reaction follows a typical electrophilic substitution mechanism, this can be explained by the activation of the aromatic ring for the electrophilic attack. Figure 5.4 shows the effect of substituents on the aromatic ring in terms of reactivity and regioselectivity. As Figure 5.4 shows, phenol is expected to be the most

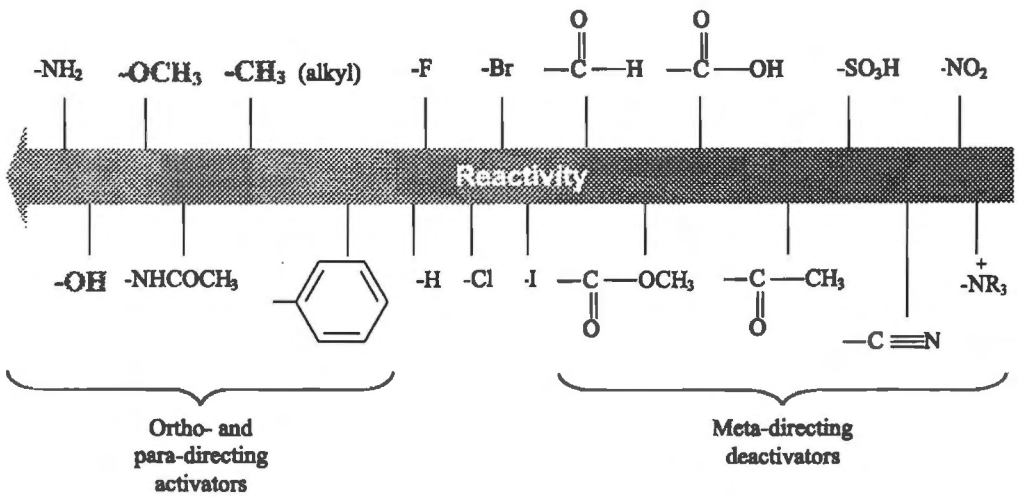

Figure 5.4: Influence of the substituent on the aromatic ring (redrawn from McMurry (1992))

reactive molecule for an electrophilic attack, followed by anisole and toluene. Ramaswamy et al. (1994) reported a very similar trend in reactivity for aromatic hydroxylation over TS-1 and TS-2 and suggested an electrophilic substitution mechanism. The fact that deactivated aromatic rings do not react and the order of reactivity obtained in this work suggest that the reaction could indeed be an electrophilic attack caused by a relatively weak electrophile.

Although a radical mechanism cannot completely be excluded, the fact that no meta-hydroxylated products could be detected in the phenol and anisole hydroxylation is strongly in favour of an heterolytic, electrophilic mechanism. Meta-cresol was formed in the toluene hydroxylation due to the weaker ortho/para-directing effect of the methyl group at the aromatic ring. In studies by Khouw et al. (1994) and Clerici and Ingallina (1993), the absence of typical by-products originating from a radical intermediates was reported, thus also favouring a heterolytic mechanism. Further evidence for the absence of radical intermediates was given by Clerici (1991) and Bhaumik and Tat-

sumi (1998), who studied the epoxidation of allyl chlorides and the epoxidation of linear alkenes in chlorinated solvents, respectively. No chlorinated isomers were found in the product spectrum, pointing again to the absence of major amounts of radicals under mild reaction conditions.

5.3.2 Selectivity

5.3.2.1 Reaction mechanism

Whereas many propositions for a reaction mechanism in epoxidations, alkane oxidations and ammoximations over TS-1 and Al-free Ti-beta exist in the literature, no detailed suggestions for a reaction mechanism in aromatic hydroxylations can be found. A reaction mechanism for the hydroxylation of phenol consistent with the experimental observations in this work is therefore proposed. This reaction mechanisms is then also applied to the anisole and toluene hydroxylation.

To explain the selectivities and the pronounced solvent effects observed in aromatic hydroxylations, the attention must be first focused on the active site. The formation of peroxo species with titanium (IV) is well known; a wide range of titanium compounds produce peroxo derivates on reaction with basic, neutral and acid solutions of hydrogen peroxide. The active site in titanium-substituted silicates is also believed to be a titanium-peroxo species, formed by reaction of hydrogen peroxide with titanium incorporated in the silica environment. Clerici et al. (1992) were the first authors to succeed in the isolation of titanium peroxides in TS-1 using a basic environment; the TS-1 peroxides obtained were stable even after vacuum-drying of the catalyst. Only when Ti(IV) is isolated and in tetrahedral coordination, good catalytic performance was observed. UV-VIS diffuse reflectance and ESR measurements reported by Geobaldo et al. (1992) and Prakash and Kevan (1998) as well as results from many other groups [Astorino et al. (1995), Sheldon et al. (1998b), Sheldon et al. (1998a), Deo et al. (1993)] confirmed that titanium is indeed in tetrahedral coordination in freshly calcined, non-hydrated (and phase-pure) samples. However, with the application of very sensitive characterisation techniques, it had been shown that reversible hydrolysis at least one Ti-O-Si bond with the formation of Ti-OH and Si-OH groups takes place in TS-1. Geobaldo et al. (1992) reported line broadening and a red-shift of diffuse reflectance UV-VIS spectra of TS-1 upon hydration, which was interpreted as a change in the coordination sphere of the titanium atom. de Castro-Martins et al. (1994) applied cyclic voltammetry to characterise the environment of the titanium site in TS-1 and confirmed the hydrolysis of Ti-O-Si lattice bonds to titanol and silanol groups as well as a higher coordination of titanium in the presence of water. X-ray absorption techniques proved to be a very efficient tool to characterise the coordination of titanium in TS-1. In an EXAFS study by Pei et al. (1993), it was again shown that well-manufactured, dehydrated TS-1 samples contain titanium only in tetrahedral coordination. However, by applying a combination of EXAFS and XANES spectroscopy, a number of groups showed the expansion of the coordination

sphere of titanium in the presence of polar molecules. In a EXAFS-XANES study, Behrens et al. (1991) reported the reversible hydration of titanium in TS-1 to a five-or six-coordinated species. Using the same technique, Bordiga et al. (1994a) and Bolis et al. (1999) characterised the Ti(IV) coordination sphere in the presence of water and ammonia. Coordination numbers between five and six were reported upon adsorption of water or NH_3 onto the sample. Lamberti et al. (1998) came to the same conclusion in a similar study comparing various spectroscopic techniques. Van der Waal *et al.* [van der Waal and van Bekkum (1997), van der Waal (1998)] and Astorino et al. (1995) reported the expansion of the titanium coordination sphere to six not only upon hydration but also upon adsorption of alcohols onto TS-1 using DR UV-VIS spectroscopy. An increase in Ti-O bond length upon adsorption of protic molecules has been reported in many studies [Astorino et al. (1995), Bolis et al. (1999), Bordiga et al. (1994a)]. Prakash and Kevan (1998) reported the coordination of only one alcohol molecule, thus proposing a penta-coordinate titanium centre.

Summarising the above mentioned literature reports, two statements seem generally to be well founded. Firstly, it can be concluded that hydrolysis of Ti-O-Si bonds takes place upon reaction with water or hydrogen peroxide; this hydrolysis is reversible since the original state can be restored by heating or outgassing the sample. Secondly, polar molecules such as alcohols, water and ammonia coordinate to the titanium and expand its coordination sphere. The exact coordination number is however still under debate; values from 4.5 to 6 have been reported. Figure 5.5 shows possible configurations of the active site in TS-1 without (species **c**) and with coordination of 1 or 2 protic solvent molecules (species **b** and **a**). For the development of a reaction mechanism, the different

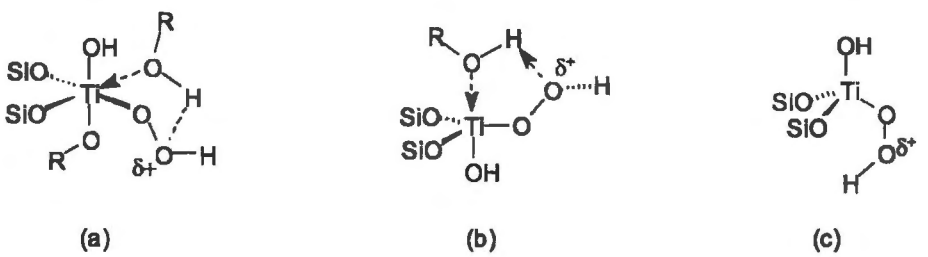

(a) (b) (c)

Figure 5.5: Possible configurations of the hydroperoxo-titanium active site: (a) hexa-coordinate octahedral, (b) penta-coordinate trigonal bipyramidal, (c) tetracoordinate tetrahedral

configurations of the active site have to be considered. Additionally, possible intermediates formed in the hydroxylation of the aromatic ring and geometric constraints imposed by the zeolite micropores have to be taken into account.

Aromatic hydroxylations are most likely to follow an electrophilic substitution mechanism. It is therefore proposed that the terminal OH of the titanium hydroperoxo group is the electrophile that attacks the aromatic ring (polarisation of the Ti-OOH group is indicated in Figure 5.5). To further

support this hypothesis, a phenol hydroxylation experiment with tert-butylhydroperoxide and Al-free Ti-beta was conducted. Even though TBHP may not penetrate the pores of TS-1, there is ample space in the pores of Ti-beta to activate the Ti-sites, as is well known for epoxidation reactions [Blasco et al. (1998)]. However, no phenol hydroxylation occurs with Al-free Ti-beta when TBHP is the oxidant. This strongly suggests that the aromatic hydroxylation over titanium substituted molecular sieves follows a different reaction mechanism than epoxidation reactions. An electrophilic attack of the aromatic ring using species **c** in Figure 5.5 as the intermediate was suggested by Ramaswamy *et al.* [Ramaswamy and Sivasanker (1993), Ramaswamy et al. (1994)]. A mechanism involving a similar electrophilic intermediate has been suggested by Reddy and Jacobs (1996) for the hydroxylation of amines. A 5-membered ring with hydrogen bonds between methanol and the peroxo group at the titanium site (species **a** and **b** in Figure 5.5) has been proposed in most publications as the active intermediate complex for TS-1 catalyzed reactions in methanol [Clerici (1993), Clerici and Ingallina (1993), Khouw et al. (1994), Martens et al. (1993), van der Pol and van Hooff (1993)]. In the presence of protic solvents, a reaction mechanism for the para-hydroxylation involving species **b** is therefore proposed and shown in Figure 5.6. The coordination of protic solvent molecules results

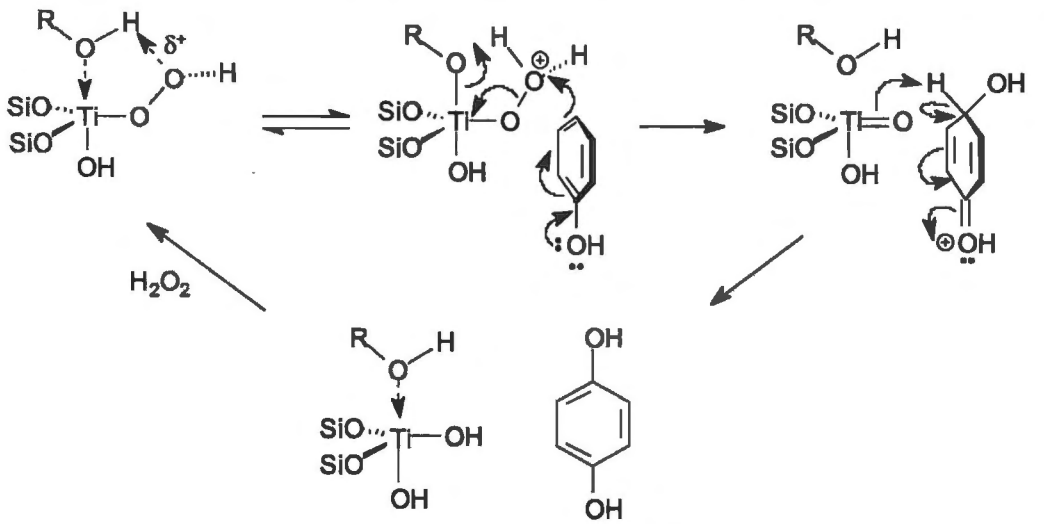

Figure 5.6: Proposed reaction mechanism for the formation of hydroquinone in phenol hydroxylation

in an increase of the size of the active titanium site. Hydrogen bonds of the phenolic OH with solvent OH groups will make the phenol molecule more bulky. Phenol, hydrogen-bonded to solvent molecules, will approach the bulky titanium site with the OH group pointing away from the titanium site (see Figure 5.6), yielding hydroquinone.

On the other hand, in non-protic solvents, phenol can take over the role of the protic solvent molecule. Although water is always present, its concentration in the hydrophobic TS-1 and Al-free

Ti-beta pores is expected to be low, as indicated by the extremely high adsorption constants for phenol in both TS-1 and Al-free Ti-beta with water as a solvent (Table 4.29 and Table 4.30). Thus, the existence of titanium sites without protic molecules coordinated is proposed (species **c** in Figure 5.5). In that case another pathway is opened, i. e. the conversion via penta-coordinated (trigonal bipyramidal) Ti site, involving coordination of phenol to Ti peroxo species yielding catechol. The proposed mechanism for the formation of catechol involving phenol coordination to the titanium active site is shown in Figure 5.7. This will be the case in aprotic solvents, such as acetone. Protic

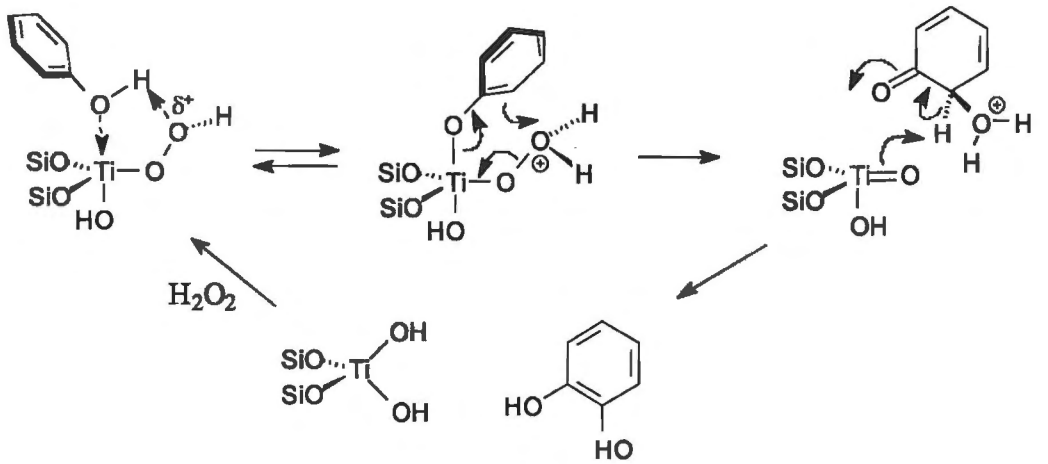

Figure 5.7: Proposed reaction mechanism A for the formation of catechol via phenol coordination

solvents such as methanol will compete with phenol, so that this pathway is not dominant in these solvents.

Formation of catechol can also take place without coordination of phenol to Ti peroxo species; ortho-hydroxylation of phenol via a 6-membered transition state involving phenol is shown in Figure 5.8, bearing in mind that the trajectory of attack of the electrophilic OH group is nearly orthogonal to the plane of the aromatic ring. As for the catechol formation mechanism proposed in Figure 5.7, this scenario is only likely in the absence of coordinated protic solvent molecules since hydrogen bonds of the latter with the titanium peroxo group (species **a** and **b** in Figure 5.5) would destabilise H-bonding of the phenolic OH with the OOH group.

5.3.2.2 Influence of the substrate

The reaction pathways proposed for ortho- and para-hydroxylation of phenol can also be applied to the hydroxylation of anisole and toluene. Neither the anisole nor the toluene molecule possess an OH group, hence a scenario according to Figure 5.7, involving coordination of the aromatic molecule to the titanium site, is not possible for anisole and toluene. However, the formation of

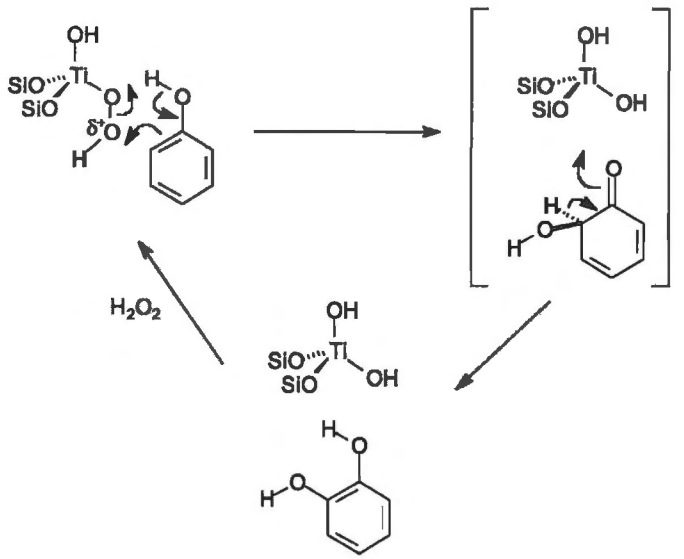

Figure 5.8: Proposed reaction mechanism B for the formation of catechol without phenol coordination

para-hydroxylated isomers shown for phenol in Figure 5.6 is also possible in the anisole and toluene hydroxylation, as well as mechanism B for the formation of ortho-hydroxylated products (Figure 5.8, without the proton transfer to the internal oxygen of the peroxo group).

In the TS-1 catalyzed anisole hydroxylation, more para-isomer was formed than in the phenol hydroxylation for all solvents. With one pathway less available for the ortho-hydroxylation, para-hydroxylation becomes more likely. This can be explained by the size and the polarity of the substituent. In the para-hydroxylation reaction mechanism (see in Figure 5.6), the substituent is pointing away from the active site due to the increased bulkiness of the titanium active site with coordinated methanol molecules. This effect is expected to be more pronounced for anisole since the methoxy group is more bulky than the OH group; a slight steric hindrance for ortho-hydroxylation is also possible. The methyl group of the anisole molecule might also be repelled by the hydrophilic nature of the titanium hydroperoxo site.

In the case of the toluene hydroxylation, more ortho-hydroxylation occurred than in the phenol hydroxylation in all solvents. This can also be explained by the nature of the substituent. The methyl group is generally much less o/p-directing than the hydroxy or the methoxy group (see Figure 5.4). Consequently, with two ortho-positions available for hydroxylation, more ortho isomer is expected. This argument is supported by the fact that between 15 and 20 % of meta-cresol was also formed in the toluene hydroxylation. Meta-cresol can form either by direct meta-attack on the aromatic ring or by initial attack at ortho- or para-position followed by migration of the OH group as shown in the schemes 5.9 and 5.10. Figure 5.9 shows possible intermediates in the toluene hydroxylation

formed by the electrophilic attack of the terminal OH of the titanium hydroperoxo group, leading to ortho- and meta-hydroxylation. The attack of the electrophilic OH group at the ortho position

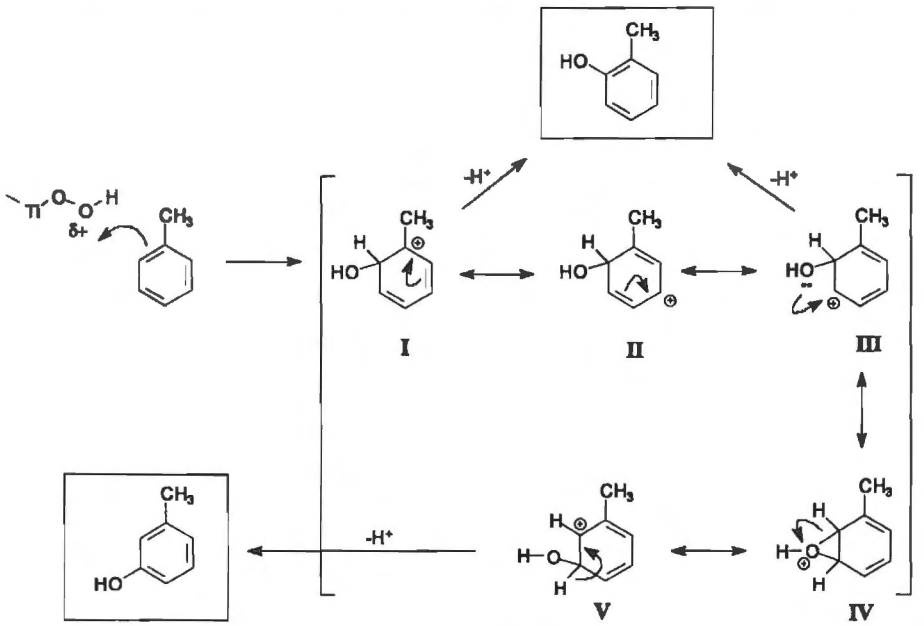

Figure 5.9: Possible scheme for the formation of ortho- and meta-cresol in the toluene hydroxylation

leads to the resonance stabilised carbocations **I** - **III**. In the intermediate **III** the carbocation can be trapped by the adjacent hydroxyl group to form the oxonium intermediate **IV**. This can subsequently open up to either yield back intermediate **III** or the other way to yield intermediate **V**, which can then aromatise by losing the proton (to the titanium site) to give meta-cresol. However, since the carbocation **I** has the lowest energy (being a tertiary carbocation), the extent of formation of **IV** and **V** is expected to be relatively small. When the electrophilic attack occurs in para position, a reaction scheme with a similar series of intermediates is obtained and is shown in Figure 5.10. The para-attack of the electrophilic hydroxyl group generates the resonance stabilised intermediates **I** - **III**, similar to the ortho attack. The intermediates **I** and **III** are however identical and therefore could give rise to the same oxonium ions **IV**, which can then open up to yield intermediate **V** and subsequently meta-cresol.

A similar scheme to the one shown in Figure 5.9 and Figure 5.10 for the toluene hydroxylation can also be drawn for the hydroxylation of phenol and anisole. Figure 5.11 shows possible intermediates formed in the anisole hydroxylation. After the electrophilic attack at the anisole molecule, the intermediates **I** - **III** can be formed, similar to the toluene hydroxylation. However, in the anisole hydroxylation, the additional and very important resonance intermediate **VII** arises from donation of the oxygen electrons from the methoxy oxygen. The combination **I** - **VII** would therefore ren-

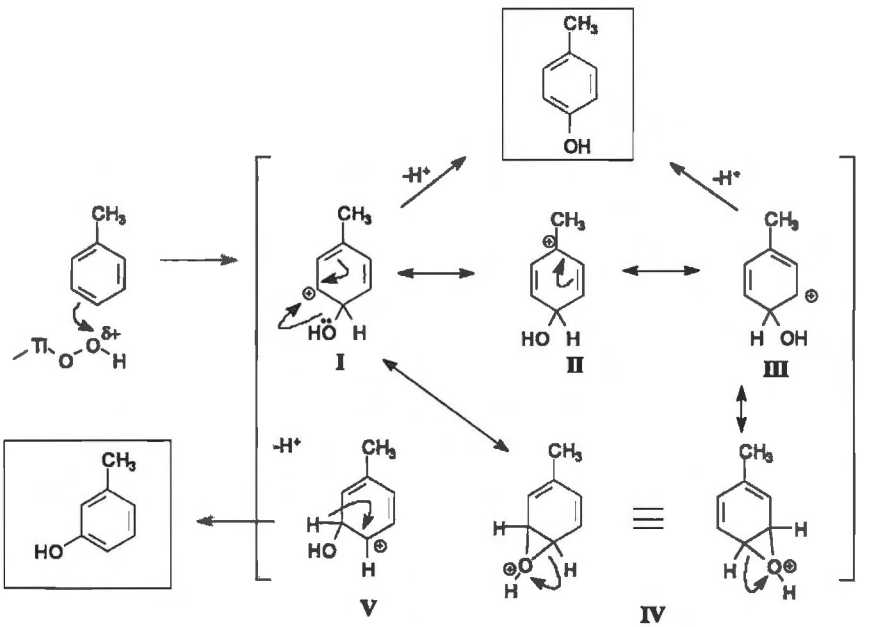

Figure 5.10: Possible scheme for the formation of para- and meta-cresol in the toluene hydroxylation

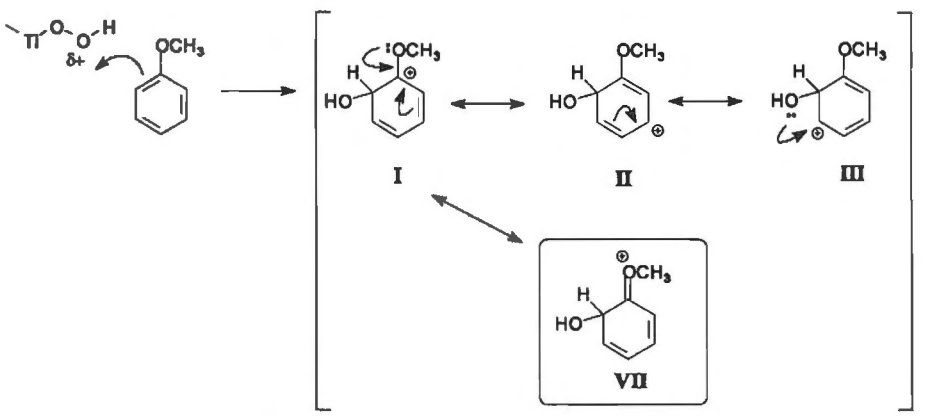

Figure 5.11: Possible intermediates in the anisole hydroxylation

der the probability for the other intermediates less significant. As a consequence, the formation of meta-anisole, which could occur from intermediate **III**, becomes inhibited. The same argumentation applies for the phenol hydroxylation, explaining the absence of the meta-isomer resorcinol (which was only detected in trace amounts) in the product mixture.

The selectivities based on the reactants follow a similar trend as the activities. Peroxide efficiencies and selectivities based on aromatic substrate decreased in the order phenol > anisole > toluene. As the reaction rate for hydroxylation decreases, side reactions such as peroxide decomposition and polymerisation of aromatic molecules (substrate and products), become relatively more important.

Particularly for the toluene hydroxylation, reaction conditions different from the 'standard' reaction conditions had to be chosen in this work to improve the selectivities and peroxide efficiencies. Some studies in the literature report higher selectivities based on both H_2O_2 and aromatic substrate due to the higher reaction temperatures and lower conversions. Since TS-1 is not a very efficient catalyst for peroxide decomposition under reaction conditions, an increase in temperature favours the desired hydroxylation reaction.

5.3.2.3 Influence of the solvent

The reaction mechanisms presented above can be used to explain the solvent effects observed in the aromatic hydroxylation reactions. However, the special environment of the zeolite micropores has to be taken into account to interpret the selectivities obtained in different solvents. Furthermore, the influence of the external surface also has to be considered. The solvent effects observed in the phenol, anisole and toluene hydroxylation are first discussed for TS-1; shape selectivity effects and a comparison to the results obtained for Al-free Ti-beta and the influence of the external surface are discussed in the following paragraphs.

In the TS-1 catalyzed phenol hydroxylation, an overall p/o-ratio of 2.14, 1.29 and 0.84 was obtained in methanol, water and acetone, respectively (see Table 4.6). These values are in line with most literature reports (see Table 2.3). Protic solvents such as water and methanol favoured the formation of hydroquinone, whereas more catechol was formed in aprotic solvents such as acetone. This can qualitatively be explained by the reaction mechanisms presented above. In aprotic solvents, a reaction path for ortho-hydroxylation through coordination of phenol is opened (see Figure 5.7) or, alternatively, hydrogen-bonding of the phenolic OH with the hydroperoxo group of the titanium site creates a configuration where the ortho-position is closer to the electrophile attacking the aromatic ring (see Figure 5.8). When protic solvents are present, they coordinate to the titanium site and significantly increase its size. This could significantly narrow the TS-1 channels, leading to a geometric constraint for an approaching phenol molecule. With the OH group pointing away from the active centre (which could be enhanced if it is hydrogen-bonded to protic solvent molecules), para-hydroxylation occurs (see Figure 5.6). This scenario corresponds to a transition-state shape selectivity induced by protic solvents in TS-1.

Different results were obtained for the anisole hydroxylation over TS-1. Para-hydroxy-anisole was always preferentially formed and the selectivities did not depend as strongly on the solvent as was observed for the phenol hydroxylation. In acetone and methanol, the overall p/o-ratios were 2.08 and 2.75, respectively (see Table 4.15), which compares well to most literature data shown in Table 2.4. This can be explained by the fact that the methoxy group is more bulky than the OH group. The size of the substituent could hinder ortho-hydroxylation significantly by favouring an orientation

with the methoxy group pointing away from the titanium site, thus favouring para-hydroxylation in all solvents. A slightly enhanced para-formation in protic solvents was however observed and can be explained by the same mechanism as for the formation of hydroquinone in the phenol hydroxylation.

In the toluene hydroxylation, trends similar to the phenol hydroxylation were obtained. Protic solvents strongly enhanced the formation of para-cresol. However, the product preferentially formed with TS-1 was always ortho-cresol. In acetone and methanol, the overall p/o-ratio was 0.47 and 0.85, respectively. Additionally, 17 and 16 % of meta-cresol were detected in the reaction mixture with acetone and methanol, respectively. The selectivity enhancement towards para-hydroxylated isomer observed in protic solvents can be explained with the same mechanism as shown for the phenol hydroxylation in protic solvents (see Figure 5.6). However, ortho-hydroxylation was generally preferred over para-hydroxylation, which can be attributed to the weaker o/p-directing effect of the methyl group (see Figure 5.4). With two positions available for ortho-hydroxylation, the product distribution is shifted towards the statistical value. The appearance of meta-cresol in the product mixture, which was hardly influenced by the solvent, confirms weaker directing effect of the methyl group.

For all hydroxylation reactions investigated, the peroxide efficiency (i.e. the selectivity based on H_2O_2) was higher in acetone than in methanol. This can also be explained by the lower amount of free peroxide with acetone as the solvent as discussed in section 5.3.1.1. The influence of the H_2O_2 concentration was shown in section 4.2.5.1; lower H_2O_2 concentrations improved the peroxide efficiency. Since acetone lowers the free peroxide concentration in a series of reversible reactions (see Figure 5.1), a higher selectivity compared to methanol is expected. Furthermore, the acetone-H_2O_2 complexes are relatively stable under reaction conditions [Sauer and Edwards (1971)] and peroxide loss through decomposition of the latter is not too severe. With methanol however, loss of hydrogen peroxide occurs through oxidation of methanol, although this reaction proceeds at a relatively low reaction rate [Deo et al. (1993), Maspero and Romano (1994)]. In the phenol hydroxylation, the highest peroxide efficiencies were obtained with water as the solvent. This can be explained by the fact that there are no interactions of H_2O_2 with water that could lead to side reactions and to peroxide loss.

5.3.2.4 The role of the pore geometry - shape selectivity effects

The comparison of the product selectivities obtained with the medium-pore titanium silicalite TS-1 and the large pore Al-free Ti-beta can be used to answer the question whether shape selectivity plays a role in the aromatic hydroxylation reactions studied in this work. If the pore geometry imposes a geometric constraint on the reaction, then different product distributions should be obtained with both catalysts. However, since very small crystallites were used in the TS-1 reactions, the influence

of the external surface also has to be taken into account.

When TS-1 and Al-free Ti-beta crystals with a similar diffusional path length were compared for a phenol hydroxylation in water, p/o-ratios of 1.31 and 0.45 were obtained for TS-1 and Al-free Ti-beta, respectively (see Table 4.10). This strongly suggests that the pore geometry controls the product distribution. The preferential formation of hydroquinone in TS-1 and catechol in Al-free Ti-beta is a proof for the existence of shape selectivity in the pores of the TS-1.

In the medium-size TS-1 pores, the coordination of methanol (or other protic solvent molecules) increases the size of the titanium active site and significantly restricts the space available for reaction. Consequently, more para-isomer is obtained. Figure 5.12 shows a TS-1 pore including a titanium hydroperoxo site with coordinated methanol and a phenol molecule in a configuration for para-hydroxylation according to the proposed mechanism in Figure 5.6.

The structures shown in Figure 5.12 - 5.14, taken from the database of the International Zeolite Association (2001), are simplified for the sake of clarity. The framework is displayed as sticks and the molecules are displayed as 'ball-and-stick'-models; when displayed with their respective van-der-Waals radii it becomes even more apparent that there is indeed a geometric constraint for a phenol molecule when solvent molecules are coordinated to the titanium site. Figure 5.13 shows a TS-1 pore including a titanium hydroperoxo site with no solvent molecule coordinated and a phenol molecule in a configuration for ortho-hydroxylation according to the mechanism proposed in Figure 5.7). Without coordinated protic solvent molecule at the titanium active site, there is clearly more space available for the phenol molecule and the phenolic OH can hydrogen-bond to the active site. In this configuration, the ortho-position of the phenol molecule is closer to the Ti-OOH group and catechol is preferentially formed.

From both Figure 5.12 and Figure 5.13 it can be seen that the phenol molecule has to adopt a 'flat' configuration when in the narrow TS-1 channels; it seems unlikely that there is enough space for the molecule to be in an orientation with the OH group perpendicular to the channel direction. In the large-size pores of Al-free Ti-beta however, this orientation is possible. Figure 5.14 shows an Al-free Ti-beta pore including a titanium hydroperoxo site with coordinated methanol and a phenol molecule (perpendicular to the channel direction). In the phenol hydroxylation catalyzed by Al-free Ti-beta, catechol was always the preferred product, indicating the absence of shape selectivity effects in this catalyst and confirming the existence of shape selectivity in TS-1. This is further supported by the fact that the solvent only had a minor influence on the product selectivity in Al-free Ti-beta. With methanol, water and acetone as the solvents the p/o-ratios obtained were 0.56, 0.42, and 0.38, respectively. The weakly para-enhancing effect of protic solvents in Al-free Ti-beta and the excess of hydroquinone obtained in TS-1 with protic solvents are in line with a transition-state shape selectivity that can be amplified by the presence of protic solvent molecules in the zeolite channels. Figure 5.12 and 5.13 demonstrate the space restrictions for a phenol molecule in the narrow TS-1

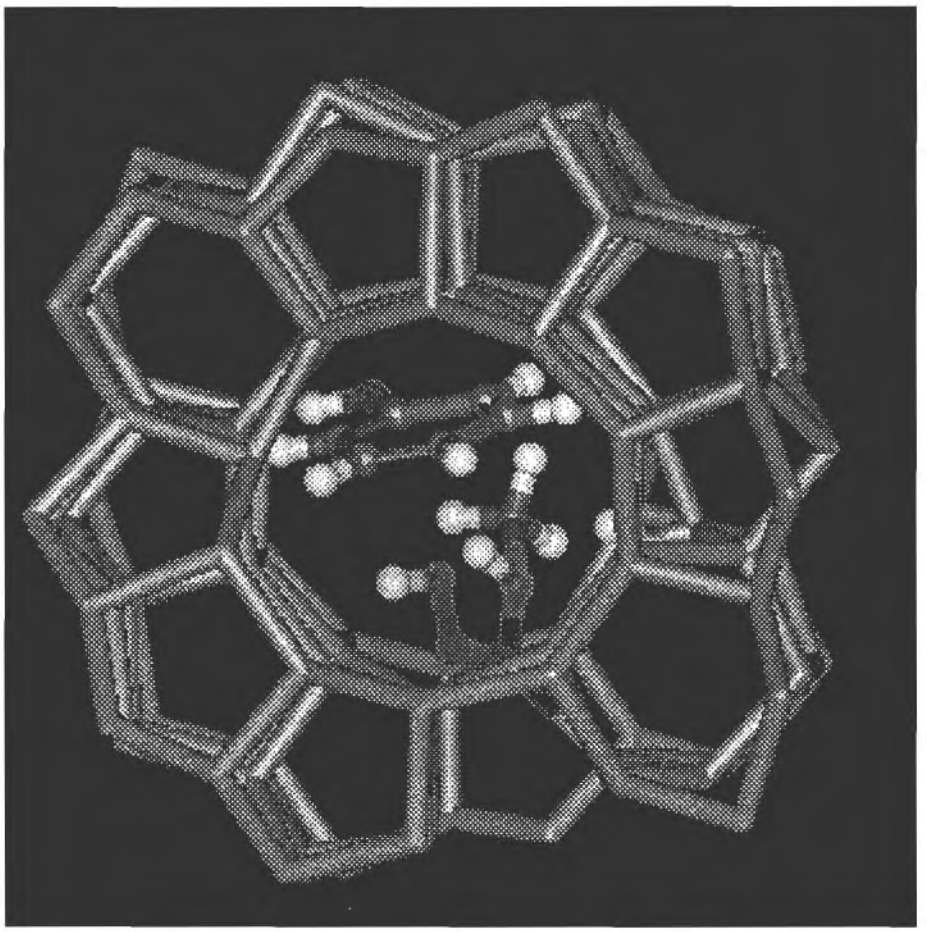

(a) (grey: zeolite framework; brown: carbon; red: oxygen: white: hydrogen; blue: titanium)

Figure 5.12: TS-1 pore with methanol coordinated to titanium peroxo group and adsorbed phenol molecule

channels and show that methanol coordinated to the titanium active site will render these constraints more severe. In the large pores of Al-free Ti-beta however, there is ample space for the phenol molecule even in the presence of a more bulky titanium centre with coordinated methanol as shown in Figure 5.14.

The product distributions obtained with protic and aprotic solvents and with the medium-pore TS-1 and the large-pore Al-free Ti-beta consistently support the hypothesis of shape selectivity enhanced by protic solvents in TS-1. Higher p/o-ratios were obtained in the TS-1 catalyzed anisole hydroxylation as compared to the phenol hydroxylation; para-hydroxyanisole was always preferentially formed. In acetone and methanol, the product p/o-ratios were 2.08 and 2.75, respectively. Thus, the change from aprotic to protic solvent did not result in the inverse of selectivity that was ob-

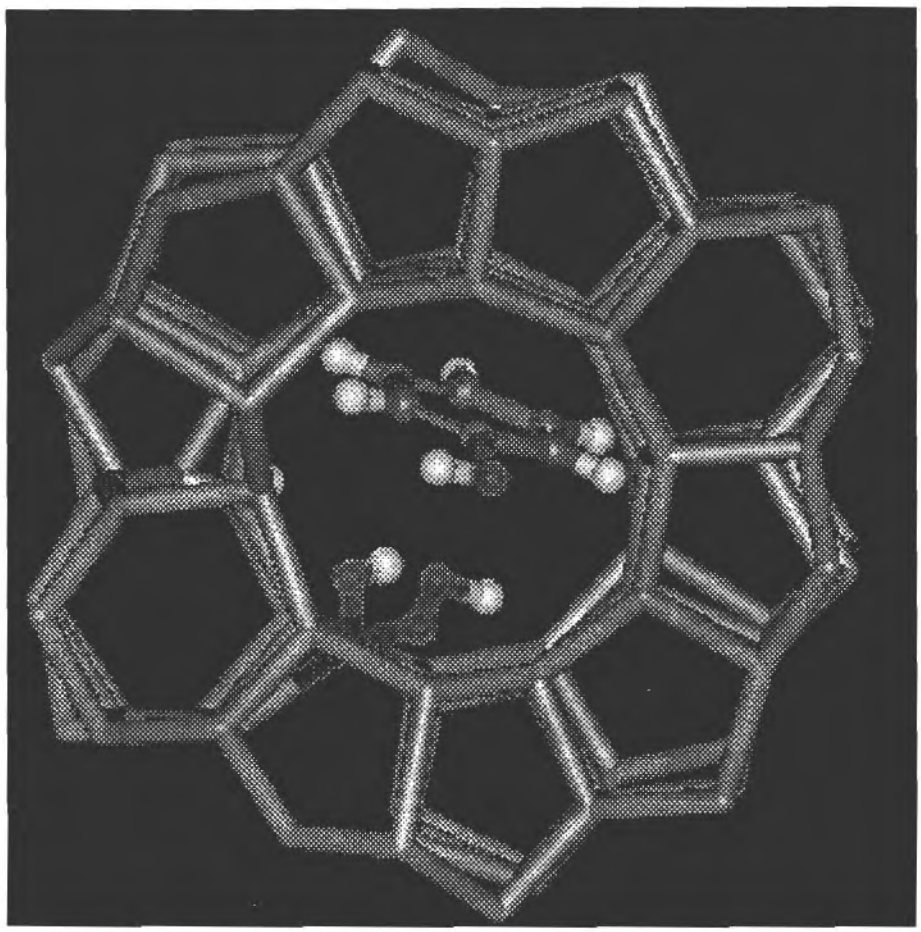

(a) (grey: zeolite framework; brown: carbon; red: oxygen; white: hydrogen; blue: titanium)

Figure 5.13: TS-1 pore with titanium peroxo group and adsorbed phenol molecule

served for the phenol hydroxylation. Although para-formation was enhanced in methanol, this effect was much weaker in the anisole hydroxylation. These results are in line with the reaction mechanism and the shape selectivity effect proposed for the phenol hydroxylation; a more bulky substituent such as the methoxy group of anisole would further favour para-hydroxylation, explaining the excess of para-hydroxyanisole. The bulkiness of the substituent could therefore 'overshadow' the para-directing effect of the protic solvent by directing the hydroxylation towards the para-position itself. However, the extremely high para-hydroxyanisole selectivities obtained with Al-free Ti-beta seem to contradict the previous argumentation. The p/o-ratios obtained in Al-free Ti-beta were 6.61 and 10.87 with acetone and methanol, respectively. As for the phenol hydroxylation, the less restricting environment of Al-free Ti-beta pores was expected to result in more ortho-hydroxyanisole being

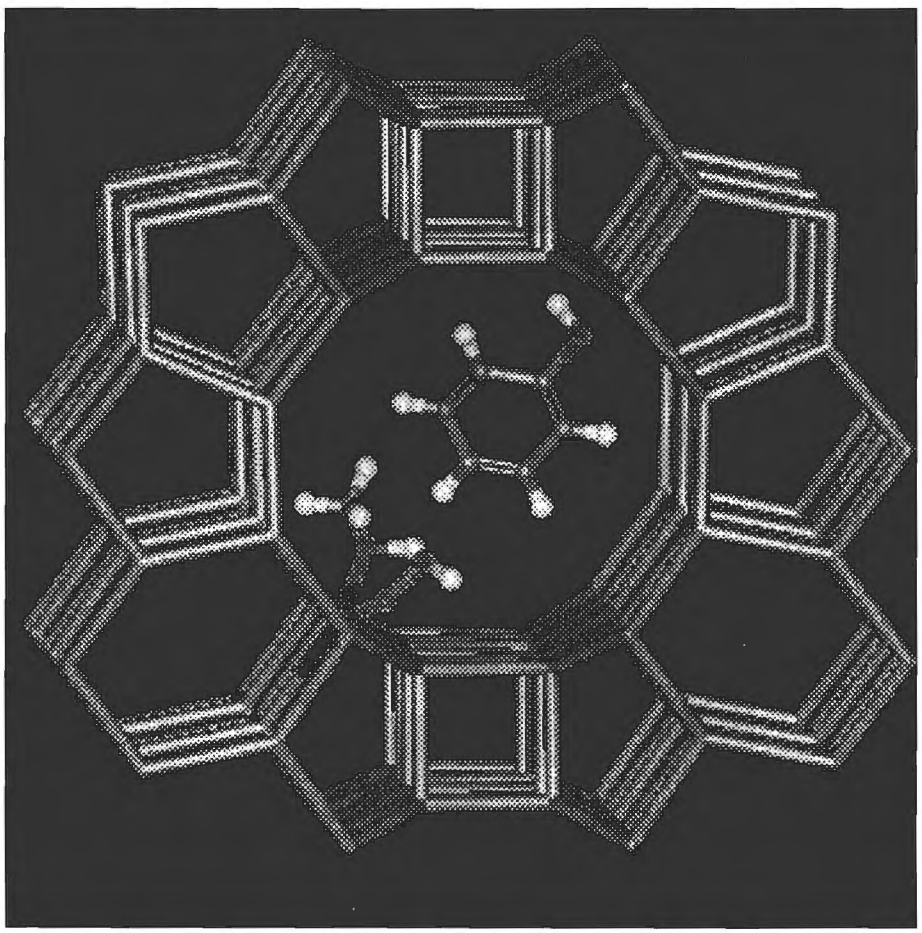

(a) (grey: zeolite framework; brown: carbon; red: oxygen: white: hydrogen; blue: titanium)

Figure 5.14: Al-free Ti-beta pore with methanol coordinated to titanium peroxo group and adsorbed phenol molecule

formed. A possible explanation for the exceptionally high para-selectivity in the anisole hydroxylation over Al-free Ti-beta is the ability of the organic molecule to adopt a different configuration in the larger pores of this catalyst. Figure 5.14 demonstrates that an aromatic molecules is able to rotate into a position where it is perpendicular to the channel direction, the substituent pointing away from the titanium site and towards the zeolite wall. This configuration is not possible in TS-1. An aromatic molecule having a relatively apolar substituent would preferably adopt a configuration with the substituent pointing away from the hydrophilic titanium centre. However, it has to be noted that the aromatic ring and the hydroperoxo group cannot be in the same plane for reaction since the electrophilic attack has to occur nearly orthogonally to the aromatic plane. Adsorption measurements presented in Table 4.30 demonstrate the hydrophobicity of the framework; Henry's constants

decrease with increasing polarity of the molecule. Thus, the walls of Al-free Ti-beta, as expected for a highly siliceous solid, prefer hydrophobic molecules. Apolar substituents on aromatic rings (such as a methoxy group) would therefore be repelled by the hydrophilic titanium peroxo site and point towards the zeolite wall. In this configuration, the para position of the molecule is closer to the titanium active centre and para-hydroxylation preferentially occurs. The presence of hydrogen-bonded or coordinated methanol molecules at the Ti-OOH site might further favour this orientation, explaining higher para-selectivity in methanol. The hypothesis of a different orientation of the aromatic molecule in Al-free Ti-beta is also consistent with the high ortho-selectivities for the hydroxylation of phenol over Al-free Ti-beta. The highly polar phenolic OH would be expected to point towards the hydrophilic titanium centre, favouring the ortho-position for the electrophilic attack.

In the toluene hydroxylation over TS-1, ortho-cresol was always the preferentially formed product. In acetone and methanol as the solvents, the p/o-ratios obtained were 0.47 and 0.62, respectively (see Table 4.19). Additionally, meta-cresol was also formed; the amount of meta-cresol was however hardly dependent on the solvent. In acetone and methanol, 16% and 17% of meta-cresol were detected in the cresol fraction, respectively. Mechanisms leading to the formation of meta-cresol were shown in Figure 5.9 and Figure 5.10. Although an excess of ortho-cresol was always obtained, protic solvents enhanced the formation of para-cresol significantly. This follows a trend similar to the phenol hydroxylation, suggesting again a shape selective reaction in TS-1 which is amplified by protic solvents. A comparison of the isomer distribution obtained with TS-1 and Al-free Ti-beta shows a trend similar to the anisole hydroxylation. In Al-free Ti-beta, more para-cresol was formed than in TS-1. In acetone and methanol, the p/o-ratios obtained with Al-free Ti-beta were 1.76 and 2.96, respectively. As opposed to TS-1, the solvent also influenced the formation of meta-cresol in Al-free Ti-beta. In acetone and methanol, 13% and 20% of meta-cresol was detected in the cresol fraction, respectively. As for the anisole hydroxylation, these observations can also be explained by a different orientation of the toluene molecule in Al-free Ti-beta due to the absence of geometric constraints.

5.3.3 The role of the external surface

The fact that only 82% of the total surface area of the small TS-1 crystals used in this work ($d_{crystal}$ = 0.1 μm) is located at the internal surface, whereas both large Al-free Ti-beta ($d_{crystal}$ = 2 - 5 μm) and large TS-1 crystals ($d_{crystal}$ = 3×10×45 μm) have 98.5% of their active sites located internally is an indication of the potential importance of the external surface with nano-size TS-1 crystals. Diffusional limitations in the phenol hydroxylation with TS-1 have clearly been shown in literature reports [van der Pol et al. (1993)] and were confirmed in this work; large TS-1 crystals showed a much lower activity than the small crystals. The latter were therefore used for the reaction and

kinetic studies to avoid mass transfer limitations, raising the question of the influence of the external surface on both activity and selectivity. Tuel and Ben Taarit (1993) used a non-calcined TS-1 sample for a study of the phenol hydroxylation. With the template blocking the access to the zeolite pores, the activity was assigned exclusively to the external surface. However, these results could not be reproduced here. Experimental results were found to be dependent on the treatment of the sample after synthesis. The cycle-wise CVD of TEOS technique allows for selective deactivation of the external surface through silanisation of the small TS-1 crystallites without significantly narrowing the entrances of the micropores. Using parent and silanised TS-1 crystals for kinetic studies then enables decoupling of internal and external activity and selectivity.

5.3.3.1 Characterisation of TS-1 modified by CVD of TEOS

To evaluate changes upon silanisation, silanised small TS-1 crystallites after 20 cycles of TEOS deposition were characterised using physico-chemical methods.

No change was detected in crystallinity (XRD), surface area and micropore volume (BET) and titanium incorporation (DR UV-VIS). SEM pictures showed no separate amorphous phase and no change in agglomeration of the crystallites. Evidence for the deposition of silica at the external surface of the crystallites is the increase of the average Si/Ti-ratio of the external rim of the crystals as determined by EDX.

In a thermogravimetric study of the first CVD deposition cycle under typical silanisation conditions, it was shown that significant amounts of TEOS adsorbed onto the external surface of the catalyst. The remaining TEOS on the external surface after flushing with inert carrier corresponded to $\approx$ 40 % of the amount calculated for a full monolayer. This demonstrates the necessity for the repetition of the CVD cycles to achieve full surface inertisation. The mass increase after calcination in air was small but detectable ($\approx$ 0.4 wt.%). Although the the thermogravimetric study was only conducted for one silanisation cycle it indicates the deposition of SiO_2 at the external surface of small TS-1 crystallites.

In an extensive gas-phase pulse adsorption study, pore-mouth narrowing of -blockage was characterised by injection of various tracer hydrocarbons into columns of parent and silanised TS-1. Conclusions were based on the first and second moments of the peak responses determined at different temperatures. Good correlations in van't Hoff plots showed the suitability of the experimental setup. A drastic decrease in the Henry's constant upon silanisation would indicate the (partial) exclusion of the hydrocarbon from the pore system caused by the silanisation procedure. However, the Henry's constants and adsorption activation energies, based on the peak first moments, showed no consistent change upon silanisation and can only be interpreted as scatter originating from the error of the method. The peak second moment is an indication for the presence of diffusional resistances.

Both pore mouth narrowing and -blockage would result in additional mass transfer resistances and increase the peak second moment. However, as also observed for the adsorption constants, no trend in the peak second moment was found upon progressive silanisation. For all tracer hydrocarbons injected, the changes in the second moment of the pulse responses were not consistent with an increase in mass transfer resistance. No trend with increasing external surface inertisation was observed. Based on the results of the pulse gas-phase adsorption study, it can be concluded that the pore entrances of the small TS-1 crystallites were not significantly affected by the silanisation procedure even after 20 cycles of CVD of TEOS.

The cycle-wise CVD of TEOS technique was applied with the aim of completely deactivating the external surface of TS-1. Röger et al. (1998) and Weber (1998) used the cracking of 1,3,5-triisopropylbenzene (which cannot enter the pores of H-ZSM-5) to probe the external surface activity of H-ZSM-5. Upon cycle-wise CVD of TEOS treatment, H-ZSM-5 completely lost its activity for the 1,3,5-triisopropylbenzene cracking reaction, which was taken as proof for complete external surface deactivation. In the course of this work an attempt was made to find a suitable test reaction for the external surface activity of TS-1. It was shown that 1-naphthol is not able to penetrate the pores of TS-1 under reaction conditions. Some activity for the 1-naphthol hydroxylation was expected due to the relatively high external surface area of the small TS-1 crystals. However, no hydroxylated products were detected. The only reaction observed was a very low conversion of 1-naphthol to tars, which probably caused a rapid deactivation of the external surface. Furthermore, the epoxidation of trans-diphenyl-ethylene (trans-stilbene), which is also not expected to enter the pores of TS-1, was also tested as a potential reaction to probe the external surface activity. TS-1 was completely inactive for this reaction since no conversion of trans-stilbene could be detected. This observation confirms results reported by van der Waal et al. (1998b), who investigated the epoxidation of bulky alkenes over TS-1 and Al-free Ti-beta. Despite the use of small crystals (having a significant external surface area), TS-1 was completely inactive for the epoxidation of norbornene, a bulky cyclic alkene with too large a kinetic diameter to enter the TS-1 pores [van der Waal et al. (1998b)]. It is not clear whether a deactivation phenomenon or other factors are responsible for the inactivity of TS-1 for a reaction with very bulky molecules at the external surface. A suitable test reaction to exclusively probe TS-1 external surface activity could not be established.

5.3.3.2 Activity of internal and external surface

The role of the external surface was found to be significant and dependent on the solvent for all hydroxylation reactions. The observed rate constants for sites at the external surface were consistently about an order of magnitude larger than those at the internal surface. Principally, diffusional constraints could also account for the difference between the observed rate constants for sites at

the external surface and those in the intracrystalline voids. The small TS-1 crystal used for the kinetic experiments were ca. 0.1 μm. Based on the diffusion measurements in this work or literature values [van der Pol et al. (1993)], the effectiveness factor for the small crystallites should be close to 1. Thus, it can be assumed that no mass transfer limitations were present in the hydroxylation experiments with the small TS-1 crystals.

Phenol hydroxylation In the TS-1 catalyzed phenol hydroxylation with water as the solvent, the consumption of phenol mainly takes place on the external surface. The contribution of the internal surface to the overall rate of phenol consumption amounts to only 31%. The small contribution of the internal surface to the rate of consumption of phenol can be explained by the strong adsorption of phenol in TS-1 using water as a solvent. Due to competitive adsorption, the hydrogen peroxide concentration near the active sites inside the pore system of TS-1 (internal surface) will be very low. This will result in a low observed rate for the consumption of phenol in the pores. With methanol and acetone as a solvent the internal surface contributed to the overall rate of consumption of phenol to 54 and 36 %, respectively. The difference between methanol and acetone can be explained by the formation of acetone peroxides and hydroperoxides (see Figure 5.1), which are too bulky to react with titanium sites in the pores. The concentration of free hydrogen peroxide in the liquid phase and consequently in the pores of TS-1 is significantly lowered through equilibrium reactions of acetone and H_2O_2; the 'release' of hydrogen peroxide from these compounds will take place in the bulk solution and thus favour reaction at the external surface sites. Thus, in acetone the internal surface contributes less to the overall reaction compared to the reaction done in methanol. This is supported by the slower decomposition of H_2O_2 during phenol hydroxylation. On the basis of the rate constants obtained for hydrogen peroxide decomposition on silanised and non-silanised TS-1, the contribution of the external surface to the rate of non-selective hydrogen peroxide decomposition amounts to 53, 63, and 72 % for water, methanol, and acetone, respectively. As a consequence of lower H_2O_2 concentrations in the pores with water and acetone as solvents, the decomposition rates were higher at the external surface with these solvents. Decoupling internal and external surface activity clearly demonstrates that the majority of the tar formation was also taking place at the external surface of the zeolite. With water, methanol, and acetone as the solvents, the external surface contributed to 96, 80, and 72 %, respectively to the overall formation of tars. As 'tars' are generally high molecular weight and hence bulky compounds, their formation inside the microchannels is less likely. However, the rate constants for tar formation at the internal surface were not zero and the thermogravimetric analysis of the recovered catalyst after reaction revealed the deposition of tars also on the silanised zeolite. This indicates a formation of tars or bulky tar precursors either in the micropores or at the pore mouth.

Anisole hydroxylation In the anisole hydroxylation, the external surface of TS-1 played an equally important role. In methanol and acetone, the contribution of the external surface to the total anisole consumption was 84 and 56 %, respectively. The particularly high value with methanol as a solvent can be explained by the high K value of anisole in methanol. High concentrations of anisole cause a lower concentration of the second reactant H_2O_2 in the pores, thus a lower contribution of the internal surface is observed in methanol as compared to acetone. For the non-selective H_2O_2 decomposition during anisole hydroxylation, the external surface activity in methanol and acetone amounts to 56 and 57 % of the overall decomposition rate, respectively. The same explanation as for the phenol hydroxylation also applies for the anisole hydroxylation; higher H_2O_2 concentration in the bulk solution than in the pores renders the external sites more active than the internal surface sites also for the decomposition reaction. As observed for the phenol hydroxylation, the tar formation mainly occurs at the external surface of the zeolite. In methanol and acetone, the external surface sites contributed to 85 and 82 % to the total formation of tars, respectively.

Toluene hydroxylation The role of the external surface is similarly important in the toluene hydroxylation. In methanol and acetone, the contribution of the external surface to the total consumption of toluene amounts to 63 and 59 %, respectively. The same arguments apply as for the phenol and anisole hydroxylation. A slightly less pronounced influence of the external surface was found for the non-selective H_2O_2 decomposition and the tar formation in the toluene hydroxylation. The external surface activity in methanol and acetone amounts to 51 and 46 % of the overall decomposition rate, respectively. For the tar formation, the external surface sites contributed to 71 and 64 % of the total rate of formation in methanol and acetone, respectively.

5.3.3.3 Product selectivity

While the importance of the external surface in terms of the activity of the catalyst was highlighted in the previous section, the most interesting implication of decoupling internal and external activity is the comparison of the product distribution. By comparing the rates of formation of the different isomers, shape selectivity effects generated by the pores of the catalyst can be identified.

Phenol hydroxylation The comparison of the phenol hydroxylation over small and large crystals of TS-1 gives a first indication of a possible shape selective reaction in the TS-1 pores. The p/o-product ratio over large TS-1 crystals was larger than over small TS-1 crystals when compared at the final phenol conversion. The fact that more of the para-isomer is obtained when a higher fraction of the active sites is located inside the pores suggests a shape selective reaction in the pores. However, the product distributions had to be compared at relatively low conversions due to the low activity of large TS-1 crystals in the phenol hydroxylation. The reaction times to reach comparable

conversion levels were very different (≈ 4 h for small TS-1 crystals and ≈ 24 h for large crystals) and the influence of side reactions such as subsequent polymerisation of reaction products is difficult to estimate. The comparison of the rate constants obtained with parent and silanised small TS-1 crystals is therefore more conclusive.

The contribution of the external surface to the rate of formation of the ortho-isomer catechol is significant. The contribution of the external surface to the total rate of catechol formation was 64, 47, and 68 % for water, methanol and acetone as a solvent, respectively. Thus, with the exception of the reaction in methanol, the majority of catechol was formed on the external surface. For the formation of hydroquinone, the contribution of the external surface sites to the formation of hydroquinone is dependent on the solvent nature. With water and acetone, 59 and 54 % of the total rate of hydroquinone formation can be assigned to the external surface, respectively; in methanol, the contribution of the external surface was only 27 %. This lower contribution of the external surface for catechol formation and the higher contribution of the external surface for hydroquinone formation confirms that a shape selective reaction takes place in the pores of TS-1 particularly with methanol as a solvent. This becomes even more apparent when looking at the ratio of the activity of the internal and external surface sites for the formation of catechol and hydroquinone (see Table 4.13). In all solvents, this p/o-ratio was higher for the internal surface sites. Whereas the difference was not very pronounced for water, a clear para-directing effect was obtained in acetone and methanol, the latter being the most selective solvent. On the external surface, a particular solvent effect was observed. In the protic solvents water and methanol, hydroquinone formation was preferred over catechol formation. In acetone, as an aprotic solvent, catechol was preferentially formed.

Anisole hydroxylation The trends obtained in the anisole hydroxylation were similar to those in the phenol hydroxylation. However, the reaction in methanol exhibited an exceptionally high activity of the external surface for the formation of both para-hydroxyanisole and ortho-hydroxyanisole. The external surface contributed to 85 and 82 % of the total rate of formation of ortho-hydroxyanisole and para-hydroxyanisole, respectively. This highlights again that the reaction in methanol is largely taking place at the external surface, a results of either low concentrations of H_2O_2 or a severely geometrically constrained reaction in the pores. In acetone, the contribution of the external surface to the total rate of ortho-hydroxyanisole and para-hydroxyanisole formation was 58 and 46 %, respectively. Thus, the reaction is taking place to a larger extent inside the pores. The p/o-ratios based on the rate of formation of ortho- and para-isomer for the internal and external surface reveal that an excess of para-hydroxyanisole was always obtained, even at the external surface. As observed in the phenol hydroxylation, the p/o-ratio was always higher at the internal sites, although the differences are not as large. In methanol, the p/o-ratio (based on the rate constants) was 2.67 and 2.26 for internal and external sites, respectively. The para-directing shape selective effect of the pores

was more pronounced in acetone, for which the internal and external p/o-ratios were 2.37 and 1.51, respectively.

Toluene hydroxylation The results for the toluene hydroxylation are somewhat more difficult to interpret due to the formation of the meta-isomer, but the trends are in line with the results obtained for the phenol and anisole hydroxylation. Internal and external surface roughly contribute equal amounts to the formation of all isomers in both methanol and acetone, the influence of the external surface being slightly higher in methanol. Surprisingly, the formation of meta-cresol was hardly influenced by the solvent or the pore structure. Only a slight increase in the p/m-product ratio from 2.24 to 2.42 in methanol and from 1.69 to 1.81 in acetone was observed when comparing external and internal surface, respectively. This might be explained on mechanistic grounds as shown in Figure 5.9 and Figure 5.10. However, the p/o-ratios at the internal and external surface confirm again that the TS-1 pores impose a geometric constraint on the hydroxylation reaction. More para-cresol was formed inside the pores for both methanol and acetone. Ortho-cresol was always preferentially formed in acetone; the distribution of the cresol isomers at the external surface is close to the statistical value. In methanol, the para-enhancing effect of the pores was most pronounced; an excess of ortho-cresol was obtained at the external surface, whereas para-cresol was preferentially formed inside the pores.

5.3.3.4 External surface effects common for all substrates

Although each reaction shows a different, solvent dependent product distribution, some common results for all hydroxylation reactions can be summarised.

The influence of the external surface was significant in all cases. The generally higher activity of the external surface can be assigned to a relatively low concentration of hydrogen peroxide in the pores; the hydrophobic framework of TS-1 results in a low affinity towards polar molecules such as water and H_2O_2. The external sites are however exposed to the concentrations in the bulk solution, which translates into a higher activity.

The presence of shape selectivity in the TS-1 pores was proven for all reactions. The reaction inside the pores consistently produces more of the para-hydroxylated isomer than the external surface reaction for all solvents and all substrates tested. No shape selectivity is expected at the external surface since there are no geometric constraints for the reaction, thus more ortho-hydroxylation occurs. In the TS-1 pores, an increase in the amount of the para-product formed was observed in the presence of protic solvents. Thus, the shape selective effect in the pores of TS-1 is enhanced by protic solvents, which coordinate to the titanium sites, rendering them more bulky and hence further constraining the space available for reaction.

Non-selective reactions such as peroxide decomposition and formation of tars mainly take place at the external surface in all hydroxylation reactions. The exposure of sites located at the external surface to much higher peroxide concentrations than present inside the pores (due to the hydrophobicity of TS-1) could lead to a different type of titanium site with more than one hydroperoxo group. The formation of two hydroperoxo groups at the same titanium atom has been postulated by van Laar et al. (1999). Alternatively, H_2O_2 molecules could compete for coordination at the titanium peroxo site as shown in Figure 5.15. These rather unstable complexes could liberate singlet oxygen

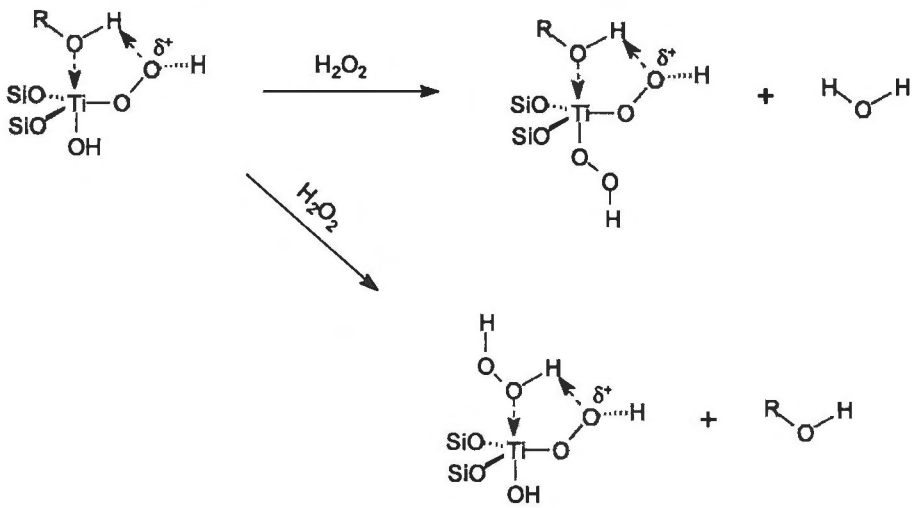

Figure 5.15: Proposed titanium sites on the external surface of TS-1

[van Laar (2001), van Laar et al. (1999)] that is quenched to its triplet state, decreasing the oxidant selectivity and leading to overoxidation and subsequent coke formation. These particular sites are poisoned with the tars as the reaction progresses, explaining the observed shift in selectivity towards the isomer with a lower rate of polymerisation in water and methanol. Since acetone is a good solvent for tars, the poisoning of these sites is partly prevented and the shift in selectivity is much less pronounced.

5.4 Application of Al-free Ti-beta and Ti-HMS for the hydroxylation of substituted naphthalenes

The hydroxylation of substituted naphthalenes is an interesting application for Al-free Ti-beta since these compounds are not expected to be able to enter the pores of TS-1. This was confirmed by the very low activity of TS-1 for both the hydroxylation of 1-naphthol and of 2-methyl-naphthalene. The naphthalenes only reacted slowly and non-selectively at the external surface of TS-1, which was

deactivated by tar formation.

Similar to the results obtained in the hydroxylation of benzenes, the main reaction over the mesoporous Ti-HMS was also tar formation and decomposition of H_2O_2, a result of the framework hydrophilicity of these materials.

The hydroxylation of 1-naphthol over Al-free Ti-beta mainly yielded the desired product 1,4-naphthoquinone with a 60 % selectivity and 81 % peroxide efficiency. A good selectivity (88 %) and peroxide efficiency (59 %) was also obtained for the hydroxylation of 2-methyl-naphthalene, although the conversion of the naphthalene was relatively low (2.4 %). These results highlight that substituted naphthalenes can efficiently be oxidised to their respective naphthoquinones over Al-free Ti-beta. However, to achieve higher conversions and better selectivities, the reaction conditions have to be optimised.

Chapter 6

Concluding remarks

The hydroxylation of phenol, anisole and toluene over TS-1, Al-free Ti-beta and Ti-HMS was investigated with the aim of understanding the key parameters influencing activity and product selectivity in aromatic hydroxylations over titanium-containing molecular sieves. An overall second-order kinetic model to fit the reaction data of all hydroxylation reactions was developed and good model fits were achieved in all cases. For TS-1 and Al-free Ti-beta, only a minor deactivation was observed, which was taken into account by weighting the initial reaction data. In the case of Ti-HMS however, a major deactivation through tar formation was observed. Since the side reactions were dominant in the Ti-HMS catalyzed phenol hydroxylation, the reaction data were not suitable for a comparison to TS-1 and Al-free Ti-beta. An additional problem with all batches of mesoporous titanosilicates synthesised in this work was significant leaching of titanium from the framework.

The cycle-wise CVD of TEOS technique was successfully applied to silanise the external surface of nano-size ($d_{crystal}$ = 0.1 μm) TS-1 crystals. Physico-chemical techniques confirmed the deposition of SiO_2 at the external surface of the crystallites. A suitable test reaction to selectively probe the external surface activity of TS-1 could not be found. However, a kinetic study of the phenol hydroxylation using parent and progressively silanised small TS-1 crystals showed that the inertisation of the external surface is complete after 20 cycles of CVD of TEOS. A gas-phase pulse chromatographic adsorption study demonstrated that no additional mass transfer resistances are present after 20 cycles of silanisation. Applying the cycle-wise CVD of TEOS technique under the mild conditions chosen in this work, it was possible to selectively deactivate the external surface of TS-1 without significantly narrowing or blocking the pore entrances.

By applying the kinetic model to the reaction data obtained from experiments using parent and external surface-deactivated TS-1, it was possible to decouple the activities of the internal and external surface. On the basis of the internal and external rate constants for reactant consumption and product formation, the influence of the external surface in terms of both activity and selectivity could be evaluated. Other methods to distinguish between internal and external activity of TS-1, such as

coking of the external surface or the use of non-calcined TS-1 samples, were not reproducible. If larger crystals with a smaller amount of external surface sites are used, the reaction becomes severely diffusion limited and conversions and selectivities are low.

Using the cycle-wise CVD of TEOS technique, the role of the external surface was found to be important. The rate constants for the reaction at the external surface were always at least an order of magnitude larger for all reactions, which can be explained by a relatively low concentration of hydrogen peroxide in the TS-1 pores due to their hydrophobicity. Being exposed to the (much higher) H_2O_2 concentrations in the bulk solution, the external surface sites exhibit a significantly higher activity. The external surface also showed much higher activity for non-selective reactions, i.e. peroxide decomposition and tar formation. A study of H_2O_2 decomposition over small and large TS-1 crystals revealed that the majority of the peroxide is decomposed at the external surface, which can also be attributed to higher peroxide concentrations at the external surface. This could also result in the formation of titanium (dihydroperoxo) species, which have a limited stability. As a result of peroxide decomposition at the external surface, tars are formed through overoxidation of hydroxylated products. The significant reduction of tar formation upon silanisation, expressed as tar deposition on the catalyst or as tar formation rate constant, confirmed that the external surface is also mainly responsible for non-selective conversion of the aromatic reactant. The external surface also exhibits different selectivities compared to the internal surface. In all aromatic hydroxylation reactions over TS-1, more of the ortho-hydroxylated isomer was formed at the external surface. This proves the presence of shape selectivity in the TS-1 pores for all hydroxylations as no geometric constraints are imposed on the reaction at the external surface. The role of the external surface was solvent dependent, which can be explained by different competitive adsorption of reactants and products. Another factor is the ability of the solvent to dissolve the tars formed at the external surface during reaction. Parts of the external surface become deactivated in the course of the reaction and a shift in the product selectivity is observed as these sites are eliminated.

The question whether shape selectivity plays a role in aromatic hydroxylations over titanium-substituted zeolites was investigated by comparing the medium-pore TS-1 and the large-pore Al-free Ti-beta. In the phenol hydroxylation, TS-1 showed a much higher selectivity towards the para isomer, which is consistent with a shape selective reaction in the pores. Since the Al-free Ti-beta pores are larger, more ortho isomer was formed. The opposite was however observed in the anisole and toluene hydroxylation, where much higher para-selectivities were observed with Al-free Ti-beta. This effect can be explained by the ability of the aromatic molecules to adopt a different configuration in the pores of Al-free Ti-beta. In Al-free Ti-beta, apolar substituents at aromatic ring such as the methyl group of anisole and toluene, will point away from the polar titanium hydroperoxo site towards the framework walls. This configuration, driven by the hydrophobicity of the framework and the hydrophilicity of the active site, is not possible in TS-1 due to space restrictions.

Diffusional limitations in TS-1 catalyzed aromatic hydroxylations have repeatedly been reported, but very little data about the diffusivity of aromatics in TS-1 is available in the literature. The ZLC method was therefore applied to measure (binary) intracrystalline counterdiffusivities in TS-1. The suitability of the method was demonstrated by thoroughly investigating key parameters that could affect the determination of the diffusivity values, such as flow rate, concentration of the substrate, amount of catalyst and blank response of the system. The intracrystalline diffusivities measured with the ZLC method were about an order of magnitude larger than literature values. However, the diffusivities reported in the literature were determined under reaction conditions. Additional space restrictions generated by reactive species in the pores could explain the lower values. An activation energy of 20.4 kJ/mol was found for the diffusion of phenol in TS-1, which is in the same order as comparable diffusivity values for silicalite or H-ZSM-5. The role of the solvent and the role of the substrate in the diffusion of aromatics in TS-1 was also investigated. A slower diffusion of the aromatic was observed when the compound was strongly adsorbed in the zeolite pores. Thus, the solvent has an influence on the transport properties of aromatic molecules in TS-1 by altering the interactions with the zeolite walls. The influence of the pore size on intraporous mass transport was evaluated by comparing the diffusion of phenol in TS-1 and Al-free Ti-beta. As expected, the intracrystalline diffusion of phenol was significantly faster in the larger-pore Al-free Ti-beta.

A chromatographic liquid-phase pulse method was used to characterise the adsorption properties of aromatics in TS-1 and Al-free Ti-beta with different solvents. The adsorption study highlighted the hydrophobic nature of both catalysts as non-polar compounds were generally more strongly adsorbed than polar molecules. Large Henry's constants for aromatics with water as the solvent and small K values for water in methanol and acetone confirmed the hydrophobicity of the zeolite pores. As a consequence, intraporous concentrations of H_2O_2 are likely to be very low, which is a key factor for framework stability and for the high selectivities observed for TS-1 and Al-free Ti-beta. Aromatics were generally more strongly adsorbed in methanol compared to acetone, explaining the higher activity of the catalyst obtained when methanol was used as a solvent.

Adsorption effects are largely responsible for the different activities observed for TS-1 and Al-free Ti-beta with different solvents. The general order of activity obtained was water >> methanol > acetone, which correlates to the Henry's adsorption constant of the aromatic reactant in the catalyst with the respective solvent. An additional factor when acetone is used as a solvent is the lower concentration of free H_2O_2, caused by the reversible formation of various acetone peroxides and hydroperoxides. The lower free hydrogen peroxide concentration translates into a lower activity in acetone.

An increase of the catalyst crystallites size results in the reaction rate being controlled by the mass transfer in the micropores for both TS-1 and Al-free Ti-beta. This confirms literature results, where severe diffusional limitations on the rate of phenol hydroxylation over TS-1 were reported

when small and large crystals were compared. Although these diffusional limitations were more severe for the medium-pore TS-1 as compared to the large-pore Al-free Ti-beta, the phenol hydroxylation over Al-free Ti-beta ($d_{crystal}$ = 0.9 μm) was also influenced by diffusion. This was confirmed by calculating catalyst effectiveness factors for TS-1 and Al-free Ti-beta in the phenol hydroxylation using the measured intracrystalline diffusivities for phenol and the observed rate constants. On the basis of the effectiveness factors and after elimination of adsorption effects, the intrinsic activities of TS-1 and Al-free Ti-beta can be calculated. TS-1 showed a significantly higher intrinsic activity than Al-free Ti-beta for the hydroxylation of phenol. However, the intracrystalline diffusivity of phenol under reaction conditions might be lower than the binary diffusion coefficient measured with the ZLC method. If this is the case, the effect would be expected to be more important in the smaller pores of TS-1, hence the difference in intrinsic activity would be even larger than calculated in this work.

For both TS-1 and Al-free Ti-beta, the activity for hydroxylation decreased in the order phenol > anisole > toluene. This can be explained by the activation of the aromatic ring by the substituent, which corresponds to the order expected for an electrophilic substitution. Based on this observation and on results reported in the literature, an electrophilic substitution is the most likely mechanism for aromatic hydroxylations over titanium-containing zeolites.

The active site in titanium silicalite catalyzed hydroxylations is a titanium hydroperoxo species formed upon reaction of framework titanium with H_2O_2; when TBHP was used as the oxidant, no hydroxylation occurred. A reaction mechanism involving an electrophilic attack of the aromatic ring by the terminal OH of the titanium hydroperoxo group was therefore proposed. Due to the nature of the resonance-stabilised reaction intermediates, exclusive ortho- and para-hydroxylation occurs in the case of phenol and anisole, whereas the meta isomer is also formed in the toluene hydroxylation.

A pronounced influence of the solvent on the product distributions was observed. Particularly in TS-1, para-selectivity was enhanced in protic solvents. It is therefore suggested that the solvent plays an active role in the reaction path. Protic solvents can coordinate to the framework-incorporated titanium atom, increasing its coordination sphere to 5 or 6 and rendering the active site significantly more bulky. Monosubstituted benzenes have a kinetic diameter close to the dimensions of the TS-1 pores; a more bulky active site therefore imposes a geometric constraint on the reaction inside the pores, favouring the formation of the para-isomer. In the absence of protic solvents, phenol can compete for coordination to the titanium or, alternatively, hydrogen-bond to the Ti-OOH group. In this case, the ortho-position of the phenol molecule is geometrically favoured for the electrophilic attack and ortho-hydroxylation occurs. Since the methylether group of anisole is more bulky than the phenolic OH and anisole cannot coordinate to the titanium site, more para-hydroxylation was observed in the anisole hydroxylation. Due to the less ortho/para-directing effect of the methyl group, all three isomers were formed in the toluene hydroxylation. Coordinated protic solvent molecules

may also alter the hydrophilicity of the active site, favouring a configuration with the substituent of the aromatic ring pointing away from the active site and leading to favour para-hydroxylation.

Future outlook and recommendations

It has to be noted that all aromatic hydroxylation reactions were investigated under standardised reaction conditions in this work. These conditions are not optimised to achieve optimum selectivities based on the aromatic reactant and hydrogen peroxide. Superior selectivities reported in the literature are due to lower feed ratios of H_2O_2 to the aromatic reactant and higher reaction temperatures. Particularly for the slower anisole and toluene hydroxylation reactions, higher reaction temperatures would significantly improve the peroxide efficiency, an important factor from an industrial point of view. This also applies for the 2-methyl-naphthalene oxidation to vitamin K_3 over Al-free Ti-beta, a particularly interesting example for an industrial application.

Literature results indicate that it might also be interesting to investigate triphase conditions where no solvent is used. Higher para-selectivities and activities were reported, but a more thorough investigation of engineering aspects such as design of the experimental setup is needed.

A general remark from both an industrial and a research point of view is that all reactions should be investigated in a continuous system to circumvent the 'classical' problems of batch reaction investigations and to confirm the results obtained in this work.

The question whether TS-1 is intrinsically more active than Al-free Ti-beta for aromatic hydroxylations was partly answered in the course of this work. An extended comparison of TS-1 and Al-free Ti-beta involving more compounds and solvents would be of interest. However, to make exact statements, diffusion measurements under reaction conditions and the determination of the intraporous hydrogen peroxide concentration are necessary. Both tasks have not yet been accomplished and more research on these topics has to be done. The liquid-phase ZLC method might be an appropriate tool; hydrogen peroxide could be co-fed at very low temperatures (where the hydroxylation reaction is sufficiently slow) and the diffusivity of aromatics could be measured in the presence of Ti-OOH sites in the pores. The same applies for the measurement of H_2O_2 adsorption in titanosilicates, which might be possible at very low temperatures and could then be extrapolated to reaction conditions.

Concerning the application of Al-free Ti-beta, it could be shown that this novel material has the potential to become a useful catalyst for aromatic hydroxylation reactions. Its hydrophobicity, similar to that of TS-1, renders the framework stable under reaction conditions when H_2O_2 is used as the oxidant. Although apparently slightly less active than TS-1 for the hydroxylation of monosubstituted benzenes, the oxidation of naphthalenes is only feasible with Al-free Ti-beta. The results obtained for the oxidation of 1-naphthol and 2-methyl-naphthalene are encouraging and optimising

the reaction conditions would lead to higher conversions. It might also be interesting to test the catalytic properties of Al-free Ti-beta for other compounds that are too bulky for TS-1, such as other substituted naphthalenes, anthracenes and highly-substituted aromatics.

The synthesis procedure for Al-free Ti-beta is not yet optimised since even the seeded synthesis results in relatively large crystals, for which mass transfer limitations were observed. It would therefore be of great interest to synthesise smaller crystals. Promising methods are the promoter-induced synthesis method developed by Kumar et al. (1996) (which could easily be extended to the synthesis of Al-free Ti-beta), the steam-assisted crystallization method presented by Ogura (2001), or the crystallization in the presence of very small amounts of aluminium as shown by Tatsumi and Jappar (1998).

References

Aiken III, J. D. and Finke, R. G. (1999). A review of modern transition-metal nanoclusters: their synthesis, characterization, and application in catalysis. *Journal of Molecular Catalysis A: Chemical*, 145:1–44.

Allain, M., Germain, A., and Figueras, F. (1994). The formation of para-benzoquinone and the mechanism of the hydroxylation of phenol by hydrogen peroxide. *Catalysis Letters*, 28:409–415.

Anunziata, O. A., Pierella, L. B., and Beltramone, A. R. (1999). Synthesis of menadione over selective oxidation zeolites. *Journal of Molecular Catalysis A: Chemical*, 149:255–261.

ASI Instruments (2001). Dielectric constants table. *www.asiinstr.com*.

Astorino, E., Peri, J. B., Willey, R. J., and Busca, G. (1995). Spectroscopic characterization of silicalite-1 and titanium silicalite-1. *Journal of Catalysis*, 157:482–500.

Awum, F., Narayan, S., and Ruthven, D. (1988). Measurement of intracrystalline diffusivities in NaX zeolite by liquid chromatography. *Industrial Engineering Chemical Research*, 27(8):1510–1515.

Bartram, M. E. and Moffat, H. K. (1996). TEOS surface chemistry on SiO_2 at CVD temperatures and pressures. In Besmann, T. M., Allendorf, M. D., Robinson, M., and Ulrich, R. K., editors, *Proceedings of the 13th International Conference on Chemical Vapor Deposition*. The Electrochemical Society Proceedings Series, Pennington. 842-853.

Behrens, P., Felsche, J., Vetter, S., Schulz-Ekloff, G., Jaeger, N. I., and Niemann, W. (1991). A XANES and EXAFS investigation of titanium silicalite. *Journal of the Chemical Society Chemical Communications*, 678-680.

Bhaumik, A., Kumar, P., and Kumar, R. (1996). Baeyer-Villiger rearrangement catalysed by titanium silicate molecular sieve (TS-1)/H_2O_2 system. *Catalysis Letters*, 40:47–50.

Bhaumik, A. and Kumar, R. (1995). Titanium silicate molecular sieve (TS-1)/H_2O_2 induced triphase catalysis in the oxidation of hydrophobic organic compounds with significant enhancement of

activity and para-selectivity. *Journal of the Chemical Society Chemical Communications*, 349-350.

Bhaumik, A., Mukherjee, P., and Kumar, R. (1998). Triphase catalysis over titanium-silicate molecular sieves under solvent-free conditions I. Direct hydroxylation of benzene. *Journal of Catalysis*, 178:101–107.

Bhaumik, A. and Tatsumi, T. (1998). Selective dihydroxylation over titanium silicate molecular sieves. *Journal of Catalysis*, 176:305–309.

Bittar, A. and Kaliaguine, S. (1992). Acid-base lewis sits in titanium silicalites. *Research on Chemical Intermediates*, 18:49.

Blasco, T., Camblor, M. A., Corma, A., Esteve, P., Guil, J. M., Martinez, A., Perdigon-Melon, J. A., and Valencia, S. (1998). Direct synthesis and characterization of hydrophobic aluminium-free Ti-beta zeolite. *Journal of Physical Chemistry B*, 102:75–88.

Blasco, T., Camblor, M. A., Corma, A., and Perez-Pariente, J. (1993). The state of Ti in titanosilicates isomorphous with zeolite β. *Journal of the American Chemical Society*, 115:11806–11813.

Bolis, V., Bordiga, S., Lamberti, C., Zecchina, A., Carati, A., Rivetti, F., Spano, G., and Petrini, G. (1999). A calorimetric, IR, XANES and EXAFS study of the adsorption of NH_3 on Ti-silicalite as a function of the sample pre-treatment. *Microporous and Mesoporous Materials*, 30:67–76.

Bordiga, S., Boscherini, F., Coluccia, S., Genoni, F., Lamberti, C., Leofanti, G., Marchese, L., Petrini, G., Vlaic, G., and Zecchina, A. (1994a). XAFS study of Ti-silicalite: structure of framework Ti(IV) in presence and in absence of reactive molecules (H_2O, NH_3). *Catalyis Letters*, 26:195–208.

Bordiga, S., Coluccia, S., Lamberti, C., Marchese, L., Zecchina, A., Boscherini, F., Buffa, F., Genoni, F., Leofanti, G., Petrini, G., and Vlaic, G. (1994b). XAFS study of Ti-silicalite: structure of framework Ti (IV) in the presence and absence of reactive molecules (H_2O, NH_3) and comparison with ultraviolet-visible and IR results. *Journal of Physical Chemistry*, 98:4125–4132.

Boulicault, L., Brandani, S., and Ruthven, D. M. (1998). Liquid phase sorption and diffusion of branched and cyclic hydrocarbons in silicalite. *Microporous and Mesoporous Materials*, 25:81–93.

Brandani, S. and Ruthven, D. M. (1995). Analysis of ZLC desorption curves for liquid systems. *Chemical Engineering Science*, 50(13):2055–2059.

Camblor, M. A., Constantini, M., Corma, A., Esteve, P., Gilbert, L., Martinez, A., and Valencia, S. (1996). Synthesis and catalytic activity of aluminium-free zeolite Ti-beta oxidation catalyst. *Journal of the Chemical Society Chemical Communications*, 1339-1340.

Camblor, M. A., Corma, A., and Perez-Pariente, J. (1993). Infrared spectroscopic investigation of titanium in zeolites. A new assignment of the 960 cm^{-1} band. *Journal of the Chemical Society Chemical Communications*, 557-558.

Carati, A., Flego, C., Massara, E. P., Millini, R., Carluccio, L., Parker Jr., W. O., and Bellussi, G. (1999). Stability of Ti in MFI and Beta structures: a comparative study. *Microporous and Mesoporous Materials*, 30:137–144.

Cavalcante Jr., C. L., Brandani, S., and Ruthven, D. M. (1997). Evaluation of the main diffusion path in zeolites from ZLC desorption curves. *Zeolites*, 18:282–285.

Ceijka, J., Zilkova, N., Wichterlova, B., Eder-Mirth, G., and Lercher, J. A. (1996). Decisive role of transport rate of products for zeolite para-selectivity: Effect of coke deposition and external surface silylation on activity and selectivity of HZSM-5 in alkylation of toluene. *Zeolites*, 17:265–271.

Chen, L. Y., Jaenicke, S., and Chuah, G. K. (1997). Thermal and hydrothermal stability of framework-substituted MCM-41 mesoporous materials. *Microporous Materials*, 12:323–330.

Ching, C. B. and Ruthven, D. M. (1988). A liquid phase chromatographic study of sorption and diffusion of glucose and fructose in NaX and KX zeolite crystals. *Zeolites*, 8:68–73.

Chu, Y. F., Keweshan, C. F., and Vansant, E. F. (1989). Control of pore-opening size of zeolites. In Karge, H. G. and Weitkamp, J., editors, *Zeolites as Catalysts, Sorbents and Detergent Builders*, volume 37 of *Studies in Surface Science and Catalysis*. Elsevier Science Publishers B. V., Amsterdam.

Clerici, M. G. (1991). Oxidation of saturated hydrocarbons with hydrogen peroxide, catalyzed by titanium silicalite. *Applied Catalysis A: General*, 68:249–261.

Clerici, M. G. (1993). Catalytic oxidations with hydrogen peroxide: new selective catalysts. In Guisnet, M., editor, *Heterogeneous catalysis and fine chemicals III*, volume 78 of *Studies in Surface Science and Catalysis*. Elsevier Science Publishers B. V.

Clerici, M. G. and Ingallina, P. (1993). Epoxidation of lower olefins with hydrogen peroxide and titanium silicalite. *Journal of Catalysis*, 140:71–83.

Clerici, M. G., Ingallina, P., and Millini, R. (1992). Titanium silicalite-1 peroxides. In von Ballmoos, R., Higgins, J. B., and Treacy, M. M. J., editors, *Proceedings of the 9th International Zeolite Conference*. Butterworth-Heinemann, Montreal. 445-451.

Corma, A., Esteve, P., and Martinez, A. (1996a). Kinetics of the oxidation of alcohols by hydrogen peroxide on Ti-beta zeolite: the influence of alcohol structure on catalyst reactivity. *Applied Catalysis A: General*, 143:87–100.

Corma, A., Esteve, P., and Martinez, A. (1996b). Solvent effects during the oxidation of olefins and alcohols with hydrogen peroxide on Ti-beta catalyst: The influence of the hydrophilicity-hydrophobicity of the zeolite. *Journal of Catalysis*, 161:11–19.

Corma, A., Esteve, P., Martinez, A., and Valencia, S. (1995). Oxidation of olefins with hydrogen peroxide and tert-butyl hydroperoxide on Ti-beta catalyst. *Journal of Catalysis*, 152:18–24.

Dartt, C. B. and Davis, M. E. (1996). Characterization and catalytic activity of titanium containing SSZ-33 and aluminium-free zeolite beta. *Applied Catalysis A: General*, 143:53–73.

Davies, A. (1961). *Organic Peroxides*. Butterworth.

de Castro-Martins, S., Tuel, A., and Ben Taarit, Y. (1994). Cyclic voltammetric characterization of titanium silicalite TS-1. *Zeolites*, 14:130–136.

Denayer, J. F. and Baron, G. V. (1998). Chromatographic study of adsorption of n-alkanes on zeolites at high temperatures. *Journal of Physical Chemistry*, 102(17):3077–3081.

Deo, G., Turek, A. M., Wachs, I. E., Huybrechts, D. R. C., and Jacobs, P. A. (1993). Characterization of titania silicalites. *Zeolites*, 13:365–373.

Di Renzo, F., Gomez, S., and ad F. Fajula, R. T. (2000). In *12th International Congress on Catalysis*, volume 130 of *Studies in Surface Science and Catalysis*, page 1631. Elsevier Science Publishers.

Duncan, W. L. and Möller, K. P. (2000). On the diffusion of cyclohexane in ZSM-5 measured by zero-length-column chromatography. *Industrial Engineering Chemistry Research*, 39(6):2105–2113.

Duncan, W. L. and Möller, K. P. (2001). The effect of a crystal size distribution on ZLC experiments. *Chemical Engineering Science*, submitted.

Duprey, E., Beaunier, P., Springueil-Huet, M.-A., Bozon-Verduraz, F., Fraissard, J., Manoli, J.-M., and Bregeault, J.-M. (1997). Characterization of catalysts based on titanium silicalite, TS-1, by physicochemical techniques. *Journal of Catalysis*, 165:22–32.

Eic, M. and Ruthven, D. M. (1988). A new experimental technique for measurement of intracrystalline diffusivity. *Zeolites*, 8:40–45.

Ferrini, C. and Kouwenhoven, H. W. (1990). Modified zeolites for oxidation reactions. In Centi, G. and Trifiro, F., editors, *New Developments in Selective Oxidation*, volume 48 of *Studies in Surface Science and Catalysis*. Elsevier Science Publishers B. V., Amsterdam. 52-60.

Gallot, J. E. and Kaliaguine, S. (1997). Oxidation of hydrocarbons by hydrogen peroxide over Ti catalysts: Kinetics and mechanistic studies. *Progress in Catalysis*, 6:87.

Geobaldo, F., Bordiga, S., Zecchina, A., Giamello, E., Leofanti, G., and Petrini, G. (1992). DRS UV-VIS and EPR spectroscopy of hydroperoxo and superoxo complexes in titanium silicalite. *Catalysis Letters*, 16:109–115.

Hancu, D. and Beckmann, E. J. (2001). Generation of hydrogen peroxide directly from H_2 and O_2 using CO_2 as the solvent. *Green Chemistry*, 3(2):80–86.

Hess, W. T. (1995). *Kirk-Othmer Encyclopedia of Chemical Technology*, volume 13. Wiley, New York, fourth edition.

Höft, E., Kosslick, H., Fricke, R., and Hamann, H.-J. (1996). Titanium containing molecular sieves as catalysts for selective oxidation reactions with hydrogen peroxide. *Journal für praktische Chemie*, 338:1–15.

Hsu, B.-Y. and Cheng, S. (1999). Synthesis and catalytic properties of Ti-substituted SAPO molecular sieves. *Journal of Molecular Catalysis A: Chemical*, 149:7–23.

Huybrechts, D. R. C., Bruycker, L. D., and Jacobs, P. A. (1990). Oxyfunctionalization of alkanes with hydrogen peroxide on titanium silicalite. *Nature*, 345:240–242.

Impens, N. R. E. N., van der Voort, P., and Vansant, E. F. (1999). Silylation of micro-, meso-, and non-porous oxides: a review. *Microporous and Mesoporous Materials*, 28:217–232.

International Zeolite Association (2001). Database of Zeolite Structures. *www.iza.com.*

Kapoor, M. P., Trong On, D., Gallot, J. E., and Kaliaguine, S. (1997). Hydrolytic cleavage of epoxy ring during the epoxidation of alkenes over boron modified titanium silicalite of MFI topology. *Catalysis Letters*, 43:127.

Kärger, J. and Ruthven, D. M. (1992). *Diffusion in Zeolites and Other Microporous Materials*. John Wiley & Sons, Inc., New York.

Khouw, C. B., Dartt, C. B., Labinger, J. A., and Davis, M. E. (1994). Studies on the catalytic oxidation of alkanes and alkenes by titanium silicates. *Journal of Catalysis*, 149:195–205.

Kimura, M., Sugihara, Y., Hanabusa, K., Shirai, H., and Kobayashi, N. (1999). Dendritic metallophthalocyanines - synthesis, electrochemical properties, and catalytic activities. *Chem. Europ. J.*, 5(12):3495–3511.

Kraushaar-Czarnetzki, B. and van Hooff, J. H. C. (1989). A test reaction for titanium silicalite catalysts. *Catalysis Letters*, 2:43–48.

Kulawik, K., Schulz-Ekloff, G., Rathousky, J., Zukai, A., and Had, J. (1995). Hydroxylation of phenol over Ti-MCM-41 and TS-1. *Collection of the Czechian Chemical Communications*, 60:451–456.

Kumar, R. and Bhaumik, A. (1998). Triphase, solvent-free catalysis over the TS-1/H_2O_2 system in selective oxidation reactions. *Microporous and Macroporous Materials*, 21:497–504.

Kumar, R., Bhaumik, A., Ahedi, R. K., and Ganapathy, S. (1996). Promoter-induced enhancement for the crystallization rate of zeolites and related molecular sieves. *Nature*, 381:2987–300.

Kumar, R., Mukherjee, P., and Bhaumik, A. (1999). Enhancement in the reaction rates in the hydroxylation of aromatics over TS-1/H_2O_2 under solvent-free triphase conditions. *Catalysis Today*, 49:185–191.

Kumar, R., Raj, A., Kumar, S. B., and Ratnasamy, P. (1994). Convenient synthesis of crystalline microporous transition metal silicates using complexing agents. In Weitkamp, J., Karge, H. G., and Hölderich, W., editors, *Zeolites and Related Microporous Materials: State of the Art 1994*, volume 84 of *Studies in Surface Science and Catalysis*. Elsevier Science Publishers B. V. 109-116.

Lamberti, C., Bordiga, S., Arduino, D., Zecchina, A., and Geobaldo, F. (1998). Evidence of the presence of two different framework Ti(IV) species in Ti-silicalite-1 in vacuo conditions: an EAXFS and a photoluminescence study. *Journal of Physical Chemistry B*, 102(33):6382.

Langhendries, G. (1999). *Liquid Phase Hydrocarbon Oxidation: From Transition Metal to Catalytic Membrane Reactor*. PhD thesis, Vrije Universiteit Brussel.

Langhendries, G., De Vos, D. E., Baron, G. V., and Jacobs, P. A. (1999). Quantitative sorption experiments on Ti-zeolites and relation with α-olefin oxidation by H_2O_2. *Journal of Catalysis*, 186:1–11.

Levenspiel, O. (1979). *The Chemical Reactor Omnibook*. OSU Book Stores, Inc., Corvallis, OR, USA.

Lin, Y.-S. and Ma, Y. H. (1989). A comparative study of liquid adsorption and diffusion in microporous and macroporous adsorbents. *Industial Engineering Chemistry Research*, 28:622–630.

Marchal, C., Tuel, A., and Ben Taarit, Y. (1993). Selective oxidation of substituted aromatics using different peroxides. In Guisnet, M., editor, *Heterogeneous Catalysis and Fine Chemicals III*, volume 78 of *Studies in Surface Science and Catalysis*. Elsevier Science Publisher B. V. 447-454.

Martens, J. A., Buskens, P., Jacobs, P. A., van der Pol, A., van Hooff, J. H. C., Ferrini, C., Kouwenhoven, H. W., Kooyman, P. J., and van Bekkum, H. (1993). Hydroxylation of phenol with hydrogen peroxide on EUROTS-1 catalyst. *Applied Catalysis A: General*, 99:71–84.

Maspero, F. and Romano, U. (1994). Oxidation of alcohols with H_2O_2 catalyzed by titanium silicalite-1. *Journal of Catalysis*, 146:476–482.

McMurry, J. (1992). *Organic Chemistry*. Brooks/Cole Publishing, California, third edition.

Milestone, N. B. and Sahasrabudhe, N. S. (1999). Synthesis of microporous metallosilicates using ammonium hexafluoro complexes of metals in a fluoride medium. In Treacy, M. M. J., Marcus, B. K., Bisher, M. E., and Higgins, J. B., editors, *Proceedings of the 12th International Zeolite Conference*, Warrendale. Materials Research Society. 1901-1908.

Millini, R., Massara, E. P., Perego, G., and Bellussi, G. (1992). Framework composition of titanium silicalite-1. *Jounal of Catalysis*, 137:497–503.

Moreau, P., Hulea, V., Gomez, S., Brunel, D., and Renzo, F. D. (1997). Oxidation of sulfoxides to sulfones by hydrogen peroxide over ti-containing zeolites. *Applied Catalysis A: General*, 155:253–263.

Moro-oka, Y. (1998). Reactivities of active oxygen species and their roles in the catalytic oxidation of inactive hydrocarbon. *Catalysis Today*, 45:3–12.

Neys, P. E. F., Vankelecom, I. F. J., Parton, R. F., Dehaen, W., L'abbe, G., and Jacobs, P. A. (1997). The oxidation of cyclic alcohols from an aqueous solution by manganese porphyrins embedded in a polydimethylsiloxane membrane. *Journal of Molecular Catalysis A: Chemical*, 126:L9–L15.

Notari, B. (1988). Synthesis and catalytic properties of titanium containing zeolites. In Grobet, P. J., editor, *Innovation in zeolite materials science*, volume 47 of *Studies in surface science and catalysis*. Elsevier Science Publishers B. V., Amsterdam. 413-426.

Notari, B. (1991). Titanium silicalite: A new selective oxidation catalyst. In Grasselli, R. K. and Sleight, A. W., editors, *Structure-activity and selectivity relationships in heterogeneous catalysis*. Elsevier Science Publishers, B.V., Amsterdam. 243-256.

Notari, B. (1996). In Eley, D. D., Haag, W. O., and Gates, B. C., editors, *Advances in Catalysis*, volume 41 of *Studies in Surface Science and Catalysis*, page 253. Academic Press, San Diego.

Ogura, M. (2001). *Journal of Catalysis*, 199:41.

Parton, R. F., Uytterhoeven, L., and Jacobs, P. A. (1991). Iron-phthalocyanine encaged in zeolite Y and VPI-5 molecular sieve as catalysts for the oxyfunctionalization of n-alkanes. In Guisnet, M., Barrault, M., Bouchoule, C., Dupey, D., Perot, G., Maurel, R., and Montassier, C., editors, *Heterogeneous Catalysis and Fine Chemicals II*, volume 59 of *Studies in Surface Science and Catalysis*. Elsevier Science Publishers B. V. 395-406.

Patai, S. (1974). *The Chemistry of the Quinonoid Compounds*, volume 1. John Wiley & Sons.

Pei, S., Zajac, G. W., Kaduk, J. A., and Faber, J. (1993). Re-investigation of titanium silicalite by X-ray absorption spectroscopy: are the novel titanium sites real? *Catalysis Letters*, 21:333–344.

Perego, G., Bellussi, G., Corno, C., Taramasso, M., Buonomo, F., and Esposito, A. (1990). Titanium-silicalite: A novel derivative in the pentasil family. In Centi, G. and Trifiro, F., editors, *New Developments in Selective Oxidation*, volume 55 of *Studies in Surface Science and Catalysis*. Elsevier Science Publishers, B. V., Amsterdam. 129-136.

Petrini, G., Cesana, A., Albertini, G. D., Genoni, F., Leofanti, G., Padovan, M., Paparatto, G., and Roffia, P. (1991). Deactivation phenomena on Ti-silicalite. In Bartholomew, C. H. and Butt, J. B., editors, *Catalyst Deactivation 1991*, volume 60 of *Studies in Surface Science and Catalysis*. Elsevier Science Publishers B. V.

Prakash, A. M. and Kevan, L. (1998). Reducibility and adsorbate interactions of Ti in titanosilicate molecular sieve TS-1. *Journal of Catalysis*, 178:586–597.

Ramaswamy, A. V. and Sivasanker, S. (1993). Selective oxidation reactions over titanium and vanadium metallosiliçate molecular sieves. *Catalysis Letters*, 22:239–249.

Ramaswamy, A. V., Sivasanker, S., and Ratnasamy, P. (1994). Selective oxidation reactions over metallosilicate molecular sieves: a comparison of titanium and vanadium silicates with MEL structure. *Microporous Materials*, 2:451–458.

Ratnasamy, P. and Kumar, R. (1995). Selective oxidation with redox metallosilicates in the production of fine chemicals. In Bonneviot, L. and Kaliaguine, S., editors, *Zeolites: A refined tool for designing catalytic sites*, volume 78 of *Studies in surface science and catalysis*. Elsevier Science Publishers, B. V. 367-376.

Ratnasamy, P. and Sivasanker, S. (1996). *Process for the conversion of phenol to hydroquinone and catechol.* U.S. Patent no. 5,493,061, New Delhi, India.

Reddy, J. S. and Jacobs, P. A. (1996). Selective oxidation of secondary amines over titanium silicalite molecular sieves, TS-1 and TS-2. *Catalysis Letters*, 37:213–216.

Reddy, J. S. and Sayari, A. (1995). volume 94 of *Studies in Surface Science and Catalysis*, page 309. Elsevier Science Publishers.

Rhee, C. H. and Lee, J. S. (1996). Thermal and chemical stability of titanium-substituted MCM-41. *Catalysis Letters*, 40:261–264.

Rigutto, M. S., de Ruiter, R., Niederer, J. P. M., and van Bekkum, H. (1994). volume 84 of *Studies in Surface Science and Catalysis*, page 2245. Elsevier Science Publishers.

Röger, H. P., Krämer, M., Möller, K. P., and O'Connor, C. T. (1998). Effects of in-situ chemical vapour deposition using tetraethoxysilane on the catalytic and sorption properties of ZSM-5. *Microporous and Macroporous Materials*, 21:607.

Ruthven, D. M., Eic, M., and Richard, E. (1991). *Zeolites*, 11:647–654.

Ruthven, D. M. and Stapleton, P. (1993). Measurement of liquid phase counter-diffusion in zeolite crystals by the ZLC method. *Chemical Engineering Science*, 48(1):89–98.

Sastre, G. and Corma, A. (1999). Relation between Lewis acidity of Ti-beta and TS-1 zeolites. A quantum-chemical study. *Chemical Physics Letters*, 302:447–453.

Sauer, M. C. V. and Edwards, J. O. (1971). The reactions of acetone and hydrogen peroxide. I. The primary adduct. *Journal of Physical Chemistry*, 75(19):3004–3011.

Schulz-Ekloff, G. and Ernst, S. (1999). *Preparation of Solid Catalysts*, page 405. Wiley-VCH, Weinheim.

Schwan, P. (2001). *Transient Measurement of Diffusion during Reaction Conditions.* PhD thesis, University of Cape Town.

Sealy, S. and Möller, K. P. (1998). Separation of linear and branched paraffins on silanized silicalite-1. unpublished results. Department of Chemical Engineering, University of Cape Town.

Shanani, G. H., Gunardson, H. H., and Easterbrook, N. C. (1996). Consider oxygen for hydrocarbon oxidations. *Chemical Engineering Progress*. 66-75.

Sheldon, R. A. (1990). Catalytic oxidations in the manufacture of fine chemicals. In Centi, G. and Trifioro, F., editors, *New developments in selective oxidations*, volume 55 of *Studies in surface science and catalysis*. Elsevier Science Publishers B. V., Amsterdam. 52-60.

Sheldon, R. A. (1997). Redox molecular sieves as heterogeneous catalysts for liquid phase oxidations. In Grasselli, R. K., Oyama, S. T., Gaffney, A. M., and Lyons, J. E., editors, *3rd World Congress on Oxidation Catalysts*, volume 110 of *Studies in Surface Science and Catalysis*. Elsevier Science Publishers B. V., Amsterdam. 151-175.

Sheldon, R. A., Arends, I. W. C. E., and Lempers, H. E. B. (1998a). Liquid phase oxidation at metal ions and complexes in constrained environments. *Catalysis Today*, 41:387–407.

Sheldon, R. A. and Dakka, J. (1994). Heterogeneous catalytic oxidations in the manufacture of fine chemicals. *Catalysis Today*, 19:215–246.

Sheldon, R. A., Wallau, M., Arends, I. W. C. E., and Schuchard, U. (1998b). Heterogeneous catalysts for liquid-phase oxidations: Philisophers' stones or trojan horses? *Accounts of Chemical Research*, 31:485–493.

Smith, J. M. (1981). *Chemical Engineering Kinetics*. Chemical Engineering Series. McGraw-Hill Book Company, London, third edition.

Tanev, P. T., Chibwe, M., and Pinnavaila, T. J. (1994). Titanium-containing mesoporous molecular sieves for catalytic oxidation of aromatic compounds. *Nature*, 368:321–323.

Taramasso, M. and Perego, G. (1983). *U.S. Patent 4,410,501*. ENICHEM.

Tatsumi, T. and Jappar, N. (1998). *Journal of Physical Chemistry B*, 102:7126.

Taylor, W. I. and Battersby, A. R. (1967). *Oxidative Coupling of Phenols*. Edward Arnold, London.

Thangaraj, A., Eapen, M. J., Sivasanker, S., and Ratnasamy, P. (1992). Studies on the synthesis of titanium silicalite, TS-1. *Zeolites*, 12:943–950.

Thangaraj, A., Kumar, R., and Ratnasamy, P. (1990). Direct catalytic hydroxylation of benzene with hydrogen peroxide over titanium-silicate zeolites. *Applied Catalysis*, 57:L1–L3.

Thangaraj, A., Kumar, R., and Ratnasamy, P. (1991a). Catalytic properties of crystalline titanium silicates II. Hydroxylation of phenol with hydrogen peroxide over TS-1 zeolites. *Journal of Catalysis*, 131:294–297.

Thangaraj, A., Puthoor, L., and Sivasanker, S. (1994). Solvent effects in the hydroxylation of phenol with H_2O_2 over TS-1. *Indian Journal of Catalysis*, 33 A:255–258.

Thangaraj, A., Sivasanker, S., and Ratnasamy, P. (1991b). Catalytic properties of crystalline titanium silicalites III. Ammoximation of cyclohexanone. *Journal of Catalysis*, 131:394–400.

Thiele, E. W. (1939). *Industrial Engineering Chemistry*, 31:916.

Trong On, D., Kapoor, M. P., Bonneviot, L., and Kaliaguine, S. (1997). Catalytic epoxidation of *alpha*-pinene over bifunctional mesoporous molecular sieves. *Catalysis Letters*, 44(3):171.

Trong On, D., Kapoor, M. P., and Kaliaguine, S. (1996). Epoxidation of olefins over new amorphous material having different acidic functions. *Journal of the Chemical Society Chemical Communications*, page 1161.

Trong On, D., Kapoor, M. P., Thibeault, E., Gallot, J. E., Lernay, G., and Kaliaguine, S. (1998). Influence of high-energy ball milling on the physico-chemical properties of titanium silicalite TS-1. *Microporous and Macroporous Materials*, 20:107.

Tuel, A. (1996). Crystallization of titanium silicalite-1 (TS-1) from gels containing hexanediamine and tetrapropylammonium bromide. *Zeolites*, 16:108–117.

Tuel, A. (1998). Crystallization of TS-1 in the presence of alcohols: Influence on Ti incorporation and catalytic activity. *Catalysis Letters*, 51:59–63.

Tuel, A. and Ben Taarit, Y. (1993). Comparison between TS-1 and TS-2 in the hydroxylation of phenol with hydrogen peroxide. *Applied Catalysis A: General*, 102:69–77.

Tuel, A. and Ben Taarit, Y. (1994a). Influence of the nature of silicon and titanium alkoxides on the incorporation of titanium in TS-1. *Applied Catalysis A: General*, 110:137–151.

Tuel, A. and Ben Taarit, Y. (1994b). Synthesis of titanium silicalite-1 using hexapropyl-1,6-hexanediammonium ions as templating agent. *Zeolites*, (14):594–599.

Tuel, A., Moussa-Khouzami, S., Ben Taarit, Y., and Naccache, C. (1991). Hydroxylation of phenol over TS-1: surface and solvent effects. *Journal of Molecular Catalysis*, 68:45–52.

van der Pol, A. J. H. P. and van Hooff, J. H. C. (1992). Parameters affecting the synthesis of titanium silicalite 1. *Applied Catalysis A: General*, 92:93–111.

van der Pol, A. J. H. P. and van Hooff, J. H. C. (1993). Oxidation of linear alcohols with hydrogen peroxide over titanium silicalite 1. *Applied Catalysis A: General*, 106:97–113.

van der Pol, A. J. H. P., van Hooff, J. H. C., and Verduyn, A. J. (1993). Comparison between gas chromatography and high-performance liquid chromatography analysis of the reaction products formed by the hydroxylation of phenol. *Applied Catalysis A: General*, 96:L13–L20.

van der Pol, A. J. H. P., Verduyn, A. J., and Hooff, J. H. C. (1992). Why are some titanium silicalite-1 samples active and others not? *Applied Catalysis A: General*, 92:113–130.

van der Waal, J. C. (1998). *Synthesis, Characterization and Catalytic Application of Zeolite titanium beta*. PhD thesis, Technische Universiteit Delft.

van der Waal, J. C., Kooyman, P. J., Jansen, J. C., and van Bekkum, H. (1998a). Synthesis and characterization of alumium-free zeolite titanium beta using di(cyclohexylmethyl)dimethylammonium as a new and selective template. *Microporous and Macroporous Materials*, 25:43–57.

van der Waal, J. C., Rigutto, M. S., and van Bekkum, H. (1998b). Zeolite titanium beta as a selective catalyst in the epoxidation of bulky alkenes. *Applied Catalysis A: General*, 167:331–342.

van der Waal, J. C. and van Bekkum, H. (1997). Zeolite titanium beta: A versatile epoxidation catalyst. Solvent effects. *Journal of Molecular Catalysis A: Chemical*, 124:137–146.

van Laar, F. M. P. R. (2001). *Generation of Singlet Oxygen with Heterogeneous Catalysts*. PhD thesis, Katolieke Universiteit Leuven.

van Laar, F. M. P. R., de Vos, D., Vanoppen, D. L., Pierard, F., Brodkorb, A., Mesmaker, A. K.-D., and Jacobs, P. A. (1999). In Treacy, M. M. J., Marcus, B. K., Bisher, M. E., and Higgins, J. B., editors, *Proceedings of the 12th International Zeolite Conference*, Warrendale. Materials Research Society.

Vayssilov, G. N., Popova, Z., Bratinova, S., and Tuel, A. (1997). Liquid phase oxidation of alkylaromatic hydrocarbons over titanium silicates. In Grasselli, R. K., Oyama, S. T., Gaffney, A. M., and Lyons, J. E., editors, *3rd World Congress on Oxidation Catalysis*, volume 110 of *Studies in Surface Science and Catalysis*. Elsevier Science Publisher B. V. 909-918.

Vogel, A. I. (1959). *Quantitative Inorganic Analysis*. Longmans, Green and Co. Ltd, London, second edition.

Wan, K. T. and Davis, M. E. (1994). Design and synthesis of a heterogeneous asymmetric catalyst. *Nature*, 370:449–458.

Wang, I., Ay, C.-L., Lee, B. L., and Chen, M.-H. (1988). In Philips, M. J. and Ternan, M., editors, *Proceedings of the 9th International Congress on Catalysis*, Montreal. Chemical Institute of Canada. 324.

Weber, R. W. (1998). *The Inertisation of the Zeolites ZSM-5, Mordenite and Beta by Chemical Vapour Deposition using Tetraethoxysilane*. PhD thesis, University of Cape Town.

Winkhofer, N., Voigt, A., Dorn, H., Roesky, H. W., Steiner, A., Stalke, D., and Reller, A. (1994). Stable silanetriols as building blocks for the synthesis of titanasilasesquilxanes-model compounds for titanium-doped zeolites. *Angewandte Chemie International Edition English*, 33(13):1352–1354.

Wu, P., Komatsu, T., and Yashima, T. (1998). Hydroxylation of aromatics with hydrogen peroxide over titanosilicates with MOR and MFI structures: effect of Ti peroxo species on the diffusion and hydroxylation activity. *Journal of Physical Chemistry B*, 102:9297–9303.

Wulff, H. P. (1971). *GB Patent 1,249,079*. Shell Oil.

Zhang, G., Sterte, J., and Schoeman, B. (1995). Discrete colloidal crystals of titanium silicalite-1. *Journal of the Chemical Society Chemical Communications*, 2259-2260.

Zukowski, J., Sybilska, D., and Jurczak, J. (1985). Resolution of ortho, meta, and para isomers of some disubstituted benzene derivates via α- and β-cyclodextrin inclusion complexes, using reversed-phase high performance liquid chromatography. *Analytical Chemistry*, 57:2215–2219.

Appendix A

Publications

Journal publications

U. Wilkenhöner, G. Langhendries, F. van Laar, G. V. Baron, D. W. Gammon, P. A. Jacobs and E.van Steen, "Influence of pore and crystal size of crystalline titano-silicates on phenol hydroxylation in different solvents", *Journal of Catalysis* **202**, in print

U. Wilkenhöner, D. W. Gammon and E. van Steen, "On the role of the titanium active site in the phenol/anisole hydroxylation over titanium substituted crystalline silicates", in "Zeolites and Mesoporous Materials at the Dawn of the 21st Century", *Proceedings of the 13th International Zeolite Conference*, Montpellier, France, 2001, *Studies in Surface Science and Catalysis* **135**, A. Galarneau, F. Di Renzo, F. Fajula and J. Vedrine, eds.

U. Wilkenhöner, W. Duncan and E. van Steen, "Measurement of liquid-phase diffusivities of aromatics in TS-1 and Al-free Ti-beta using the ZLC method", in preparation

Oral conference presentations

U. Wilkenhöner, D. W. Gammon and E. van Steen, "Mechanistic insights in the phenol hydroxylation over crystalline titanium silicates", 2nd Indopacific Conference on Catalysis, Pune, India, February 2001

U. Wilkenhöner, D. W. Gammon and E. van Steen, "Optimisation of phenol hydroxylation over crystalline titanium silicates", Leuven Summer School on Catalysis, AtoFina Catalysis Chair/Katolieke Universiteit Leuven, Oostende, Belgium, October 2000

Conference poster presentations

U. Wilkenhöner, D. W. Gammon and E. van Steen, "Improving the selectivity and reducing the coke formation in the phenol hydroxylation with the system TS-1/H_2O_2", Chemical Engineering R&D 1999, South African Institution of Chemical Engineering, Cape Town, South Africa, October 1999

U. Wilkenhöner, D. W. Gammon and E. van Steen, "Improving the selectivity and reducing the coke formation in the phenol hydroxylation with the system TS-1/H_2O_2", CATSA Catalysis Conference, Catalysis Society of South Africa, Rustenburg, South Africa, November 1999

U. Wilkenhöner, D. W. Gammon and E. van Steen, "Kinetics and diffusion in the phenol hydroxylation with TS-1/H_2O_2", Leuven Summer School on Catalysis, AtoFina Catalysis Chair/Katolieke Universiteit Leuven, Oostende, Belgium, October 2000

Appendix B

List of chemicals

Table B.1: List of products

Name	Supplier	Purity
Acetone	Merck	HPLC grade
Aerosil 200	Degussa	99.9%
Ammonium fluoride (NH_4F)	Merck	p.a
Ammonium hexafluorotitanate ($(NH_4)_2TiF_6$)	Aldrich	p.a
Aluminium chloride hexahydrate	Acros	p.a
Anisole	Aldrich	99.9%
o-hydroxy-anisole (guajacol)	Merck	99%
p-hydroxy-anisole	Merck	99%
β-cyclodextrin	Aldrich	p.a., for HPLC
Catechol (o-dihyroxybenzene)	Saarchem	99.9%
m-cresol	Aldrich	99.9%+
o-cresol	Aldrich	99.9%+
p-cresol	Aldrich	99.9%+
Dodecylamine	Fluka	99.9%
Ethanol	Saarchem	HPLC grade (dried over 4A molecular sieve)
Hydroflouric acid, 40% in water	Fluka	p.a
Hydrogen peroxide, 30% in water	BDH	p.a
Hydroquinone (p-dihyroxybenzene)	BDH	99.9%
Magnesium sulphate	Merck	p.a
Methanol	Merck	HPLC grade
2-methyl-naphthalene	Acros	99%
1-naphthol	Aldrich	99.9%

Name	Supplier	Purity
1,4-naphthoquinone	Merck	99%
2-methyl-1,4-naphthoquinone (menadione, vitamin K_3)	Merck	99.9%
Nitric acid, 55% in water	Saarchem	p.a
Phenol	Aldrich	99.9%
Phosphoric acid, 85% in water	BDH	p.a
Potassium iodide	Saarchem	p.a.
2-propanol	Saarchem	HPLC grade (dried over 4A molecular sieve)
Sulfuric acid conc.	Saarchem	p.a.
t-butylhydroperoxide (t-BuOOH) 70% in water	Acros	p.a
Tetrabutyl orthotitanate (TBOT)	Alfa	99.9%+
Tetraethyl orthosilicate (TEOS)	Aldrich	99%+
Tetraethyl orthotitanate (TEOT)	Alfa	99.9%+
Tetraethylammonium hydroxide (TEAOH) 20% or 40% in water	Alfa	99.9%+ ($Na^+ + K^+ < 50$ ppm)
Tetrapropylammonium bromide (TPABr)	Fluka	p.a
Tetrapropylammonium hydroxide (TPAOH) 20% in water	Alfa	99.9%+ ($Na^+ + K^+ < 50$ ppm)
Toluene	Aldrich	99.9%

Appendix C

Physico-chemical catalyst characterisation data

C.1 X-ray diffraction

C.1.1 TS-1

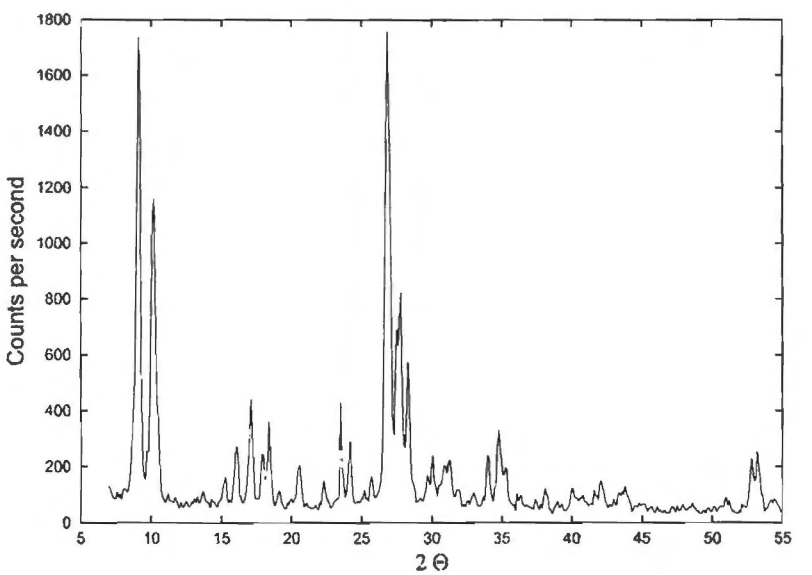

Figure C.1: XRD pattern of small TS-1 crystals

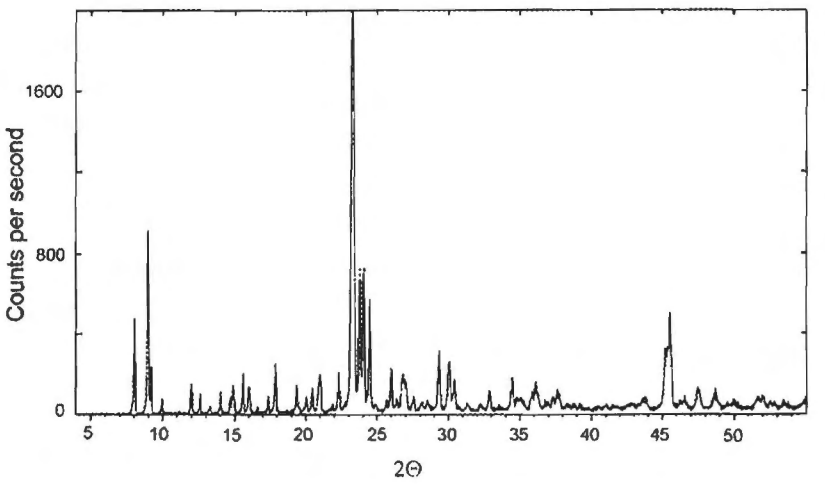

Figure C.2: XRD pattern of large TS-1 crystals

C.1.2 Al-free Ti-beta

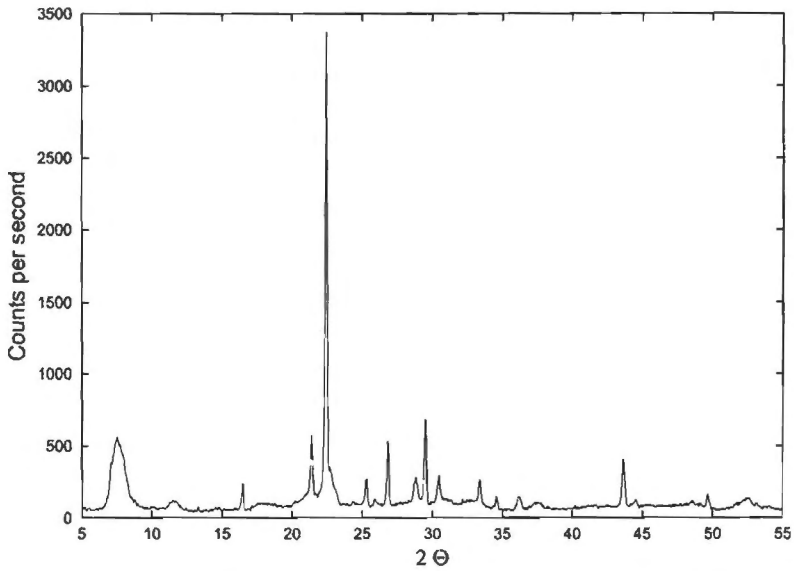

Figure C.3: XRD pattern of Al-free Ti-beta (large and small crystals)

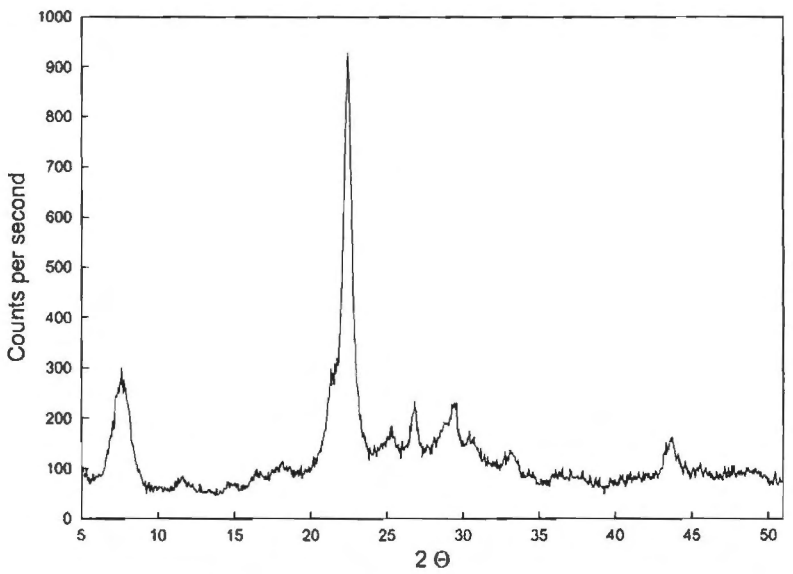

Figure C.4: XRD pattern of dealuminated Al-beta seeds

C.1.3 Ti-HMS

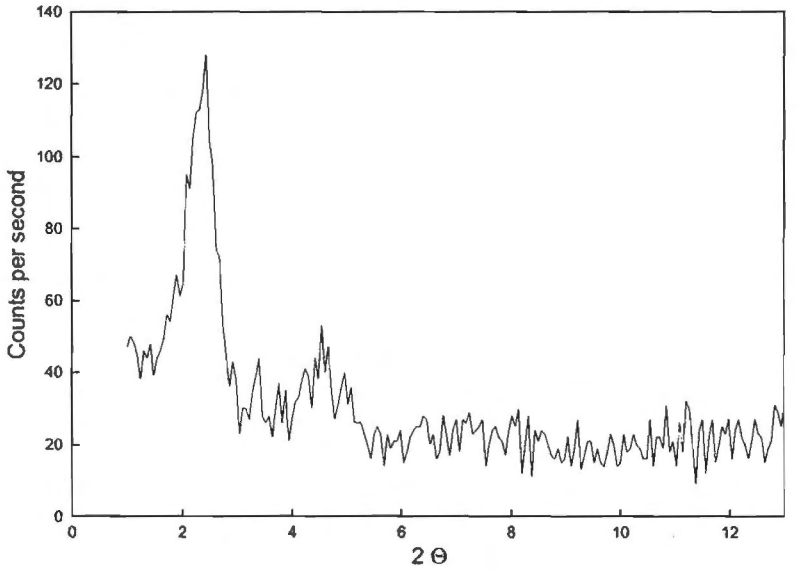

Figure C.5: XRD pattern of Ti-HMS

C.2 Diffuse reflectance UV-Vis spectra

The diffuse reflectance spectra of all catalysts used for reaction work are displayed in Figure 4.1. The spectrum of TiO_2 (anatase) is also given for comparison. Wavelengths were corrected using the absorption edge of anatase. The normalised diffuse reflectance is plotted as F(R) in Kubela-Munk according to:

$$F(R_m) = \frac{(1 - \frac{R_m}{R_\infty})^2}{2\frac{R_m}{R_\infty}} \qquad (C.1)$$

Where R_∞ was obtained from the reflection of highly pure MgO or from a certified standard of Labsphere (SRS-99-010).

C.3 Chemical composition

The titanium content of the catalysts as measured by AAS of the dissolved catalyst and by EDX of the catalyst powder, is shown in Table C.1.

Table C.1: Titanium content of catalysts

Catalyst	Si/Ti (AAS)	Si/Ti (EDX)
TS-1 small[1]	33	30
TS-1 small (sil.)[2]	33	60
TS-1 large[3]	33	35
Al-free Ti-beta[4]	40	45
Ti-HMS	50	-

[1]TS-1 of $d_{crystal}$ = 0.1 μm; [2]small TS-1 crystals after CVD of TEOS for 20 cycles; [3]TS-1 of $d_{crystal}$ = 3×10×45 μm; [4]Al-free Ti-beta of $d_{crystal}$ = 2 - 5 μm

C.4 Scanning electron micrographs

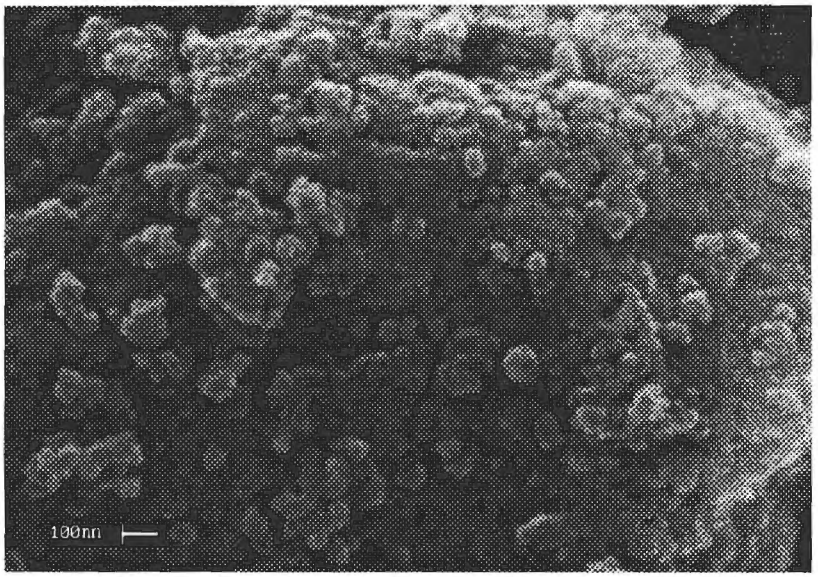

Figure C.6: SEM picture of dealuminated beta seeds

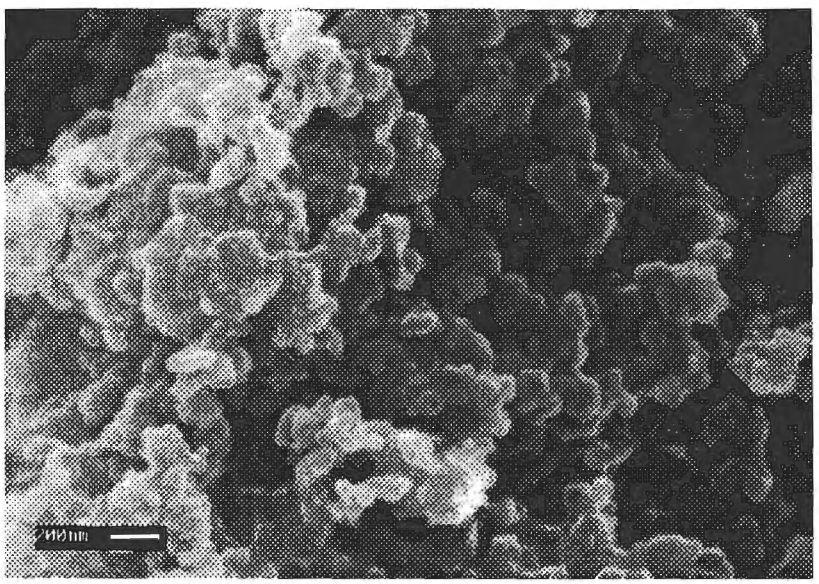

Figure C.7: SEM picture of Ti-HMS

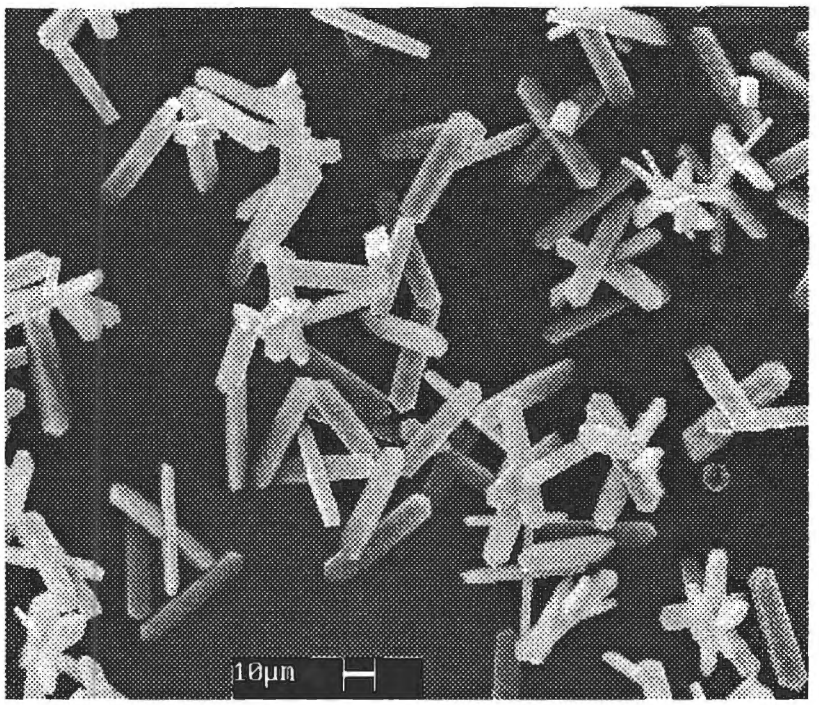

Figure C.8: SEM picture of large TS-1 crystals

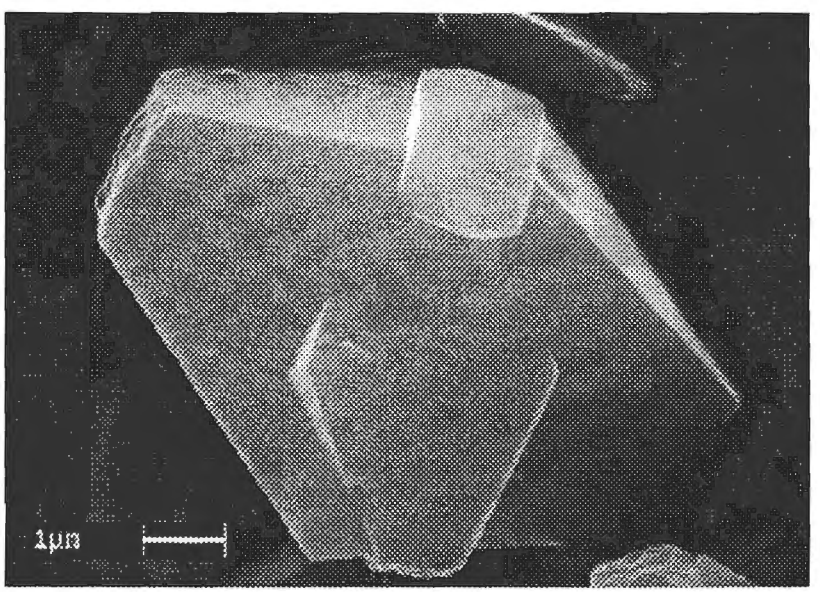

Figure C.9: SEM of large Al-free Ti-beta crystals

Appendix D

Data evaluation and work-up

The following equations were used to evaluate conversions, selectivities, the peroxide efficiency and the product p/o-ratio:

$$X_i(t)\,[\%] = \frac{C_{i,0} - C_i(t)}{C_{i,0}} \cdot 100\% \tag{D.1}$$

$$S_{H_2O_2}(t)\,[\%] \equiv H_2O_2eff.(t)\,[\%] = \frac{C_o(t) + C_m(t) + C_p(t)}{C_{H_2O_2,0} - C_{H_2O_2}(t)} \cdot 100\% \tag{D.2}$$

$$S_i(t)\,[\%] = \frac{C_o(t) + C_m(t) + C_p(t)}{C_{i,0} - C_i(t)} \cdot 100\% \tag{D.3}$$

$$\frac{p}{o} - ratio(t) = \frac{C_p(t) + C_{PBQ}(t)}{C_o(t)} \tag{D.4}$$

The concentrations of the aromatic compounds were determined by HPLC analysis using the following equation:

$$C_i = \frac{A_i \cdot \rho_f}{SF_i \cdot m_{sample}} \tag{D.5}$$

where A_i is the peak area of compound i, SF_i the sensitivity factor of compound i, m_{sample} the withdrawn sample mass in the analysis solutions and ρ_f the density of the reaction mixture. The sensitivity factors were repeatedly determined with calibration solutions of known concentrations according to

$$SF_i = \frac{A_i}{n_i} \tag{D.6}$$

Figure D.1 shows an example for the determination of a sensitivity factor using a Beckman 168 diode array detector (injection of 25 μl calibration solution with sample loop).

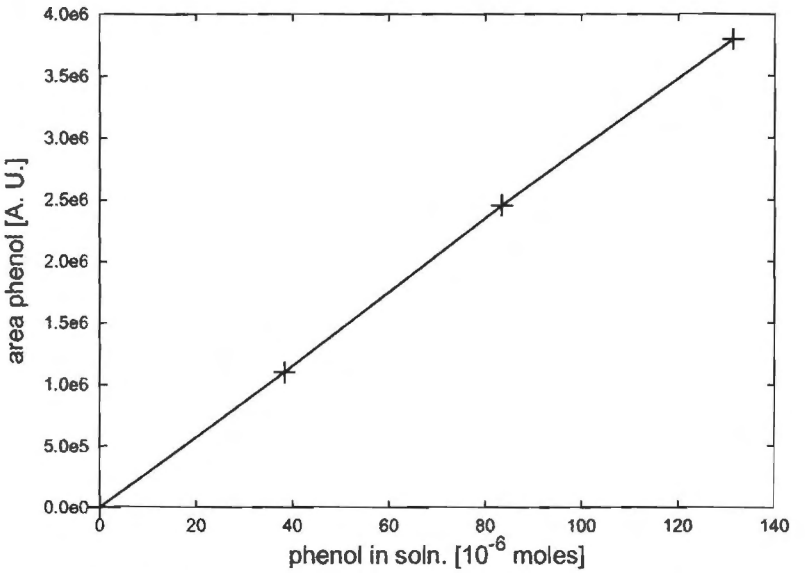

Figure D.1: Determination of sensitivity factor of phenol

Appendix E

Analysis results

Figure E.1 - E.6 show typical chromatograms obtained from HPLC analysis of the reaction mixture samples. Samples were withdrawn from the reaction mixture, immediately filtered with 0.2 μm Millipore disk filters, and diluted to 50 - 100 ml with methanol/H_2O (the sample work-up is described more detailedly in the experimental section).

E.1 Phenol hydroxylation

Mobile phase	:	Acetonitrile/H_2O (25 : 75), buffer: H_3PO_4 85 % (0.8ml/l) / TEA (1 ml/l)
Flow rate	:	1 ml/min
Stationary phase	:	Luna C_{18} 5μm reverse-phase column 250×5 mm
Detector	:	Diode array @ 280 nm

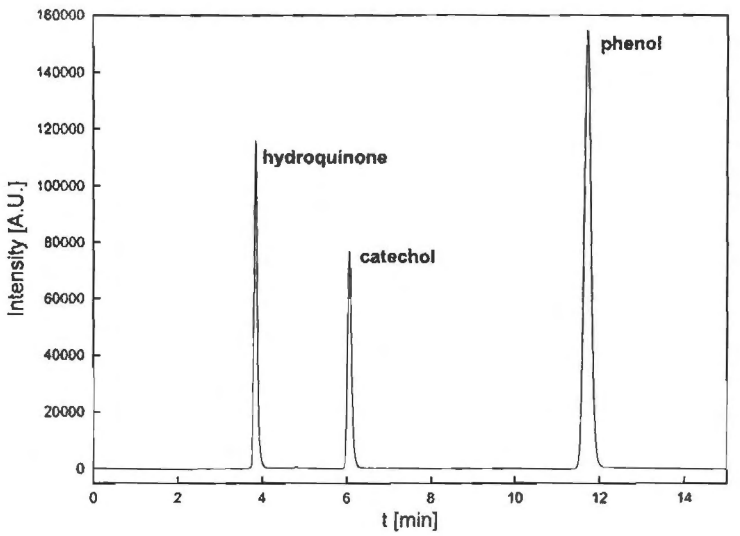

Figure E.1: Typical HPLC chromatogram for phenol hydroxylation reaction mixtures

E.2 Anisole hydroxylation

Mobile phase : Acetonitrile/H_2O (35 : 65), buffer: H_3PO_4 85 % (0.8ml/l) / TEA (1 ml/l)
Flow rate : 1 ml/min
Stationary phase : Luna C_{18} 5μm reverse-phase column 250×5 mm
Detector : UV @ 280 nm

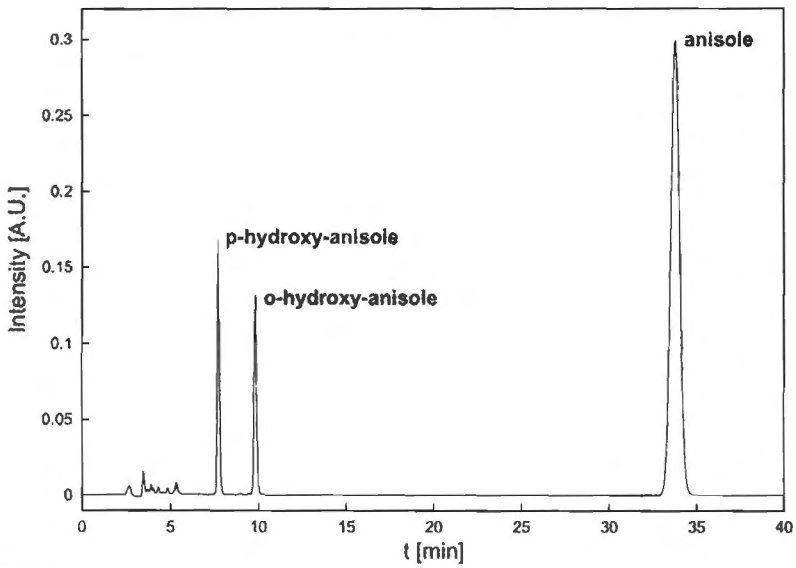

Figure E.2: Typical HPLC chromatogram for anisole hydroxylation reaction mixtures

E.3 Toluene hydroxylation

To achieve a satisfactory separation of the toluene hydroxylation reaction mixtures, β-cyclodextrin was added to the mobile phase in the HPLC analysis. The formation of complexes of β-cyclodextrin with the cresol isomers resulted in a perfect separation. Figure E.3 shows the cavity of a β-cyclodextrin molecule.

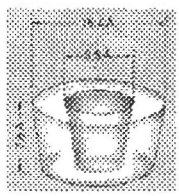

Figure E.3: Cavity of a β-cyclodextrin molecule

Mobile phase : t = 0 min - 20 min: Methanol/H_2O (30 : 70) + β-cyclodextrin (0.5 g/l)
t = 20 min - 40 min: Methanol/H_2O (60 : 40),
Flow rate : 1 ml/min
Stationary phase : Luna C_{18} 5μm reverse-phase column 250×5 mm
Detector : UV @ 280 nm

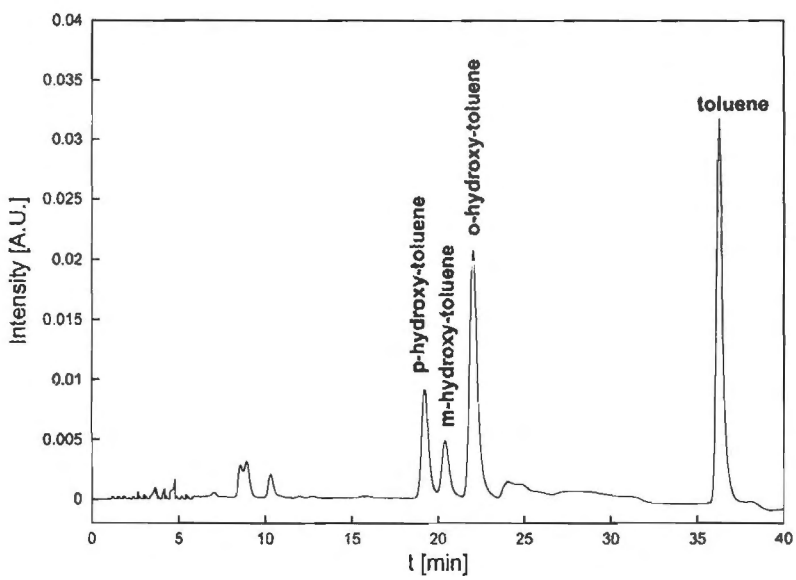

Figure E.4: Typical HPLC chromatogram for toluene hydroxylation reaction mixtures

E.4 Hydroxylation of 1-naphthol

Mobile phase : Acetonitrile/H_2O (50 :50), buffer: H_3PO_4 85 % (0.8ml/l) / TEA (1 ml/l)
Flow rate : 1 ml/min
Stationary phase : Luna C_{18} 5μm reverse-phase column 250×5 mm
Detector : UV @ 280 nm

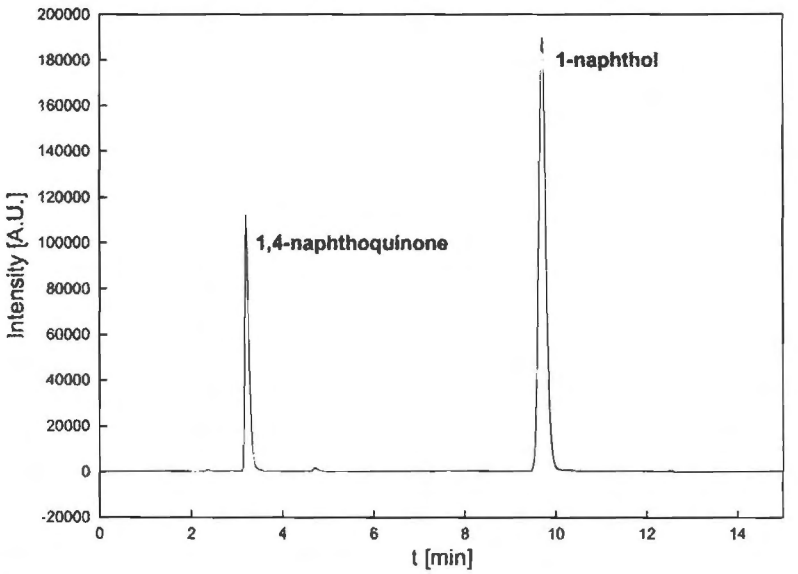

Figure E.5: Typical HPLC chromatogram for 1-naphthol hydroxylation reaction mixtures

E.5 Hydroxylation of 2-methyl-naphthalene

Mobile phase : Acetonitrile/H_2O (70 :30), buffer: H_3PO_4 85 % (0.8ml/l) / TEA (1 ml/l)
Flow rate : 1 ml/min
Stationary phase : Luna C_{18} 5μm reverse-phase column 250×5 mm
Detector : UV @ 290 nm

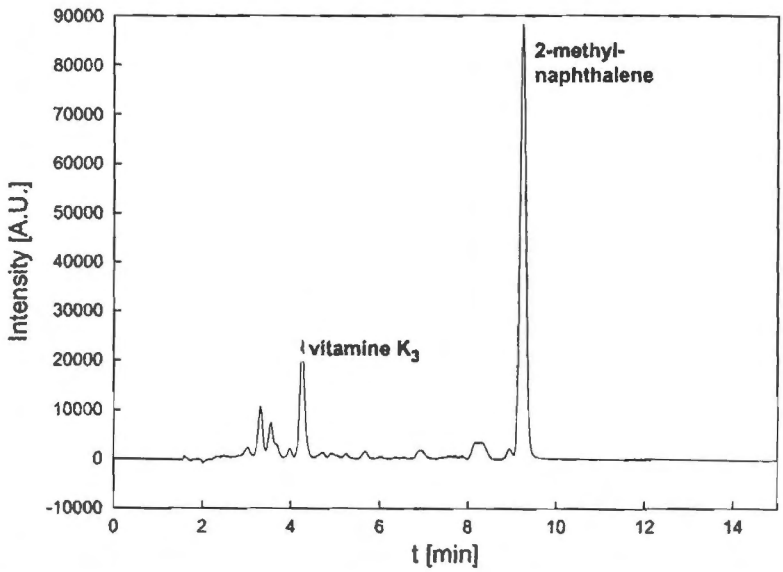

Figure E.6: Typical HPLC chromatogram for 2-methyl-naphthalene hydroxylation reaction mixtures

Appendix F

Kinetics

F.1 Kinetic model

An overall second-order kinetic model (first order in both the aromatic reactant and hydrogen peroxide) as described in section 4.2.2 was chosen to represent the measured concentration-time data of the hydroxylation of phenol, anisole and toluene. A brief evaluation of the reaction order and a justification of the kinetic model is given below.

According to the reaction mechanism proposed in section 5.3.2.1, the aromatic compound reacts with a titanium hydroperoxo species to form the hydroxylated product in an irreversible reaction:

$$Ar + Ti(OOH) \xrightarrow{k_1} ArOH + Ti \tag{F.1}$$

$$hence: \quad r_{Ar} = \frac{dC_{Ar}}{dt} = k_1 C_{Ar} C_{Ti(OOH)} \tag{F.2}$$

Where Ar represents the aromatic reactant and $ArOH$ the hydroxylated reaction product. The active titanium species $Ti(OOH)$ (possible configurations of the active site are displayed in Figure 5.5) is formed via reaction of incorporated titanium (Ti) with hydrogen peroxide (see also Clerici et al. (1992)), which can be regarded as either a reversible (equation F.3) or as an irreversible reaction (equation F.4):

$$Ti + H_2O_2 \overset{K_{TiOOH}}{\rightleftharpoons} Ti(OOH) \tag{F.3}$$

$$Ti + H_2O_2 \xrightarrow{k_{Ti(OOH)}} Ti(OOH) \tag{F.4}$$

Where the sum of hydroperoxo titanium sites $Ti(OOH)$ and "free" titanium sites Ti equals the total amount of titanium sites in the catalyst:

$$C_{Ti,tot} = C_{Ti} + C_{Ti(OOH)} \tag{F.5}$$

If the formation of titanium hydroperoxo species is assumed to be reversible (equation F.3), the rate equation F.1 becomes

$$\frac{dC_{Ar}}{dt} = k_1 K_{Ti(OOH)} C_{Ti,tot} \cdot C_{Ar} \cdot C_{H_2O_2} \cdot \frac{1}{1 + K_{Ti(OOH)} C_{H_2O_2}} \tag{F.6}$$

For relatively low concentrations of hydrogen peroxide (which is the case in the hydrophobic pores of TS-1 and Al-free Ti-beta), this expression becomes (with $k_1^* = k_1 K_{Ti(OOH)} C_{Ti,tot}$)

$$\frac{dC_{Ar}}{dt} \cong k_1^* \cdot C_{Ar} \cdot C_{H_2O_2} \tag{F.7}$$

which is the overall second-order expression used for the kinetic evaluations in this work. If the titanium hydroperoxo formation is assumed to be irreversible, the rate equation F.1 becomes (assuming pseudo-steady state)

$$\frac{dC_{Ar}}{dt} = k_1 C_{Ti,tot} \cdot C_{Ar} \cdot C_{H_2O_2} \cdot \frac{1}{\frac{k_1}{k_{Ti(OOH)}} C_{Ar} + C_{H_2O_2}} \tag{F.8}$$

At a low concentration of hydrogen peroxide and with $\frac{k_1}{k_{TiOOH}} C_{Ar} \approx$ const. (at low conversions of the aromatic), the rate equation can be approximated with a second-order expression similar to equation F.7 (with $k_1^* = k_1 \cdot \frac{1}{\frac{k_1}{k_{Ti(OOH)}} C_{Ar} + C_{H_2O_2}}$).

F.2 Kinetic constants

F.2.1 Phenol hydroxylation

Table F.1: Kinetic constants for phenol hydroxylation over TS-1 after progressive cycle-wise CVD treatment

rate constant $[\frac{l}{mol \cdot m^2 \cdot s}]$	no. silanisation cycles				
	0	5	10	15	20
k_1	1.18E-05	9.35E-06	8.32E-06	7.06E-06	6.73E-06
k_2	3.26E-07	4.20E-08	3.47E-09	1.22E-08	9.98E-09
k_3	5.07E-06	3.94E-06	3.47E-06	2.79E-06	2.64E-06
k_4	5.68E-06	4.32E-06	4.00E-06	3.92E-06	3.80E-06
k_5	2.43E-07	2.36E-07	1.25E-07	3.42E-08	6.19E-08
k_6	5.04E-09	3.22E-09	2.66E-09	4.00E-09	2.00E-09
k_t	1.02E-06	1.08E-06	8.55E-07	3.52E-07	2.96E-07

T = 60 °C, 30 ml water, 1.2 g phenol, 0.6 ml H_2O_2 (30 % in H_2O), 0.12 g TS-1 ($d_{crystal}$ = 0.1 μm)

Table F.2: Observed rate constants for phenol hydroxylation over parent and silanised TS-1 and large TS-1 crystals in different solvents

	TS-1							
rate constant	Water				Methanol		Acetone	
$[\frac{l}{mol \cdot m^2 \cdot s}]$	parent[1]	silanised[2]	large[3]	coked[4]	parent	silanised	parent	silanised
k_1	5.32e-6	2.02e-6	1.41e-7	2.89e-6	1.38e-6	9.23e-7	7.93e-7	3.45e-7
k_2	2.94e-6	1.70e-6	4.09e-8	5.50e-6	2.88e-6	1.30e-6	3.32e-8	1.14e-8
k_3	1.61e-6	7.07e-7	4.986e-8	8.97e-7	3.23e-7	2.10e-7	3.32e-7	1.29e-7
k_4	2.43e-6	1.23e-6	7.86e-8	1.28e-6	6.94e-7	6.24e-7	2.57e-7	1.46e-7
k_5	1.07e-6	2.36e-7	6.85e-7	2.28e-7	2.25e-7	1.41e-7	7.81e-8	1.51e-8
k_6	2.52e-6	4.15e-8	1.98e-8	2.41e-8	1.44e-7	1.04e-7	6.28e-9	4.04e-9
k_t	1.46e-6	8.23e-8	1.26e-8	7.13e-7	3.59e-7	8.86e-8	2.04e-7	6.98e-8

T = 60 °C, 5 ml solvent, 1.2 g phenol, 0.6 ml H_2O_2 (30 % in H_2O), 0.12 g TS-1; [1]small TS-1 crystals (0.1 μm), not modified; [2]small TS-1 crystals after CVD of TEOS for 20 cycles; [3]large TS-1 crystals of 3×10×45 μm; [4]small TS-1 crystals coked before reaction

Table F.3: Kinetic constants for phenol hydroxylation over TS-1 with Al-free Ti-beta of different crystal sizes

rate constant $[\frac{l}{mol \cdot m^2 \cdot s}]$	Al-free Ti-beta	
	large crystals[1]	small crystals[2]
k_1	6.25e-7	1.19e-6
k_2	3.71e-7	4.45e-7
k_3	3.84e-7	6.88e-7
k_4	1.59e-7	2.77e-7
k_5	3.75e-6	6.47e-6
k_6	3.49e-7	6.78e-7
k_t	8.19e-8	2.23e-7

T = 60 °C, 5 ml water, 1.2 g phenol, 0.6 ml H_2O_2 (30 % in H_2O), 0.12 g Al-free Ti-beta; [1]Al-free Ti-beta of 2 - 5 μm; [2]Al-free Ti-beta of ca. 0.9 μm

F.2.2 Anisole hydroxylation

Table F.4: Observed rate constants for anisole hydroxylation over parent and silanised TS-1 and Al-free Ti-beta in different solvents

	TS-1				Al-free Ti-beta[3]	
rate constant	Methanol		Acetone		Methanol	Acetone
$[\frac{l}{mol \cdot m^2 \cdot s}]$	parent[1]	silanised[2]	parent	silanised		
k_1	5.67e-7	9.01e-8	2.05e-7	1.08e-7	1.73e-7	6.04e-8
k_2	5.24e-7	2.25e-7	2.12e-7	2.44e-7	3.36e-7	1.66e-7
k_3	1.23e-7	1.82e-8	5.89e-8	2.98e-8	1.25e-7	4.07e-9
k_4	2.84e-7	4.85e-8	1.09e-7	7.05e-8	1.32e-7	2.57e-8
k_5	1.53e-7	1.39e-7	9.39e-8	6.80e-8	2.41e-7	1.94e-7
k_6	4.85e-9	3.04e-9	2.29e-8	1.26e-9	1.19e-7	1.21e-7
k_t	1.60e-7	2.34e-8	3.70e-8	8.03e-9	2.83e-8	3.06e-8

T = 60 °C, 5 ml solvent, 1.2 g anisole, 0.6 ml H_2O_2 (30 % in H_2O), 0.18 g catalyst; [1]small TS-1 crystals ($d_{crystal}$ = 0.1 μm), not modified; [2]small TS-1 crystals after CVD of TEOS for 20 cycles; [3]Al-free Ti-beta of $d_{crystal}$ = 2 - 5 μm

F.2.3 Toluene hydroxylation

Table F.5: Observed rate constants for toluene hydroxylation over parent and silanised TS-1 and Al-free Ti-beta in different solvents

	TS-1				Al-free Ti-beta	
rate constant	Methanol		Acetone		Methanol	Acetone
$[\frac{l}{mol \cdot m^2 \cdot s}]$	parent[1]	silanised[2]	parent	silanised		
k_1	1.02e-7	4.15e-8	6.73e-8	3.11e-8	3.35e-8	2.33e-8
k_2	5.69e-7	3.04e-7	2.18e-7	1.31e-7	4.91e-7	1.25e-7
k_3	2.28e-8	8.99e-9	2.25e-8	1.06e-8	2.27e-9	9.25e-10
k_4	8.71e-9	4.55e-9	5.95e-9	3.19e-9	1.46e-9	6.56e-10
k_5	1.95e-8	1.18e-8	1.02e-8	5.88e-9	6.09e-9	1.69e-10
k_6	3.25e-8	2.12e-8	3.35e-8	7.18e-9	1.02e-7	9.02e-8
k_7	2.23e-8	5.19e-9	1.57e-8	9.87e-9	1.77e-8	1.22e-8
k_8	5.97e-9	3.10e-9	4.74e-8	6.55e-9	2.16e-9	9.77e-10
k_t	5.14e-8	5.70e-9	2.87e-8	1.14e-8	2.37e-8	2.15e-8

T = 60 °C, 5 ml solvent, 1.2 g toluene, 0.6 ml H_2O_2 (30 % in H_2O), 0.3 g catalyst; [1]small TS-1 crystals (0.1 μm), not modified; [2]small TS-1 crystals after CVD of TEOS for 20 cycles